

**Design, Synthesis and Biological Evaluation of
Anti-Cancer and Anti-Parasitic
Histone Deacetylase Inhibitors**

Inaugural-Dissertation

zur Erlangung des Doktorgrades
der Mathematisch-Naturwissenschaftlichen Fakultät
der Heinrich-Heine-Universität Düsseldorf

vorgelegt von

Katharina Stenzel

aus Omsk

Düsseldorf, März 2017

Aus dem Institut für Pharmazeutische und Medizinische Chemie
der Heinrich-Heine-Universität Düsseldorf

Gedruckt mit der Genehmigung der
Mathematisch-Naturwissenschaftlichen Fakultät der
Heinrich-Heine-Universität Düsseldorf

Referent: Prof. Dr. Thomas Kurz
Korreferent: Prof. Dr. Matthias Kassack

Tag der mündlichen Prüfung: 03.07.2017

Eidesstattliche Erklärung

Ich versichere an Eides statt, dass die Dissertation von mir selbständig und ohne unzulässige fremde Hilfe unter Beachtung der „Grundsätze zur Sicherung guter wissenschaftlicher Praxis an der Heinrich-Heine-Universität Düsseldorf“ erstellt worden ist.

Diese Dissertation wurde in der vorgelegten oder einer ähnlichen Form noch bei keiner anderen Institution eingereicht und es wurden bisher keine erfolglosen Promotionsversuche von mir unternommen.

Ort, Datum

Katharina Stenzel

Acknowledgements

At first I would like to thank my advisor Prof. Dr. Thomas Kurz for giving me the opportunity to work on various interesting and challenging projects and for the continuous support of my Ph.D. study and related research. Thank you for sharing the scientific knowledge, your great encouragement, and for allowing me to work independently. Furthermore, I would like to thank him for his support to attend scientific meetings, the mentorship, and for bringing me in touch with various scientists all over the world.

I want to thank JProf. Dr. Finn Hansen for the motivating discussions and his encouragement. I greatly appreciate his dedication; it was a pleasure to work with him both on a personal and professional level.

I would also like to acknowledge the efforts and to thank Prof. Dr. Matthias Kassack for co-directing this thesis and him and Dr. Alexandra Hamacher for a long and successful collaboration.

Further, I would like to thank Prof. Dr. Katherine Andrews for the great collaboration during our projects and for welcoming me in her Tropical Parasitology Lab at the Griffith University, Queensland, Australia. I could learn a lot during my work in her group and enjoyed the great atmosphere. I also want to thank the whole group, especially MJ Chua and Jessica Engel for their help and all the memories.

I also want to thank our cooperation partner Prof. Dr. InKyeom Kim, Dr. Hae-Ahm Lee and the whole group at the Kyungpook National University School of Medicine, Department of Pharmacology in Daegu, Republic of Korea. During my stays I could learn a lot and I want to thank you very much for the nice cooperation and the hospitality.

Further I would like to thank Dr. Marc Remke and Viktoria Marquardt from the Medical Faculty of the Heinrich-Heine-University Duesseldorf and Prof. Dr. Holger Gohlke and Dr. Christoph Gertzen from the Computational Pharmaceutical Chemistry group of the Pharmaceutical and Medicinal Chemistry Institute of the Heinrich-Heine-University Duesseldorf for their support during our cooperation. I also want to thank Prof. Dr. Jung and Dr. Johanna Senger from the Institute of Pharmaceutical Sciences at the University Freiburg, Vicky M. Avery and Sandra Duffy from the Griffith Institute for Drug Discovery at the Griffith University Queensland in Australia and Elizabeth Winzeler, Stephan Meister and Yevgeniya Antonova-Koch from the Department of Pediatrics at the University of California in San Diego.

I also would like to thank the whole Institute of Pharmaceutical and Medicinal Chemistry of the Heinrich-Heine-University Düsseldorf. Especially I want to thank Beate Lungerich and Simon Herkenhöner for their support and contribution to this work.

Thank you all for your individual part that made this work possible.

Of course, a big "Thanks!" to my labmates for the stimulating discussions, help and for all the fun we had. All past and present members of the working group: Thanks for your help, the laughs and the memories. I am going to miss you so much and hope we will never lose sight of each other!

Special thanks to my close friends - my "non-DNA" family, for being there in great and bad times. Thank you for the different perspectives looking at life. I am a better person through knowing awesome people like you exist.

Finally, I would like to thank my family, who always believed in me, for their love and support on every step of the way. Thank you so much, this work would not have been possible without you!

Für meine Familie

Table of Contents

Abbreviations	V
1 Introduction.....	1
1.1 Histone deacetylases.....	1
1.1.1 Epigenetic machineries.....	1
1.1.2 Antagonistic actions of histone acetyltransferases and histone deacetylases.....	2
1.1.3 HDAC classification	3
1.1.4 Histone deacetylase multi-protein complexes	5
1.1.5 HDAC substrates	6
1.1.6 Pharmacophore model of HDAC inhibitors	7
1.2 Effects of HDAC inhibition on tumor cells, cancer onset, progression and treatment	8
1.2.1 Key effects of HDAC inhibition.....	8
1.2.2 Known mutations in HDAC/HAT genes and expression abnormalities.....	10
1.2.3 Therapeutic implications and sensitivity of tumor cells	11
1.2.4 HDACi approved for cancer treatment	11
1.2.5 Drug combinations with HDACi for cancer treatment.....	13
1.2.6. Isoform-selective HDACi - the next step in therapy?.....	14
1.3 HDACs in non-cancer human disorders	16
1.4 Parasitic approaches of HDACi.....	17
1.5 HDACs as novel target in malaria treatment.....	17
1.5.1 <i>Plasmodium</i> species and life cycle.....	17
1.5.2 Malaria as a public health challenge - disease and pathology.....	19
1.5.3 Malaria prevention and treatment	20
1.5.4 Drug resistances and the search for new generation drugs	23
1.5.5 Anti-malarial activity of HDACi - <i>Pf</i> HDACs as novel target	24
1.6 HDAC as novel target in schistosomiasis treatment	26
1.6.1 Schistosomiasis as a public health challenge.....	26
1.6.2 The need for new drugs for schistosomiasis.....	27
1.6.3 Anti-schistosomal activity of HDACi - <i>Sm</i> HDACs as novel target.....	28
2 Aims of the thesis	30
3 Publication I - Alkoxyurea-based Histone Deacetylase Inhibitors Increase Cisplatin Potency in Chemoresistant Cancer Cell Lines	32
3.1 Project background	32
3.2 Project overview and results.....	33

4 Publication II - Design and Synthesis of Terephthalic acid-based Histone Deacetylase Inhibitors with Dual Stage anti- <i>Plasmodial</i> Activity.....	36
4.1 Project background	36
4.2 Project overview and results.....	37
5 Publication III - Isophthalic acid-based HDAC Inhibitors as Potent Inhibitors of HDAC8 from <i>Schistosoma mansoni</i>	39
5.1 Project background	39
5.2 Project overview and results.....	39
6.1 Summary.....	42
6.2 Zusammenfassung.....	44
7 Manuscripts.....	47
7.1 Manuscript I.....	47
Supporting Information.....	62
7.2 Manuscript II.....	77
Supporting Information.....	88
7.3 Manuscript III.....	97
8 References.....	107

List of Publications

Manuscripts in revision and submitted manuscripts included in this thesis

- I. **K. Stenzel (40%)[#]**, A. Hamacher[#], F. K. Hansen, C. G. W. Gertzen, J. Senger, V. Marquardt, L. Marek, M. Marek, C. Romier, M. Remke, M. Jung, H. Gohlke, M. U. Kassack^Δ, T. Kurz^Δ
- Alkoxyurea-Based Histone Deacetylase Inhibitors Increase Cisplatin Potency in Chemoresistant Cancer Cell Lines
- J. Med. Chem.* 2017, 60, 5334 – 5348 (DOI: 10.1021/acs.jmedchem.6b01538)
- II. **K. Stenzel (70%)**, M. J. Chua, S. Duffy, J. Antonova, S. Meister, A. Hamacher, M. U. Kassack, E. Winzeler, V. M. Avery, T. Kurz, K. T. Andrews^Δ, F. K. Hansen^Δ
- Design and Synthesis of Terephthalic Acid-based Histone Deacetylase Inhibitors with Dual Stage anti-*Plasmodium* activity
- ChemMedChem* 2017, 12, 1627 – 1636 (DOI: 10.1002/cmdc.201700360)
- III. **K. Stenzel (60%)**, A. Chakrabarti, J. Melesina, F. K. Hansen, J. Lancelot, S. Herkenhöner, B. Lungerich, M. Marek, C. Romier, R. J. Pierce, W. Sippl, Manfred Jung, T. Kurz
- Isophthalic Acid-Based HDAC Inhibitors as Potent Inhibitors of HDAC8 from *Schistosoma mansoni*
- Arch. Pharm. Chem.* 2017, 350, e1700096

Other publications

- IV. F. K. Hansen, S. D. M. Sumanadasa, **K. Stenzel**, S. Duffy, S. Meister, L. Marek, R. Schmetter, K. Kuna, A. Hamacher, B. Mordmüller, M. U. Kassack, E. A. Winzeler, V. M. Avery, K. T. Andrews and T. Kurz. Discovery of HDAC Inhibitors with Potent Activity Against Multiple Malaria Parasite Life Cycle Stages. *Eur. J. Med. Chem.* 2014, **82**, 204-213.
- V. D. Diedrich, **K. Stenzel**, E. Hesping, Y. Antonova-Koch, S. Duffy, G. Fisher, M. Mackwitz, S. Meister, T. Kurz, V. M. Avery, E. A. Winzeler, J. Held, K. T. Andrews, F. K. Hansen
- One-pot, multicomponent synthesis and structure-activity relationships of peptoid-based histone deacetylase inhibitors targeting malaria parasites
(manuscript in preparation)
- VI. V. Krieger, A. Hamacher, M. R. H. Zwinderman, C. Schrenk, C. G. W. Gertzen, **K. Stenzel**, T. Kurz, H. Gohlke, F. Dekker, M. U. Kassack, F. K. Hansen

Diversity-oriented synthesis of peptoid-based class I selective histone deacetylase (HDAC) inhibitors
(manuscript in preparation)

Poster presentations

Katharina Stenzel, Alexandra Hamacher, Finn. K. Hansen, Christoph. G. W. Gertzen, Michael Leven, Johanna. Senger, Martin Marek, Christophe Romier, Manfred Jung, Holger Gohlke, Mathias. U. Kassack, Thomas Kurz Alkoxyurea-based Histone Deacetylase "*Inhibitors Increase Cisplatin Chemosensitivity*" (poster presentation)
German Pharmaceutical Society Annual Conference 2016, Munich, Germany, 4 – 7 October, 2016

Katharina Stenzel, Alexandra Hamacher, Finn. K. Hansen, Christoph. G. W. Gertzen, Michael Leven, Linda. Marek, Johanna. Senger, Martin Marek, Christophe Romier, Manfred Jung, Holger Gohlke, Mathias. U. Kassack, Thomas Kurz "*New potent and selective HDAC6 inhibitors with quinoline-based cap groups possess improved activity against chemoresistant cancer cells*" (poster presentation)
Frontiers in Medicinal Chemistry 2016, German Chemical Society Conference, Bonn, Germany, 13 – 16 March, 2016

Katharina Stenzel, Alexandra Hamacher, Finn K. Hansen, Linda Marek, Matthias U. Kassack, Thomas Kurz "Synthesis and anticancer activity of HDAC inhibitors with alkoxyurea linker and quinoline-based cap groups" (poster presentation)
Korean Society of Pharmacology Annual Autumn Congress 2015, Daegu, Republik Korea, 05 – 06 November, 2015

Katharina Stenzel, Alexandra Hamacher, Finn K. Hansen, Christoph G. Gertzen, Michael Leven, Linda Marek, Johanna Senger, Martin Marek, Christophe Romier, Manfred Jung, Holger Gohlke, Matthias U Kassack, Thomas Kurz "Alkoxyurea-based HDAC Inhibitors with quinoline cap groups possess improved activity against chemoresistant cancer cells" (poster presentation)
German Pharmaceutical Society Annual Conference 2015, Duesseldorf, Germany, 23 – 25 September 25, 2015

Oral presentations

Synthesis and anticancer activity of HDAC inhibitors with alkoxyurea linker and quinoline-based cap groups. (oral presentation) November 2015, Lecture at Kyungpook National University, School of Medicine, Republik Korea

Classical chemistry and Solid Phase chemistry for synthesis of novel Hydroxamate-based Histone Deacetylase (HDAC) Inhibitors. (oral presentation) November 2014, Lecture at Kyungpook National University, School of Medicine, Republik Korea

Abbreviations

acetyl-CoA	Acetyl coenzyme A
ACT	Artemisinin-based Combination Therapies
AMC	7-Aminocoumarin
Asp	Aspartic acid
bp	Base pair
Boc	<i>tert</i> -Butyloxycarbonyl protecting group
BSA	Bovine Serum Albumin
°C	Degree Celsius
CDI	1,1'- Carbonyldiimidazole
CDT	1,1'- Carbonylditriazole
CI	Combination indices
CisR	Cisplatin resistant subclone
CpG	Cytosine-phosphate Guanine
CQ	Chloroquine
DHFR	Dihydrofolate reductase
DHPS	Dihydropteroate synthase
DR	Death receptor
EEF	Exo-erythrocytic form
EMA	European Medicines Agency
Et	Ethyl group
EtOH	Ethanol
FAS	Death receptor, also known as apoptosis antigen 1
FDA	Food and Drug Administration
Gadd45	Growth arrest and DNA-damage-inducible protein
<i>e.g.</i>	<i>Exempli gratia</i> , Latin for "for example"
<i>et al.</i>	<i>Et alii</i> , Latin for "and others"
HAT	Histone acetyltransferase
HDAC	Histone deacetylases
HDACi	Histone deacetylase inhibitor
His	Histidine
HIV	Human Immunodeficiency Virus
h	Hours
Hsp90	Heat shock protein 90
HTS	High Throughput Screening
IC ₅₀	Inhibitory concentration (IC), Concentration of component where response is reduced by half
kg	Kilogram

Lys	Lysine
MeOH	Methanol
Met	Methionine
MTT	3-(4,5-dimethylthiazol-2-yl)-2,5-diphenyltetrazolium bromide
mRNA	Messenger RNA
min	Minutes
MW	Microwave
Na	Sodium
NMM	4-Methylmorpholine
p53	Tumor protein p53
<i>Pf</i>	<i>Plasmodium falciparum</i>
<i>Pf</i> HDAC	<i>Plasmodium falciparum</i> histone deacetylase
<i>Pf</i> LSG	<i>Plasmodium falciparum</i> NF54 late stage gametocytes (IV-V)
<i>Pb</i>	<i>Plasmodium berghei</i>
Phe	Phenylalanine
PZQ	Praziquantel
RT	Room Temperature
ROS	Reactive oxygen species
SAHA	Vorinostat (N-hydroxy-N'-phenyl-octanediamide)
SI	Selectivity Index
<i>Sm</i>	<i>Schistosoma mansoni</i>
<i>Sm</i> HDAC	<i>S. mansoni</i> histone deacetylase
TF	Transcription factors
THF	Tetrahydrofuran
TNF	Tumor necrosis factor
TPP	Target product profile
TRAIL	Tumor Necrosis Factor Related Apoptosis Inducing Ligand
Trp	Tryptophan
TSA	Trichostatin A
Tyr	Tyrosine
UPS	Ubiquitin and proteasome system
W	Watt
WAF1(p21)	Cyclin-dependent kinase inhibitor 1
WHO	World Health Organisation
ZBG	Zinc Binding Group

These authors contributed equally to this work.

Δ These authors share the senior authorship

1 Introduction

1.1 Histone deacetylases

1.1.1 Epigenetic machineries

The definition of Epigenetics is changes in gene function that do not involve alterations in the primary sequence of nucleic acids. Such modification can be meiotically inherited to the next generation. Factors such as diet and lifestyle leave epigenetic footprints across the human genome and influence susceptibilities to diseases. Epigenetic changes are crucial for many cellular processes and organism functions like metabolic processes. The most important epigenetic modifications are the methylation of cytosine-phosphate guanine (CpG) islands within the DNA and an array of different posttranslational modifications of the histone proteins including the acetylation of amino acids in the N-terminal histone tails.^{1,2}

Chromatin remodelling is a central mechanism in the epigenetic regulation of gene transcription and expression. The human genome is packaged into chromatin, a dynamic macromolecular complex that consists of DNA, histones, and non-histone proteins and can assume different levels of condensation. In general, condensed chromatin, called heterochromatin, mediates transcriptional repression, whereas transcriptionally active genes are in areas of open euchromatin. DNA-binding transcription factors (TFs) recruit chromatin-modifying complexes and have better access to euchromatin compared with a condensed conformation.^{3,4}

DNA methylation is an epigenetic modification used for long-term silencing of gene expression.⁵ The so-called CpG islands are regions in the DNA where the bases cytosine and guanine repetitively alternate. Methylation takes place only at CpG dinucleotides, at the 5-position of the cytosine ring, almost exclusively within CpG islands.⁶ The alterations in chromatin structure caused by methylation change the interactions between proteins and DNA and leads typically to a decrease in the rate of transcription, however hypermethylation also occurs in regions of active genes.⁷ Most CpG islands are found in the proximal promoter regions and are generally unmethylated in normal cells. Their methylation is often associated with the inappropriate transcriptional silencing of genes and hypermethylation within the promoter region of tumor-suppressor genes are hallmarks of malignancy.⁸

Jenuwein and Allis proposed in 2001 that different combinations of chromatin modifications constitute a so-called histone code and thereby extend the amount of information stored in the genetic sequence.⁹ The histone code is defined by the modifications that regulate the transcriptional activity of specific genes and the activity of transcription regulating multiprotein complexes.¹⁰ The combinatorial nature of post-translational modifications seems to reveal that the histone code considerably extends the information potential of the DNA code.

Histones are formed by a globular domain and a more flexible NH₂ terminus protruding from the nucleosome (so-called histone tails). The N-terminal tail regions of histones undergo a wide variety of modifications and are the most important sites for histone modifications (Figure 1).

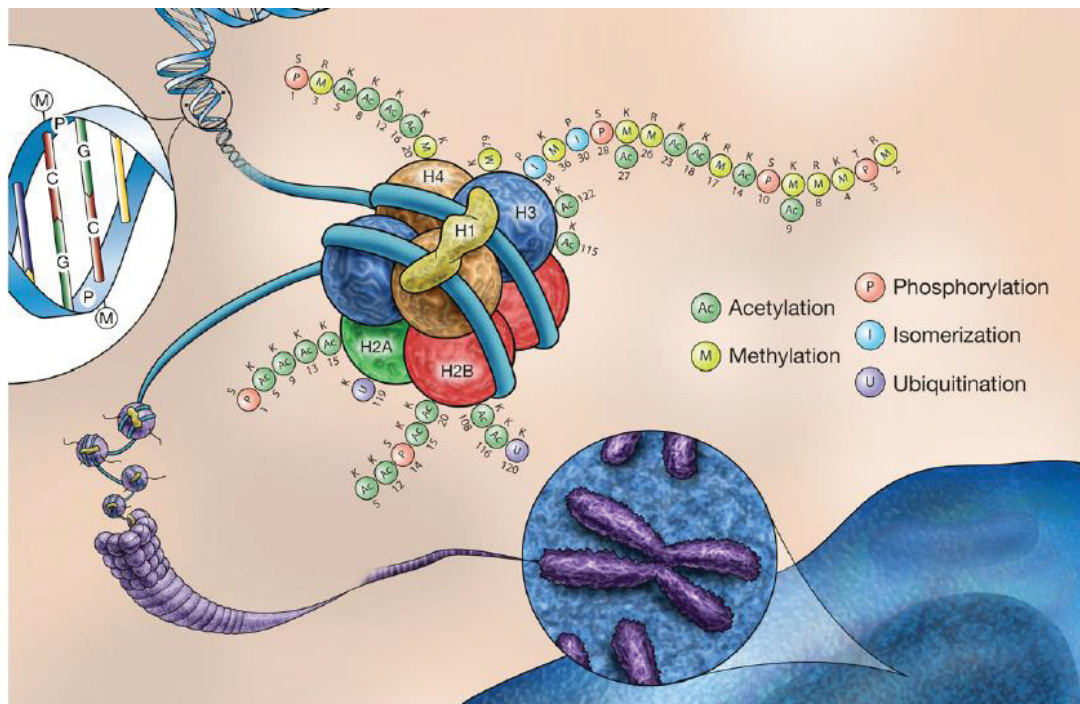


Figure 1. Schematic presentation of specific sites of histone modifications in the amino termini of core histones and the nucleosome as the fundamental repeating units of chromatin. The nucleosome consists of a double-stranded DNA wrapped around a histone octamer. Different possible histone modifications at core histones and DNA methylation at CpG dinucleotides are shown. Picture from: ¹¹

Several post-translational modifications take place on the tail domains of histones, including acetylation, phosphorylation, methylation, ubiquitination, and isomerization (Figure 1). The basic unit of packaging is called nucleosome, consisting of two copies of each core histone H4, H3, H2B, H2A and 147 bp of DNA wrapped around this core. The binding between the DNA and histones is achieved by ionic interactions between basic amino acid residues in the histones and the acidic sugar phosphate backbone of the DNA.¹² Histone post-translational modifications provide an important regulatory framework for DNA repair, gene expression, mitosis, meiosis and other mechanisms.

1.1.2 Antagonistic actions of histone acetyltransferases and histone deacetylases

Lysine acetylation occurs on residues in the N-terminal tails of histones and is controlled by the antagonistic actions of two families of enzymes, histone acetyltransferases (HATs) and histone deacetylases (HDACs). HATs use acetyl-CoA to transfer an acetyl group to the ϵ -amino group of the lysine moieties. Acetyl groups neutralize the positive charges on the basic histone tails, thereby weakening electrostatic interactions between the histones and the negatively charged phosphate backbone of the DNA. HDACs promote the removal of the acetyl group from the acetylated residue, resulting in the release of an acetate molecule. Based on their function, HDACs can be described as

epigenetic erasers, as well as phosphatases and demethylases. The antagonists of erasers are the epigenetic writers like HATs and DNA methyltransferases. Epigenetic readers identify specific histone recognition sequences and recruit other chromatin remodelling proteins. The reading protein modules are classified into several subgroups, among them the bromodomain-containing histone acetylation readers.

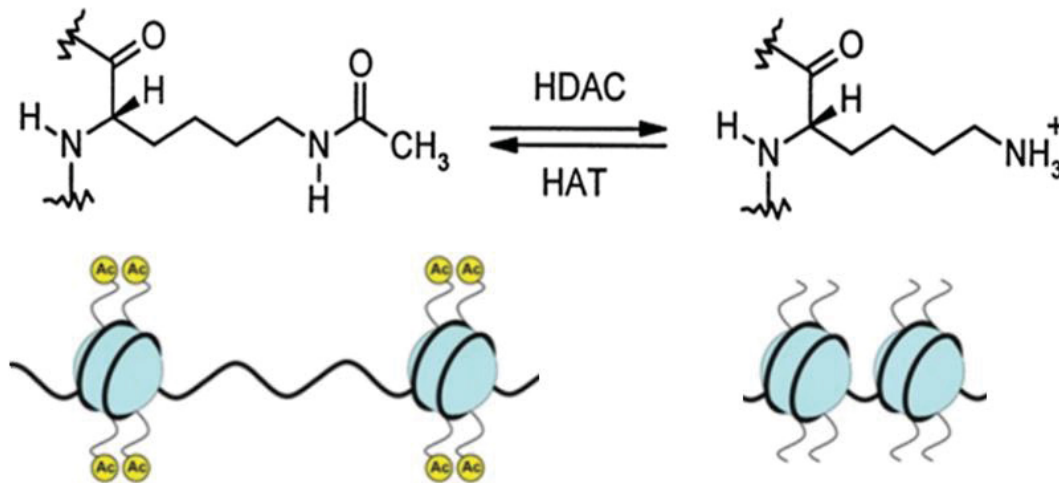


Figure 2. Acetylation and deacetylation of lysine residues in histone tails by histone acetyltransferases (HATs) and histone deacetylases (HDACs) alter the structure of the chromatin. Picture: modified from¹³

Within the nucleosome, positively charged hypoacetylated histones are tightly bound to the phosphate backbone of DNA, maintaining chromatin in a transcriptionally silent state. Acetylation neutralizes the positive charge, disrupting tertiary structures in chromatin and thereby enhancing access of TFs, transcriptional regulatory complexes, and RNA polymerases to promoter regions of DNA. However, in some cases histone acetylation is involved in transcriptional activation.¹⁴

HDACs are part of a high number of complex regulatory mechanisms. By removing acetyl groups from ϵ -amino lysines of proteins, HDACs not only alter transcription, but also influence alternative posttranslational lysine modifications such as ubiquitination. Ubiquitination is an enzymatic process that involves the bonding of an ubiquitin protein to a substrate protein, followed by inactivation and degradation by the proteasome. There is a direct link between acetylation and ubiquitination and both often occur on the lysines. The balance between acetylation and ubiquitylation influences the stability of the substrate protein. As a result, HDACs are able to decrease the half-life of several substrates by exposing the lysine residue for ubiquitylation.^{15, 16}

1.1.3 HDAC classification

An extensive phylogenetic analysis of HDACs¹⁷ shows that HDACs are members of an ancient enzyme family found in animals, plants, fungi and bacteria. 18 human HDACs have been grouped in two families and four classes on the basis of their homology to yeast proteins and their co-factor dependence. The three HDAC classes I/II/IV contain 11 "classical" Zn^{2+} -dependent enzymes whereas class III comprises seven nicotinamide adenine dinucleotide (NAD^+) dependent enzymes (Figure 3).¹⁸

The class I/II/IV HDACs consists of an 8-stranded parallel β sheet placed between a number of α helices. These HDACs differ in size and structural organization but share a similar catalytic core that uses Zn^{2+} as co-factor, located at the bottom of the binding pocket.

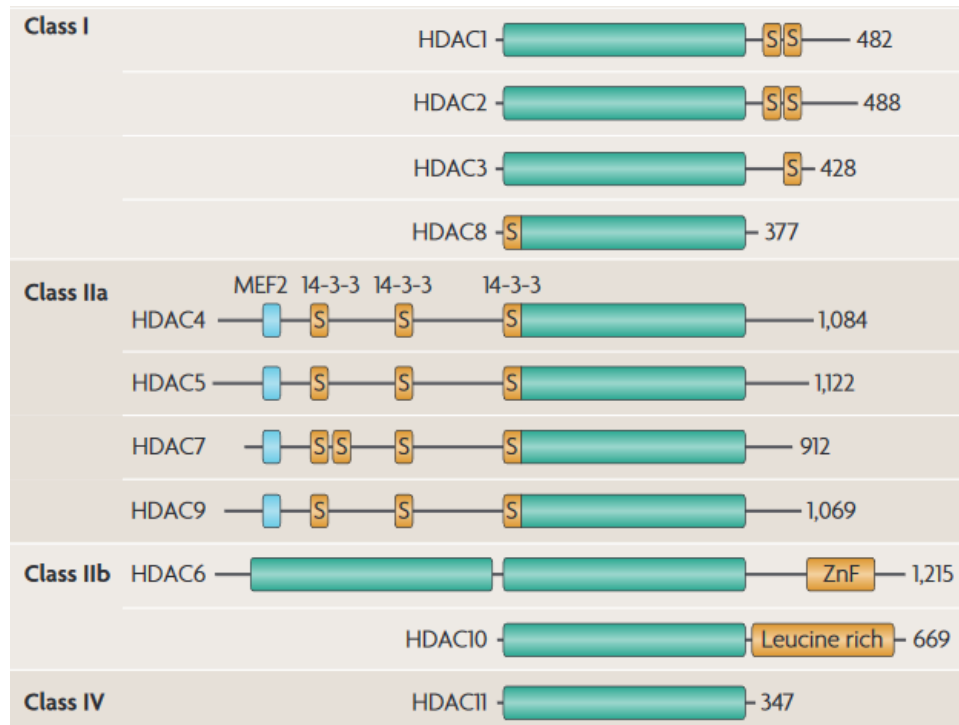


Figure 3. Mammalian classes of HDACs. Green rectangles indicate the conserved HDAC domain; numbers following the HDAC domain indicate the number of amino acids. Myocyte enhancer factor 2 (MEF2)-binding sites are marked by a blue square; 14-3-3, binding sites for the 14-3-3 chaperone protein; S, serine phosphorylation sites; ZnF, zinc finger. Picture from: ¹⁹

Structurally unrelated to the other classes, class III is characterized by NAD^+ dependency. Class III HDACs, called sirtuins, are widely expressed and have a broad range of biological functions. Among others, sirtuins participate in the regulation of oxidative stress, DNA repair and metabolism. The two HDAC families, the sirtuins and the classical HDACs, are evolutionarily conserved amongst prokaryotes and humans. However, sirtuins are not affected by the conventional HDAC inhibitors (HDACi) and will not be discussed any further.

Class I HDACs, consisting of HDAC1, 2, 3 and 8, are considered as nuclear proteins, however, HDAC3 navigates between the nucleus and the cytoplasm. Phylogenetic analysis suggests that HDAC1, 2, 3 and 8 can be further subdivided into class Ia (HDAC1 and 2), class Ib (HDAC3) and class Ic (HDAC8).¹⁷ With the exception of HDAC8,²⁰ a specific characteristic of class I HDACs is their inclusion in large macro-protein complexes. These complexes often involve more than one HDAC subunit and are frequently in association with co-repressor proteins. Especially HDAC1 and HDAC2 interact with each other, forming the catalytic core of several multi-protein complexes.

HDAC4, 5, 6, 7, 9 and 10 are members of the HDAC class II and are relatively large proteins which can shuttle between cytoplasm and nucleus but are mainly localized in the cytoplasm. While class I HDACs are ubiquitously expressed in humans, class II HDACs show tissue specific expression. This class can be further divided into class IIa (HDAC4, 5, 7 and 9) and class IIb (HDAC6 and 10). The presence of a double deacetylase domain is a characteristic for class IIb HDACs. Class IIa is defined by a bipartite structure with a C-terminal HDAC domain and a large N-terminal adaptor domain, characterized by the binding sites for the transcription factor myocyte enhancer factor 2 (MEF2) and for the chaperone protein 14-3-3.²¹ The N-terminal adaptor domain mediates the HDAC class II interactions with tissue-specific transcription factors and co-repressors. Class IIa HDACs navigate between the nucleus and the cytoplasm and have non-histone proteins as primary targets. The class IIb subfamily has two members, HDAC6 and HDAC10. HDAC6 is the only enzyme containing two non-identical catalytic domains and a C-terminal zinc finger domain. HDAC6 is localized exclusively in the cytoplasm, where its main target is α -tubulin.^{22, 23} HDAC10 is found in the nucleus and cytoplasm. It also contains a partial^a second catalytic domain.^{22, 24, 25} The specific substrates of HDAC10 remain unknown and HDAC 10 might function as a recruiter rather than as a deacetylase.²⁵

Class IV is composed by HDAC11 alone. This is the most recently identified isoform. HDAC11 shares conserved residues with both class I and II. Its expression patterns and function are only partially understood.^{26, 27}

1.1.4 Histone deacetylase multi-protein complexes

HDACs (with the exception of HDAC8) belong to multiprotein complexes, which catalyse the cleavage of acetyl residues from histones and other proteins. These multiprotein complexes include transcriptional activators, proteins, other isoforms and/or cofactors.²⁸⁻³⁰ Although HDACs are unable to bind directly to DNA, the multi-protein complexes are recruited to promoters by interaction with specific transcription factors. These protein clusters are one of the difficulties in designing new HDACi, leading to the problem that inhibition on isolated enzymes isoforms does not always match the *in vivo* findings. The enzymatic or physical effect of HDACs on the activity of other HDAC family members and HDAC multi-protein complexes requires further investigation in the future.

A particularly high number of HDAC containing complexes have been described for class I HDACs, which are targeted to specific genomic regions by interactions with DNA binding factors such as nuclear receptors and transcription factors.³¹ HDAC1 and HDAC2 are mainly found in Mi2/NURD complex, the Sin3 complex and the CoREST complex.³²⁻³⁵ HDACs of different classes can co-exist in the same macromolecular complex. The catalytic domain of HDAC4 interacts with HDAC3 within the large NCoR/SMRT nuclear co-receptor complex. HDAC4 contains minimal intrinsic deacetylase

^a The second catalytic domain is vestigial and is thought to be dysfunctional in HDAC10.

activity, however, the enzyme is essential for HDAC activity and for transcriptional repression of target genes by this complex.³⁶

1.1.5 HDAC substrates

Deacetylation of histones in promoters is generally associated with the formation of heterochromatin and transcriptional inactivation, however exceptions are known and some genes were found to be activated by HDACs.³⁷ Apart from histones, other proteins in the cytoplasm and nucleus can be deacetylated by HDACs. As for histones, acetylation is considered as part of a complex set of post-translational modifications often working cooperatively to regulate the function of the modified protein. A growing list of acetylated proteins is currently available and it is supposed that in human cells more than 1750 proteins can be acetylated at lysine residues.³⁸ The dynamic acetylation and deacetylation of non-histone proteins is critical for many cellular processes. While a large number of non-histone HDAC substrates have been identified, the molecular and biological activity of non-histone protein deacetylation have yet to be characterized for the majority of these targets.

Inhibition of HDACs has been shown to significantly affect the acetylation of various tissue-specific or ubiquitous non-histone proteins. HDAC substrates are for example transcription factors (p53, c-Myb and FOXP3),³⁹⁻⁴¹ nuclear receptors (glucocorticoid receptor),⁴² and cytoplasmic proteins (e.g. Hsp90 and α -tubulin).²² Further examples are cell-cycle regulating proteins, e.g. retinoblastoma protein,⁴³ which are involved in many physiological and pathological processes. There is an intense connectivity between post-translational modifications of cell-cycle proteins and the epigenetic regulation of gene expression, where HDACs has an important role at both levels.

HDAC6 plays a central role in cytoskeleton regulation, cell-cell interaction and in angiogenesis^{44, 45} It is the only HDAC isoform which is able to deacetylate α -tubulin, a protein subunit of microtubules. The polypeptide α -tubulin is involved in cytoskeletal structural integrity and cellular motility.⁴⁶ Inhibition of HDAC6 leads to hyperacetylation of the chaperone protein Hsp90 and reduces the chaperone association with its client proteins.⁴⁷ In cells HDAC6 does not catalyse the removal of acetyl groups from histones. HDAC6 deacetylates histones *in vitro*, but there is no evidence for its activity *in vivo*.^{48, 49}

The activity of HDACs on non-histone proteins is a key aspect of HDAC function and the search for additional substrates is ongoing. However, it should not be ignored that histones are by far the most abundant HDAC substrates and histone acetylation surely represents a key target for the action of most HDACs.

1.1.6 Pharmacophore model of HDAC inhibitors

The eleven classical HDACs are characterized by a highly conserved catalytic domain from bacteria to humans and the study of its crystal structures assisted in the development of potent HDACi. The catalytic domain is formed by approximately 300-400 amino acids⁵⁰ and HDAC6 contains two such domains. The HDAC isoforms share the same folding pattern as well as similarity in the binding pocket. The chain conformation within the catalytic domain is similar among all known HDAC structures. Three residues coordinate the Zn^{2+} ion (His, Asp, Asp) and two histidine residues coordinate the zinc binding group of the ligand. A significant difference between the isoforms is a catalytic tyrosine, which is conserved in all HDACs except in vertebrate class IIa HDACs. This tyrosine is replaced by histidine in class IIa HDACs and is considered to act as a transition-state stabilizer.⁵¹

Many HDACi structurally mimic acetyl-lysine and are characterized by a widely accepted pharmacophore model. The morphology of the HDACi pharmacophore, exemplified by vorinostat (suberoyl anilide hydroxamic acid) in Figure 4, consists of three substructures. A metal-binding moiety that binds the catalytic metal atom within the HDAC active site (Zn^{2+} -binding group, ZBG), a hydrophobic linker or spacer to fit in the catalytic tunnel and a cap-group, which binds to the rim of the substrate channel.⁵² A connecting unit is often present between the cap-group and the linker region.

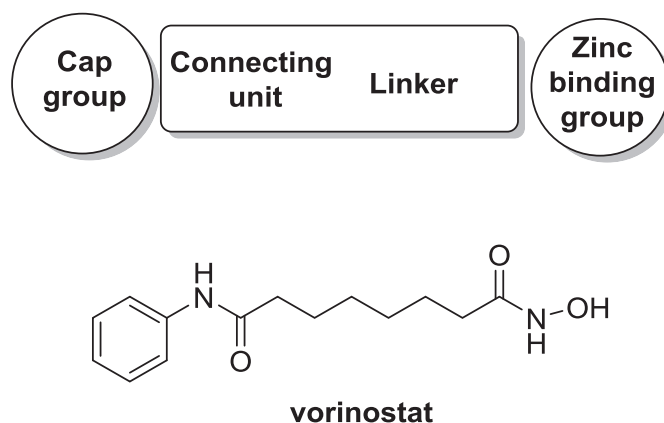


Figure 4. General HDACi pharmacophore model exemplified by vorinostat.

The metal binding moiety of these compounds bind the Zn^{2+} ion, which blocks the active site and keeps the HDAC in its inactive form. HDACi can be classified as members of at least four classes, based on their structure. One common classification is to HDACi containing a hydroxamic acids, e.g. trichostatin A and vorinostat. A second group contains a short-chain fatty acid, e.g. sodium butyrate. Third group contains a cyclic tetrapeptides, e.g. romidepsin. The fourth group contains benzamides, e.g. MS-275.⁵³ In addition several other possible classifications have been suggested after the discovery of a large number of highly diverse HDACi over the last decades. Today, the most frequent used ZBGs remains to be hydroxamic acid (e.g. vorinostat) and benzamide (e.g. MS-275). The most commonly used linkers are aliphatic chains (e.g. six carbon chain in vorinostat), aromatic rings (e.g.

phenylene in MS-275) or vinyl-aromatic structures (e.g. styryl in PXD-101). Recent studies have shown that all pharmacophore units have an impact on the isoform profile of HDACi.⁵⁴ However, many exceptions from the pharmacophore model have been described. For example, lacking the cap or the linker unit.⁵⁵ For a deeper understanding of HDACi properties see part 1.2.4 of the introduction.

1.2 Effects of HDAC inhibition on tumor cells, cancer onset, progression and treatment

1.2.1 Key effects of HDAC inhibition

HDACi are primarily known as anticancer agents and are therefore investigated for their mode of action and clinical efficacy. For a long time cancer was considered to result from a wide variety of genetic and genomic alterations, such as amplifications, translocations, deletions, insertions, and point mutations. However, it became increasingly evident that the development of cancer and persistence may not only be caused by genetic mutations but also by epigenetic modifications. The global pattern of histone acetylation is dysregulated in cancer, which results in chromosomal abnormalities and may result in hyperactivation of oncogenes and the deactivation of tumor suppressor genes.

Acetylation of histones and non-histone proteins play a key role in carcinogenesis. The genes induced by the presence of a HDACi are mainly involved in cell growth, differentiation, changes in gene expression, induction of apoptosis, cell cycle arrest and inhibition of angiogenesis and metastasis.⁵⁶ Interestingly, HDACi induce accumulation of hyperacetylated histones in most regions of chromatin, but only a small number of expressed genes (around 10% according to analyses using DNA microarrays) show a change in transcription patterns.⁵⁷

Tumor growth arrest caused by HDACi can not only be explained on the basis of gene expression⁵⁸, but also by alternative mechanisms. HDACi can cause accumulation of acetylated proteins that are regulators of cell-cycle progression, for example the retinoblastoma protein pRb, TFs such as p53 or glucocorticoid and thyroid hormone receptors. In Table 1, key effects of HDACi on tumor cells are summarized.

Table 1. Key anti-tumor activities of HDACi.

Biological effect	Key effects of HDACi
Cell death	<ul style="list-style-type: none"> -Induction of apoptosis through the intrinsic and extrinsic apoptosis pathways -Enhanced ROS (reactive oxygen species) production and decreased production of free radical scavengers -Accumulation of DNA damage through transcriptional downregulation of DNA repair proteins

Cell cycle arrest	<ul style="list-style-type: none"> -Induction of cell cycle arrest, often in combination with other effects, such as cell death and differentiation -Cells that are resistant to apoptosis undergo cell cycle arrest, where G1/S phase-induced arrest is dominant over G2/M phase-induced arrest.
Differentiation	-Induction of tumor cell differentiation
Inhibition of angiogenesis	-Suppression of pro-angiogenic gene expression
Tumor immunogenicity and regulation of immune cell subsets	<ul style="list-style-type: none"> -Enhancement of immunogenicity -Enhancement of antigen-presenting capacity -Inhibition of dendritic cell differentiation and function -Increase of tumor killing by natural killer cells and cytotoxic T cells -Increase of differentiation and function of CD8+ T cells -Suppression of inflammatory cytokine production

The result of HDACi treatment is most often an induction of tumor cell apoptosis.⁵⁹ Using preclinical models, a direct link between HDACi-induced tumor cell apoptosis and therapeutic efficacy has been described.^{59, 60} HDACi induce apoptosis using at least two different mechanisms.⁶¹ The first mechanism is also called the extrinsic pathway. This mechanism is activated through apoptotic signal transduction cascades mediated by members of the TNF (tumor necrosis factor) death-receptor family (e.g. DR4, DR5 and FAS) and their ligands (e.g. TRAIL or FASL).⁶² The second important mechanism is the intrinsic cell-death pathway, also known as ROS (reactive oxygen species) pathway or the mitochondrial apoptotic pathway.⁶³ The intrinsic pathway has a substantial role in chemotherapy and radiation induced cell death and is controlled by the Bcl2 family proteins in the mitochondria.

HDACi cause increased production of reactive oxygen species (ROS), which has been described as a significant factor in the pro-apoptotic character of HDACi. Tumor cells treated with HDACi showed higher concentration of ROS compared to HDACi treated non-proliferative cells. In addition, the thioredoxin concentration in tumor cells is reduced. The activity of redox proteins (thioredoxins and/or peroxiredoxins) plays an important role in protection of cells from ROS. It is assumed that reduced thioredoxin concentration in tumor cells is one of the reasons for tumor cells sensitivity to HDACi-induced apoptosis.^{64, 65}

HDACi cause an inhibition of cell proliferation by inducing cell-cycle arrest in G1 and/or G2 phase, thereby inhibiting cell growth and/or inducing apoptosis of transformed cells.⁵⁹ HDACi induced activation of the intrinsic apoptotic pathway is not yet fully understood. It is assumed that HDACi

cause global changes in gene expression, which increases expression of pro-apoptotic proteins. Several mechanisms are involved in the induction of cell cycle arrest caused by HDACi. The most relevant is an increased expression of genes that participate in the regulation of the cell cycle such as *CDKN1A* (*p21*), which encodes the cyclin-dependent kinase inhibitor WAF1 (*p21*).⁶⁶ This tumor suppressor protein prevents the dimerization of cyclin dependent kinases and cyclins. This leads for example to hypophosphorylation of the key tumor suppressor protein pRb and its two relatives p107 and p130 and results in suppression of cell proliferation and a cell-cycle arrest in the G1 phase.^{66, 67}

HDACi were historically identified on the basis of their ability to induce tumor cell differentiation.⁶⁸ The differentiation is associated with the ability to cause cell cycle arrest in G1 and/or G2 phase and leads to inhibition of cell growth.⁵⁹ The HDACi concentrations necessary to cause growth inhibition correlate with those needed to induce hyperacetylation of histones.⁶⁹

Angiogenesis is a pivotal component of the progression and metastasis of solid tumors and haematological malignancies. The anti-angiogenic properties of HDACi have been associated with decreased expression of pro-angiogenic genes. The vascular endothelial growth factor (VEGF), basic fibroblast growth factor (bFGF), hypoxia-inducible factor-1 α (HIF1 α), angiopoietin, and endothelial nitric oxide synthase (eNOS) are downregulated after HDACi treatment.⁷⁰⁻⁷² These effects decrease the nutrient supply, thus leading to an inhibition of the metastatic spread of the tumor.⁵⁹ Upregulation of gene expression of metastatic suppressors and down regulation of genes that promote metastasis are also responsible for the anti-metastatic character of HDACi.^{73, 74}

Growing evidences indicate that HDACi lead to an augmentation of the host immune response by an increased cytokine secretion.⁷⁵ Immunomodulatory effects can result in an increased recognition of malignant cells by the immune system due to an increased expression of tumor-associated antigens. These immunomodulatory effects may contribute to the anti-tumor activity of HDACi.

1.2.2 Known mutations in HDAC/HAT genes and expression abnormalities

The interest for HDACs as therapeutic targets results from the observation that HDACs are overexpressed or deregulated in various human tumor types. Various studies in cancer cell lines and tumor tissue revealed changes in protein acetylation, particularly on histones, while an abnormal expression of HDACs enzymes has been found in a broad range of cancer types.⁵⁹ However, it could not be shown that aberrant expression of HDACs can be a primary oncogenic effect.

In several cancer types overexpression of individual HDACs correlated with significant decreases in disease-free survival rate and overall survival.⁷⁶ Expression of HDAC1, 5, and 7 can be used as a molecular biomarker for tumor tissue versus normal tissue and is even able to predict poor patient prognosis independent of other variables such as tumor type and disease progression.⁷⁶ Furthermore, knockdown of HDACs can induce a range of anti-tumor effects such as cell cycle arrest and inhibition of proliferation and induction of apoptosis. In general, expression of class I HDACs

tends to be higher in tumor samples compared to the corresponding normal tissue. In other studies key events of tumor genesis, like the epigenetic repression of the tumor suppressor gene *CDKN1A* (encoding the cyclin-dependent kinase inhibitor WAF1 (p21)) has been linked to an overexpression of HDACs.⁷⁷ In contrast, class II HDACs are downregulated in some tumor samples and high expression correlated with a better prognosis.⁷⁸ Examples are known that HDAC6 overexpression correlates with better prognosis.⁷⁹ Summarized, the level of HDAC expression and/or histone acetylation is not necessarily a suitable indication of clinical sensitivity to oncologic drugs.

Recently, mutations in the HAT genes *CREBBP* and *EP300* were linked to several tumor types. As expected, the inactivating mutations decreased tumor acetylation, and HDACi would be a possible complementary treatment to regain an epigenetic balance.^{80,81}

1.2.3 Therapeutic implications and sensitivity of tumor cells

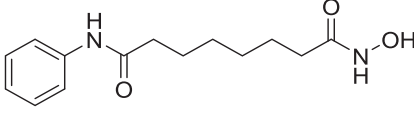
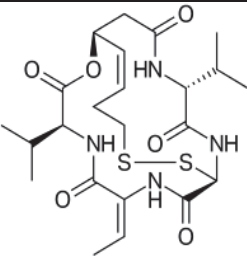
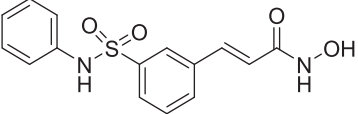
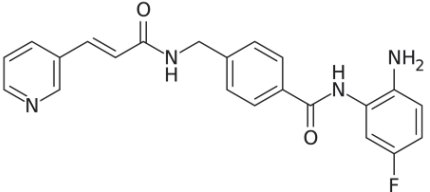
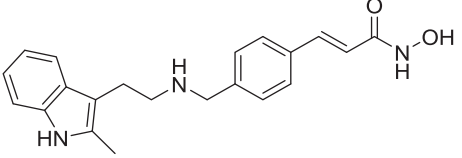
HDACs are regarded as promising therapeutic targets for cancer treatment due to their critical role in the regulation of transcription of key genes, controlling cellular functions such as cell proliferation, cell cycle regulation and apoptosis.⁸² The treatment of normal and tumor cells with HDACi result in an accumulation of hyperacetylated histones. Nevertheless, tumor cells appear to be more sensitive to the growth inhibition and apoptotic effects of these agents than normal cells.⁸³

It was suggested, that tumor cells rely on specific epigenetic pathways and are unable to adapt to an 'epigenetic error' caused by HDACi treatment, whereas normal cells utilize alternative compensatory pathways.⁸⁴ Furthermore, the induction of death receptors and ligands was also demonstrated to be a tumor-cell-selective response to HDACi.^{60,85} Due to increased levels of the protective thioredoxin in normal but not in tumor cells by HDACi treatment, reactive oxygen species (ROS) accumulate only in tumor cells but not in healthy cells.⁶⁵ Interestingly, HDACi also kill nonproliferating tumor cell, whereas normal cells remain unaffected.⁸⁶ However, the exact anticancer mechanisms of HDACi still need further investigation.

1.2.4 HDACi approved for cancer treatment

HDACs are among the most promising therapeutic targets for hematological malignancies and solid tumors. Several HDACi are approved by the FDA (Food and Drug Administration), the China FDA and the EMA (European Medicines Agency) and more than 18 HDACi are in clinical development (phase I/II). Lymphomas are the most common blood cancer type, occurring when lymphocytes mature and multiply uncontrollably. Nowadays, therapeutic efficacy of HDACi have been demonstrated for the treatment of non-Hodgkin lymphoma of the type cutaneous T-cell lymphoma (CTCL), peripheral T-cell lymphoma (PTCL), acute myeloid leukaemia as well as for Hodgkin's lymphoma.

Table 1. Characteristics of approved HDACi.

Structure and name	Clinical application	Classification
 <p>vorinostat (SAHA) Zolinza® Merck</p>	<p>- FDA approved in 2006 for cutaneous T-cell lymphoma (CTCL) and peripheral T-cell lymphoma (PTCL)</p> <p>- Approved alone or in combination</p>	-pan-HDACi, hydroxamate
 <p>romidepsin (FK228) Istodax® Gloucester</p>	-FDA approved in 2009 for cutaneous T-cell lymphoma (CTCL) and peripheral T-cell lymphoma (PTCL)	-Class I HDACi, prodrug, cyclic peptide
 <p>belinostat (PXD101) Beleodaq® Topo Target</p>	-FDA approved in 2014 for peripheral T-cell lymphoma (PTCL)	-pan-HDACi, hydroxamate
 <p>chidamide (HBI-8000) Epidaza®</p>	- chinese FDA approved in 2015 for peripheral T-cell lymphoma (PTCL)	- pan-HDACi, benzamide
 <p>panobinostat (LBH-589) Farydak® Novartis</p>	- FDA and EMA approved in 2015 for multiple myeloma (combination therapy)	-pan-HDACi, hydroxamate

Cutaneous T-cell lymphoma (CTCL) and peripheral T-cell lymphoma (PTCL) are rare forms of non-Hodgkin's lymphoma.^{87,88} Vorinostat, romidepsin and belinostat have been clinically approved for CTCL and/or PTCL by the US FDA. Vorinostat (SAHA, Zolinza[®]) and belinostat (PXD101, Beleodaq[®]) are hydroxamate-based pan-HDACi^b. Romidepsin (FK-228; Istodax[®]) is a pro-drug and is the only approved cyclic tetrapeptide.⁸⁹ Chidamide (HBI-8000) was developed and approved for relapsed or refractory peripheral T-cell lymphoma (PTCL) in China.^{90, 91} Additionally, panobinostat (LBH-589, Farydak[®]) has recently been approved by the FDA and the EMA for a combination therapy for certain patients with multiple myeloma, one of the most common blood cancers. Panobinostat is currently also investigated for the treatment of acute lymphocytic leukaemia and prostate cancers.⁹²

1.2.5 Drug combinations with HDACi for cancer treatment

Chemoresistance is the major problem limiting anticancer drug-based therapeutic approaches. Novel strategies to prevent the development and to overcome chemoresistance are urgently needed. Drug resistances occur against classical cytostatic agents and targeted therapies as e.g. kinase inhibitors. For this reason multi-drug therapies with combined anticancer agents operating in different mechanisms became a standard treatment to prevent drug resistance and to produce synergistic or at least additive effects in various tumors. Chemoresistance may be due to epigenetic alterations leading to defects in the apoptotic pathway. HDACi have been investigated for the combined treatment in several types of cancer therapies, resulting in different degrees of success and various combinations have also been investigated in clinical trials.^{93,56}

DNA hypermethylation is associated with certain cancer genes and DNA methyltransferases inhibitors are effective anticancer agents that cause increased apoptosis in tumor cells.⁹⁴⁻⁹⁶ Several preclinical studies combining HDACi with inhibitors of DNA methyl transferases revealed synergistic antitumor activity.⁹⁷

Promising initial results have been described after combining HDACi with ROS-generating agents such as the tyrosine kinase inhibitors adaphostin.⁹⁸ Cancer cells are known to have higher levels of ROS compared to normal cells and HDACi have been shown to induce oxidative stress in different types of cancer cells.

A further successful strategy is the combination therapy involving HDACi and proteasome inhibition. After treatment of multiple myeloma cells with the proteasome inhibitor bortezomib, the cells became more sensitive to vorinostat and increasing apoptosis was observed.⁹⁹⁻¹⁰² Early phase clinical trials demonstrated an increase in anti-tumor effects of vorinostat in combination with bortezomib in patients suffering from multiple myeloma.¹⁰³⁻¹⁰⁶ In 2015 the HDACi panobinostat (Farydak[®]) was approved for combination therapy with bortezomib (Velcade[®]) for patients who no longer respond to one of the most effective treatments for multiple myeloma, the proteasome inhibition.¹⁰⁷

^b Pan-HDACi inhibit all types and isoforms of HDACs.

An important approach for cancer therapy is the combination of HDACi with DNA damaging chemotherapeutics.¹⁰⁸ Numerous studies showed synergism or additive effects by combining HDACi and DNA-damaging agents such as topoisomerase inhibitors, inhibitors of DNA synthesis, DNA-intercalators and agents covalently modifying DNA (i.e. doxorubicin, epirubicin, cisplatin, 5-fluorouracil, etoposid, mephalan, ellipticine, and temozolomide).¹⁰⁹⁻¹¹⁴ The use of HDACi permits the utilization of lower amounts of therapeutics and could lead to less undesirable side effects due to the DNA-damaging drugs. The HDACi induced sensitization of cells to DNA-damaging drugs is explained by the influence of HDACi on the chromatin structure. The decondensation of chromatin after HDACi treatment induces the relaxed condition, which makes the chromatin more susceptible to DNA damaging drugs. Exposing several human cancer cells to the HDACi trichostatin A or vorinostat prior to etoposide, ellipticine, doxorubicin or cisplatin increased the cytotoxicity of these drugs. After such an exposure the expression of p53, WAF1 (p21), and Gadd45 proteins was significantly increased.¹¹⁵ One of the observed effects after treatment with HDACi in combination with DNA-damaging agents was an increased level of proapoptotic proteins like Bim and Bmf.¹¹⁶ Two more possible effects of the cotreatment are impaired DNA repair and interference with genes important for survival after treatment with DNA damaging agents.¹¹⁷

1.2.6. Isoform-selective HDACi - the next step in therapy?

The contribution of HDACs to tumor development can be due to complex mechanisms other than HDAC overexpression, making a deeper investigation of HDAC isoforms necessary. Common pan-HDAC inhibitors have massive side effects and poor anti-cancer activity against solid tumors. Non isoform-selective HDACi could increase the risk of toxic side effects and definitely limit their use as research tools. Most of the first generation HDACi are not selective towards specific isozymes. In the last years, HDACi with proposed selectivity for several HDAC isoforms have been developed and several of these second-generation HDACi are currently in clinical trials. However, the questions remain whether agents that selectively target a specific HDAC are beneficial. It still has to be demonstrated in clinic if isoform selectivity provides substantial advantages over pan-HDAC inhibition.^{118, 119}

1.2.6.1 Possible applications of selective HDAC1 inhibition

The members of the HDAC class I family are deregulated in many cancers. Overexpression of HDAC1 has been found in gastric, breast, pancreatic, hepatocellular, lung, and prostate carcinomas and in most of these cases HDAC1 up-regulation is associated with a poor outcome.^{120, 121} High expression of HDAC1, HDAC2 and HDAC3 was shown in renal cell cancer, colorectal and gastric cancer as well as in classical Hodgkin's lymphoma.^{122, 123} In a different study analysing breast tumors, HDAC1 and HDAC3 expression correlate with estrogen and progesterone receptor expression suggesting HDAC1 and HDAC3 as an independent prognostic marker.¹²⁴ Taken together, these studies point towards the

overexpression of class I HDACs, in particular HDAC1, as a cancer marker associated with poor prognosis and all these could be examples for future application of HDAC1 selective HDACi.

1.2.6.2 Possible applications of selective HDAC6 inhibition

Since HDAC6 inhibition has no impact on the DNA state it could be a better drug target than other isoforms. HDAC6 knockout mice are the only HDAC mutant mice with no obvious phenotype except for increased α -tubulin acetylation.¹²⁵ Among the Zn^{2+} -dependent HDACs, HDAC6 is functionally and structurally unique. This isoform is primarily present in the cytosol and thus cannot be considered strictly as an epigenetic enzyme. HDAC6 is the only HDAC isoform able to deacetylate α -tubulin *in vitro* and *in vivo* and does not catalyze histone deacetylation *in vivo*.⁴⁶

Due to its unique mode of action HDAC6 has been suggested to be a particularly suitable target for cancer therapy. In addition to its two catalytical domains HDAC6 has a C-terminal ubiquitin-binding zinc finger domain.¹²⁶ HDAC6 counteracts the toxic effects of misfolded protein accumulations by being involved in the two important protein degradation pathways, the aggresome-autophagy pathway and the ubiquitin and proteasome system (UPS).^{127, 128} HDAC6 function can be seen as a bridge between UPS and the autophagy pathway. HDAC6 binds polyubiquitinated proteins through its ubiquitin-binding domain and delivering to the dynein motor. Polyubiquitinated proteins are then directed to the aggresome for the subsequent lysosome degradation.¹²⁹ Due to the rapid protein turnover cancer cells rely heavily on the protein degradation pathways and are more sensitive to proteasome inhibition than non-transformed cells.^{127, 130, 131} As mentioned in part 1.2.4 in 2015 the pan-HDAC-inhibitor panobinostat (Farydak®) was approved together with the proteasome inhibitor bortezomib (Velcade®).¹⁰⁰⁻¹⁰² Combination of proteasome inhibitors with an HDAC inhibitor case cytotoxicity by inhibiting the UPS and the aggresome pathway. Dual targeting of protein degradation pathways with the selective HDAC6 and bortezomib have been shown to be synergistic in lymphoma. The use of a HDAC6 selective HDAC inhibitor could be beneficial in comparison to pan-HDACi and several trials showed promising results.^{105, 132-134}

HDAC6 regulates the formation of chaperone complexes of Hsp90 client proteins.^{47, 135} The reduced chaperone activity results in polyubiquitination and proteasomal degradation of a number of cancer-related proteins, for example the epidermal growth factor receptor (EGFR).^{136, 135} By deacetylation of cortactin, an actin remodeling protein, HDAC6 plays a central role in cytoskeleton mediated processes.⁴⁵ HDAC6 modulates cell motility by altering the acetylation level of cortactin and overexpression of HDAC6 has been connected to invasive metastatic behavior of tumor cells.¹³⁷ HDAC6 inhibition could act protective and has been shown to result in impaired cell motility.⁴⁵

Taken together, HDAC6 is involved in regulation of several critical cellular functions linked to cancer. Generally, high levels of HDAC6 expression have been associated with tumor-genesis.^{138, 139} Elevated levels of HDAC6 were documented in myeloblastic cell lines, in acute myeloid leukemia blasts and in

some breast cancers.^{138, 140-142} However, in a different study HDAC6 expression in breast cancer was also associated with better survival and was higher in small tumors, low histologic grade, and in estrogen and progesterone receptor-positive tumors.⁷⁹ In oral squamous cell carcinoma significantly higher HDAC6 expression was found in carcinoma versus non-transformed cells. Additionally, in the same study HDAC6 expression was increased in advanced stage cancers compared with early stage.¹⁴⁰ HDAC6 has been shown to be required for oncogenic tumor formation and potential regulatory role of HDAC6 in the malignant transformation process was suggested.¹³⁸ Interestingly, after inactivation of HDAC6, resistance to oncogenic transformation and reduction of tumor cell growth was observed.¹³⁸ The deacetylase activity was required for HDAC6 to support malignant tumorigenic growth, pointing to a possible pharmacologic inhibition of HDAC6 enzymatic activity for antitumor effects.¹³⁸

1.3 HDACs in non-cancer human disorders

Due to the important role of HDAC enzymes in transcriptional regulation and beyond, an aberrant HDAC activity can lead to the development of several pathologies. A wide variety of conditions have been related to HDAC dysfunctions.

A large number of brain disorders are associated with imbalances in protein acetylation. Epigenetic phenomena and HDACs are involved in nervous system and psychiatric disorders.¹⁴³ HDACi have been investigated in several animal models of neurodegenerative diseases, including Huntington's disease, Alzheimer's disease, Parkinson's disease and spinal muscular atrophy.^{144, 145} For example, inhibition of HDAC3 was able to reduce the expression of Huntington's disease-associated genes and prevented Huntington's disease-associated eye neurodegeneration in a *Drosophila melanogaster* model.¹⁴⁶ In this study, HDAC1 and a pan-HDAC inhibition showed positive results in the Huntington's disease model. Isoform-specific inhibitors could be more efficacious, with less toxicity.¹⁴⁶ Especially selective inhibition of HDAC3 could be beneficial in neurodegenerative diseases.

Several studies revealed that HDACs are implicated in various aspects of the immune response, including the innate and adaptive system.¹⁴⁷ The adaptive immune response is subject to epigenetic regulation and HDACi have demonstrated preclinical efficacy in several rodent models of inflammatory conditions and in clinical samples taken from patients with an autoimmune disease.^{148, 149}

A link from HDAC activity to human cardiovascular disease is also emerging.¹⁵⁰ HDACs are fundamentally important in cardiac development and have the potential to regulate many aspects of cardiovascular diseases. HDACs regulate hypertrophy, fibrosis and inflammation.¹⁵¹⁻¹⁵³ Additionally, a role for HDACs in cardiomyopathy associated with metabolic diseases such as uncontrolled diabetes mellitus is also proposed.¹⁵⁴

Activation of latent hepatitis B virus and Epstein-Barr virus has been observed in patients with cancer following treatment with romidepsin.¹⁵⁵ According to these observations, HDACi recently have been suggested as an antiviral therapeutic strategy. Cells infected with integrated latent proviruses are able to evade the immune system and escape from a pharmacological attack. HIV production could be enhanced *in vitro* by either class I-selective or pan-HDACi, which could help to overcome the challenge of latent virus reservoirs. The reactivation of latent virus could be induced in infected cell lines and in resting CD4⁺T cells from patients receiving antiretroviral therapy.¹⁵⁶ Preclinical results were already reproduced in a clinical study in patients with latent HIV infection.¹⁵⁷

1.4 Parasitic approaches of HDACi

The need for new anti-parasitic drugs drives drug discovery research globally. HDACi are a promising class of new potential anti-parasitic agents.¹⁵⁸ The potential of HDACi as anti-parasitic agents was first observed when the cyclic tetrapeptide apicidin was found to have anti-parasitic activity.¹⁵⁹ Interestingly, some human parasites share characteristics with malignant tumors. Parasites are considered to be similar to tumors in the intense metabolic activity and a dependence on lactate fermentation as an energy source within the human host.^{160, 161} Moreover, parasites exhibit a high rate of cell division without the control of the host^{162, 163} and are almost invisible to the host's immune responses. Parasites like schistosomes achieve this by adsorbing host determinants onto their surface.¹⁶⁴ In case of *Plasmodium* parasites allelic variability in different clones is thought to enable an effective immune evasion.^{165, 166}

The discovery of suitable candidates for the therapy of tropical diseases can be based on several approaches. The *de novo* drug discovery and rational structure based design, phenotypic screening of chemical libraries or the so-called piggybacking of established drugs are common strategies.¹⁶⁷⁻¹⁶⁹ The piggyback approach is based on reusing chemical scaffolds, previously validated for other diseases.¹⁶⁸ Targeting protein acetylation is a starting point for identifying new anti-parasitic drugs. The potential to use HDACi as new anti-parasitic agents was reported several times.^{170, 171} Addressing epigenetic enzymes and especially the inhibition of HDACs have been shown to be a promising strategy for many parasites. HDACs are recognized as an anti-parasitic target in several major human parasitic pathogens; *Plasmodium*, *Toxoplasma*, *Trypanosoma*, *Schistosoma*, and *Lieshmania*.^{172, 173}

1.5 HDACs as novel target in malaria treatment

1.5.1 *Plasmodium* species and life cycle

Malaria is caused by protozoan parasites of the genus *Plasmodium*. The six malaria parasites species infecting humans are *Plasmodium falciparum*, *P. vivax*, *P. ovale* (two species),¹⁷⁴ *P. malariae* and *P. knowlesi*.¹⁷⁵ *P. falciparum* and *P. vivax* are mainly responsible for the burden of the malaria disease. *P. falciparum* is most prevalent on the African continent, it is the species most commonly associated with severe and complicated disease and causes the most deaths from malaria. *P. vivax* has a wide geographic distribution in Africa, Asia and South America. It can develop in the *Anopheles*

mosquito vector at lower temperatures and form the dormant liver stage known as hypnozoite. However, the risk of infection with *P. vivax* is low as *P. vivax* needs a certain protein to invade red blood cells. This protein is encoded by the Duffy gene, which is missing in most of the African population.¹⁷⁶

The main species that infect humans (*P. falciparum*, *P. vivax*, *P. malariae*, and *P. ovale*) and the rodent species used in various model systems, such as *P. berghei* and *P. yoelii* have comparable life cycles (Figure 5).

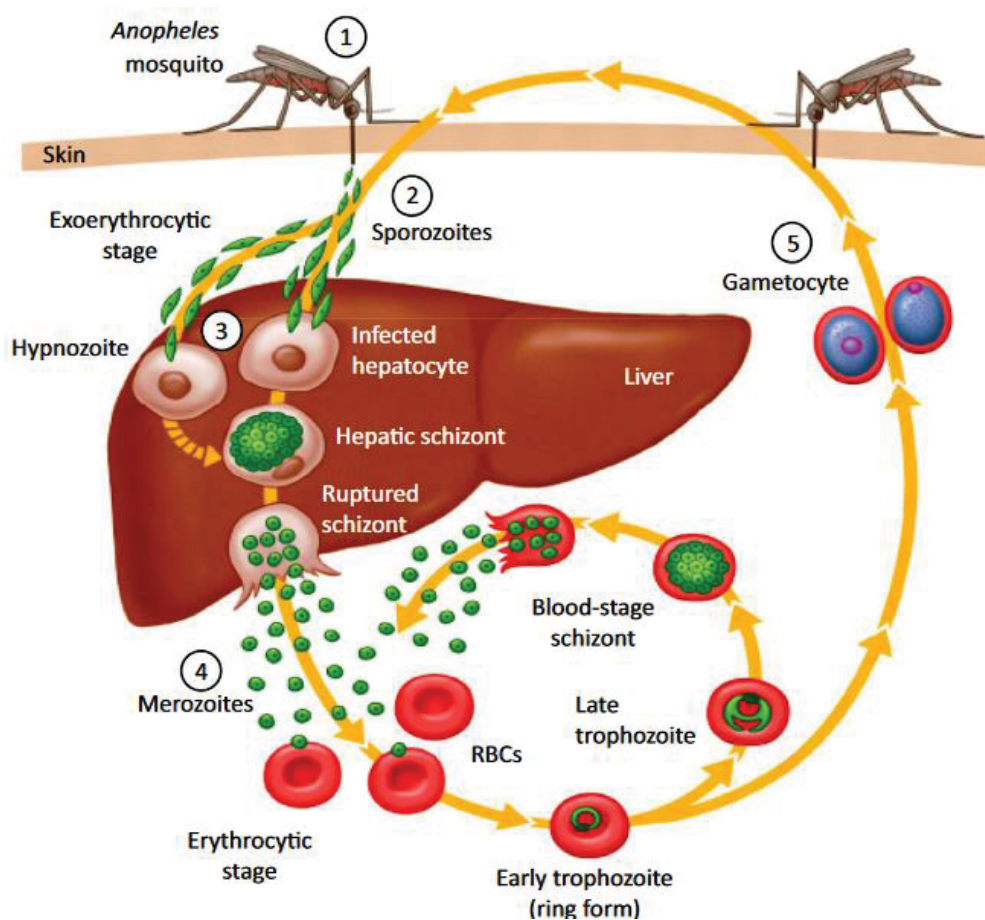


Figure 5. Life cycle of *Plasmodium* parasite. (1) Infection is precipitated by the bite of an *Anopheles* spp. mosquito. (2) Sporozoites enter the bloodstream. (3) In the liver, parasites undergo a replicative round within hepatic cells. The parasites then egress from the liver as merozoites and invade red blood cells. (4) Blood-stage parasites proceed through asexual replication. (5) Merozoites differentiate into male and female gametocytes. Picture from:¹⁷⁷

The life cycle of *P. falciparum* is extremely complex with multiple intracellular and extracellular stages of development in both the *Anopheline* mosquito vector and the human host. The infection of humans begins with the bite of an infected female *Anopheles* mosquito (1, Figure 5), causing the transfer of sporozoite-stage parasites. Sporozoites migrate to the liver (2, Figure 5), where they invade hepatocytes and mature to hepatic schizonts. This is followed by asexual replication of the parasite inside hepatocytes, forming thousands of merozoites per hepatocyte over a period of approximately two weeks. For malaria species *P. vivax* and *P. ovale* parasites can remain dormant in

the liver as hypnozoites (**3**, Figure 5) and cause relapses weeks to years after the primary infection. When merozoites are released into the circulation, each merozoite can infect an erythrocyte (**4**, Figure 5). The infection and subsequently following destruction of red blood cells leads to fever, anaemia, and cerebral malaria and even to death if not treated adequately. During the erythrocytic phase, the parasite metabolizes the host's hemoglobin to hemozoin, which is also called malaria pigment.¹⁷⁸ Within this stage the parasite replicates in erythrocytes by cell division (schizogony). During this asexual cycle, the parasite can commit to sexual development, differentiating into a male or female gametocyte.¹⁷⁹ The distinct morphology of gametocytes compared to the asexual blood stages is reflected in their unique pattern of gene expression.¹⁸⁰ Male and female gametocytes are the components of the malaria parasite life cycle which are taken up from an infected host bloodstream by mosquitoes and thus mediate disease transmission (**5**, Figure 5). The uptake of mature gametocytes by a feeding mosquito followed by the further development of the parasite in the mosquito midgut completes the *P. falciparum* life cycle.

1.5.2 Malaria as a public health challenge - disease and pathology

Malaria still represents one of the major health challenges mankind is facing today. The vector-borne tropical disease primarily affects the poorest and most vulnerable communities. Statistically, Africa suffered 92% of all malaria caused deaths in 2015, followed by South-East Asia with 6%.¹⁸¹ According to the World Health Organization Malaria Report 2016, there were approximately 212 million cases of malaria and 429 000 estimated deaths worldwide in 2015. The tropical disease is one of the reasons of poverty. African children under the age of 5 and pregnant woman carry the heaviest burden. Despite its high morbidity and mortality, as well as its social and economic impacts in malaria-endemic countries, for many years malaria was not of commercial priority for the pharmaceutical industry. However, the research efforts are growing. The decade-long scale up of vector control interventions, the introduction of rapid diagnostic tests and the availability of highly efficacious artemisinin-based combination therapy (ACT) led to a globally significant reduction of malaria cases.¹⁸²

The course of disease is determined by a combination of parasite-specific virulence factors like host inflammatory responses, age, and genetic disposition.^{183, 184} In areas with stable endemicity, year-round malaria transmission continually exposes and re-exposes the community to the bites of infected mosquitoes, resulting in a persisting low-level parasitemia and established immunity. Only the asexual replication cycle is responsible for symptomatic disease, the exoerythrocytic liver stages and sexual blood stages are not known to cause organ dysfunction.¹⁸⁵ Severe manifestations of malaria mainly affect infants and young children in highly endemic areas. Possible complications which are associated with the manifestation of malaria are severe anaemia caused by the destruction of red blood cells and cerebral malaria caused by obstruction of small vessels of the brain. The clinical outcome of the malaria disease ranges from nearly asymptomatic infection to death.^{184, 186}

1.5.3 Malaria prevention and treatment

1.5.3.1 Prevention

One of the most common and most affordable methods of malaria prevention are vector control strategies, for example the use of insecticide-treated mosquito nets.¹⁸⁷ Indoor residual spraying utilizing the insecticide dichlorodiphenyltrichloroethane (DDT) and improved sanitation eradicated malaria from many parts of the world. However, DDT is considered to be a human carcinogen and due to its massive side effects on environment and human health the use of this insecticide has almost been stopped.¹⁸⁸

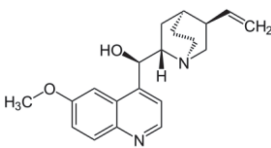
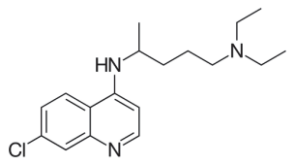
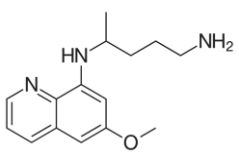
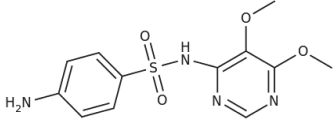
Today malaria remains to be endemic in tropical Africa and many parts of Asia. Some of the reasons are that eradication programs are often still difficult to implement, insufficient funding, inadequate health infrastructure as well as poverty and lack of education. In addition to that, development of insecticide resistance by the mosquito and drug resistance by the parasite have been documented.¹⁸⁹ Mosquitoes resistant to pesticides enhance the global health burden massively as personal protection measures and vector control strategies like indoor house spraying, personal repellents and other remain the most practical method for wide-scale malaria control.¹⁸⁹⁻¹⁹¹ In Africa, intermittent preventive therapy is advocated in some high-risk populations.^{192, 193} The objective of preventive chemotherapies is to prevent malarial illness by maintaining therapeutic drug levels in the blood throughout the period of greatest malarial risk.

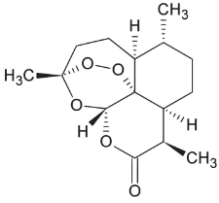
Numerous eradication programs and intensive research efforts focused on the development of a malaria vaccine.¹⁹⁴ A practical and effective vaccine that is suitable for immunization of people living in endemic areas is still not available.^{177, 189, 194, 195} The development of an effective prophylactic vaccine is highly challenging as the parasite has various sophisticated mechanisms to avoid the host immune system. During the various life-cycle stages, the parasite synthesizes an assortment of possible targets, which have been used for the development of vaccines. The recently developed vaccine RTS,S (Mosquirix™) showed disappointing preliminary results in Phase III trials. The efficacy of this vaccine was reported to be lower than 16.8% declining to 0% over 4 years.^{196, 197} However, efforts to develop other vaccines with increased efficacy are ongoing.¹⁹⁸ Since no malaria vaccine is yet available, antimalarial drug treatments and prophylaxis remain the most efficient strategies to control infections.

1.5.3.2 Antimalarial drugs

Antimalarial drugs remain to be fundamental for malaria prevention and treatment. However, no new antimalarial drug has reached the market in the past decades. The approved drugs are based on the following compound families: aryl amino alcohols (e.g. quinine, lumefantrine, mefloquine), antifolates (e.g. sulphadoxine and pyrimethamine), 4-aminoquinolines (e.g. chloroquine), 8-aminoquinolines (e.g. primaquine), and peroxides (artemisinin and its derivatives).

Table 2. Examples of main families of antimalarial drugs.

Drug family and example	Mechanism of action	Note
aryl aminoalcohols: e.g. quinine 	- Interfere with the haem digestion ¹⁹⁹	- Massive side effects - Clinical resistance to quinine occurs at low level - Mainly for treating severe malaria, often with antibiotics
quinoline derivatives: 4-aminoquinolines e.g. chloroquine 	- Block the polymerization of the toxic byproduct of haemoglobin degradation, haem, into insoluble and non-toxic pigment granules. ²⁰⁰	- Former first-line treatment for uncomplicated malaria - Massive resistances ²⁰¹⁻²⁰³
8-aminoquinolines e.g. primaquine 	- Primaquine eliminates liver-stage parasites, including dormant forms of <i>P. vivax</i> . ¹⁹⁹ - Mechanism is not exactly known	- Primaquine causes haemolysis in glucose-6-phosphate-dehydrogenase-deficient humans. ²⁰⁴
antifolates: e.g. sulfadoxine 	- Antifolates target two enzymes of the biosynthesis of tetrahydrofolate, the dihydropteroate synthase (DHPS) and dihydrofolate reductase (DHFR). ²⁰⁵	- Massive resistances ²⁰⁶
artemisinin derivatives: e.g. artesunate	-The peroxide lactone group of the sesquiterpene lactone endoperoxidases releases reactive oxygen species. ²⁰⁷	- Resistance in South East Asia and other regions ^{208, 209}

	<p>- The resulting free radical selectively binds to membrane proteins ultimately resulting in lysis of the parasite.²⁰⁷</p>	<p>- Fast-acting drug of Artemisinin-based Combination Therapies (ACTs), combined with a long-acting partner drug.</p>
-----------------------------------------------------------------------------------	-----------------------------------------------------------------------------------------------------------------------------------------	------------------------------------------------------------------------------------------------------------------------

The cinchona alkaloids, like quinine, are natural products extracted from the bark of *Cinchona* plants. Quinine was already used during the early 17th century to treat malaria and it was the first widely used antimalarial drug.¹⁹² In the late nineteenth century, synthetic derivatives of 8-aminoquinoline (e.g. primaquine, Table 3) and 4-aminoquinoline (e.g. chloroquine) have been developed. The mode of action of chloroquine is to block the polymerization of the toxic by-product of haemoglobin degradation, haem, into insoluble and non-toxic pigment granules.²⁰⁰ Chloroquine is a safe, and in absence of resistant parasites, highly effective in treatment of blood stages, and was the most important anti-malarial drug for decades. However, the way of treatment and prophylaxis has been changed by the worldwide spread of parasite drug-resistance, especially to chloroquine.^{202, 203} Nowadays almost all *P. falciparum* parasites are resistant to chloroquine. Primaquine's mechanism of action is not completely understood. It is known that primaquine severely disrupts the metabolic processes of plasmodial mitochondria.²¹⁰ Primaquine is the only drug effective against liver stages, including the dormant hypnozoite stages of *P. vivax* and *P. ovale*.²¹¹

Antifolates interfere with enzymes in the folate metabolism.²⁰⁵ This pathway is essential to malaria parasite survival and antifolates enable an effective causal prophylactic and therapeutic use. Some antifolates act synergistically when used in combination since they affect different steps of the pathway. The most common antifolate combinations consist of an inhibitor of dihydrofolate reductase (DHFR) combined with a dihydropteroate synthase (DHPS) inhibitor. The two components of combination (pyrimethamine, proguanil or dapsone as a DHFR and sulfalene or sulfadoxine as a DHPS inhibitor) act as synergists with each other, enhancing their activity and reducing the propensity for resistance development. However, resistances against this drugs have been reported.²¹²⁻²¹⁴ The development of antifolate agents for malaria therapy derived from attempts to treat leukaemia. Interestingly, antifolate drugs, also known as folate antagonists, restrain the production of folic acid. The folic acid deficiency hinders a rapid division of cells, making antifolates commonly used anti-cancer agents to treat various forms of cancer.^{215, 216}

The sesquiterpene lactone and endoperoxide artemisinin was isolated first in 1972 by chinese scientists from the leaves of the sweet wormwood *Artemisia annua*. In 2015 this discovery was awarded with the Nobel Prize in Medicine. The peroxide within the 1,2,4-trioxane system of artemisinins is essential for antimalarial activity. It is assumed that peroxides, generally reactive entities, act as prodrugs and generate reactive oxygen species (ROS). It was suggested that the

peroxide group of Artemisinin becomes unstable inside the parasite due to high iron concentrations and releases ROS. However, the mechanism of radical generation and of parasite death are still matters of debate.²¹⁷ High iron concentrations are also common in cancerous cells and artemisinin is undergoing early testing for the treatment of cancer.²¹⁸

Nowadays, an artemisinin combination therapy (ACT) is recommended by the World Health Organization (WHO) as the first-line treatment for *P. falciparum* malaria in all endemic regions. The excellent effectiveness and tolerability of ACTs brought new optimism into efforts to eliminate malaria. Artemisinin and its derivatives are potent, fast and act on all asexual blood stages (rings, trophozoites, and schizonts). The combination of an artemisinin derivative with a second antimalarial drug, usually with drugs with longer elimination half-lives and a different mode of action, has become the standard treatment.²¹⁹ Globally, the number of ACT treatment courses procured from manufacturers increased from 11 million in 2005 to 337 million in 2014.¹⁸² However, the use of ACTs in poorer regions is limited by their high costs of ACTs and cases of artemisinin resistance have been reported for many years.^{209, 220-223}

1.5.4 Drug resistances and the search for new generation drugs

Current drugs are often limited by low efficacy, side effect issues, and high costs. Growing insecticide resistances and spread of parasite resistances to the available drugs are two reasons for growing concern. Malaria caused by *P. vivax* is generally still treatable with chloroquine. However, chloroquine-resistance is now widely disseminated throughout malaria-endemic regions.^{201, 222, 224} The emergence and spread of chloroquine-resistant *P. falciparum*, the most lethal form of human malaria, are major obstacles in the control of the disease. Similar concerns have been raised about artemisinin resistance.^{209, 220} The combination of drugs with different mechanisms of action is one way to address the problem of drug resistances.¹⁸⁵ Monotherapies have been replaced with a combination of two drugs employing different modes of action.

Desirable properties for the next generation of anti-parasitic and especially anti-malaria drugs have been discussed extensively.^{201, 225, 226} The target product profile (TPP) of the new anti-malarial drugs should include high potency and selectivity for the parasite, suitability for mass administration, a high barrier for resistances, and appropriate pharmacokinetic properties. In addition, new drugs/drug combinations also need to be affordable, as they are mainly needed in the poorest countries. A high efficacy against drug resistant parasites and an excellent safety profile are required as the two groups at most risk of malaria are children and pregnant women.²²⁵⁻²²⁹

In the past, the focus of malaria research has been set on the *P. falciparum* species and drugs against the blood stages of the parasite, which is justified by the need of treatment and prevention of the disease.²²⁸ To achieve eradication of malaria, drugs active against all *Plasmodium* stages would be preferable.^{225, 230} Only one drug (primaquine, Table 3) completely eliminates *P. vivax* and *P. ovale*

hypnozoites and thus provides a radical cure.^c However, primaquine requires repeated dosing²³¹ and is toxic to individuals with glucose-6-phosphate dehydrogenase deficiency, which is a common condition in malaria-endemic regions.²⁰⁴

To stop relapse, *Plasmodium* liver stages need to be targeted.^{226,232} If infection can be blocked at this stage, there will be no pathology. Moreover, the low number of dormant hypnozoites substantially reduces the likelihood of the selection of drug-resistant parasites.^{233,234} The development of drugs with liver stage activity suffers from the highly complex biology of *Plasmodium* species. Recent studies revealed a high number of genes and proteins that are expressed only during the liver stage.²³⁵⁻²³⁷ There are several challenges on the way to true causal prophylactic drugs,²³⁸ among them the eminent technical difficulties in studying *Plasmodium* species liver stages.

In order to limit parasite transmissions to the mosquito, it is necessary to target the gametocytes of the malaria parasite.^{239,240} The number and infectivity of *P. falciparum* gametocytes depend on the drug and its efficacy.²⁴¹ Some anti-malarial drugs act not only against symptomatic asexual erythrocytic parasites but also indirectly on gametocytes by inducing an increase in gametocytogenesis, which leads to a potential increase in transmission.^{240, 241} Therefore, drug performances also need to be evaluated for the ability to limit transmission.^{239, 240}

The global aim of the research community must become the eradication of malaria. This will ultimately require an integrated strategy that includes new and old drugs, vaccines, vector control strategies and public health measures.

1.5.5 Anti-malarial activity of HDACi - PfHDACs as novel target

The development of *Plasmodium* parasites through the different stages of its life cycle is driven by the epigenetic control of the gene expression.^{242, 243} The protection from the host's immune response by means of genetic variation is of central importance for the pathogenesis of the parasite.^{165, 166} Switching gene expression, controlled by dynamic chromatin changes, is an example of the excellent adaptation of parasites to survive in the human host and its dependency on epigenetic mechanisms. Multiple drug resistance has necessitated new efforts in the search for new drugs, which operate by novel mechanisms of action. The epigenetic regulation is therefore an interesting target for anti-parasitic agents.^{244,245,246}

HDACs are important regulators of transcription in *P. falciparum* and the inhibition of PfHDACs is a possible mechanism to target the parasite.^{171, 247-251} Pan-inhibitors of human HDACs, such as vorinostat (SAHA) and trichostatin A (TSA) cause hyperacetylation of *P. falciparum* histones and have potent antimalarial activity *in vitro*. Five HDAC encoding genes have been annotated in the genome of *P. falciparum*. Three of these genes encode proteins with homology to human class I and II HDACs,

^c Radical cure: complete elimination of all forms of the *Plasmodium* parasite from the human host, including hypnozoites.

two further genes encode NAD⁺ dependent class III homologues. The class I homologue *PfHDAC1* is localized in the parasite nucleus and transcribed across the *P. falciparum* life cycle. It is involved in the post-translational modification of histone and non-histone *Plasmodium* proteins.^{172, 228, 252} *PfHDAC1* is the only available recombinant *PfHDAC* enzyme.²⁵² This isoform has the most similarity to HDACs of other species, with 61% sequence identity compared to the human orthologue human HDAC1 and 62% to human HDAC2. Unfortunately the high sequence identity of *PfHDAC1* hinders the development of parasite-selective HDACi.

Less is known about the class II *PfHDAC* homologues *PfHDAC2* and *PfHDAC3*.²⁴³ Contrary to *PfHDAC1*, the structures of *PfHDAC2* and *PfHDAC3* are unknown. The class II HDAC enzymes have less sequence conservation with their human orthologues than *PfHDAC1*. Both are predicted to be high molecular weight proteins and a knock-down of *PfHDAC3* inhibits asexual-stage growth and development.²⁴³ *PfHDAC2* and 3 lack any homology outside the HDAC core²⁴³ and share less than 14% amino acid identity to each other. Interestingly, they also have limited homology to HDACs class II of other species.²⁴³ The lack of recombinant *PfHDAC2* and 3 as well as the lack of all *PfHDACs* crystal structures significantly complicates the rational design of anti-malarial HDACi targeting this isoforms.

The inhibition of human HDAC1 is highly correlated with toxicity.^{42, 253, 254} Therefore HDACi with low activity against human class I enzymes and in particular against human HDAC1 and 2 are suitable starting points for the development of anti-*Plasmodial* HDACi. Homology models of *PfHDAC1* have predicted that the active site of *PfHDAC1* is highly conserved with that of human HDACs. However, the predicted structures also display differences at the entrance of the active site and foot pocket.²⁵⁵ The problem of strong structure similarities between *PfHDAC1*, as predicted, and human HDACs is a difficulty, which is pronounced for many parasitic epigenetic targets.²⁵⁶

The activity of several anti-tumor HDACi has been profiled against *Plasmodium* parasites and most of the compounds do not exhibit selectivity for the parasite versus human cells.¹⁵⁸ However, some HDACi compounds, such as WR301801 and SB939, showed significantly higher *in vitro* selectivity for asexual intraerythrocytic stage parasites than for mammalian cells (Figure 6).^{170, 171}

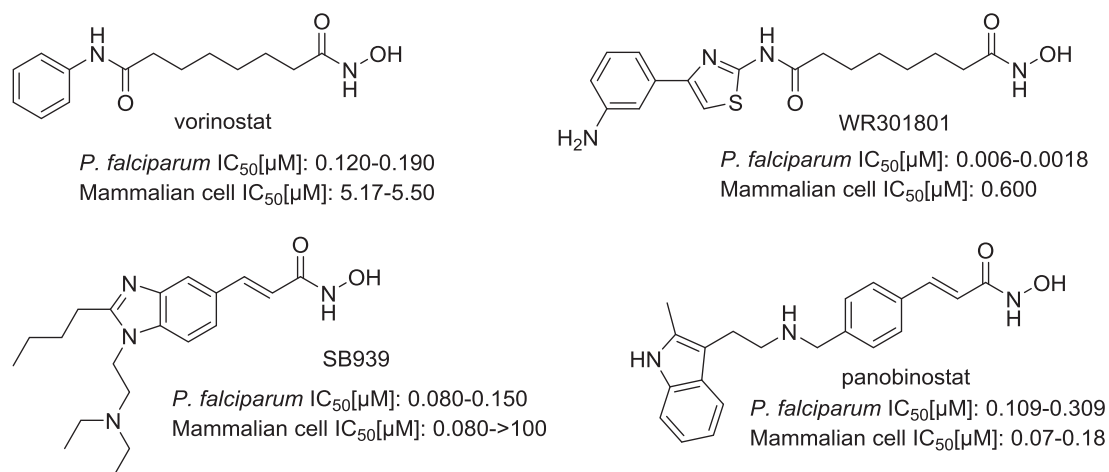


Figure 6. Chemical structures of HDACi, their *in vitro* activity against asexual blood stages of *P. falciparum* and cytotoxicity against mammalian cells.^{158, 170, 171}

Most anti-plasmodial HDACi show significant cytotoxicity against mammalian cells.^{170, 171} Undesired toxicity of HDACi in the human host remains to be a challenge using this new mechanism of action. In terms of *in vivo* efficacy promising results have been described already in mouse malaria models. SB939 and WR301801 (Figure 6) are two of the most promising anti-plasmodial HDACi. In a murine model of cerebral malaria SB939 was able to prevent the development of cerebral malaria-like symptoms when administered orally to *P. berghei* ANKA-infected mice.¹⁷⁰ In case of WR301801 the study outcome was dependent on the routes of delivery of the compound. When administered by intraperitoneal injection WR301801 was able to cure mice.²⁵⁷ However, this compound failed to effect a cure in *P. berghei* infected mice when given in oral administration.¹⁷¹

1.6 HDAC as novel target in schistosomiasis treatment

1.6.1 Schistosomiasis as a public health challenge

Bilharzia, or schistosomiasis, is caused by the trematode flatworm species *Schistosoma*. It is one of the major neglected human tropical diseases.^{258, 259} The main human disease-causing species are *Schistosoma mansoni*, *Schistosoma haematobium*, and *Schistosoma japonicum*, each with different intermediate snail host and distribution.^{259, 260} According to WHO statistics schistosomes cause at least 300,000 deaths yearly and infect around 230 million people worldwide.²⁶¹ Under risk are individuals having contact with contaminated freshwater sources and specially children under the age of 14.²⁶² The number of deaths due to schistosomiasis is difficult to estimate because of hidden pathologies such as liver, kidney failure and bladder cancer. The disease is prevalent in at least 78 countries and the health impact has been estimated to be near to that of malaria, HIV/AIDS and tuberculosis.²⁶¹ A majority of its burden occurs in Africa, where *S. haematobium* and *S. mansoni* are endemic, especially in poor communities without access to safe drinking water and adequate sanitation.²⁶³

Larvae of the endoparasite *Schistosoma* penetrate the skin and develop into male and female worms which pair up and live together in the blood vessels for years. Female worms mated with males produce hundreds of eggs which are passed out of the body in the urine or faeces. Others remain trapped in the body and cause damage to internal organs. Although mortality attributable to schistosomiasis is relatively low, morbidity can be severe and long lasting.²⁶³⁻²⁶⁵

The complexity of the *Schistosoma* species is reflected in a large genome and transcriptome.²⁶⁶ The life-cycle includes radical morphological modifications and exhibits diverse phenotypes. There are two major forms of schistosomiasis - intestinal and urogenital.^{263, 267} In intestinal schistosomiasis, there is a progressive enlargement of the liver and spleen, intestinal damage, and hypertension of the abdominal blood vessels.²⁶⁴ In urinary schistosomiasis, the clinical picture shows progressive damage to the bladder, urethra and kidneys.²⁶⁷ Chronic disease contribute to major organ damage, so reducing the severity of symptoms is critical to the management of schistosomiasis.

1.6.2 The need for new drugs for schistosomiasis

Schistosomiasis is among the neglected parasitic diseases with a very limited number of drugs available for treatment.^{264, 268} No effective vaccines have yet been developed and there is currently no indication that a vaccine is likely to become available any time soon.²⁶⁹

Since praziquantel (PZQ) was introduced for treatment of schistosomiasis it has been widely used in schistosome-endemic areas for more than 30 years and remains to be the drug of choice till now.²⁶⁸ PZQ has replaced other anti-schistosomal drugs becoming the only drug of choice, which makes the search for alternative chemotherapeutic urgent. PZQ is considered to be safe, effective and relatively cheap. Given one single oral dose of 40 mg/kg it has an overall cure rate of 60-90% in individuals living in areas endemic for infection (defined by clearance of eggs from urine or stools).²⁵⁸ The application of PZQ is limited to adult worms, which has been shown in *in vitro* tests and has been confirmed by clinical data.^{270, 271} While the global use of PZQ is scaling up, PZQ does not prevent re-infection and its mechanism of action is not identified.²⁷²

The WHO strategy for schistosomiasis control focuses on periodic, large-scale treatment with PZQ (preventive chemotherapy) of affected populations. There is also a growing concern about reports from patients not cured by multiple doses.^{271, 273, 274} Mass treatment with a single drug increase the likelihood of the development of drug-resistant parasite strains. The development of resistance and the selection of resistant isolates that are stably resistant in the absence of drug pressure have been confirmed in the laboratory.^{272, 275-277} Besides these observations, resistant populations have already been characterized in endemic areas²⁷⁰ and the selection of field strains of schistosome that are resistant to PZQ is more and more likely.

1.6.3 Anti-schistosomal activity of HDACi - *SmHDACs* as novel target

Schistosomes are endoparasites which possess a large genome and utilize epigenetic tools and mechanisms to control their complex lifestyle.²⁷⁸ The parasite has a dynamic epigenetic machinery that is necessary for the extensive phenotypic changes during the life cycle. In the *S. mansoni* genome several HDACs are encoded.^{279, 280} Treatment of schistosomes with HDACi caused an overall increase of protein acetylation and dose-dependent mortality of schistomula and adult worms.²⁸⁰⁻²⁸² HDACi caused accumulation of acetylated cellular proteins, more particularly of histone H4 and, to a lesser extent, H3 and induced a programmed cell death pathway in schistosomes.²⁸⁰ While the exact mechanisms are not understood yet, the effector caspases 3/7 seem to play an essential role.^{280, 282} There is also evidence that HDACi treatment affects metamorphosis of *Schistosoma* parasites and blocks transformation of *S. mansoni* larvae from the free-swimming miracidia into the intramolluskal sporocyst.²⁷⁹ Taken together, HDACi treatment of schistosomes can lead to chromatin remodeling, modified regulation of gene expression and induced programmed cell death, which could explain the susceptibility of the parasite.

Recent studies highlighted *SmHDAC8* as a promising therapeutic target for the treatment of schistosomiasis.^{256, 283, 284} Interestingly, in contrast to the nuclear localization of the human HDAC8 orthologue, the predicted subcellular localization of *SmHDAC8* is cytosolic.²⁸² The HDACi trichostatin A, vorinostat and valproic acid inhibited *SmHDAC8* activity at all life cycle stages.^{280, 281} Bioinformatic genome analyses revealed six Zn²⁺-utilizing HDACs in *S. mansoni*,^{281, 285} three of them are orthologues of class I HDACs, namely *SmHDAC1*, 3, and 8. As the human HDAC2 is the outcome of a vertebrate-specific duplication of the *HDAC1* gene²⁸⁶, no human HDAC2 orthologue was identified in schistosome genomes. *SmHDAC1* and *SmHDAC3* are highly conserved compared with the human orthologues, while *SmHDAC8* contains several insertions in the protein sequence. *SmHDAC4*, 5, and 6 have not been functionally characterized yet and represent class II HDACs.^{278, 285} Homologous genes for the remaining human class II isoforms HDACs 7, 9, and 10 and the single class IV member HDAC11 are not present in schistosomes. In addition to the Zn²⁺-dependent HDACs, five NAD⁺-dependent sirtuins have been identified in the *S. mansoni* genome. According to phylogenetic analysis they can be described as orthologues of mammalian Sirt1,2, 5, 6, and 7.²⁸⁷

Only *S. mansoni* class I HDACs (*SmHDAC1*, *SmHDAC3*, and *SmHDAC8*) have been cloned and characterized so far.²⁸¹ All three class I *SmHDACs* are expressed at all life-cycle stages, with *SmHDAC8* transcripts always being observed as the most abundant isoform.²⁸⁰ In contrast, human HDAC8 shows the lowest level of expression of the four class I HDACs in human.²⁸⁸ Compared to the orthologue HDAC8 enzymes of other organisms, *SmHDAC8* contains a significant number of alterations. Sequence alignment showed that the essential residues for HDAC activity are conserved, but the whole protein sequence contains six extensions of between 4 and 17 amino acids. These insertions are located outside the active site, probably not influencing the catalytic mechanism and

are not present in any other known HDAC8 family member.^{281, 289} *S. mansoni* HDAC8 has only one single active site amino acid substitution compared with human HDAC8. A methionine (Met 274) in human HDAC8 is substituted to a histidine (His 292) in *Sm*HDAC8 pocket, that accommodates the aliphatic part of the substrate or inhibitor. The presence of a polar residue replacing a hydrophobic one reduces the hydrophobic character of the active site of *Sm*HDAC8. This exchange could be a key feature to design *Sm*HDAC8-specific inhibitors.^{283, 284, 290} Furthermore, X-Ray analysis revealed that the *Sm*HDAC8 contains amino acid substitutions around the catalytic pocket which allow a change in the configuration of the side chain of a phenylalanine (Phe 151). In the schistosomal enzyme the Phe 151 side chain is free to adopt a flipped-out configuration, allowing the pocket to accommodate bigger substrates or inhibitors.²⁸⁴ All these make *Sm*HDAC8 a promising target for the development of new, schistosome-specific drugs.

2 Aims of the thesis

The objective of this work was the development and synthesis of anti-cancer and anti-parasitic HDACi.

The goal of the first project was the synthesis of alkoxyurea-based HDACi with antiproliferative and chemosensitising properties. Currently it is under discussion if isoform-selective HDACi could be beneficial for a more effective chemotherapy compared to pan-inhibitors, enabling a more precise therapeutic use and fewer side effects.²⁹¹ The model that HDACi act only by influencing gene transcription is oversimplified and non-genomic functions regulated by HDACs are important in oncogenesis as well.^{137, 138} Starting from the prototype-compound LMK214 we reasoned that the modification of the cap should lead to a novel type of HDACi with HDAC6 preference (Figure 7). We planned to synthesize an alkoxyurea-based HDACi library and to evaluate the antiproliferative and chemosensitising properties of the compounds in the working group of Prof. Dr. Kassack. Further biological characterization of the novel compounds and docking studies were intended to be performed by additional cooperation partners.

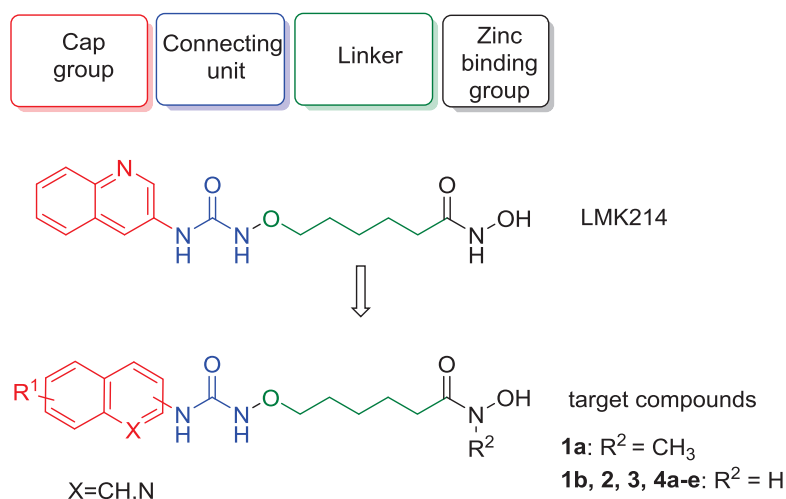


Figure 7. Alkoxyurea-based HDACi: strategy and target compounds.

The aim of the second part of the thesis was the development of anti-parasitic HDACi using the piggyback approach.¹⁶⁸

In cooperation with the working group of Prof. Dr. Katherine Andrews we planned to screen our diversity orientated Kurz-group HDACi-library to find suitable anti-plasmodial lead structures. The design of the anti-plasmodial HDACi was guided by several aimed properties of the target compounds. The inhibition of human HDAC1 is highly correlated with toxicity.^{42, 254, 292, 293} Toxic side effects of class I HDACi and other broad spectrum HDACi hinder the application of class I-selective

HDACi in areas outside of oncology.²⁵³ We hypothesized that HDACi with low activity against human class I enzymes and in particular against HDAC1 are more likely to be suitable starting points for the development of anti-plasmodial HDACi with high parasite-selectivity. To evaluate the anti-plasmodial activity, the compounds were intended to be assessed against the asexual blood stages of the *P. falciparum* 3D7 strain and the multidrug-resistant Dd2 strain. This work was planned to be done by me in the Tropical Parasitology Lab of the Griffith Institute for Drug Discovery, in cooperation with Prof. Dr. Kathy Andrews. To determine the parasite selectivity, the cytotoxicity of the compounds against human cell lines was planned to be evaluated. Additionally we planned to verify the mode of action and the *in vitro* activity against early-stage and late stage *P. falciparum* gametocytes and *P. berghei* exo-erythrocytic stages.

In initial studies a dose- and time dependent mortality of schistosomula could be induced by HDACi.^{256, 280, 284} It was suggested that the structural divergence of *SmHDAC8* and the abundance of its transcript make it a promising target for drug development.²⁸¹ *SmHDAC8* is phylogenetically distant from its orthologues. Interestingly, *SmHDAC8* mRNAs are expressed at all schistosome life-cycle stages at higher levels than *SmHDAC1* and 3, while human HDAC8 shows the lowest level of expression of the human class I HDACs.^{281, 288} One goal of this thesis was the development of anti-schistosomal HDACi, targeting *SmHDAC8*. In cooperation with Prof. Dr. Jung we intended to start our work with a screening of our Kurz-group HDACi-library to identify suitable *SmHDAC8* inhibiting lead structures.

3 Publication I

Alkoxyurea-based Histone Deacetylase Inhibitors Increase Cisplatin Potency in Chemoresistant Cancer Cell Lines

K. Stenzel (40%)[#], A. Hamacher[#], F. K. Hansen, C. G. W. Gertzen, J. Senger, V. Marquardt, L. Marek, M. Marek, C. Romier, M. Remke, M. Jung, H. Gohlke, M.U. Kassack^Δ, T. Kurz^Δ

J. Med. Chem. 2017, 60, 5334 – 5348 (DOI: 10.1021/acs.jmedchem.6b01538)

Contributions to this project:

- Synthesis of all precursors and target compounds (but not the prototype compounds **1a** and **1b**, Figure 8), analysis of all novel chemical structures and target compounds
- Collection of data, analysis and interpretation of data, participation in writing of the manuscript, review and revision of the manuscript

3.1 Project background

Today HDAC6 is widely discussed as a therapeutic target for epigenetic drug discovery. HDAC6 does not catalyze histone deacetylation *in vivo*^{48, 49} and stands out from other members of the HDAC family in almost exclusively deacetylating cytoplasmic proteins. HDAC6 is involved in the regulation of several critical cellular functions linked to cancer, the best-studied is the role in the removal of misfolded proteins.^{127, 128} Additionally, functions in oncogenic tumorigenesis and correlation between HDAC6 expression and tumor aggressiveness have been described.^{138, 294} These studies are pointing to HDAC6 as a possible target in cancer treatment. Therefore HDAC6 provides a strategy in treating disease without affecting DNA modification. However, highly selective HDAC6 compounds generated only weak cytotoxic and antiproliferative activity in several tumor cells^{293, 295} and additional HDAC class I activity could be beneficial. Ricolinostat has been examined as monotherapy and in combination^d in a phase II study in multiple myeloma and lymphoma. This HDAC6 preferential inhibitor has 10 to 20-fold lower potency for class I HDACs 1, 2, and 3. This compound showed promising study results and it is expected that ricolinostat can be dosed more frequently with better tolerability than the approved pan-HDAC inhibitor panobinostat^{133, 296, 292}

Clinical application of standard chemotherapy drugs is often associated with resistance and toxicity, posing urgent demand for combination therapy. A promising strategy to increase the efficacy of chemotherapy drugs is the combination treatment with low doses of HDACi.²⁹⁷ It is increasingly

^d Combination with bortezomib (proteasome inhibitor, Velcade[®]) and dexamethasone (used to treat many inflammatory and autoimmune conditions, often given to counteract certain side effects of their antitumor treatments)

recognized that the combination of HDACi with drugs such as platinum compounds (e.g. cisplatin) provides synergistic effects in the treatment of haematological and solid tumors, probably through HDACi-generated increased accessibility of DNA.^{108-111, 298}

3.2 Project overview and results

HDAC6 selective inhibitors often contain bulky or branched cap groups due to the fact that HDAC6 possesses a significantly wider channel rim compared to other HDAC isoforms.^{134, 299} The lead structure LMK214 (Figure 7) of the novel compound library showed potent inhibition of HDAC6 (IC_{50} 52 nM) and HDAC1 (IC_{50} 189 nM), low activity against HDAC8 (IC_{50} >10 μ M) and no inhibition of HDAC4 up to a concentration of 10 μ M. Due to these preliminary results we performed a docking study in order to understand the selectivity profile of compound LMK214. Based on the results a series of analogues as potential HDAC6 inhibitors were designed and synthesized, focusing our structural modifications on the cap group.

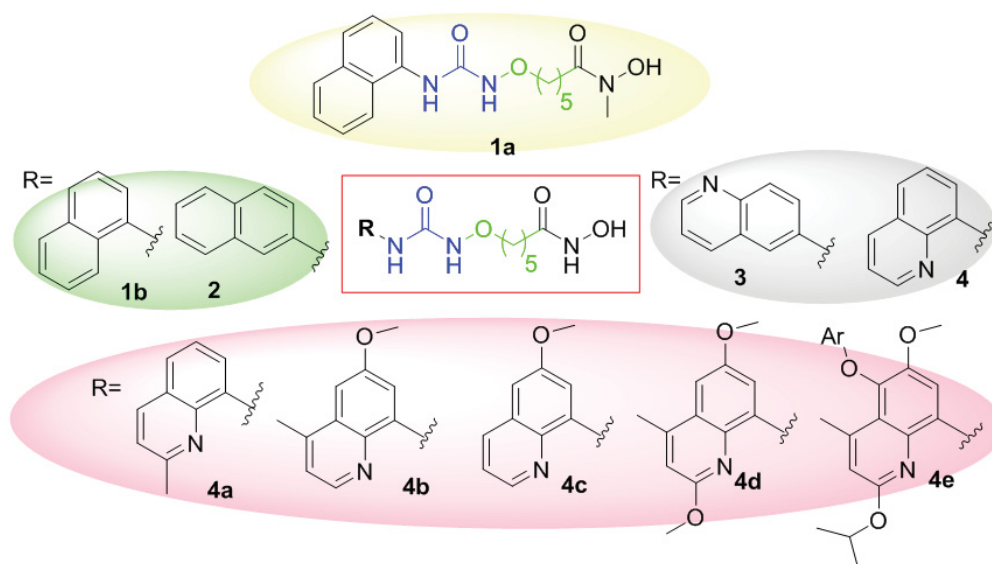
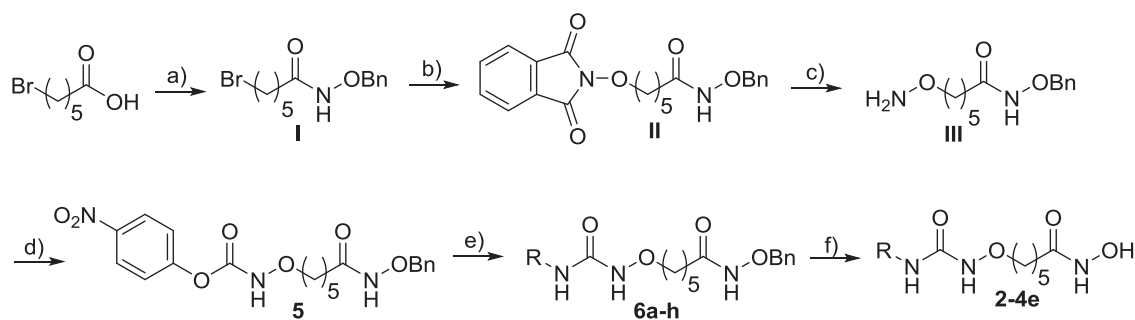


Figure 8. Target compounds of this study. Ar = 3-(trifluoromethyl)benzyl

The synthesized novel alkoxyurea-based HDACi are characterized by a substituted quinoline or naphthyl cap group and an alkoxyurea connecting unit linker region. The intended HDACi **2-4e** (Figure 8) were prepared according to a novel and straightforward microwave-assisted synthetic protocol allowing the systematic variation of the cap moiety (Scheme 1).



Scheme 1. Synthesis of alkoxyurea-based HDACi **2-4e**. R: defined in Figure 8. Reagents and conditions: (a) Isobutyl chloroformate, NMM, benzyloxylamine, THF, 3 h; (b) Et₃N, hydroxyphthalimide, CH₃CN, reflux, 5 h; (c) Methylhydrazine, CH₂Cl₂, -10 °C, 3 h; (d) Pyridine, ClCO₂C₆H₄NO₂, CH₂Cl₂, RT, THF, 3 h; (e) R-NH₂, Et₃N, THF, MW, 100 W, 70 °C, 0.5 h; (f) Pd/C, H₂ (1 bar), MeOH, RT, 3 h.

The activation of the aminoxy group of compound **III** was performed using 4-nitrophenyl chloroformate to obtain the 4-nitrophenyl carbamate **5**. Attempts to introduce the alkoxyurea moiety using 1,1'-carbonyldiimidazole (CDI)- or 1,1'-carbonylditriazole (CDT)-mediated coupling protocols did not provide the targeted asymmetrical alkoxyureas **6a-h** at all or only in a low yield. In an optimized protocol we utilized microwave heating in order to improve reaction times and yields (Scheme 1, yields 83-91%). In the last step a catalytic hydrogenation provided the alkoxyurea-based HDACi **2-4e** in 54-72% yield (Scheme 1).

The biological evaluation of the target compounds included MTT cytotoxicity assays³⁰⁰ and cellular HDAC assays using the cell-permeable substrate Boc-Lys(ε-Ac)-AMC. Upon deacetylation by cellular HDACs (all but class IIa) the substrate is cleavable by trypsin, releasing the fluorescent coumarin derivative.^{301, 302} For assessment of the antiproliferative activity the tumor cell lines Cal27 (human tongue squamous carcinoma cell line) and A2780 (human ovarian carcinoma cell line) as well as their cisplatin resistant sublines were used.^{303, 304} Some of the compounds showed similar or improved effects compared to vorinostat in the whole-cell HDAC assay but significantly enhanced cytotoxic effects against the human cell line Cal27 and its cisplatin resistant subline Cal27 CisR.

The HDAC6 inhibitory activity of compounds **4b-d** was further validated by investigation of the acetylation status of α-tubulin and H3 histone. Incubation of Cal27 and Cal27 CisR cells with **4b-d** resulted in a hyperacetylation of H3 histone and α-tubulin, confirming the inhibition of HDAC6 in a more complex cellular environment.²² Based on their antiproliferative effects and HDAC inhibition, the three most potent compounds were selected for isoform profiling against human HDAC1, HDAC4, HDAC6, and HDAC8. In particular compound **4d** demonstrated strong inhibition of HDAC6 (IC₅₀ 2.8 nM), selectivity over HDAC8 (SI: 550) and HDAC4 (SI >3500), and moderate preference over HDAC1 (SI: 15).

The HDAC isoform profiling confirmed the results of our docking study. HDAC6 inhibitory activity of **4d** was 2-9-fold higher than of **4b** and **4c** and even 19-fold higher in comparison to the lead structure LMK214. In HDAC4 no docking configuration of our compounds could be identified. Thus, decoration of the quinoline moiety with small hydrophobic groups did result in improved binding affinities as hypothesized from the initial docking studies.

In the next step we studied the effect of pretreatment with the three most active compounds **4b-d** 48 h prior to cisplatin in the cell lines Cal27 and Cal27 CisR. The drug combination studies with cisplatin showed for all three selected compounds a markedly enhancement of cisplatin-induced cytotoxicity and a synergistic anti-tumor effect with combination indices (CI) below 0.9. In particular compound **4d** showed a 11.2 fold enhancement of cisplatin sensitivity in the cisplatin resistant subline Cal27 CisR.

4 Publication II

Design and Synthesis of Terephthalic acid-based Histone Deacetylase Inhibitors with Dual Stage anti-*Plasmodial* Activity

K. Stenzel (70%), M. J. Chua, S. Duffy, J. Antonova, S. Meister, A. Hamacher, M. U. Kassack, E. Winzeler, V. M. Avery, T. Kurz, K. T. Andrews^Δ, F. K. Hansen^Δ

ChemMedChem 2017, 12, 1627 – 1636 (DOI: 10.1002/cmdc.201700360)

Contributions to this project:

- Synthesis of all precursors and target compounds, analysis of all novel chemical structures and target compounds
- *P. falciparum* *in vitro* growth inhibition assays (³H-hypoxanthine based assay against 3D7 and Dd2 *P. falciparum* parasite strains), initial mode of action studies and initial mammalian cell toxicity assays
- *In vitro* human HDAC assay
- Collection of data, analysis and interpretation of data, participation in writing of the manuscript

4.1 Project background

The global agenda is striving for elimination and ultimately eradication of malaria disease.^{226, 227, 305} Generally anti-malarial compounds with a new mechanism of action are preferable.²²⁵ HDACs have been shown to be important regulators of transcription in *P. falciparum* and the inhibition of PfHDACs is a possible mechanism to kill the parasite.^{171, 247-250} However, undesired toxicity of HDACi in the human host remains to be a major challenge on the way to safe anti-malarial drugs using this new mechanism of action. Development of new drug candidates that are not only active against asexual intra-erythrocytic stage malaria parasites is necessary. Drugs with activity against liver and sexual gametocyte stage parasites are needed to enable prophylaxis and interruption of transmission.^{226, 227} Previous results suggest that it may be possible to develop HDACi that target multiple malaria parasite life cycle stages.²⁴⁹ High cytotoxicity can be considered as a general problem for the first generation of anti-malarial HDACi. Thus, next generation anti-malarial HDACi should possess lower cytotoxicity against mammalian cells while at least retaining or improving the anti-plasmodial activity.

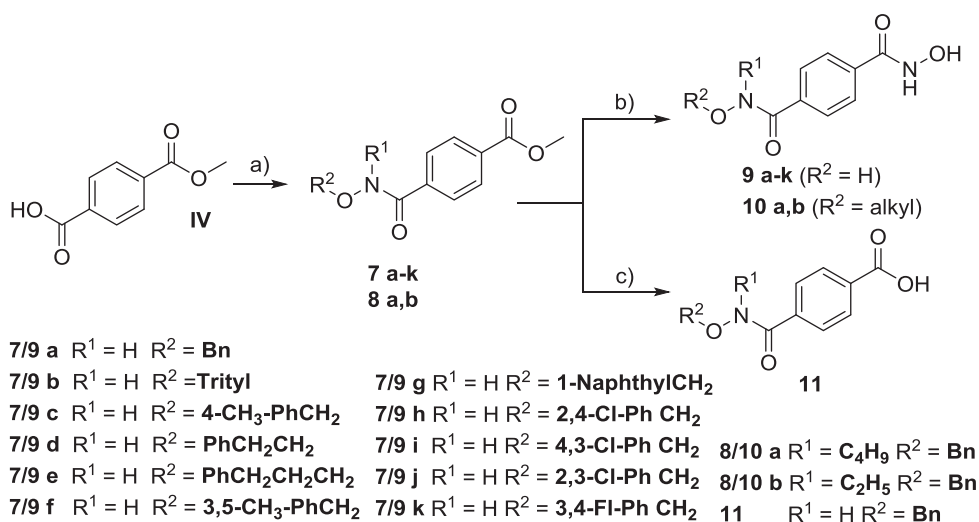
In our previous study a mini-library of HDACi was constructed using a straightforward solid-phase supported synthesis. Several compounds from this set displayed potent *in vitro* activity against asexual stages and in addition some of the HDACi showed nanomolar activity against all three life cycle stages tested (asexual blood stages, exo-erythrocytic stages and gametocyte stages). Compared

to the reference compound vorinostat the parasite selectivity was increased, but unfortunately, most compounds from this series showed significant cytotoxicity against mammalian cells resulting in only moderate parasite selectivity.²⁴⁹

Recent publications implies that highly selective human HDAC6 are weak in antiproliferative activity.²⁹³ Generally, the inhibition of human HDAC1 is highly correlated with toxicity.^{42, 254, 293} We hypothesized that HDACi with low activity against human class I HDAC enzymes and in particular against human HDAC1 are more likely to be suitable starting points for the development of anti-plasmodial HDACi with high parasite-selectivity.

4.2 Project overview and results

HDAC6-preferential and selective HDACi often contain a sp^2 -hybridized carbon atom in α -position related to the ZBG, bulky or branched cap groups and a hydroxamic acid group as ZBG.^{306, 307} In this work we investigated the anti-plasmodial activity of a series of hydroxamate-based HDACi containing an terephthalic acid alkoxyamide-based connecting unit linker region. The compounds **9a-k** were synthesized using a simple two-step protocol starting from the *O*-substituted hydroxylamine derivatives and mono-methyl terephthalate **IV** (Scheme 2). The *N*-alkylated intermediates **8a** and **8b** were prepared by a reaction of **IV** with *N,O*-disubstituted hydroxylamines furnishing the desired alkoxyamides. Finally, a hydroxylaminolysis provided the target compounds **9a-k** and **10a,b**. To investigate whether the hydroxamic acid can be replaced by a carboxylic acid, the methyl ester **7a** was hydrolyzed to yield the desired free carboxylic acid **11**.



Scheme 2. Synthesis of terephthalic-based HDACi (**9a-k**, **10a** and **10b**, **11**). Reagents and conditions: a) isobutyl chloroformate, NMM, $R^2\text{ONH}_2$, THF, 3 h, 67-93%; or $R^2\text{ONHR}^1$, CDI, RT, 77-79%; b) $\text{H}_2\text{NOH}\cdot\text{HCl}$, Na, MeOH dry, 70 °C, 3 h, 41-83%; c) (i) KOH, MeOH, H_2O , 90 °C, 5-6 h; (ii) HCl, H_2O , 92%.

The HDACi **9a-k**, **10a,b** and **11** were first tested against the 3D7 strain of *P. falciparum* using a ^3H -hypoxanthine incorporation assay. The screening revealed that 11 of 14 compounds tested (**9a-k**) showed IC_{50} values $\leq 1 \mu\text{M}$, **10b** had less potent activity with IC_{50} values $\leq 5 \mu\text{M}$ while **10a** and **11** were

not active ($IC_{50} >5 \mu\text{M}$). Notably, compound **9f**, bearing a 3,5-dimethylbenzyl group was the most active compound in this series ($IC_{50} 0.090 \mu\text{M}$). Subsequently, we assessed the anti-plasmodial activity against the multidrug-resistant *P. falciparum* Dd2 strain and observed similar IC_{50} values and structure-activity relationships. This indicates that resistance mechanisms developed in the Dd2 line do not affect the *in vitro* activity of this series of anti-Plasmodial HDACi.

To investigate the selectivity for asexual blood stage *P. falciparum* parasites cytotoxicity of all compounds was evaluated against human embryonic kidney 293 cell line HEK293. All compounds, except **9g**, exhibited IC_{50} values in the double-digit micromolar range which can be seen as relatively low cytotoxicity against human cells. The five most active asexual intraerythrocytic stage inhibitors (**9a**, **9c**, **9e**, **9f**, and **9g**) showed human cell IC_{50} values from 8.3 to 29.7 μM and calculated selectivity indices (SI; human cell $IC_{50}/P. falciparum IC_{50}$) of greater than 100. Additionally the five most active asexual intraerythrocytic stage inhibitors (**9a**, **9c**, **9e**, **9f**, and **9g**) were tested against the human liver carcinoma cell line HepG2. The compounds showed IC_{50} values higher than 50 μM and 37 μM in case of **9g**. Compound **9f**, the most active compounds from this series (3D7 $IC_{50} 0.090 \mu\text{M}$), was >100-fold more cytotoxic towards the *P. falciparum* 3D7 and Dd2 cell lines versus normal mammalian cell line HEK293 and >450-fold in comparison with HepG2 cells.

To proof the mode of action of the compounds protein hyperacetylation assays were carried out. Consistent with the expected outcome representative compounds were shown to hyperacetylate *P. falciparum* histone H4. When a sub-set of compounds were also screened *in vitro* for their activity against early-stage and late stage *P. falciparum* gametocytes only moderate activity was observed ($IC_{50} >2 \mu\text{M}$). Additionally the pre-selected compounds were tested against exoerythrocytic liver stages. Interestingly, compound **9f**, bearing a 3,5-dimethylbenzyl group, showed potent activity against *P. berghei* exo-erythrocytic stages ($IC_{50} 0.180 \mu\text{M}$) and >270-fold selectivity for exo-erythrocytic forms over HepG2 cells.

5 Publication III

Isophthalic acid-based HDAC Inhibitors as Potent Inhibitors of HDAC8 from *Schistosoma mansoni*

K. Stenzel (60%), A. Chakrabarti, J. Melesina, F. K. Hansen, J. Lancelot, S. Herkenhöner, B. Lungerich, M. Marek, C. Romier, R. J. Pierce, W. Sippl, Manfred Jung, T. Kurz

Arch. Pharm. Chem. 2017, 350, e1700096

Contributions to this project:

- Synthesis or supervision of the synthesis of all precursors and target compounds, analysis of all novel chemical structures and target compounds
- Collection of data, analysis and interpretation of data, participation in writing of the manuscript

5.1 Project background

For prevention of schistosomiasis no vaccine will be available in near future and for treatment mass administration of communities with a single administration of the anti-helminthic drug PZQ is recommended.³⁰⁸ While the global use of PZQ is scaling up, it does not prevent reinfections and its mechanism of action is not known. PZQ is rapidly becoming the only available drug, which increase the likelihood of the development of drug-resistant parasite strains. There is growing concern regarding reports from patients not cured by multiple doses of PZQ.^{271, 273, 274} Observations of resistant isolates have already been documented in endemic areas²⁷⁰ and the selection of field strains of schistosome that are resistant to PZQ is more and more likely.

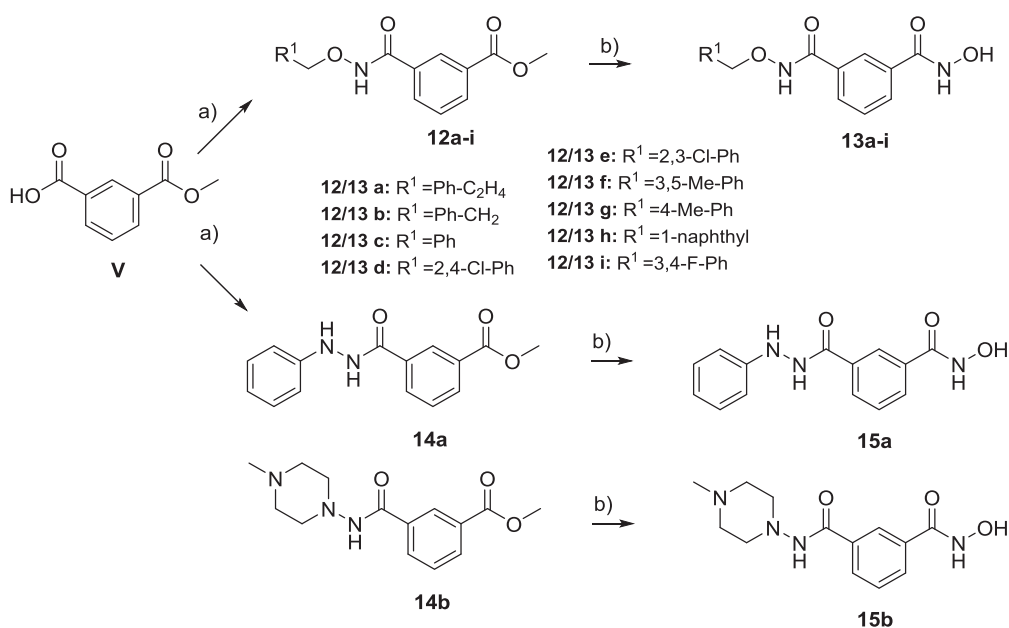
*Sm*HDAC8 has been identified as a potential target for anti-parasitic therapy. Transcripts of *Sm*HDAC8 are expressed at higher levels than *Sm*HDAC3 and *Sm*HDAC1 during all life cycle stages,²⁸¹ pointing at specific and vital functions in the parasite life cycle. The situation is different with human HDAC8. The enzyme shows relatively low level of expression and human HDAC8 inhibitors have the most limited effect on the human acetylome among all isoforms. Studies of human HDAC8 compounds showed that they exhibit a low effect on cell proliferation, indicating that the inhibition does not result in intrinsic toxicity. Limited toxicity of human HDAC8 inhibitors has been reported in several cell types.^{42, 309, 310} All these make *Sm*HDAC8 a promising target for the development of new species-selective drugs.

5.2 Project overview and results

In this project we combined the meta-substituted benzohydroxamate with an alkoxyamide connecting unit and various cap groups. The alkoxyamide group was used as a connecting unit which

presumably can enable charge-assisted hydrogen bonds due to the additional polarization of the N–H bond.^{109, 249} In order to probe whether these groups can serve as an alternative connecting unit in addition compounds with hydrazide-based connecting units have been synthesized.

Using a straightforward two-step protocol the target compounds were synthesized from the mono-methyl isophthalate and the *O*-substituted hydroxylamines and hydrazine derivatives. The alkoxyamide intermediates **12a-i** and hydrazides **14a,b** were treated with an excess of hydroxylamine hydrochloride in the presence of methanolic sodium methoxide and afforded the desired target compounds **13a-i** and **15a,b**.



Scheme 3. Synthesis of alkoxyamide-based and the hydrazide-based HDACi **13a-i**, **15a** and **15b**. Reagents and conditions: a) CDI, CH₂Cl₂, R¹-ONH₂ or R¹R²-NNH₂, RT, 0.5 h, 12 h; b) 1) NaOMe, MeOH, NH₂OH·HCl, 70° C, 3-5 h. 2) NaOH, NH₂OH, MeOH, CH₂Cl₂, 0° C, RT, 12 h.

In a primary screen for inhibition of *Sm*HDAC8 and representative human HDAC isoforms (HDAC1, HDAC6 and HDAC8) all compounds showed significant inhibition of *Sm*HDAC8 deacetylase activity, moderate inhibition of human HDAC6 and only very low inhibition of human HDAC1. Most compounds inhibited human HDAC8 in similar fashion as *Sm*HDAC8, however compounds **13d** and **15a** revealed a stronger inhibition of *Sm*HDAC8 in comparison to human HDAC8. Based on this primary screening, HDACi **13d** and **15a** and the unsubstituted prototype compound **13c** have been investigated further. All three tested compounds demonstrated high selectivity for *Sm*HDAC8 over the major human HDAC isoforms HDAC1 and HDAC6. The three compounds showed IC₅₀ values in the range of 0.33–0.75 μM against *Sm*HDAC8 and **13d** and **15a** showed a preference for *Sm*HDAC8 over its human orthologue.

Structural analyses at high resolution are useful tools in the development of novel potent and selective anti-schistosomal HDACi. Docking studies using the available human HDAC1, human HDAC8 and *Sm*HDAC8 structures were carried out allowing rationalization of the observed biochemical data. It has been shown that two important hydrogen bonds of the alkoxyamide connecting unit to Lys20 and His292 contribute to the high activity of **13d** against *Sm*HDAC8.

Additionally, a cell cytotoxicity assay in the human cell line HeK293 and in the human cell line HeLa was performed. In agreement with the finding that all of the tested inhibitors exhibited only low activity against human HDAC isoforms HDAC1 and HDAC6, the cytotoxicity of compounds **13d** and **15a** in the human cell system was very low.

We next analyzed the phenotypic activity of the most promising derivatives **13d** and **15a** on parasites in culture by examining their effects on the viability of the larvae (schistosomula) and the stability of adult worm pairs in culture. Our compound **13d** showed only very moderate and not dose-dependent toxicity toward schistosomula at 10 μ M and **15a** showed only slight activity. Both compounds couldnt significantly affect adult worm pairing during 5 days of culture *in vitro*.

6.1 Summary

This work deals with the design, synthesis and biological evaluation of anti-cancer and anti-parasitic HDACi. Three HDACi-sets were synthesized and analyzed. The biological evaluation was performed in cooperation with a high number of international collaborators. Additional to the compound synthesis, the author of this thesis was involved in the biological characterization of the anti-parasitic properties of the compounds and in the performance of the *in vitro* human HDAC isoform assay.

Depending on the target in each project, we hypothesized a certain HDACi isoform-profile as beneficial or disadvantageous. Experience from previous projects in our group and from other groups, compound screenings and *in vitro* experiment results contributed to an improved understanding of structure-activity relationships. The design of the compounds was primarily guided by the aimed isoform profile properties. Docking studies and mode of action investigations helped to expand our knowledge within the research projects. The collection and analysis of all these information enabled an optimisation of the lead structures toward the targeted anti-cancer or anti-parasitic properties.

Project 1: Alkoxyurea-based HDACi increase cisplatin potency in chemoresistant cancer cell lines

In the first project we present the synthesis and biological evaluation of novel and potent alkoxyurea-based HDACi with quinoline- or naphthyl cap group, an alkoxyurea connecting unit linker region and a hydroxamic acid Zn^{2+} -binding group. Compound **4d** displays slightly higher HDAC inhibition in the cellular HDAC assay compared to vorinostat and significantly enhanced cytotoxic effects against the tumor cell line Cal27 and A2780 as well as their cisplatin resistant sublines. The HDAC isoform profiling was in line with the results of the docking study and revealed that compounds **4b-d** are inhibitors with HDAC6 preference and nanomolar activity (Figure 9). Compound **4d** demonstrates strong inhibition of HDAC6 (IC_{50} 2.8 nM), moderate preference over HDAC1 (SI: 15.4) and selectivity over HDAC8 (SI: 550) and HDAC4 (SI >3500).

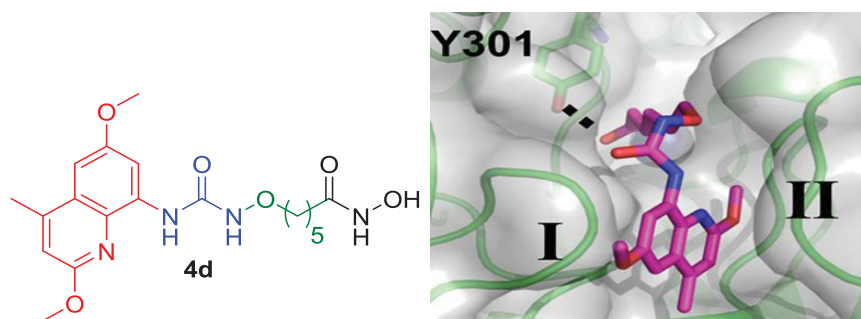


Figure 9. Compound structure of **4d** and docking pose for **4d**, identified in a homology model of HDAC6. Roman numerals indicate hydrophobic subpockets in the crevice of HDAC6.

The combination of cisplatin and compounds **4b-d** enhanced the sensitivity of the cisplatin-resistant cell line Cal27 CisR. Notably, **4d** was able to revert the cisplatin resistance in the Cal27 CisR cell line

with a shift factor of 11.2. The high acetylated H3 histone levels and acetylated α -tubulin levels found, revealed that the inhibition of HDAC1 and HDAC6 may both contribute to the enhancement of cisplatin chemosensitivity.

Project 2: Design and synthesis of terephthalic acid-based histone deacetylase inhibitors with dual stage anti-*Plasmodium* activity

Currently Zn²⁺-dependent HDACs are pharmaceutically highly investigated targets for epigenetic therapy. Chemical control of epigenetic pathways could represent a suitable possibility to attack eukaryotic parasites. Some of the terephthalic acid-based derivatives in this study are not cytotoxic at the highest concentration tested in HepG2 cells (IC₅₀ > 50 μ M). Compound **9f** was the most active compound in this series and was >450-fold more cytotoxic towards asexual blood stage parasites of *P. falciparum* 3D7 strain (IC₅₀ 0.090 μ M) versus mammalian cell line HepG2. While most work to date has focused on asexual stage parasites²²⁸ we could show that **9f** has potent activity (IC₅₀ 0.180 μ M) against exo-erythrocytic stage *P. berghei* parasites and >270-fold selectivity for exo-erythrocytic forms than versus HepG2 cells. It was possible to develop HDACi that selectively target two malaria parasite life cycle stages and **9f** may be a valuable starting point for the development of novel anti-malarial drug leads with low host cell toxicity. This generation compounds retain potent anti-plasmodial asexual blood stage activity and decreases the host cell toxicity in comparison to our last projects.^{249 248}

Project 3: Isophthalic acid-based HDAC inhibitors as potent inhibitors of HDAC8 from *Schistosoma mansoni*

A series of newly designed and synthesized alkoxyamide-based and hydrazide-based HDACi including an isophthalic linker were tested for inhibitory activity against *Sm*HDAC8 and human HDACs 1, 6, and 8. Based on the primary results, HDACi **13d**, **15a** and the unsubstituted prototype compound **13c** were further investigated. These compounds demonstrate high selectivity for *Sm*HDAC8 over the major human HDAC isoforms HDAC1 and 6. The three compounds show IC₅₀ values in the range of 0.33-0.75 μ M against *Sm*HDAC8 and **13d** and **15a** show a preference for *Sm*HDAC8 over its human orthologue. Selectivity over human HDAC8 still requires optimization, but there are strong indications that the high selectivity over human HDAC1 and 6, that we have already obtained, is of higher importance for a potential therapeutic setting. Docking studies provided insights into the putative binding modes and allowed rationalization of the observed selectivity profile. In cytotoxicity studies both tested compounds **13d** and **15a** were shown to have only very moderate effect on the viability of HEK293 and HeLa cells up to double-digit μ M range concentrations. However, the most potent derivatives **13d** and **15a** only showed moderate or no influence on the viability of *S. mansoni* schistosomula.

6.2 Zusammenfassung

Die vorliegende wissenschaftliche Arbeit beschäftigt sich mit dem Design, Synthese sowie der biologischen Evaluierung von anti-tumoralen und anti-parasitären HDACi. Die Verbindungen wurden in Zusammenarbeit mit einer großen Zahl von internationalen Kooperationspartnern biologisch evaluiert. Neben der Synthese der Verbindungen, führte die Autorin dieser Arbeit Teile der Charakterisierung der anti-parasitären Eigenschaften der Verbindungen durch, sowie den *in vitro* Assay an humanen HDAC.

In Abhängigkeit von dem Target postulierten wir ein bestimmtes HDAC-Isoformprofil als vorteilhaft oder unvorteilhaft für die Zielsetzung des jeweiligen Projektes. Durch Erfahrung aus vorangegangenen Projekten, von uns und von anderen Gruppen, durch Screenings von Verbindungen und basierend auf Resultaten aus den *in vitro* Studien, konnten wir Erkenntnisse zu Struktur-Aktivitätsbeziehungen gewinnen. Das Design der HDACi wurde durch die angestrebten Eigenschaften im HDAC-Isoformprofil maßgeblich geleitet. Dockingstudien und tieferegehende biologische Experimente zu den Wirkmechanismen halfen dabei unseren Wissensstand in den jeweiligen Projekten zu vergrößern. Das systematische Sammeln und die Analyse von allen diesen Informationen ermöglichte uns eine Optimierung der Leitstrukturen hin zu den angestrebten Eigenschaften als anti-tumorale oder anti-parasitäre HDACi.

Projekt 1: Alkoxyurea-basierte HDACi steigern die Cisplatin Aktivität in chemoresistenten Tumor-Zelllinien

Im ersten Projekt können wir die Synthese und die biologische Evaluierung von neuen und potenten Alkoxyurea-basierten HDACi mit Chinolin- oder Naphthyl Cap-Gruppe, einer Alkoxyurea Verbindungseinheit-Linker-Region und einer Hydroxamsäure-Funktion als Zink-bindende Gruppe präsentieren. Verbindung **4d** zeigte eine leicht höhere HDAC Inhibition im zellulären HDAC-Assay im Vergleich zu Vorinostat und eine signifikant gesteigerte Zytotoxizität gegen die Tumor-Zelllinie Cal27 und A2780, wie auch gegen deren Cisplatin resistenten Sub-Zelllinien.

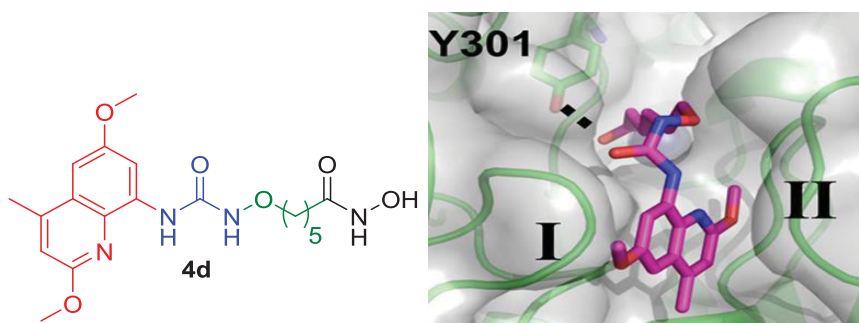


Bild 9. Struktur und Dockingergebnis der Verbindung **4d**, identifiziert im Homologiemodell der Isoform HDAC6. Die römischen Ziffern zeigen die hydrophoben Seitentaschen am Eingangsbereich zum katalytischen Zentrum.

Das ermittelte HDAC Isoform-Profil war in Übereinstimmung mit den Resultaten der Dockingstudie und zeigte, dass die Inhibitoren **4b-d** eine HDAC6-Präferenz und Aktivität im nanomolaren Bereich aufweisen (Bild 9). Verbindung **4d** zeigte eine starke Inhibierung von HDAC6 (IC_{50} 2.8 nM), eine moderate Präferenz für HDAC1 (SI: 15.4) und Selektivität über HDAC8 (SI: 550) und HDAC4 (SI >3500).

Die Kombination von Cisplatin und den Verbindungen **4b-d** verbesserte deutlich die Sensitivität der Cisplatin-resistenten Zelllinie Cal27 CisR. Die Verbindung **4d** konnte eine Aufhebung der Cisplatin Resistenz in der Cal27 CisR Zelllinie mit einem Verschiebungsfaktor von 11.2 hervorrufen. Die im Experiment gezeigte Hyperacetylierung der H3-Histone und die Acetylierung des α -Tubulins wiesen darauf hin, dass die Inhibition von HDAC1 und HDAC6 beide potentiell zur Steigerung der Cisplatin Chemosensitivität beitragen.

Projekt 2: Design und Synthese von Terephthalsäure-basierten HDACi mit Aktivität gegen zwei plasmodiale Stadien

Zur Zeit werden Zn^{2+} -abhängige HDACs pharmazeutisch in zahlreichen Studien untersucht und als mögliche Angriffs-Ziele für Epigenetik-basierte Therapien wissenschaftlich diskutiert. Die chemische Kontrolle von epigenetischen Mechanismen könnte eine geeignete Möglichkeit sein um eukaryotische Parasiten zu bekämpfen. Gemessen in der humanen HepG2 Zelllinie zeigten mehrere Terephthalsäure-basierten HDACi dieser Studie nur geringe Toxizität mit IC_{50} >50 μ M. Die Verbindung **9f** dieser Serie zeigte die höchste anti-plasmodiale Aktivität mit einem IC_{50} Wert von 0.090 μ M gegenüber asexuellen Blutstadien des *P. falciparum* 3D7 Stammes. Gleichzeitig war **9f** >450-fach mehr cytotoxisch gegenüber den asexuellen Blutstadien des *P. falciparum* 3D7 Stammes im Vergleich zu der humanen Zelllinie HepG2. Während die meisten wissenschaftlichen Arbeiten sich auf die asexuellen Stadien des Parasiten konzentrieren,²²⁸ konnten wir mit **9f** eine Verbindung entwickeln, die zudem potent ist (IC_{50} 0.180 μ M) gegenüber exo-erythrocytische Stadien von *P. berghei*. Dabei wies **9f** eine >270-fache Selektivität für die exo-erythrocytische Stadien im Vergleich zu HepG2 Zellen auf. Damit war es möglich, einen HDAC Inhibitor zu entwickeln, der selektiv gegen zwei plasmodiale Stadien wirkt. Die *in vitro* Aktivitäten und die Selektivität zeigen, dass **9f** ein interessanter Startpunkt ist für die Entwicklung von weiteren, anti-plasmodialen Verbindungen mit geringer Zytotoxizität gegen den menschlichen Wirt. Im Vergleich zu dem Vorgängerprojekt konnten wir bei den anti-plasmodialen HDACi dieser Generation die Aktivität gegen die asexuellen Blutstadien der Leitstrukturen beibehalten und gleichzeitig die Zytotoxizität gegen humane Zelllinien senken.^{249 248}

Projekt 3: Isophthalsäure-basierte HDAC-Inhibitoren als potente Inhibitoren der HDAC8 von *Schistosoma mansoni*

Eine Serie von Alkoxyamid- und Hydrazid-basierten HDACi wurde synthetisiert, deren Verbindungen einen Isophthalsäure-Linker als gemeinsames Strukturelement beinhalten. Die neuen HDACi wurden auf ihre Aktivität gegen *Sm*HDAC8 und die humanen HDACs 1, 6 und 8 getestet und **13d**, **15a** und die

unsubstituierte Prototyp-Verbindung **13c** für weitere Untersuchungen ausgewählt. Alle drei Verbindungen zeigten eine hohe Selektivität für die *SmHDAC8* im Vergleich zu den getesteten humanen HDAC-Isoformen HDAC1 und HDAC6. Die Aktivität lag bei IC_{50} Werten zwischen 0,33 und 0,75 μM gegen das *SmHDAC8* Enzym. Verbindungen **13d** und **15a** zeigten zudem eine leichte Präferenz für die *SmHDAC8* im Vergleich zu der humanen HDAC8. Diese Präferenz sollte in Zukunft weiter verbessert werden. Es ist jedoch anzunehmen, dass für einen potentiellen therapeutischen Einsatz, die bereits erreichte Selektivität über die humanen Isoformen HDAC6 und HDAC1, wichtiger ist als die Selektivität über die humane HDAC8. Dockingstudien zeigten die wahrscheinlichen Bindungseigenschaften der ausgewählten HDACi in *SmHDAC8* und humanen HDAC-Enzymen und ermöglichten eine Rationalisierung des beobachteten Isoformprofils. Verbindungen **13d** und **15a** wurden anschließend an humanen Zelllinien in Zytotoxizitäts-Untersuchungen getestet. Dabei konnte bei den verwendeten HeLa- und HEK293-Zelllinien bis zu einem doppelstelligen μM -Wert kaum oder keine Effekte auf die Zellviabilität gesehen werden. Die beiden interessantesten Verbindungen **13d** und **15a**, mit der höchsten Aktivität an *SmHDAC8* und der leichten Präferenz für *SmHDAC8* im Vergleich zur humanen HDAC8, zeigten jedoch kaum oder keine Wirkung auf die Überlebensfähigkeit von *S. mansoni* Schistosomula.

Alkoxyurea-Based Histone Deacetylase Inhibitors Increase Cisplatin Potency in Chemoresistant Cancer Cell Lines

Katharina Stenzel,^{†,○} Alexandra Hamacher,^{†,○} Finn K. Hansen,^{†,‡,§} Christoph G. W. Gertzen,[†] Johanna Senger,[§] Viktoria Marquardt,^{†,||,⊥,‡,§} Linda Marek,^{†,||} Martin Marek,[∇] Christophe Romier,[∇] Marc Remke,^{||,⊥,‡,§} Manfred Jung,^{§,||} Holger Gohlke,^{†,||} Matthias U. Kassack,^{*,†,◆} and Thomas Kurz^{*,†,◆,⊥}

[†]Institut für Pharmazeutische und Medizinische Chemie, Heinrich-Heine-Universität Düsseldorf, Universitätsstraße 1, 40225 Düsseldorf, Germany

[‡]Pharmaceutical/Medicinal Chemistry, Institute of Pharmacy, Leipzig University, Brüderstraße 34, 04103 Leipzig, Germany

[§]Institut für Pharmazeutische Wissenschaften, Albert-Ludwigs-Universität Freiburg, Albertstraße 25, 79104 Freiburg, Germany

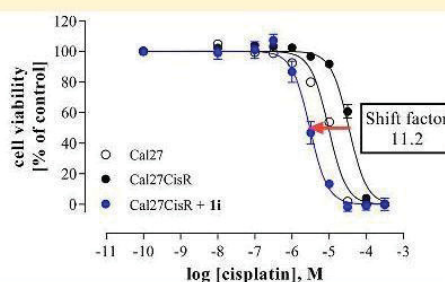
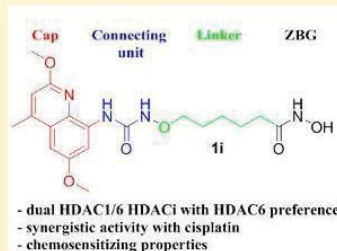
^{||}Department of Pediatric Oncology, Hematology, and Clinical Immunology, Medical Faculty, Heinrich-Heine-University, Moorenstraße 5, 40225 Düsseldorf, Germany

[⊥]Department of Neuropathology, Medical Faculty, Heinrich-Heine-University, Moorenstraße 5, 40225 Düsseldorf, Germany

[‡]Division of Pediatric Neuro-Oncogenomics, German Cancer Consortium (DKTK) and German Cancer Research Center (DKFZ), Moorenstraße 5, 40225 Düsseldorf, Germany

[∇]Département de Biologie Structurale Intégrative, Institut de Génétique et Biologie Moléculaire et Cellulaire (IGBMC), Université de Strasbourg (UDS), CNRS, INSERM, 1 Rue Laurent Fries, 67404 Illkirch Cedex, France

Supporting Information



ABSTRACT: The synthesis and biological evaluation of potent hydroxamate-based dual HDAC1/6 inhibitors with modest HDAC6 preference and a novel alkoxyurea connecting unit linker region are described. The biological studies included the evaluation of antiproliferative effects and HDAC inhibitory activity in the human ovarian cancer cell line A2780, the human squamous carcinoma cell line Cal27, and their cisplatin resistant sublines A2780CisR and Cal27CisR. The three most potent compounds **1g–i** showed IC_{50} values in the low μ M and sub- μ M range. **1g–i** revealed low nM IC_{50} values for HDAC6 with up to 15-fold preference over HDAC1, >3500-fold selectivity over HDAC4, and >100-fold selectivity over HDAC8. Furthermore, their ability to enhance cisplatin sensitivity was analyzed in Cal27 and Cal27CisR cells. Notably, a 48 h preincubation of **1g–i** significantly enhanced the antiproliferative effects of cisplatin in Cal27 and Cal27CisR. **1g–i** interacted synergistically with cisplatin. These effects were more pronounced for the cisplatin resistant subline Cal27CisR.

INTRODUCTION

The dynamic histone acetylation/deacetylation state is regulated by histone acetyltransferases (HATs) and histone deacetylases (HDACs). HDACs are clinically validated cancer targets and represent a group of 18 enzymes catalyzing the removal of acetyl groups from *N*-acetyl-lysine residues of histones and various non-histone proteins during post-translational protein modification.¹ Deacetylation causes chromatin condensation leading mainly to transcriptional suppression, whereas acetylation leads to gene activation. HDACs of classes I (HDACs 1–3, 8), IIa (HDACs 4, 5, 7, 9), IIb (HDACs 6, 10), and IV (HDAC 11) are

Zn²⁺ dependent enzymes. Class III HDACs (sirtuins) are NAD⁺ dependent deacetylases.²

HDAC inhibition can abrogate aberrant epigenetic changes associated with cancer.³ Currently, four histone deacetylase inhibitors (HDACi), vorinostat (cutaneous T-cell lymphoma; CTCL), romidepsin (CTCL and peripheral T-cell lymphoma; PTCL), belinostat (relapsed or refractory PTCL), and panobinostat (multiple myeloma; MM) have been approved

Received: December 8, 2016

Published: June 5, 2017

for cancer treatment by the FDA (Figure 1).⁴ Moreover, the class I selective benzamide-based HDACi chidamide has recently been

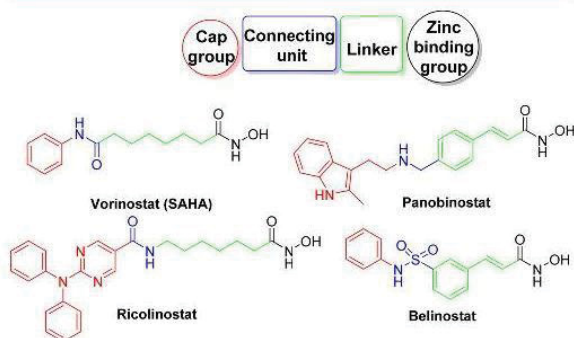


Figure 1. General pharmacophore model of HDACi.

approved in China for the treatment of relapsed or refractory PTCL.⁵ Furthermore, HDACi are under investigation for potential application as therapeutic drugs for treating a variety of diseases beyond cancer including inflammation, HIV, neurodegenerative diseases, and parasitic diseases such as malaria and schistosomiasis.^{1,6} Structurally, most HDACi are characterized by a widely accepted pharmacophore model (see Figure 1) and contain (i) a cap group (CAP) that interacts with residues at the entry point of the active site tunnel, (ii) a linker region plus a connecting unit (CU), interacting mainly with hydrophobic residues of the tunnel, and (iii) a zinc binding group (ZBG) that coordinates the catalytically essential Zn^{2+} ion at the active site. Recent results have shown that all units have an impact on the isoform profile of HDACi.⁷

Most of the first generation HDACi are pan inhibitors. To date, it is still under debate whether pan HDAC inhibitors or class-selective HDAC inhibitors will be more effective in clinical trials regarding both safety and efficacy.⁸ To address the question if pan- or class/subtype selective HDAC inhibitors show superior clinical benefit, the development of isoform and class-selective HDACi has attracted the attention of academia and industry.⁹ Experimental preclinical and clinical data suggest that the combination of HDACi with established DNA-modifying anticancer drugs (e.g., cisplatin, carboplatin, temozolomide) provides synergistic effects in the treatment of hematological and solid tumors, possibly through HDACi-mediated increased accessibility of DNA or inhibition of antiapoptotic gene expression.¹⁰

Recently, ricolinostat (ACY-1215, Figure 1), an HDAC6 preferential inhibitor with additionally potent inhibitory activity toward class I HDACs, has entered phase II clinical trials for the treatment of multiple myeloma and lymphoid malignancies.¹¹ HDAC6 is structurally unique and acts primarily via deacetylation of non-histone proteins such as α -tubulin and Hsp90. HDAC6 contains two catalytic domains and a C-terminal zinc finger region responsible for binding of ubiquitinated proteins. In addition, HDAC6 possesses a significantly wider channel rim compared to other HDACs. Therefore, HDAC6 selective inhibitors often contain bulky or branched cap groups. Moreover, an sp^2 -hybridized carbon atom in α -position related to the ZBG is often present in HDAC6-preferential and -selective HDACi.¹² The hydroxamic acid group and the α -mercaptoacetamide moiety are typical ZBGs of HDAC6-selective HDACi.¹³

Dual inhibitors, inhibiting HDAC6 and to a lesser extent HDAC class I, would help to decrease unwanted (cytotoxic) side effects of class I and still make use of beneficial effects associated with HDAC6 inhibition. We now discovered that alkoxyurea-based HDACi with quinoline cap groups can serve as potent dual HDAC1/6 inhibitors, with moderate HDAC6 preference. Herein, we report the structure-based design, straightforward synthesis, and biological evaluation of this class of HDACi with potent anticancer activity and remarkable chemosensitizing properties. Compounds were evaluated in the human ovarian cancer cell line A2780 and the adenocarcinoma cell line Cal27 and their cisplatin resistant sublines A2780CisR and Cal27CisR for antiproliferative effects and inhibition of cellular HDAC activity. Compounds **1g–i** were further tested for inhibition of selected HDAC isoforms (1, 4, 6, and 8, respectively). Molecular modeling and docking studies were performed to rationalize the observed selectivity profile. The acetylation of α -tubulin and histone H3 was analyzed in Cal27 and Cal27CisR to show HDAC6 inhibition in a complex cellular environment. Eventually, **1g–i** were shown to enhance cisplatin sensitivity in Cal27 and Cal27CisR in a synergistic manner.

RESULTS AND DISCUSSION

Design of HDAC6-Preferential HDACi with an Alkoxyurea Connecting Unit Linker Region. Recently, we studied the effects of a small library of HDACi containing alkoxyamide and alkoxyurea connecting-unit linker regions in cellular MTT and pan-HDAC assays on sensitive and chemoresistant cancer cell lines.¹⁴ Initial studies on alkoxyurea **1a** revealed only moderate cytotoxicity assessed in MTT assay against the human ovarian cancer cell lines A2780 ($IC_{50} = 10.8 \mu M$) and A2780CisR ($IC_{50} = 11.6 \mu M$) but significant HDAC inhibition in a cellular HDAC assay targeting class I and class IIb HDACs in A2780 ($IC_{50} = 1.07 \mu M$) and A2780CisR ($IC_{50} = 0.85 \mu M$).¹⁴ Due to the presence of a bulky cap group and structural similarities with ricolinostat (Figure 1), we hypothesized that **1a** might show a comparable isoform profile with preferred HDAC6 inhibition. Subsequent isoform profiling confirmed our hypothesis and revealed potent activity against HDAC6 and preference over HDACs 1, and 8 (Table 1). **1a** did not show any inhibition of HDAC4. The pan inhibitor vorinostat and the class IIa selective trifluoromethyloxadiazole (TFMO)-HDACi TMP269 were used as reference HDACi.¹⁵ On the basis of these preliminary results,

Table 1. Inhibition Activities of Compound **1a** and Vorinostat against HDAC Isoforms 1, 4, 6, and 8^a

Compound	Structure	IC_{50} [nM] of HDAC isoforms			
		HDAC1	HDAC4	HDAC6	HDAC8
1a		189 ± 20.4	>10000	51.7 ± 4.1	11170 ± 2220
vorinostat		45 ± 8	n.d.	108 ± 11	1260 ± 210
TMP269		n.d.	447 ± 30	n.d.	n.d.

^aValues of HDAC1, -6, and -8 are the mean \pm SD of three independent experiments. Values for HDAC4 were determined in duplicate by Reaction Biology Corp. (Malvern, PA, USA). n.d. = not determined.

we performed a docking study in order to understand the selectivity profile of compound **1a** and to design improved analogues.

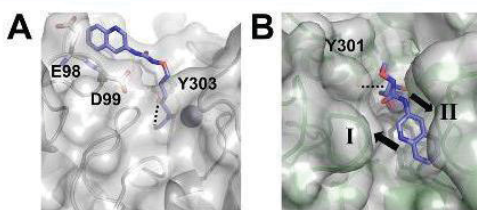


Figure 2. Docking poses for **1a** identified in HDAC1 (A) and HDAC6 (B). Hydrogen bonds are shown with dashed lines; the zinc ion is shown as a sphere. Black arrows and roman numerals indicate hydrophobic subpockets in the crevice of HDAC6.

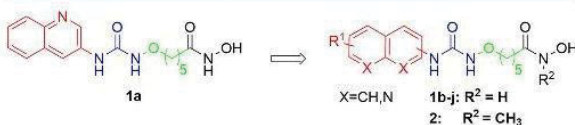


Figure 3. Lead compound **1a** and target compounds.

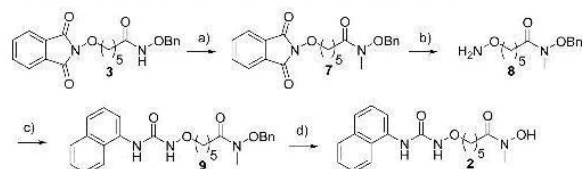
Docking of 1a and Design of 1a Derivatives. In order to understand the selectivity profile of compound **1a**, the compound was docked into the crystal structures of HDAC1 and -4, and homology models of the second catalytic domain of HDAC6 with Y301 flipped in and out. Templates for the homology modeling of HDAC6 encompass structures resulting in Y301 (numbering based on the homology model) flipped in and out. The homology models of HDAC6 had been generated and then subjected to 1 μ s of molecular dynamics simulations for identification of conformationally preferred states previously.¹⁶ X-ray crystal structures of human and zebrafish HDAC6 (PDB codes SEDU¹⁷ and SEF8¹⁷) have been released prior to submission of this manuscript.^{17,18} Our homology model is very similar to the crystal structures, as shown by a C α atom rmsd of 1.39 Å (1.56 Å) and a binding pocket (residues within 5 Å of the cocrystallized ligand) heavy atom rmsd of 1.75 Å (1.62 Å) toward the human (zebrafish) HDAC6 structure. This demonstrates the quality of our comparative modeling,¹⁶ although docking into HDAC6 crystal structures may further improve the accuracy of predicting binding modes of HDACi in HDAC6 in the future. HDACi were docked into both possible conformers of HDAC6. For docking, AutoDock3 in combination with DrugScore¹⁹ was used, as successfully applied previously.²⁰ No valid binding mode in which the zinc ion was complexed by the hydroxamic acid moiety was identified when docking **1a** to

HDAC4, in line with the experimental results (Table 1). Furthermore, the docking energies of **1a** in HDAC1 (−11.61 kcal mol^{−1}) are higher than those in HDAC6 (−13.48 kcal mol^{−1}) with Y301 flipped in (Table 5), which agrees qualitatively with the trend in IC₅₀ values (Table 1). In both HDAC isoforms, the zinc ion is complexed by the hydroxamic acid moiety of **1a**, and this moiety forms a hydrogen bond with Y303 and Y301 in HDAC1 and HDAC6, respectively. In contrast, the aromatic rings bind to different locations in both isoforms (Figure 2). In HDAC1, the quinoline ring binds to a small recess on the surface, which is partially lined by acidic residues on one side (Figure 2A). As to (de)solvation effects, this is energetically less favorable than if the recess was lined with hydrophobic residues. In HDAC6, the quinoline ring binds to a deeper crevice at the side of HDAC6 (Figure 2B), which is lined with hydrophobic residues. Together, this can explain the differences in the docking energies and IC₅₀ values of **1a** toward HDAC1 and -6. Notably, the crevice displays small hydrophobic subpockets I and II adjacent to the quinoline moiety (Figure 2B, black arrows). We thus hypothesized that derivatives of **1a** with a quinolyl moiety substituted with small hydrophobic groups will fill these subpockets, which will yield higher affinities toward HDAC6.

On the basis of the results of the docking study, we designed and synthesized a series of **1a** analogues as potential HDAC6i (Figure 3) and focused our structural modifications on the cap. Notably, we aimed at the replacement of the unsubstituted 3-quinolyl cap by (substituted) 4-quinolyl, 8-quinolyl, 1-naphthyl, and 2-naphthyl caps. In order to address the above-mentioned subpockets in the crevice of HDAC6, we intended to decorate selected compounds in positions 2, 4, and 6 of the quinoline moiety.

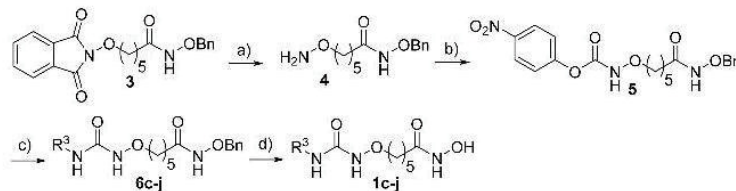
Chemistry. The synthesis of the alkoxyurea-based HDACi **1a** and **1b** has been reported previously. The synthetic protocols for the preparation of all novel HDACi are summarized in Schemes 1 and 2. The HDACi **1c–j** were prepared according to a novel and

Scheme 2. Synthesis of the Target Compound **2**^a



^aReagents and conditions: (a) CH₃I, NaH (60%), THF, rt, 16 h; (b) methylhydrazine, CH₂Cl₂, −10 °C, 3 h; (c) 1-naphthyl isocyanate, CH₂Cl₂, rt; (d) Pd/C, H₂ (1 bar), MeOH, rt, 3 h.

Scheme 1. Synthesis of the Target Compounds **1c–j**^a



^aReagents and conditions: (a) methylhydrazine, CH₂Cl₂, −10 °C, 3 h; (b) pyridine, CH₂Cl₂, ClCO₂C₆H₄NO₂, rt, 3 h; (c) R³NH₂, Et₃N, THF, microwave, 70 °C, 0.5 h; (d) Pd/C, H₂ (1 bar), MeOH, rt, 3 h.

straightforward synthetic protocol. The key intermediate **4** was obtained by deprotection of the readily available starting material

Table 2. Antiproliferative Effects of 1a–j, 2, Cisplatin, Tubastatin A, and Vorinostat in A2780, Cal27, and Their Cisplatin Resistant Sublines A2780CisR and Cal27CisR^b

Compound	R ³	Cytotoxicity IC ₅₀ [μM]			
		A2780	A2780CisR	Cal27	Cal27CisR
1a		10.8 ± 1.0	11.6 ± 0.8	3.0 ± 0.3	5.4 ± 0.5
1b		7.6 ± 0.6	7.9 ± 0.6	1.6 ± 0.1	3.9 ± 0.4
1c		1.4 ± 0.1	1.6 ± 0.1	1.7 ± 0.1	2.3 ± 0.2
1d		27.3 ± 1.0	10.5 ± 0.8	5.8 ± 0.5	7.6 ± 0.6
1e		3.0 ± 0.3	1.0 ± 0.09	1.1 ± 0.1	2.2 ± 0.2
1f		4.3 ± 0.3	1.3 ± 0.1	2.2 ± 0.2	4.7 ± 0.3
1g		1.2 ± 0.1	0.4 ± 0.03	0.9 ± 0.04	1.3 ± 0.1
1h		1.1 ± 0.09	0.3 ± 0.02	0.6 ± 0.04	1.3 ± 0.06
1i		0.8 ± 0.07	0.4 ± 0.03	1.0 ± 0.08	1.3 ± 0.08
1j		1.7 ± 0.09	3.6 ± 0.3	3.9 ± 0.1	2.9 ± 0.2
2		46.8 ± 2.8	44.2 ± 3.7	43.7 ± 3.8	65.8 ± 5.9
cisplatin		1.88 ± 0.06	13.7 ± 1.1	2.27 ± 0.2	19.8 ± 1.1
vorinostat		2.42 ± 0.2 ^a	3.12 ± 0.3 ^a	1.98 ± 0.1	1.75 ± 0.1
tubastatin A		n.d.	n.d.	4.6 ± 0.4	10.8 ± 1.0

^aData taken from ref 14. ^bValues are the mean ± SD of three independent experiments. n.d. = not determined.

3 (see Supporting Information for details). Initial attempts to introduce the alkoxyurea moiety using 1,1'-carbonyldiimidazole (CDI) mediated or 1,1'-carbonylditriazole (CDT) mediated coupling protocols^{2,1} did not provide the targeted asymmetrical alkoxyureas **6** at all, or only in a low yield, especially in the case of the aminoquinoline-based cap groups. Thus, we decided to develop an optimized protocol. The aminoxy group of compound **4** was activated using 4-nitrophenyl chloroformate to obtain the 4-nitrophenyl carbamate **5**.

The treatment of **5** with aminoquinolines or 2-naphthylamine under conventional reaction condition provided the desired alkoxyureas only in moderate yields (33–69%) and required relatively long reaction times. We therefore considered microwave heating in order to improve reaction times and yields. Best results were obtained at 70 °C and 100 W for 0.5 h. This microwave-assisted protocol allowed the synthesis of the alkoxyureas **6c–j** in good to excellent yield (83–91%). The

Table 3. Antiproliferative Effects of 1g–i, Cisplatin, and Vorinostat in Med8a and ONS76^a

Compound	R ³	Cytotoxicity IC ₅₀ [μM]	
		Med8a	ONS76
1g		1.21 ± 0.09	2.67 ± 0.21
1h		0.60 ± 0.11	0.59 ± 0.04
1i		0.59 ± 0.06	0.65 ± 0.03
cisplatin		2.81 ± 0.51	10.2 ± 0.62
vorinostat		1.34 ± 0.18	2.04 ± 0.08

^aValues are the mean ± SD of three to four independent experiments.

Table 4. HDAC Inhibition of 1a–j, 2, Cisplatin, and Vorinostat in A2780, A2780CisR, Cal27, and Cal27CisR^a

Compound	R ¹	HDAC inhibition IC ₅₀ [μM]			
		A2780	A2780 CisR	Cal27	Cal27 CisR
1a		1.1 ± 0.1	0.9 ± 0.06	1.3 ± 0.08	1.3 ± 0.07
1b		1.1 ± 0.03	0.9 ± 0.05	1.1 ± 0.04	1.0 ± 0.06
1c		5.1 ± 0.4	1.6 ± 0.1	1.0 ± 0.08	1.0 ± 0.09
1d		2.4 ± 0.2	2.0 ± 0.2	1.4 ± 0.1	1.1 ± 0.1
1e		2.1 ± 0.1	0.9 ± 0.06	0.9 ± 0.04	0.9 ± 0.06
1f		3.3 ± 0.2	1.7 ± 0.1	3.4 ± 0.3	2.8 ± 0.2
1g		1.0 ± 0.06	0.5 ± 0.02	0.9 ± 0.06	0.7 ± 0.07
1h		0.9 ± 0.05	0.4 ± 0.02	0.6 ± 0.05	0.5 ± 0.05
1i		1.7 ± 0.07	0.5 ± 0.03	0.5 ± 0.04	0.5 ± 0.04
1j		149 ± 11	n.c.	107 ± 10	56 ± 1.2
2		--	--	190 ± 16	204 ± 20
vorinostat		1.68 ± 0.04	2.82 ± 0.2	0.88 ± 0.05	0.75 ± 0.06
tubastatin A		n.d.	n.d.	16.1 ± 0.9	12.1 ± 0.4

^aValues are the mean ± SD of three independent experiments. n.d. = not determined.

Table 5. Inhibitory Activities of 1a, 1g, 1h, and 1i against Human HDAC1, HDAC4, HDAC6, and HDAC8^a

Compound	Structure	IC ₅₀ [nM] of HDAC isoforms			
		HDAC1	HDAC4	HDAC6	HDAC8
1a		189 ± 20.4	>10000	51.7 ± 4.1	11170 ± 2220
1g		51.9 ± 6.2	>10000	6.10 ± 1.5	1080 ± 120
1h		77.3 ± 6.2	>10000	24.8 ± 5.2	1220 ± 290
1i		43.2 ± 3.2	>10000	2.80 ± 0.6	1540 ± 140
vorinostat		45 ± 8	n.d.	108 ± 11	1260 ± 210
TMP269		n.d.	447 ± 30	n.d.	n.d.

^aValues of HDAC1, -6, and -8 are the mean ± SD of three independent experiments. Values for HDAC4 were determined in duplicate by Reaction Biology Corp. (Malvern, PA, USA). n.d. = not determined.

subsequent catalytic hydrogenation followed by purification by flash column chromatography afforded the novel alkoxyurea-based HDACi 1c–j in 54–72% yield (Scheme 1).

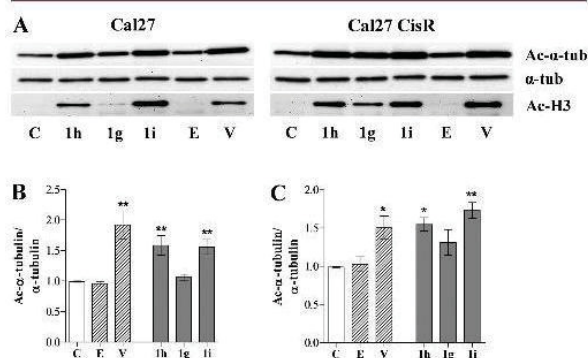


Figure 4. Compound-induced α -tubulin and histone H3 acetylation in Cal27 and Cal27CisR. (A) Representative immunoblot analysis of α -tubulin (α -tub), acetylated α -tubulin (Ac- α -tub), and acetylated histone H3 (Ac-H3) in Cal27 and Cal27CisR after compound incubation. Cal27 and Cal27CisR cells were incubated for 24 h with vehicle (C) or 1 μ M entinostat (E), vorinostat (V), 1h, 1g, or 1i, respectively. (B, C) Quantification of the immunoblots confirmed a significant increase in acetylated α -tubulin for 1h and 1i. Densitometric analysis of the protein bands of Cal27 (B) and Cal27CisR (C) were performed using ImageJ software (NIH). Data are the mean ± SD, $n = 3$. All values have been normalized to control. Statistical analysis was performed using one-way ANOVA test (* $p < 0.05$ and ** $p < 0.01$).

The *N*-methyl-substituted hydroxamic acid 2 was synthesized from the starting material 3 (Scheme 2). First, 3 was methylated with methyl iodide in the presence of sodium hydride as a base to obtain the *O*-protected *N*-methylated hydroxamic acid 7. The deprotection of the phthaloyl group afforded the aminoxy derivative 8, which was converted into the alkoxyurea derivative 9. Finally, the target compound 2 was obtained by catalytic hydrogenation (54% yield, Scheme 2).

Biological Evaluation. Determination of Antiproliferative Effects. Compounds 1c–j and 2 were first tested by MTT assay for antiproliferative effects in A2780 and Cal27, and their cisplatin resistant sublines A2780CisR and Cal27CisR. Results are presented in Table 2 together with vorinostat, tubastatin A, and cisplatin as controls. The compounds with the highest antiproliferative activity against all four cell lines are the 8-quinolyl-substituted analogues 1g–i showing IC₅₀ values in the range of 0.4–1.3 μ M. Notably, 1g–i are more active against A2780CisR compared to the native cell line A2780. In comparison to the lead structure 1a, the pan-HDAC vorinostat and 1g–i displayed higher antiproliferative effects whereas the HDAC6-selective HDACi tubastatin A was clearly less potent. The MTT assay revealed that the antiproliferative potential of the unsubstituted 2-naphthyl analogue 1c is almost comparable to the unsubstituted 8-quinolyl derivative 1e. In contrast, the 6-quinolyl derivative 1d and the 1-naphthyl derivative 1b are significantly less cytotoxic than 1c and 1e.

For further evaluation of the antiproliferative potential of this novel class of HDACi, the three most potent compounds (1g–i) were additionally tested for their efficacy in the two medulloblastoma cell lines Med8a and ONS76. The cell viability was determined after a 72 h incubation by Celltiter-Glo assay (Promega). The results presented in Table 3 underline the higher cytotoxicity of the compounds 1h,i compared to cisplatin and the pan-HDAC inhibitor vorinostat.

Cellular HDAC Inhibition. Cellular HDAC assays were performed as previously published.¹⁴ The results are summarized in Table 4. 1g–i displayed the most potent HDAC inhibitory activity with IC₅₀ values in the range of 0.4–1.7 μ M against all four cell lines. These results were in good agreement with the antiproliferative effects obtained with the MTT assay in the same cell lines, whereas the lead structure 1a displayed increased HDAC inhibition in comparison to its antiproliferative effects. Cellular HDAC inhibition was similar in native and resistant cell lines, whereas 1c and 1e–i showed a 2- to 3.4-fold higher activity in the cisplatin resistant subline A2780CisR compared to the native A2780.

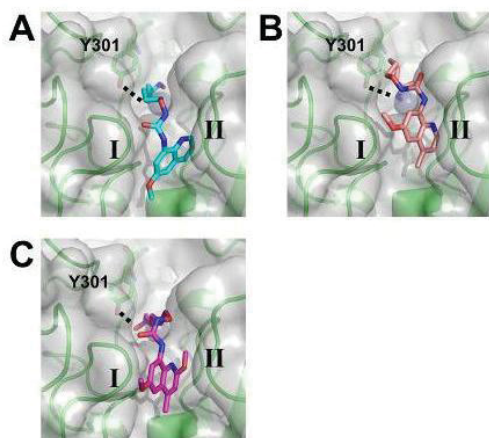


Figure 5. Docking poses for **1g** (A), **1h** (B), and **1i** (C) identified in HDAC6. Hydrogen bonds are shown as dashed lines; the zinc ion is shown as a sphere. The hydrophobic subpockets are numbered with roman numerals.

Table 6. Docking Energies for HDACi Binding to HDAC Isoforms

compd	HDAC1 ^a	HDAC4 ^a	HDAC6 ^a	HDAC8 ^a
1a	-11.61	n/a ^b	-13.48	
1g	-12.67	n/a ^b	-15.67	n/a ^b
1h	-13.36	n/a ^b	-14.52	n/a ^b
1i	-14.02	n/a ^b	-15.61	n/a ^b

^aDocking energy of the energetically most favorable configuration in the largest cluster; in kcal·mol⁻¹. ^bNo docking configuration fulfilling the criteria given in the methods section could be identified.

Inhibition of HDAC1, HDAC4, HDAC6, and HDAC8.

MTT and cellular HDAC assays identified **1g–i** as the most potent compounds. **1g–i** were therefore subjected to isoform profiling against human HDAC1, HDAC4, HDAC6, and HDAC8. Results are shown in Table 5. **1g–i** are nanomolar potency HDAC6 inhibitors (IC₅₀ in the range of 2.8–24.8 nM) and 2- to 18-fold more potent than the lead structure **1a**. **1i** demonstrated excellent selectivity over HDAC8 (SI = 550) and a preference over HDAC1 (SI = 15). HDAC6 inhibitory activity of **1i** was 2- to 9-fold higher than for **1g** and **1h** and even 18-fold higher in comparison to the lead structure **1a**.

To confirm HDAC6 inhibition in a more complex cellular environment, α -tubulin acetylation was analyzed after a 24 h incubation of 1 μ M **1g–i** in Cal27 and Cal27CisR cells. Furthermore, the ability of the potential HDAC inhibitors **1g–i** to enhance the acetylation of histone H3 was analyzed. The results of a representative Western blot analysis are shown in Figure 4.

1g–i, and vorinostat induced an accumulation of acetylated α -tubulin in comparison to the untreated control in both cell lines. This indicates that all three compounds and the reference pan-HDACi vorinostat inhibit HDAC6, whereas the HDAC1 and HDAC3 isoform-specific HDACi entinostat did not influence the amount of acetylated α -tubulin after a 24 h incubation. The α -tubulin acetylation of **1h** and **1i** was significant in comparison to the untreated control in Cal27 and Cal27CisR cells.

Furthermore, **1g–i** and vorinostat induced histone H3 acetylation indicating that they act not only as HDAC6 inhibitors. This is further supported by the fact that highly

Table 7. IC₅₀ Values (μ M) after Treatment of Cal27 and Cal27CisR with Cisplatin or in Combination with 1 μ M **1g**, 0.5 μ M **1h**, or 0.5 μ M **1i**, Respectively^a

compd	cell line			
	Cal27		Cal27CisR	
	IC ₅₀	SF	IC ₅₀	SF
cisplatin	9.13 \pm 0.5		46.4 \pm 3.1	
cisplatin + 1g 1.0 μ M	1.28 \pm 0.1	7.1	5.47 \pm 0.4	8.5
cisplatin + 1h 0.5 μ M	1.49 \pm 0.1	6.1	5.68 \pm 0.3	8.2
cisplatin + 1i 0.5 μ M	1.05 \pm 0.1	8.7	4.16 \pm 0.4	11.2
cisplatin + SAHA 1 μ M			6.80 \pm 0.2	6.8
cisplatin + tub A 10 μ M	8.30 \pm 0.2	1.1	32.0 \pm 0.3	1.5

^aSF means shift factor and was calculated as the ratio of the IC₅₀ of cisplatin alone and the IC₅₀ of the corresponding drug combination. Data shown are the mean \pm SEM of pooled data from at least three independent experiments each carried out in triplicates. All shift factors are significant (*t* test, *p* < 0.05) except for cisplatin plus tubastatin A. The used concentrations of **1g–i** were chosen on the basis of their HDAC inhibitory activity (Table 2).

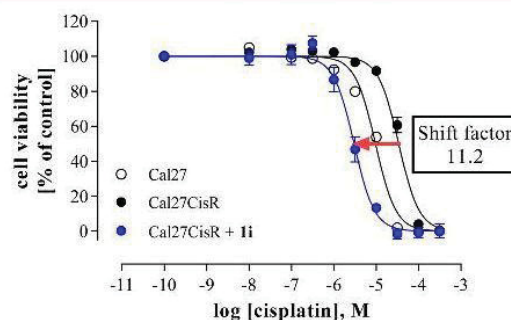


Figure 6. Treatment with **1i** restores cisplatin sensitivity of Cal27CisR cells. Cal27 (○) or Cal27CisR (●) were treated with increasing concentrations of cisplatin for 72 h. The IC₅₀ values for each cell line were determined by MTT assay. Treatment of Cal27CisR with 500 nM of **1i** 48 h prior cisplatin administration (blue dot) was able to reduce the IC₅₀ value even below the IC₅₀ of the parental cell line Cal27. The shift factor was calculated as the ratio of the IC₅₀ of cisplatin alone and the IC₅₀ of the corresponding combination with **1i** (Table 7). Data shown are the mean \pm SEM of four independent experiments each performed in triplicates.

selective HDAC6 inhibitors show only weak growth inhibition of cancer cells.²² H3 acetylation was more pronounced for **1h** and **1i**, whereas **1g** induced only a moderate acetylation of the histone core. **1g–i** showed the same or higher H3 acetylation than vorinostat. Histone acetylation induced by **1g–i** and vorinostat was more pronounced in Cal27CisR cell line than in the native cell line Cal27. Thus, acetylated H3 and acetylated tubulin levels found for **1g–i** in Figure 4 revealed that inhibition of both HDAC1 and HDAC6 may contribute to the enhancement of cisplatin chemosensitivity. Additionally, Asgar et al. reported about synergistic anticancer effects of cisplatin and vorinostat on cholangiocarcinoma cell lines.²³ Interestingly, the 24 h incubation with the class I selective HDACi entinostat resulted only in a very weak histone H3 acetylation. This unexpected effect could be attributed to the incubation time used because entinostat showed an increase of histone H3 acetylation only after a longer incubation period of 36 h.²⁴

Docking Studies. We docked compounds **1g–i** into HDACs 1, 4, 6 (with Y301 in the flipped-in conformation),

Table 8. Synergism Studies between Cisplatin and Ig–i^a

compd [nM]	Cal27					Cal27CisR				
	cisplatin [μ M]					cisplatin [μ M]				
	0.316	0.5	1	2	5	1	3.16	5	10	20
Ig										
500	0.86	0.87	0.67	0.49	0.35	*	*	0.96	0.36	0.35
600	0.79	0.77	0.57	0.37	0.34	*	*	0.60	0.36	0.37
700	*	0.97	0.63	0.43	0.32	*	0.56	0.41	0.33	0.37
800	*	0.93	0.56	0.43	0.36	0.81	0.51	0.37	0.35	0.37
900	0.77	0.60	0.54	0.40	0.37	*	0.79	0.52	0.43	0.49
1000	0.77	0.67	0.50	0.41	0.40	0.85	0.63	0.43	0.49	0.48
1500	0.82	0.74	0.64	0.60	0.55	1.00	0.52	0.47	0.51	0.62
2000	0.92	0.86	0.75	0.70	0.66	0.82	0.60	0.59	0.65	0.68
Ih										
100	*	*	*	*	0.50	*	*	*	*	0.73
200	*	*	0.76	0.39	0.29	*	*	*	0.48	0.33
300	*	*	0.44	0.31	0.25	*	*	*	0.43	0.34
400	*	0.91	0.39	0.27	0.29	*	*	0.56	0.26	0.28
500	*	0.49	0.37	0.27	0.29	*	0.71	0.28	0.25	0.26
600	0.93	0.58	0.37	0.26	0.33	*	0.51	0.25	0.20	0.21
700	0.68	0.57	0.43	0.36	0.41	*	0.28	0.21	0.21	0.25
800	0.56	0.51	0.41	0.38	0.38	1.09	0.26	0.23	0.23	0.28
Ii										
100	*	*	*	0.31	0.26	*	0.89	0.66	0.41	0.34
200	*	0.96	0.82	0.33	0.22	*	0.87	0.38	0.21	0.19
300	*	*	0.64	0.38	0.32	*	0.46	0.25	0.18	0.17
400	0.97	0.75	0.51	0.38	0.36	*	0.30	0.19	0.16	0.16
500	0.79	0.66	0.50	0.42	0.43	0.56	0.26	0.19	0.16	0.20
600	0.71	0.66	0.53	0.49	0.49	0.56	0.24	0.20	0.17	0.19
700	0.82	0.70	0.61	0.60	0.64	*	0.28	0.23	0.20	0.21
800	0.84	0.79	0.69	0.66	0.69	0.65	0.29	0.26	0.23	0.21

^aData shown are combination indices. Cal27 and Cal27CisR were treated with combinations of cisplatin and Ig, Ih, or Ii. CI (combination index) was calculated using Calcsyn 2.1 based on the Chou–Talalay method. CI > 1 indicates antagonism, CI = 1 indicates an additive effect, and CI < 0.9 indicates synergism. * means fraction affected is less than 0.20. Values are the mean of three experiments. SD is <10% of the mean.

and 8 in order to understand and explain their selectivity profile. Compounds Ig–i are the most potent inhibitors of HDAC6 evaluated in this study. All three inhibitors did not produce valid docking poses in HDAC4 and HDAC8 reflecting their high IC₅₀ values toward these isoforms. In contrast, in HDAC1 and -6, binding poses were identified for all three inhibitors similar to the ones found for 1a (Figure 5). Again, the relative change of the IC₅₀ values of the inhibitors is reflected in the relative change in docking energies (Table 6), with the compounds showing a preference for HDAC6 (Table 5). Moreover, compounds Ig–i show more favorable docking energies than 1a in HDAC6 (Table 6), in agreement with the lower IC₅₀ values toward HDAC6 for Ig–i compared to 1a (Table 5). The docking results are even sensitive enough to correctly display that Ig and Ii exhibit a similar activity toward HDAC6, while Ih is correctly predicted to be less effective (Table 5, Table 6). The docking poses (Figure 5) suggest that this difference occurs because of the quinoline moiety of Ig being quite buried in subpocket II, and Ii filling both subpockets I and II with its methoxy groups; in contrast, the urea oxygen of Ih is in unfavorably close contact to the protein. Compounds Ig and Ii could also form weak hydrogen bonds with C137 at the lower backside of subpocket I, which Ih cannot form due to the orientation of its quinoline moiety. In all, the results of the docking are in remarkably close agreement with those of the biological evaluation. Furthermore, decoration of the quinoline moiety with small hydrophobic groups resulted in improved binding affinities as hypothesized from the initial

docking studies above. Together with previous successful applications of the combination AutoDock3/DrugScore for ligand docking to HDACs,^{14,16} this corroborates the suitability of these methods for such predictive in silico studies.

Enhancement of Cisplatin-Induced Cytotoxicity. As HDACi are promising new therapeutic agents successfully combined with DNA-damaging compounds such as cisplatin,²³ the ability of Ig–i to influence the cytotoxic activity (MTT assay) of cisplatin was analyzed. Cal27 and Cal27CisR were preincubated with 1 μ M Ig, 0.5 μ M Ih, or 0.5 μ M Ii 48 h prior to cisplatin administration for another 72 h. IC₅₀ values for cisplatin alone and in combination with Ig–i are shown in Table 7.

A 48 h preincubation with Ig–i resulted in a significantly increased cisplatin sensitivity. In the native cell line Cal27, a hypersensitization with shift factors of 6.1 up to 8.7 for cisplatin was observed. This sensitizing effect was also obtained in the cisplatin resistant subline Cal27CisR. With shift factors in the range of 8.2–11.2, the enhancement of cisplatin-induced cytotoxicity was more pronounced in Cal27CisR. IC₅₀ values for cisplatin in Cal27CisR after preincubation with Ig–i were below the IC₅₀ value of the native cell line Cal27 indicating that Ig–i are able to overcome cisplatin resistance in the HNSCC cell line Cal27. The HDAC6-selective compound tubastatin A was included as control and only slightly increased cisplatin sensitivity in Cal27CisR (1.5fold) with no effect in native Cal27. This indicates that HDAC6 inhibition may be a minor factor in the in vitro chemosensitizing process and additional

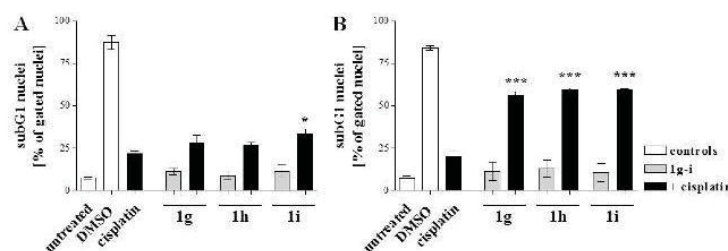


Figure 7. **1g–i** enhance cisplatin-induced apoptosis in Cal27 and Cal27CisR cells. Cal27 (A) and Cal27CisR (B) cells were preincubated with $1\ \mu\text{M}$ **1g**, $0.5\ \mu\text{M}$ **1h**, or $0.5\ \mu\text{M}$ **1i** for 48 h. Cisplatin was added in an IC_{50} concentration for each cell line (Cal27 $3\ \mu\text{M}$ (A), Cal27CisR $25\ \mu\text{M}$ (B)) and washed out after 6 h. After a further incubation period of 24 h, apoptosis was analyzed by determining the sub-G1 cell fractions by flow cytometry analysis. DMSO 10% was added for 24 h to serve as a positive control for apoptosis induction. Vehicle was added as a control for untreated cells. Gray bars depict the incubation of cells with **1g–i** only, whereas black bars show the effects of the combination of **1g–i** with cisplatin. All experimental conditions were incubated for same time periods. Data are the mean \pm SD, $n = 3$. Statistical analysis to compare the apoptosis induction by cisplatin alone and the combination of cisplatin and **1g–i** was performed using one-way ANOVA test ($*$) $p < 0.05$ and ($***$) $p < 0.001$.

class I HDAC inhibition is required to increase cisplatin sensitivity as seen for vorinostat and **1g–i**.

Figure 6 shows the effect of the most potent compound **1i** on the inhibitory activity of cisplatin at Cal27CisR cells.

To determine the type of interaction between cisplatin and **1g–i**, we performed synergism studies by using MTT assays. Cal27 and Cal27CisR cells were preincubated with eight different concentrations of **1g–i**. After 48 h, cisplatin was added in five different concentrations and incubated for 72 h similar to the combination experiments shown above. The used concentrations were chosen to achieve a fraction affected ($f_a =$ level of cellular growth inhibition) of <0.9 in the isobologram analysis. Results are shown in Table 8.

With combination indices below 0.9, the isobologram analysis revealed a synergistic effect of **1g–i** with cisplatin. As seen in the combination experiments to analyze an enhancement of cisplatin-induced cytotoxicity, the effects of **1g–i** were more pronounced for the cisplatin-resistant subline. In Cal27CisR, CI values were more than 2-fold lower in comparison to Cal27. These results underline once more the higher efficacy of **1g–i** concerning synergistic cytotoxic effects in the cisplatin resistant subline Cal27CisR.

Enhancement of Cisplatin-Induced Apoptosis. Above, we found a synergistic enhancement of cisplatin-induced cytotoxicity upon a 48 h preincubation with **1g–i**. Here, we evaluated if these results could be due to effects of **1g–i** on cisplatin-induced apoptosis. Cal27 and Cal27CisR cells were treated with $1\ \mu\text{M}$ **1g** or $0.5\ \mu\text{M}$ **1h** and **1i** for 48 h. Then, cisplatin was added in a concentration corresponding to the actual IC_{50} for each cell line (Cal27, $3\ \mu\text{M}$; Cal27CisR, $25\ \mu\text{M}$) and washed out after 6 h. Cells were cultured for another 24 h and analyzed using propidium iodide staining. Results are shown in Figure 7.

1g–i induced no significant changes in the amount of apoptotic nuclei in comparison to the untreated control for both cell lines. This indicates that the concentrations of **1g–i** used for the apoptosis assay and for the combination experiments had no apoptotic effects as single agents. However, in combination with cisplatin **1g–i** induced an increase in apoptosis in comparison to cisplatin alone. The combined treatment in Cal27 showed a significant increase in the amount of apoptotic nuclei for **1i** (33.3% in contrast to 21.8% for cisplatin alone), whereas **1g** and **1h** induced only a small increase which was not significant. In the cell line Cal27CisR, a significant increase in apoptosis induction was observed for all three compounds

(cisplatin, 20.3%; +**1g**, 56.3%; +**1h**, 59.7%; +**1i**, 59.7%) underlining again the higher activity of **1g–i** in the cisplatin-resistant subline.

CONCLUSIONS

In summary, we have developed an improved synthetic protocol for the preparation of HDACi with an alkoxyurea connecting-unit linker region. In particular, compounds **1g–i** showed remarkable inhibition of cellular HDAC activity and cytotoxicity in the human ovarian cancer cell line A2780, the human squamous carcinoma cell line Cal27, and their cisplatin resistant sublines A2780CisR and Cal27CisR. On the basis of their potent anticancer activity, **1g–i** were selected for a comprehensive biological evaluation. Isoform profiling against HDAC1, -4, -6, and -8 resulted in low nanomolar IC_{50} values for HDAC6 with up to 15-fold preference over HDAC1, >3500 -fold over HDAC4, and >100 -fold selectivity over HDAC8. Molecular modeling and docking studies were performed to rationalize the observed selectivity profile. Moreover, our data show that **1g–i** enhanced the cisplatin-induced cytotoxicity in Cal27 and Cal27CisR cells. Notably, **1g–i** interacted synergistically with cisplatin. The enhancement of cisplatin-induced cytotoxicity could be due to an increase in cisplatin-induced apoptosis. These effects are more pronounced in the cisplatin-resistant subline Cal27CisR. These new dual HDAC1/HDAC6 inhibitors may thus be promising modulators to overcome cisplatin resistance in HNSCC.

EXPERIMENTAL SECTION

Chemistry. General. All solvents and chemicals were used as purchased without further purification. The progress of all reactions was monitored on Merck precoated silica gel plates (with fluorescence indicator UV₂₅₄) using ethyl acetate/*n*-hexane as solvent system. Column chromatography was performed with Fluka silica gel 60 (230–400 mesh ASTM) with the solvent mixtures specified in the corresponding experiment. Spots were visualized by irradiation with ultraviolet light (254 nm) or staining in potassium permanganate solution following heating. Flash column chromatography was performed using prepacked silica cartridge with the solvent mixtures specified in the corresponding experiment. Melting points (mp) were taken in open capillaries on a Mettler FP 5 melting-point apparatus and are uncorrected. Proton (^1H) and carbon (^{13}C) NMR spectra were recorded on a Bruker Avance 500 (500 MHz for ^1H and 125 MHz for ^{13}C) or Bruker Avance 600 (600 MHz for ^1H and 150 MHz for ^{13}C) using chloroform-*d* or DMSO-*d*₆ as solvent. Chemical shifts are given in parts per million (ppm), relative to residual solvent peak for ^1H and ^{13}C . Elemental analysis was performed on a PerkinElmer PE 2400 CHN elemental analyzer. Analytical HPLC analysis were carried out on a

Varian Prostar system equipped with a Prostar 410 (autosampler), 210 (pumps) and 330 (UV detector) using a Phenomenex Luna Su C18(2) 1.8 μ m particle (250 mm \times 4.6 mm) column, supported by Phenomenex Security Guard cartridge kit C18 (4.0 mm \times 3.0 mm). UV absorption was detected at 254 nm with a linear gradient. The purity of all final compounds was 95% or higher.

Experimental Data. General procedures for the synthesis of HDAC inhibitors **1c–j**, **2**, and the *O*-benzyl-protected precursors **6c–j** as well as characterization data for compounds **1i** and **6i** are given below. The synthesis of all other compounds is reported in the Supporting Information.

General Procedure for the Synthesis of Compounds 1c–j, 2. A solution of the respective *O*-benzyl-protected hydroxamic acid (**6c–j**, **9**) in methanol (50 mL) was hydrogenated (1 bar) at room temperature in the presence of a catalytic amount of Pd–C (10 wt %). Upon completion of the reaction, the crude mixture was filtered through Celite to remove the catalyst and the filtrate was concentrated under reduced pressure. The residue was purified by column chromatography using CH₂Cl₂/30% methanol (9:1) as eluent (yield, 54–72%).

N-Hydroxy-6-((3-(naphthalen-2-yl)ureido)oxy)hexanamide (1c). Colorless solid; yield 65%; mp 195 °C. ¹H NMR (600 MHz, DMSO-*d*₆) δ = 10.35 (s, 1H), 9.54 (s, 1H), 8.88 (s, 1H), 8.67 (s, 1H), 8.15 (s, 1H), 7.96–7.64 (m, 4H), 7.50–7.33 (m, 2H), 3.80 (t, *J* = 6.8 Hz, 2H), 1.98 (t, *J* = 7.6 Hz, 2H), 1.81–1.59 (m, 2H), 1.61–1.48 (m, 2H), 1.42–1.28 (m, 2H) ppm. ¹³C NMR (151 MHz, DMSO-*d*₆) δ = 169.0, 157.1, 136.7, 133.4, 129.3, 127.9, 127.3, 126.9, 126.2, 124.1, 120.6, 114.9, 75.7, 32.1, 27.2, 24.9 ppm. HPLC analysis: retention time = 8.13 min; peak area, 96.48%. Method: eluent A, HPLC-grade water + 0.1% TFA; eluent B, HPLC-grade CH₃CN + 0.1% TFA; linear gradient of 30% B to 100% B over 20 min at a flow rate of 1.0 mL min⁻¹.

N-Hydroxy-6-((3-(quinolin-6-yl)ureido)oxy)hexanamide (1d). Colorless solid; yield 62%; mp 153 °C. ¹H NMR (600 MHz, DMSO-*d*₆) δ = 10.36 (s, 1H), 9.63 (s, 1H), 9.04 (s, 1H), 8.77–8.74 (m, 1H), 8.68 (s, 1H), 8.24 (m, 8.26–8.21, 2H), 7.93 (s, 2H), 7.54–7.36 (m, 1H), 3.80 (t, *J* = 6.6 Hz, 2H), 1.97 (t, *J* = 7.4 Hz, 2H), 1.72–1.60 (m, 2H), 1.60–1.47 (m, 2H), 1.40–1.28 (m, 2H) ppm. ¹³C NMR (151 MHz, DMSO-*d*₆) δ = 169.0, 157.0, 148.5, 144.3, 137.1, 135.1, 129.0, 128.2, 124.0, 121.5, 114.5, 75.7, 32.1, 27.2, 24.9 ppm. HPLC analysis: retention time = 7.09 min; peak area, 96.33%. Method: eluent A, HPLC-grade water + 0.1% TFA; eluent B, HPLC-grade CH₃CN + 0.1% TFA; linear gradient of 10% B to 100% B over 20 min at a flow rate of 1.0 mL min⁻¹.

N-Hydroxy-6-((3-(quinolin-8-yl)ureido)oxy)hexanamide (1e). Colorless solid; yield 57%; mp 123 °C. ¹H NMR (600 MHz, DMSO-*d*₆) δ = 10.36 (s, 1H), 9.96 (s, 1H), 9.91 (s, 1H), 8.92–8.87 (m, 1H), 8.67 (s, 1H), 8.48 (d, 1H), 8.41 (d, *J* = 8.2, 1.7 Hz, 1H), 7.68–7.51 (m, 3H), 3.89 (t, *J* = 6.3 Hz, 2H), 1.98 (t, *J* = 7.3 Hz, 2H), 1.76–1.64 (m, 2H), 1.61–1.52 (m, 2H), 1.51–1.42 (m, 2H) ppm. ¹³C NMR (151 MHz, DMSO-*d*₆) δ = 169.0, 156.3, 148.8, 137.6, 136.6, 134.4, 127.7, 127.0, 122.1, 120.5, 114.1, 76.0, 32.1, 27.5, 25.1, 24.9 ppm. HPLC analysis: retention time = 9.76 min; peak area, 95.44%. Method: eluent A, HPLC-grade water + 0.1% TFA; eluent B, HPLC-grade CH₃CN + 0.1% TFA; linear gradient of 10% B to 100% B over 20 min at a flow rate of 1.0 mL min⁻¹.

N-Hydroxy-6-((3-(2-methylquinolin-8-yl)ureido)oxy)hexanamide (1f). Colorless solid; yield 72%; mp 153 °C. ¹H NMR (600 MHz, DMSO-*d*₆) δ = 10.36 (s, 1H), 9.97 (s, 1H), 9.94 (s, 1H), 8.68 (s, 1H), 8.49–8.42 (m, 1H), 8.27 (s, 1H), 7.61–7.40 (m, 3H), 3.91 (t, *J* = 6.4 Hz, 2H), 2.71 (s, 3H), 2.04–1.93 (m, 2H), 1.85–1.69 (m, 2H), 1.69–1.52 (m, 2H), 1.54–1.41 (m, 2H) ppm. ¹³C NMR (151 MHz, DMSO-*d*₆) δ = 168.4, 156.7, 155.9, 136.4, 136.1, 133.3, 125.5, 125.4, 122.2, 119.7, 113.5, 75.6, 31.5, 27.1, 24.5, 24.4, 24.3 ppm. HPLC analysis: retention time = 14.17 min; peak area, 96.99%. Method: eluent A, HPLC-grade water + 0.1% TFA; eluent B, HPLC-grade CH₃CN + 0.1% TFA; linear gradient of 10% B to 100% B over 20 min at a flow rate of 1.0 mL min⁻¹.

N-Hydroxy-6-((3-(6-methoxyquinolin-8-yl)ureido)oxy)hexanamide (1g). Colorless solid; yield 59%; mp 176 °C. ¹H NMR (600 MHz, DMSO-*d*₆) δ = 10.35 (s, 1H), 10.01 (s, 1H), 9.85 (s, 1H), 8.70 (dd, *J* = 4.2, 1.6 Hz, 1H), 8.66 (s, 1H), 8.27 (d, *J* = 8.2 Hz, 1H), 8.14 (d, *J* = 2.5 Hz, 1H), 7.61–7.52 (m, 1H), 7.01 (d, *J* = 2.5 Hz, 1H), 3.97–3.82 (m, 5H), 1.98 (t, *J* = 7.2 Hz, 2H), 1.74–1.64 (m, 2H), 1.61–1.53

(m, 2H), 1.51–1.41 (m, 2H) ppm. ¹³C NMR (151 MHz, DMSO-*d*₆) δ = 168.9, 157.6, 156.2, 146.0, 135.4, 135.3, 134.2, 128.9, 122.5, 106.5, 98.5, 76.0, 55.4, 32.1, 27.5, 25.1, 24.9 ppm. HPLC analysis: retention time = 6.88 min; peak area, 95.42%. Method: eluent A, HPLC-grade water + 0.1% TFA; eluent B, HPLC-grade CH₃CN + 0.1% TFA; linear gradient of 30% B to 100% B over 20 min at a flow rate of 1.0 mL min⁻¹.

N-Hydroxy-6-((3-(6-methoxy-4-methylquinolin-8-yl)ureido)oxy)hexanamide (1h). Colorless solid; yield 61%; mp 142 °C. ¹H NMR (600 MHz, DMSO-*d*₆) δ = 10.36 (s, 1H), 9.99 (s, 1H), 9.95 (s, 1H), 8.67 (s, 1H), 8.56 (dd, *J* = 4.3, 1.7 Hz, 1H), 8.19–8.11 (m, 1H), 7.42 (d, *J* = 4.1 Hz, 1H), 6.95 (s, 1H), 3.92 (s, 3H), 3.87 (t, *J* = 6.4, 1.8 Hz, 2H), 2.65 (s, 3H), 1.98 (t, *J* = 7.5, 1.7 Hz, 2H), 1.74–1.64 (m, 2H), 1.61–1.53 (m, 2H), 1.50–1.42 (m, 2H) ppm. ¹³C NMR (125 MHz, DMSO-*d*₆) δ = 169.0, 157.5, 156.2, 145.5, 143.4, 135.9, 133.9, 128.5, 123.0, 106.0, 95.3, 76.0, 55.4, 32.1, 27.5, 25.1, 24.9, 18.4 ppm. HPLC analysis: retention time = 9.62 min; peak area, 98.50%. Method: eluent A, HPLC-grade water + 0.1% TFA; eluent B, HPLC-grade CH₃CN + 0.1% TFA; linear gradient of 10% B to 100% B over 20 min at a flow rate of 1.0 mL min⁻¹.

6-((3-(2,6-Dimethoxy-4-methylquinolin-8-yl)ureido)oxy)-N-hydroxyhexanamide (1i). Colorless solid; yield 55%; mp 162 °C. ¹H NMR (600 MHz, DMSO-*d*₆) δ = 10.34 (s, 1H), 9.94 (s, 1H), 9.59 (s, 1H), 8.66 (s, 1H), 8.13 (d, 1H), 6.96 (s, 1H), 6.92 (d, *J* = 2.7 Hz, 1H), 3.98 (s, 3H), 3.95–3.83 (m, 3H), 2.59 (s, 3H), 1.94 (t, *J* = 7.4 Hz, 2H), 1.70–1.60 (m, 2H), 1.56–1.47 (m, 2H), 1.38–1.29 (m, 2H) ppm. ¹³C NMR (151 MHz, DMSO-*d*₆) δ = 168.4, 158.7, 155.8, 155.1, 146.6, 133.6, 130.2, 124.5, 112.5, 105.7, 96.0, 75.3, 54.7, 52.1, 31.6, 27.0, 24.39, 24.32, 17.92 ppm. HPLC analysis: retention time = 14.17 min; peak area, 96.99%. Method: eluent A, HPLC-grade water + 0.1% TFA; eluent B, HPLC-grade CH₃CN + 0.1% TFA; linear gradient of 10% B to 100% B over 20 min at a flow rate of 1.0 mL min⁻¹.

N-Hydroxy-6-((3-(2-isopropoxy-4-methyl-5-(3-(trifluoromethyl)phenoxy)quinolin-8-yl)ureido)oxy)hexanamide (1j). Colorless solid; yield 54%; mp 137 °C. ¹H NMR (600 MHz, DMSO-*d*₆) δ = 10.37 (s, 1H), 10.02 (s, 1H), 9.68 (s, 1H), 8.69 (s, 1H), 8.57 (s, 1H), 7.53 (t, *J* = 8.1, 1H), 7.37 (d, *J* = 7.8, 1H), 7.12 (s, 1H), 7.03 (d, *J* = 7.8, 1H), 6.84 (s, 1H), 5.45 (sept, *J* = 6.2, 1H), 3.91 (t, *J* = 7.1, 2H), 3.75 (s, 3H), 2.52 (s, 3H), 1.98 (t, *J* = 7.4, 2H), 1.85–1.63 (m, 2H), 1.63–1.48 (m, 2H), 1.48–1.27 (m, 8H) ppm. ¹³C NMR (151 MHz, DMSO-*d*₆) δ = 168.9, 158.7, 158.6, 156.4, 147.4, 146.2, 131.9, 131.1, 130.4 (q, *J* = 32.0 Hz), 130.4, 130.3, 123.8 (q, *J* = 272.9 Hz), 119.4, 118.6, 118.2, 118.2, 116.3, 111.3, 103.7, 75.8, 67.8, 56.3, 32.1, 27.5, 24.9, 24.8, 22.2, 21.6 ppm. HPLC analysis: retention time = 18.61 min; peak area, 96.49%. Method: eluent A, HPLC-grade water + 0.1% TFA; eluent B, HPLC-grade CH₃CN + 0.1% TFA; linear gradient of 30% B to 100% B over 20 min at a flow rate of 1.0 mL min⁻¹.

N-(Benzoyloxy)-N-methyl-6-((3-(naphthalen-1-yl)ureido)oxy)hexanamide (2). Oil; yield 54%. ¹H NMR (500 MHz, DMSO-*d*₆) δ = 9.76 (s, 1H), 9.55 (s, 1H), 8.83 (s, 1H), 8.07–7.87 (m, 2H), 7.75 (d, *J* = 8.20, 1H), 7.63 (d, *J* = 7.34, 1H), 7.60–7.46 (m, 3H), 3.88 (t, *J* = 6.7 Hz, 2H), 3.07 (s, 3H), 2.37 (t, *J* = 7.7 Hz, 2H), 1.77–1.66 (m, 2H), 1.61–1.49 (m, 2H), 1.47–1.34 (m, 2H) ppm. ¹³C NMR (125 MHz, DMSO-*d*₆) δ = 172.8, 157.9, 133.6, 128.3, 128.3, 128.0, 125.8, 125.7, 125.5, 124.8, 122.4, 121.6, 75.8, 35.6, 31.4, 27.4, 25.1, 24.0 ppm. Anal. Calcd for C₁₈H₂₃N₃: C 60.51, H 8.07, N 12.45. Found: C 60.58, H 7.93, N 12.15.

N-(Benzoyloxy)-6-((1,3-dioxoisindolin-2-yl)oxy)hexanamide (3). (1) 6-Bromohexanoic acid (1.951 g, 10 mmol) was dissolved in anhydrous THF (25 mL) and cooled to –15 °C. This was treated with *N*-methylmorpholine (1.012 g, 11 mmol) followed by isobutyl chloroformate (1.502 g, 11 mmol) to form the mixed anhydride. After 15 min *O*-benzylhydroxylamine (1.232 g, 10 mmol) was added dropwise. The reaction was warmed to room temperature over 3 h and subsequently filtered. After removing the solvent in vacuo the residue was diluted in ethyl acetate/H₂O and extracted with ethyl acetate (3 \times 60 mL). The combined extracts were washed with NaHCO₃ (50 mL) and the organic layer was dried over Na₂SO₄, filtered and the solvent removed in vacuo to give the intermediate *N*-(benzoyloxy)-6-bromohexanamide (2.49 g, 8.30 mmol, 83%).

(2) *N*-Hydroxyphthalimide (1.35 g, 8.30 mmol) and *N*-(benzoyloxy)-6-bromohexanamide (2.49 g, 8.30 mmol) were dissolved in acetonitrile

(25 mL). Triethylamine (1.26 g, 12.45 mmol) was added, and the reaction mixture was refluxed for 7 h. Upon completion (TLC analysis, eluent ethyl acetate/*n*-hexane 1:1), the reaction mixture was poured into ice-water (70 g) and extracted with ethyl acetate (3 × 75 mL). The combined organic layers were washed with a saturated solution of NaHCO₃ (3 × 75 mL), dried over Na₂SO₄, and evaporated under reduced pressure to provide 3 in 79% yield. All spectroscopic data were in agreement with the literature.¹⁴

6-(Aminoxy)-*N*-(benzyloxy)hexanamide (4). Methylhydrazine (0.503 mL, 9.6 mmol) was added dropwise at -10 °C to a solution of compound 3 (2.29 g, 6 mmol) in dry CH₂Cl₂ (15 mL). The reaction mixture was stirred for 2.5 h, and the precipitate was removed by filtration. The filtrate was evaporated under reduced pressure and treated with diethyl ether (5 mL). The precipitate was removed by filtration, and a saturated solution of HCl in diethyl ether was added to the filtrate to obtain the hydrochloride of the product. The solid was collected by filtration and subsequently dissolved in water (40 mL). A saturated Na₂CO₃ solution was added until pH > 8, and the aqueous layer was extracted with ethyl acetate (3 × 50 mL). The combined organic layers were dried over Na₂SO₄ and evaporated under reduced pressure to provide 4. All spectroscopic data were in agreement with the literature.¹⁴

4-Nitrophenyl ((6-((benzyloxy)amino)-6-oxohexyl)oxy)carbamate (5). The 6-(aminoxy)-*N*-(benzyloxy)hexanamide 4 (0.252 g, 1.0 mmol) was dissolved in dry CH₂Cl₂ (30 mL), and dry pyridine (0.110 mL, 1.4 mmol) was added. The reaction was cooled down to 0 °C, and 4-nitrophenyl chloroformate (0.202 g, 1 mmol) was added under stirring in one portion. After stirring at room temperature for 3 h, the homogeneous solution was diluted with CH₂Cl₂ (100 mL) and washed with citric acid solution (10% w/w, 2 × 50 mL) and water (2 × 50 mL). The organic layer was dried over Na₂SO₄ and concentrated to afford 5 in 72% yield. Compound 5 was used directly in the next step without further purification.

General Procedure for the Microwave-Assisted Synthesis of Compounds 6c–j. 4-Nitrophenyl ((6-((benzyloxy)amino)-6-oxohexyl)oxy)carbamate 5 (0.209 g, 0.5 mmol) in dry THF (1.5 mL) was placed into a 10 mL glass pressure microwave tube equipped with a magnetic stirrer bar. Triethylamine (69 μL, 0.5 mmol) was added before the tube was closed with a silicon septum, and the reaction mixture was subjected to microwave irradiation for 0.5 h at 70 °C and 100 W. The reaction mixture was cooled to room temperature and transferred to a round bottomed flask. The solvent was evaporated, CH₂Cl₂ (100 mL) was added, and the mixture was washed subsequently with a saturated, aqueous solution of sodium hydrogen carbonate (30 mL), and water (30 mL). The organic layer was dried over Na₂SO₄, filtered, and the solvent was evaporated. The remaining residues were purified by crystallization from appropriate solvents or the crude products were purified by flash column chromatography (prepacked silica cartridge, *n*-hexane/ethyl acetate, gradient 90:10 → 0:100 in 0.5 h) to yield the desired intermediates (yield, 83–91%).

***N*-(Benzyloxy)-6-((3-(naphthalen-2-yl)ureido)oxy)hexanamide (6c).** Colorless solid; yield 85%; mp 132 °C. ¹H NMR (600 MHz, DMSO-*d*₆) δ = 10.96 (s, 1H), 9.54 (s, 1H), 8.87 (s, 1H), 8.15 (d, *J* = 1.6 Hz, 1H), 7.82 (s, 1H), 7.80 (s, 1H), 7.77 (d, *J* = 8.2 Hz, 1H), 7.69 (dd, *J* = 2.0, 8.9 Hz, 1H), 7.44 (t, *J* = 7.5 Hz, 1H), 7.41–7.30 (m, 6H), 4.78 (s, 2H), 3.79 (t, *J* = 6.7 Hz, 2H), 1.98 (t, *J* = 7.2 Hz, 2H), 1.69–1.59 (m, 2H), 1.57–1.48 (m, 2H), 1.37–1.26 (m, 2H) ppm. ¹³C NMR (150 MHz, DMSO-*d*₆) δ = 169.2, 157.1, 136.6, 136.0, 133.3, 129.3, 128.7, 128.2, 128.1, 127.9, 127.3, 126.9, 126.1, 124.1, 120.6, 114.9, 76.7, 75.6, 32.1, 27.2, 24.7, 24.7 ppm. Anal. Calcd for C₂₄H₂₇N₃; C 68.39, H 6.46, N 9.97. Found: C 68.21, H 6.37, N 9.83.

***N*-(Benzyloxy)-6-((3-(quinolin-6-yl)ureido)oxy)hexanamide (6d).** Colorless solid; yield 79%; mp 103 °C. ¹H NMR (600 MHz, DMSO-*d*₆) δ = 10.95 (s, 1H), 9.62 (s, 1H), 9.03 (s, 1H), 8.75 (dd, *J* = 4.0, 1.7 Hz, 1H), 8.26–8.16 (m, 2H), 7.92 (s, 2H), 7.50–7.42 (m, 1H), 7.51–7.27 (m, 5H), 4.78 (s, 2H), 3.80 (t, *J* = 6.7 Hz, 2H), 1.98 (t, *J* = 7.2 Hz, 2H), 1.72–1.60 (m, 2H), 1.59–1.49 (m, 2H), 1.39–1.27 (m, 2H) ppm. ¹³C NMR (151 MHz, DMSO-*d*₆) δ = 169.2, 157.0, 148.5, 144.3, 137.1, 136.0, 135.1, 129.0, 128.7, 128.2, 128.1, 123.9, 121.5, 114.5, 76.7,

75.7, 32.1, 27.1, 24.7, 24.7 ppm. Anal. Calcd for C₂₃H₂₆N₄; C 65.39, H 6.20, N 13.26. Found: C 65.11, H 6.11, N 13.01.

***N*-(Benzyloxy)-6-((3-(quinolin-8-yl)ureido)oxy)hexanamide (6e).** Colorless solid; yield 77%; mp 94 °C. ¹H NMR (600 MHz, DMSO-*d*₆) δ = 10.97 (s, 1H), 9.97 (s, 1H), 9.92 (s, 1H), 8.90 (d, *J* = 2.9 Hz, 1H), 8.49 (d, *J* = 7.5 Hz, 1H), 8.40 (d, *J* = 7.1 Hz, 1H), 7.66–7.52 (m, 3H), 7.43–7.30 (m, 5H), 4.77 (s, 2H), 3.89 (t, *J* = 6.3 Hz, 2H), 2.00 (t, *J* = 7.2 Hz, 2H), 1.74–1.64 (m, 2H), 1.62–1.51 (m, 2H), 1.51–1.42 (m, 2H) ppm. ¹³C NMR (151 MHz, DMSO-*d*₆) δ = 169.2, 156.3, 148.7, 137.6, 136.5, 136.0, 134.4, 128.7, 128.2, 128.1, 127.7, 127.0, 122.1, 120.4, 114.1, 76.7, 76.0, 32.0, 27.4, 24.9, 24.7 ppm. Anal. Calcd for C₂₃H₂₆N₄; C 65.39, H 6.20, N 13.26. Found: C 65.34, H 6.05, N 13.23.

***N*-(Benzyloxy)-6-((3-(2-methylquinolin-8-yl)ureido)oxy)hexanamide (6f).** Colorless solid; yield 89%; mp 110 °C. ¹H NMR (600 MHz, DMSO-*d*₆) δ = 10.93 (s, 1H), 9.96 (s, 1H), 9.93 (s, 1H), 8.44 (dd, *J* = 7.7, 1.4 Hz, 1H), 8.27 (d, *J* = 8.4 Hz, 1H), 7.56–7.44 (m, 3H), 7.39–7.29 (m, 5H), 4.75 (s, 2H), 3.89 (t, *J* = 6.5 Hz, 2H), 2.70 (s, 3H), 1.96 (t, *J* = 7.3 Hz, 2H), 1.78–1.70 (m, 2H), 1.60–1.52 (m, 2H), 1.47–1.39 (m, 2H) ppm. ¹³C NMR (151 MHz, DMSO-*d*₆) δ = 168.7, 156.7, 155.9, 136.4, 136.1, 135.5, 133.3, 128.2, 127.7, 127.6, 125.5, 125.4, 122.2, 119.7, 113.5, 76.1, 75.5, 31.5, 27.0, 24.4, 24.3, 24.2 ppm. Anal. Calcd for C₂₄H₂₈N₄; C 66.04, H 6.47, N 12.84. Found: C 66.07, H 6.33, N 12.77.

***N*-(Benzyloxy)-6-((3-(6-methoxyquinolin-8-yl)ureido)oxy)hexanamide (6g).** Colorless solid; yield 91%; mp 102 °C. ¹H NMR (600 MHz, DMSO-*d*₆) δ = 10.96 (s, 1H), 10.02 (s, 1H), 9.86 (s, 1H), 8.75–8.66 (m, 1H), 8.27 (dd, *J* = 8.3, 1.7 Hz, 1H), 8.15 (d, *J* = 2.8 Hz, 1H), 7.59–7.52 (m, 1H), 7.41–7.31 (m, 5H), 7.01 (d, *J* = 2.8 Hz, 1H), 4.78 (s, 2H), 3.96–3.81 (m, 5H), 2.00 (t, *J* = 7.5 Hz, 2H), 1.76–1.64 (m, 2H), 1.64–1.52 (m, 2H), 1.53–1.41 (m, 2H) ppm. ¹³C NMR (151 MHz, DMSO-*d*₆) δ = 169.2, 157.6, 156.2, 146.0, 136.0, 135.4, 135.3, 134.2, 128.9, 128.7, 128.2, 128.1, 122.5, 106.5, 98.5, 76.7, 76.0, 55.4, 32.0, 27.4, 24.9, 24.7 ppm. Anal. Calcd for C₂₄H₂₈N₄; C 63.70, H 6.24, N 12.38. Found: C 63.41, H 6.09, N 12.23.

***N*-(Benzyloxy)-6-((3-(6-methoxy-4-methylquinolin-8-yl)ureido)oxy)hexanamide (6h).** Colorless solid; yield 78%; mp 110 °C. ¹H NMR (600 MHz, DMSO-*d*₆) δ = 10.95 (s, 1H), 9.99 (s, 1H), 9.95 (s, 1H), 8.56 (d, *J* = 4.2 Hz, 1H), 8.15 (d, *J* = 2.6 Hz, 1H), 7.50–7.26 (m, 6H), 6.95 (d, *J* = 2.6 Hz, 1H), 4.76 (s, 2H), 3.91 (s, 3H), 3.86 (t, *J* = 6.3 Hz, 2H), 2.65 (s, 3H), 1.98 (t, *J* = 6.2 Hz, 2H), 1.75–1.62 (m, 2H), 1.61–1.51 (m, 2H), 1.51–1.40 (m, 2H) ppm. ¹³C NMR (151 MHz, DMSO-*d*₆) δ = 169.2, 157.5, 156.2, 145.5, 143.4, 136.0, 135.8, 133.8, 128.7, 128.5, 128.2, 128.1, 123.0, 106.0, 95.2, 76.6, 76.0, 55.4, 32.0, 27.4, 24.9, 24.7, 18.4 ppm. Anal. Calcd for C₂₅H₃₀N₄; C 64.36, H 6.48, N 12.01. Found: C 64.13, H 6.43, N 12.15.

***N*-(Benzyloxy)-6-((3-(2,6-dimethoxy-4-methylquinolin-8-yl)ureido)oxy)hexanamide (6i).** Colorless solid; yield 84%; mp 132 °C. ¹H NMR (600 MHz, DMSO-*d*₆) δ = 10.95 (s, 1H), 9.94 (s, 1H), 9.58 (s, 1H), 8.13 (d, *J* = 2.7 Hz, 1H), 7.42–7.30 (m, 5H), 6.93 (s, 1H), 6.90 (d, *J* = 2.8 Hz, 1H), 4.77 (s, 2H), 3.98 (s, 3H), 3.88 (m, 3.91–3.85, 5H), 2.57 (s, 3H), 1.96 (t, *J* = 7.3 Hz, 2H), 1.69–1.61 (m, 2H), 1.56–1.48 (m, 2H), 1.37–1.28 (m, 2H) ppm. ¹³C NMR (151 MHz, DMSO-*d*₆) δ = 169.1, 159.2, 156.3, 155.7, 147.2, 136.0, 134.1, 130.7, 128.7, 128.2, 128.1, 125.0, 113.0, 106.2, 96.5, 76.7, 75.8, 55.2, 52.6, 32.0, 27.5, 24.7, 18.4 ppm. Anal. Calcd for C₂₆H₃₂N₄; C 62.89, H 6.50, N 11.28. Found: C 62.67, H 6.44, N 11.03.

***N*-(Benzyloxy)-6-((3-(2-isopropoxy-6-methoxy-4-methyl-5-(3-(trifluoromethyl)phenoxy)quinolin-8-yl)ureido)oxy)hexanamide (6j).** Colorless solid; yield 83%; mp 109 °C. ¹H NMR (600 MHz, DMSO-*d*₆) δ = 10.95 (s, 1H), 10.01 (s, 1H), 9.67 (s, 1H), 8.56 (s, 1H), 7.52 (t, *J* = 8.1 Hz, 1H), 7.45–7.25 (m, 6H), 7.11 (s, 1H), 7.03 (dd, *J* = 8.5, 2.6 Hz, 1H), 6.84 (s, 1H), 5.44 (sept, *J* = 6.2 Hz, 1H), 4.78 (s, 2H), 3.90 (t, *J* = 6.9 Hz, 2H), 3.74 (s, 3H), 2.52 (s, 3H), 1.98 (t, *J* = 7.2 Hz, 2H), 1.73–1.64 (m, 2H), 1.62–1.47 (m, 2H), 1.39 (d, *J* = 9.5 Hz, 6H), 1.37–1.30 (m, 2H) ppm. ¹³C NMR (151 MHz, DMSO-*d*₆) δ = 169.2, 158.7, 158.6, 156.4, 147.4, 146.2, 136.1, 132.0, 131.1, 131.1, 130.4 (q, *J* = 31.93 Hz), 130.4, 128.7, 128.2, 128.1, 123.8 (q, *J* = 272.79 Hz), 119.4, 118.6, 118.2, 116.3, 111.3, 103.7, 76.7, 75.8, 67.8, 56.3, 32.1, 27.5, 24.7, 24.7, 22.2, 21.6 ppm. Anal. Calcd for C₃₅H₃₉N₄; C 61.40, H 5.74, N 8.18. Found: C 61.21, H 5.68, N 8.03.

N-(Benzyloxy)-6-((1,3-dioxoisindolin-2-yl)oxy)-N-methylhexanamide (7). Sodium hydride (0.52 g, 13.4 mmol, 60% dispersion in mineral oil) was added in portions to 4.59 g (12 mmol) of N-(benzyloxy)-6-((1,3-dioxoisindolin-2-yl)oxy)hexanamide (3) in 115 mL of THF followed by dropwise addition of methyl iodide (0.84 mL, 13.4 mmol). The reaction was stirred overnight at room temperature before it was quenched with a saturated solution of NH_4Cl (100 mL) and extracted with ethyl acetate (3×100 mL). The organic layer was dried over Na_2SO_4 , filtered, and the solvent was removed in vacuo. The crude products were purified by flash column chromatography (prepacked silica cartridge, *n*-hexane/ethyl acetate, gradient 90:10 \rightarrow 50:50 in 0.5 h) to give the intermediate N-(benzyloxy)-6-((1,3-dioxoisindolin-2-yl)oxy)-N-methylhexanamide 7 in 92% yield.²⁵

N-(Benzyloxy)-6-((1,3-dioxoisindolin-2-yl)oxy)-N-methylhexanamide (7). Oil; yield 59%. ^1H NMR (500 MHz, $\text{DMSO}-d_6$) δ = 7.86 (s, 4H), 7.52–7.30 (m, 5H), 4.89 (s, 2H), 4.11 (t, J = 6.5 Hz, 2H), 3.14 (s, 3H), 2.34 (t, J = 7.3 Hz, 2H), 1.71–1.58 (m, 2H), 1.57–1.44 (m, 2H), 1.44–1.34 (m, 2H) ppm. ^{13}C NMR (125 MHz, $\text{DMSO}-d_6$) δ = 163.2, 134.6, 129.4, 128.6, 128.5, 128.4, 123.1, 77.5, 75.1, 31.1, 31.1, 27.4, 24.8, 23.6 ppm. HPLC analysis: retention time = 3.1 min; peak area, 95.34%. Method: eluent A, 5 mM/L (385 mg/L) ammonium acetate; eluent B, HPLC-grade CH_3CN ; linear gradient of 5% B to 95% B over 20 min at a flow rate of 1.0 mL min^{-1} .

6-(Aminoxy)-N-(benzyloxy)-N-methylhexanamide (8). Synthesized from 7 according to the procedure for 4.¹⁴ Oil; yield 62%. ^1H NMR (500 MHz, $\text{DMSO}-d_6$) δ = 7.54–7.30 (m, 5H), 5.86 (s, 2H), 4.87 (s, 2H), 3.47 (t, J = 6.5 Hz, 2H), 3.13 (s, 3H), 2.30 (t, J = 7.5 Hz, 2H), 1.60–1.36 (m, 4H), 1.31–1.13 (m, 2H). ^{13}C NMR (151 MHz, $\text{DMSO}-d_6$) δ = 173.7, 134.8, 129.4, 128.6, 128.4, 75.1, 74.7, 32.7, 31.2, 27.7, 25.3, 23.9 ppm. Anal. Calcd for $\text{C}_{14}\text{H}_{22}\text{N}_2$: C 63.13, H 8.33, N 10.52. Found: C 63.11, H 8.60, N 10.39.

N-(Benzyloxy)-N-methyl-6-(3-naphthalen-1-ylureidoxy)hexanamide (9). Synthesized from 8 according to the literature.¹⁴ A solution of 1-naphthyl isocyanate (2.7 mmol) in dry CH_2Cl_2 (5 mL) was added dropwise to a solution of the aminoxy derivative 8 (3 mmol) in dry CH_2Cl_2 (15 mL). The reaction mixture was stirred overnight at room temperature and subsequently treated with petroleum ether to precipitate the product. The resulting solid was collected, washed with petroleum ether (5 mL), and dried in vacuo.

N-(Benzyloxy)-N-methyl-6-(3-naphthalen-1-ylureidoxy)hexanamide (9). Oil; yield 59%. ^1H NMR (500 MHz, $\text{DMSO}-d_6$) δ = 9.55 (s, 1H), 8.82 (s, 1H), 7.95–7.91 (m, 2H), 7.75 (d, J = 8.18, 1H), 7.63 (d, J = 7.20 Hz, 1H), 7.57–7.34 (m, 8H), 4.87 (s, 2H), 3.86 (t, J = 6.69, 2H), 3.12 (s, 3H), 2.35 (t, J = 7.37 Hz, 2H), 1.71–1.61 (m, 2H), 1.78–1.70 (m, 2H), 1.56–1.44 (m, 2H), 1.34–1.25 (m, 2H) ppm. ^{13}C NMR (151 MHz, $\text{DMSO}-d_6$) δ = 170.2, 157.9, 134.8, 133.6, 133.6, 129.4, 128.6, 128.4, 128.3, 128.0, 125.8, 125.7, 125.5, 124.7, 122.3, 121.6, 75.7, 75.0, 31.2, 27.4, 25.0, 23.8 ppm. Anal. Calcd for $\text{C}_{25}\text{H}_{29}\text{N}_3$: C 68.95, H 6.71, N 9.65. Found: C 68.75, H 6.89, N 9.20.

Amine Precursors. The amine intermediates and their precursors were synthesized according to established literature methods or were obtained from commercial suppliers. 2-Naphthylamine, 6-aminoquinoline, 8-aminoquinoline, and 2-methyl-8-nitroquinoline were obtained from commercial suppliers (Sigma-Aldrich, TCI, Alfa Aesar) and used as purchased without further purification. 8-Amino-2-methylquinoline was synthesized from 2-methyl-8-nitroquinoline.²⁶ The known intermediates 6-methoxy-4-methylquinolin-8-amine, 6-methoxyquinolin-8-amine, and 2,6-dimethoxy-4-methylquinolin-8-amine and their precursors were synthesized according to established literature methods.²⁶ The novel 2-isopropoxy-6-methoxy-4-methyl-5-(3-(trifluoromethyl)phenoxy)quinolin-8-amine was synthesized according to known procedures.²⁶

2-Isopropoxy-6-methoxy-4-methyl-8-nitro-5-(3-(trifluoromethyl)phenoxy)quinoline. A solution of the respective phenol (16.3 mmol) in DMSO (15 mL) and potassium hydroxide (0.92 g, 16.3 mmol) was heated to 100 °C for 0.5 h. The respective 2-alkoxy-5-chloro-6-methoxy-4-methyl-8-nitroquinoline (14.2 mmol) was added in one portion. The resulting dark solution was stirred at 100 °C for 2.5 h. Water (30 mL) was added slowly while keeping the temperature above 60 °C. The resulting suspension was cooled to 10 °C. The crude product

was separated by suction filtration, washed with water, and dried. The residue was then suspended in toluene (125 mL), heated to reflux in the presence of activated charcoal, and filtered through kieselgur. Toluene (100 mL) was removed by distillation at ambient pressure. The solution was cooled to 70 °C, and *n*-hexane was added (100 mL). The resulting suspension was cooled to 5 °C. The product was separated by suction filtration and washed with *n*-hexane.

2-Isopropoxy-6-methoxy-4-methyl-8-nitro-5-(3-(trifluoromethyl)phenoxy)quinoline. Yellow solid; yield 64%; mp 155 °C. ^1H NMR (500 MHz, CDCl_3) δ = 7.75 (s, 1H), 7.40 (dd, $J_1 = J_2 = 8.0$ Hz, 1H), 7.32 (d, $J = 7.7$ Hz, 1H), 7.09 (s, 1H), 6.93 (d, $J = 8.2$ Hz, 1H), 6.72 (s, 1H), 5.41 (sept, $J = 6.2$ Hz, 1H), 3.80 (s, 3H), 2.61 (s, 3H), 1.39 (d, $J = 6.2$ Hz, 6H) ppm. ^{13}C NMR (125 MHz, CDCl_3) δ = 161.7, 157.9, 146.2, 145.8, 144.4, 140.8, 135.2, 132.3 (q, $J = 32.7$ Hz), 130.4, 123.7 (q, $J = 273.2$ Hz), 121.7, 119.2 (q, $J = 3.6$ Hz), 118.2, 118.0, 112.2 (q, $J = 3.5$ Hz), 111.2, 69.4, 57.0, 23.1, 21.8. Anal. Calcd for $\text{C}_{21}\text{H}_{19}\text{F}_3\text{N}_2\text{O}_5$: C 57.80, H 4.39, N 6.42. Found: C 57.65, H 4.66, N 6.45.

2-Isopropoxy-6-methoxy-4-methyl-5-(3-(trifluoromethyl)phenoxy)quinoline-8-amine. The respective 8-nitroquinoline (3.7 mmol) and Pd–C (10%) were suspended in dry ethanol (50 mL). The reaction mixture was heated to 60 °C, and then hydrazine hydrate (0.93 g, 18.5 mmol) was added dropwise over 15 min. The reaction mixture was stirred at 60 °C for 4 h, then heated under reflux for 0.5 h. After cooling to 50 °C, Pd–C was removed by filtration through kieselgur and washed with ethanol (20 mL). After cooling to room temperature, water (50 mL) was added slowly under vigorous stirring over 0.5 h. The resulting slurry was cooled to 5 °C, filtered, and the residue was washed with a mixture of ethanol/ H_2O (1:1).

2-Isopropoxy-6-methoxy-4-methyl-5-(3-(trifluoromethyl)phenoxy)quinoline-8-amine. Colorless solid; yield 44%; mp 91 °C. ^1H NMR (500 MHz, CDCl_3) δ = 7.33 (dd, $J_1 = J_2 = 8.0$ Hz, 1H), 7.21 (d, $J = 7.7$ Hz, 1H), 7.05 (s, 1H), 6.94 (dd, $J = 8.2, 2.0$ Hz, 1H), 6.77 (s, 1H), 6.61 (s, 1H), 5.46 (sept, $J = 6.2$ Hz, 1H), 4.69 (s, 2H), 3.75 (s, 3H), 2.54 (s, 3H), 1.41 (d, $J = 6.2$ Hz, 6H) ppm. ^{13}C NMR (126 MHz, CDCl_3) δ = 159.6, 158.9, 148.2, 146.0, 141.1, 131.9 (q, $J = 32.6$ Hz), 131.3, 130.0, 128.6, 123.9 (q, $J = 272.3$ Hz), 120.6, 118.2, 118.0 (q, $J = 3.8$ Hz), 116.4, 112.0 (q, $J = 3.7$ Hz), 99.3, 67.8, 56.7, 23.0, 22.0 ppm. Anal. Calcd for $\text{C}_{21}\text{H}_{21}\text{F}_3\text{N}_2\text{O}_3$: C 62.06, H 5.21, N 6.89. Found: C 62.01, H 5.60, N 6.80.

Molecular Modeling. Docking Studies. For the molecular docking, compounds 1a, 1g, 1h, and 1i were drawn with ChemDraw Ultra,²⁷ converted into a 3D structure, and energy minimized with Moloc using the MAB force field.²⁸ The HDACi were then docked into crystal structures of HDAC1 (PDB code 4BKX²⁹), HDAC4 (PDB code 4CBT³⁰), and HDAC8 (PDB code 4RNO³¹) and into a homology model of HDAC6, which was already successfully used by us to predict HDACi binding mode models,¹⁶ utilizing AutoDock3³² as a docking engine and the DrugScore³³ distance-dependent pair-potentials as an objective function, as described in ref 20. In the docking, default parameters were used with the exception of the clustering rmsd cutoff, which was set to 2.0 Å, to consider the flexibly connected saturated and unsaturated carbon cycles. Docking solutions with more than 20% of all configurations in the largest cluster were considered sufficiently converged. The configuration in the largest cluster with the lowest docking energy and with a distance of <3 Å between the hydroxamic acid oxygen and the zinc ion in the binding pocket was used for further evaluation.

Biological Evaluation. Reagents. Cisplatin was purchased from Sigma (Germany), propidium iodide (PI) was purchased from Santa Cruz Biotechnology (Germany), and tubastatin A and entinostat were purchased from Selleckchem (Germany). Vorinostat was synthesized according to known procedures.³⁴ All other reagents were supplied by PAN Biotech (Germany) unless otherwise stated.

Cell Lines and Cell Culture. The human ovarian carcinoma cell line A278 was obtained from European Collection of Cell Cultures (ECACC, Salisbury, U.K.). The human tongue cell line Cal27 was obtained from the German Collection of Microorganisms and Cell Cultures (DSMZ, Germany). The corresponding cisplatin resistant CisR cell lines were generated by exposing the parental cell lines to

weekly cycles of cisplatin in an IC_{50} concentration over a period of 24–30 weeks as described in Gosepath et al.³⁵ and Eckstein et al.³⁶ The human medulloblastoma cell lines ONS76 and Med8a were a kind gift of the KMT laboratory (Department of Pediatric Oncology, Hematology and Clinical Immunology, Heinrich Heine University Düsseldorf, Germany).

All cell lines were grown at 37 °C under humidified air supplemented with 5% CO_2 in RPMI 1640 (A2780) or DMEM (Cal27, ONS76, Med8a) containing 10% fetal calf serum, 120 IU/mL penicillin, and 120 μ g/mL streptomycin. The cells were grown to 80% confluency before using them for the appropriate assays.

In Vitro Testing of HDAC1, -6, and -8.³⁷ OptiPlate-96 black microplates (PerkinElmer) were used with an assay volume of 60 μ L. Human recombinant HDAC1 (BPS Bioscience, catalog no. S0051) or human recombinant HDAC6 (BPS Bioscience, catalog no. S0006) was diluted in incubation buffer (50 mM Tris-HCl, pH 8.0, 137 mM NaCl, 2.7 mM KCl, 1 mM $MgCl_2$, and 1 mg/mL BSA). An amount of 52 μ L of this dilution was incubated with 3 μ L of different concentrations of inhibitors in DMSO and 5 μ L of the fluorogenic substrate ZMAL (Z-(Ac)Lys-AMC)³⁸ (126 μ M) at 37 °C. After a 90 min incubation time 60 μ L of the stop solution (33 μ M trichostatin A (TSA) and 6 mg/mL trypsin in trypsin buffer (Tris-HCl 50 mM, pH 8.0, NaCl 100 mM)) were added. After a following incubation at 37 °C for 30 min, the fluorescence was measured on a BMG LabTech POLARstar OPTIMA plate reader (BMG LabTech, Germany) with an excitation wavelength of 390 nm and an emission wavelength of 460 nm. For the inhibition of human HDAC8 1/2-AREAPLATE-96 F microplates (PerkinElmer) with an assay volume of 30 μ L were used. Human HDAC8 enzyme was obtained as described before.³⁹ An amount of 22.5 μ L of enzyme diluted in incubation buffer (50 mM KH_2PO_4 , 15 mM Tris, pH 7.5, 3 mM $MgSO_4 \cdot 7 H_2O$, 10 mM KCl) was mixed with 2.5 μ L of inhibitor in DMSO and 5 μ L of Z-Lys(*ε*-trifluoroacetyl)-AMC (150 μ M). The plate was incubated at 37 °C for 90 min. An amount of 30 μ L of the stop solution (see HDAC1 and HDAC6) was added, and the plate was incubated again at 37 °C for 30 min. Measurement was performed as described for HDAC1/6.

In Vitro Testing of HDAC4. The in vitro inhibitory activity of compounds 1a and Ig-i against HDAC4 isoform was performed at Reaction Biology Corp. (Malvern, PA) with a fluorescent based assay according to the company's standard operating procedure. The IC_{50} values were determined using 10 different concentrations with 3-fold serial dilution. TMP269 was used as reference compound.

MTT Cell Viability Assay. The rate of cell survival under the action of test substances was evaluated by an improved MTT assay as previously described.^{14,40} The assay is based on the ability of viable cells to metabolize yellow 3-(4,5-dimethylthiazol-2-yl)-2,5-diphenyl-tetrazolium bromide (MTT, Serva, Germany) to violet formazan that can be detected spectrophotometrically. In brief, A2780 and Cal27 cell lines were seeded at a density of 5000 and 2500 cells/well in 96-well plates (Corning, Germany). After 24 h, cells were exposed to increased concentrations of the test compounds. Incubation was ended after 72 h, and cell survival was determined by addition of MTT solution (5 mg/mL in phosphate buffered saline). The formazan precipitate was dissolved in DMSO (VWR, Germany). Absorbance was measured at 544 and 690 nm in a FLUOstar microplate reader (BMG LabTech, Offenburg, Germany).

CellTiter-Glo Luminescent Cell Viability Assay. ONS76 and Med8a were seeded at a density of 1000 and 2000 cells/well in 384-well plates (Corning) and incubated with increasing concentrations of the test compounds. After 72 h the Celltiter Glo reagent was added, and after shaking the plates for 2 min and a subsequent incubation time of 10 min the luminescent signals were read on a Spark 10M microplate reader (Tecan).

Combination Experiments. For the investigation of the effect of Ig-i on cisplatin induced cytotoxicity, the compounds were added 48 h before cisplatin administration. After 72 h, the cytotoxic effect was determined with a MTT cell viability assay. Calcsyn software 2.1 (Biosoft, U.K.) was used to calculate the combination index (CI) as a quantitative measure of the degree of drug interactions.

Whole-Cell HDAC Inhibition Assay. The cellular HDAC assay was based on an assay published by Ciossek et al.⁴¹ and Bonfils et al.⁴² with minor modifications as described in ref 14. Briefly, human cancer cell lines Cal27/Cal27CisR and A2780/A2780CisR were seeded in 96-well tissue culture plates (Corning, Germany) at a density of 1.5×10^4 cells/well in a total volume of 90 μ L of culture medium. After 24 h, cells were incubated for 18 h with increasing concentrations of test compounds. The reaction was started by adding 10 μ L of 3 mM Boc-Lys(*ε*-Ac)-AMC (Bachem, Germany) to reach a final concentration of 0.3 mM.⁴³ The cells were incubated with the Boc-Lys(*ε*-Ac)-AMC for 3 h under cell culture conditions. After this incubation, 100 μ L/well stop solution (25 mM Tris-HCl (pH 8), 137 mM NaCl, 2.7 mM KCl, 1 mM $MgCl_2$, 1% NP40, 2.0 mg/mL trypsin, 10 μ M vorinostat) was added and the reaction was developed for 3 h under cell culture conditions. Fluorescence intensity was measured at excitation of 320 nm and emission of 520 nm in a NOVOstar microplate reader (BMG LabTech, Offenburg, Germany).

Measurement of Apoptotic Cells. Cal27 and Cal27CisR cells were seeded at a density of 3×10^4 cells/well in 24-well plates (Sarstedt, Germany). Cells were treated with Ig-i and cDDP alone or in combination for the indicated time points. Supernatant was removed after a centrifugation step, and the cells were lysed in 500 μ L of hypotonic lysis buffer (0.1% sodium citrate, 0.1% Triton X-100, 100 μ g/mL PI) at 4 °C in the dark overnight. The percentage of apoptotic nuclei with DNA content in sub-G1 was analyzed by flow cytometry using the CyFlow instrument (Partec, Germany).

Immunoblotting. Cells were treated with 1 μ M Ig-i or vehicle for 24 h. The pan-HDACi vorinostat and the HDAC1 and -3 selective inhibitor entinostat were used as controls. Cell pellets were dissolved with lysis buffer 6 (Bio-Techne, Germany) and clarified by centrifugation. Equal amounts of total protein (20 μ g) were resolved by SDS-PAGE and transferred to polyvinylidene fluoride membranes. Blots were incubated with primary antibodies against acetylated α -tubulin, α -tubulin, and acetyl histone H3 (Lys24) (Santa Cruz Biotechnology, Germany). Immunoreactive proteins were visualized using luminol reagent (Santa Cruz Biotechnology, Heidelberg, Germany) with an Intas imager (Intas, Germany). Densitometric analysis was performed on scanned images using the ImageJ software (National Institutes of Health).⁴⁴

Data Analysis. Concentration–effect curves were constructed with Prism 4.0 (GraphPad, San Diego, CA) by fitting the pooled data of at least three experiments performed in triplicates to the four-parameter logistic equation. Statistical analysis was performed using *t* test or one-way ANOVA.

■ ASSOCIATED CONTENT

● Supporting Information

The Supporting Information is available free of charge on the ACS Publications website at DOI: 10.1021/acs.jmedchem.6b01538.

Coordinates information for structure representation (PDB)

Molecular formula strings and some data (CSV)

Characterization data of compounds 1c–j and 6c–j and of the precursors and general procedures (PDF)

■ AUTHOR INFORMATION

Corresponding Authors

*M.U.K.: phone, +49 211 81-14587; fax, +49 211 81-13847; e-mail, Matthias.kassack@uni-duesseldorf.de.

*T.K.: phone, +49 211 81-14984; fax, +49 211 81-13847; e-mail, Thomas.kurz@uni-duesseldorf.de.

ORCID

Finn K. Hansen: 0000-0001-9765-5975

Manfred Jung: 0000-0002-6361-7716

Holger Gohlke: 0000-0001-8613-1447

Thomas Kurz: 0000-0002-9474-4224

Author Contributions

○K.S. and A.H. contributed equally to this work.

Author Contributions

◆M.U.K. and T.K. share the senior authorship.

Notes

The authors declare no competing financial interest.

‡L.M. passed away on October 20, 2011.

Authors will release the atomic coordinates and experimental data upon article publication.

ACKNOWLEDGMENTS

The authors thank the COST Action CM1406 (Epigenetic Chemical Biology EPICHEMBO) for support. J.S. and M.J. thank the Deutsche Forschungsgemeinschaft (DFG, Grant Ju295/13-1) for funding. V.M. thanks the Duesseldorf School of Oncology (funded by the Comprehensive Cancer Center Duesseldorf/Deutsche Krebshilfe and the Medical Faculty HHU Duesseldorf) for funding. This work was supported by institutional funds from the Centre National de la Recherche Scientifique (CNRS), the Institute National de la Santé et de la Recherche Médicale (INSERM), and the Université de Strasbourg. The Deutsche Forschungsgemeinschaft (DFG) is acknowledged for funds used to purchase the UHR-TOF maxIS 4G, Bruker Daltonics, Bremen HRMS instrument used in this research.

ABBREVIATIONS USED

CisR, cisplatin resistant subclone; HDAC, histone deacetylase; HDACi, histone deacetylase inhibitors; MTT, 3-(4,5-dimethylthiazol-2-yl)-2,5-diphenyltetrazolium bromide; Pd/C, palladium on activated carbon; rt, room temperature; THF, tetrahydrofuran

REFERENCES

- (1) Falkenberg, K. J.; Johnstone, R. W. Histone deacetylases and their inhibitors in cancer, neurological diseases and immune disorders. *Nat. Rev. Drug Discovery* **2014**, *13*, 673–691.
- (2) Seto, E.; Yoshida, M. Erasers of histone acetylation: the histone deacetylase enzymes. *Cold Spring Harbor Perspect. Biol.* **2014**, *6*, a018713.
- (3) (a) Wagner, J. M.; Hackanson, B.; Lubbert, M.; Jung, M. Histone deacetylase (HDAC) inhibitors in recent clinical trials for cancer therapy. *Clin. Epigenet.* **2010**, *1*, 117–136. (b) Keller, K.; Jung, M. Histone deacetylase (HDAC) inhibitors in recent clinical trials for cancer therapy. In *Epigenetic Therapy of Cancer Preclinical Models and Treatment Approaches*, 1st ed.; Lubbert, M., Jones, P. A., Eds.; Springer-Verlag: Berlin, 2014; pp 227–255, DOI: 10.1007/978-3-642-38404-2_10.
- (4) (a) Prince, H. M.; Bishton, M. J.; Johnstone, R. W. Panobinostat (LBH589): a potent pan-deacetylase inhibitor with promising activity against hematologic and solid tumors. *Future Oncol.* **2009**, *5*, 601–612. (b) Garnock-Jones, K. P. Panobinostat: first global approval. *Drugs* **2015**, *75*, 695–704.
- (5) Shi, Y.; Dong, M.; Hong, X.; Zhang, W.; Feng, J.; Zhu, J.; Yu, L.; Ke, X.; Huang, H.; Shen, Z.; Fan, Y.; Li, W.; Zhao, X.; Qi, J.; Huang, H.; Zhou, D.; Ning, Z.; Lu, X. Results from a multicenter, open-label, pivotal phase II study of chidamide in relapsed or refractory peripheral T-cell lymphoma. *Ann. Oncol.* **2015**, *26*, 1766–1771.
- (6) (a) Rasmussen, T. A.; Schmeltz Sogaard, O.; Brinkmann, C.; Wightman, F.; Lewin, S. R.; Melchjorsen, J.; Dinarello, C.; Ostergaard, L.; Tolstrup, M. Comparison of HDAC inhibitors in clinical development: effect on HIV production in latently infected cells and T-cell activation. *Hum. Vaccines Immunother.* **2013**, *9*, 993–1001.

(b) Azzi, A.; Cosseau, C.; Grunau, C. Schistosoma mansoni: developmental arrest of miracidia treated with histone deacetylase inhibitors. *Exp. Parasitol.* **2009**, *121*, 288–291. (c) Hansen, F. K.; Skinner-Adams, T. S.; Duffy, S.; Marek, L.; Sumanadasa, S. D.; Kuna, K.; Held, J.; Avery, V. M.; Andrews, K. T.; Kurz, T. Synthesis, antimalarial properties, and SAR studies of alkoxyurea-based HDAC inhibitors. *ChemMedChem* **2014**, *9*, 665–670. (d) Hansen, F. K.; Sumanadasa, S. D.; Stenzel, K.; Duffy, S.; Meister, S.; Marek, L.; Schmetter, R.; Kuna, K.; Hamacher, A.; Mordmuller, B.; Kassack, M. U.; Winzeler, E. A.; Avery, V. M.; Andrews, K. T.; Kurz, T. Discovery of HDAC inhibitors with potent activity against multiple malaria parasite life cycle stages. *Eur. J. Med. Chem.* **2014**, *82*, 204–213. (e) Trenholme, K.; Marek, L.; Duffy, S.; Pradel, G.; Fisher, G.; Hansen, F. K.; Skinner-Adams, T. S.; Butterworth, A.; Ngwa, C. J.; Moecking, J.; Goodman, C. D.; McFadden, G. L.; Sumanadasa, S. D.; Fairlie, D. P.; Avery, V. M.; Kurz, T.; Andrews, K. T. Lysine acetylation in sexual stage malaria parasites is a target for antimalarial small molecules. *Antimicrob. Agents Chemother.* **2014**, *58*, 3666–3678.

(7) Micelli, C.; Rastelli, G. Histone deacetylases: structural determinants of inhibitor selectivity. *Drug Discovery Today* **2015**, *20*, 718–735.

(8) Kim, K. P.; Park, S. J.; Kim, J. E.; Hong, Y. S.; Lee, J. L.; Bae, K. S.; Cha, H.; Kwon, S. K.; Ro, S.; Cho, J.; Kim, T. W. First-in-human study of the toxicity, pharmacokinetics, and pharmacodynamics of CG200745, a pan-HDAC inhibitor, in patients with refractory solid malignancies. *Invest. New Drugs* **2015**, *33*, 1048–1057.

(9) (a) Andreu-Vieyra, C. V.; Berenson, J. R. The potential of panobinostat as a treatment option in patients with relapsed and refractory multiple myeloma. *Ther. Adv. Hematol.* **2014**, *5*, 197–210. (b) Ganai, S. A. Novel approaches towards designing of isoform-selective inhibitors against class II histone deacetylases: The acute requirement for targeted anticancer therapy. *Curr. Top. Med. Chem.* **2016**, *16*, 2441–2452.

(10) (a) Stiborova, M.; Eckschlager, T.; Poljakova, J.; Hrabeta, J.; Adam, V.; Kizek, R.; Frei, E. The synergistic effects of DNA-targeted chemotherapeutics and histone deacetylase inhibitors as therapeutic strategies for cancer treatment. *Curr. Med. Chem.* **2012**, *19*, 4218–4238. (b) Ong, P. S.; Wang, X. Q.; Lin, H. S.; Chan, S. Y.; Ho, P. C. Synergistic effects of suberoylanilide hydroxamic acid combined with cisplatin causing cell cycle arrest independent apoptosis in platinum-resistant ovarian cancer cells. *Int. J. Oncol.* **2012**, *40*, 1705–1713.

(11) Santo, L.; Hideshima, T.; Kung, A. L.; Tseng, J. C.; Tamang, D.; Yang, M.; Jarpe, M.; van Duzer, J. H.; Mazitschek, R.; Ogier, W. C.; Cirstea, D.; Rodig, S.; Eda, H.; Scullen, T.; Canavese, M.; Bradner, J.; Anderson, K. C.; Jones, S. S.; Rajee, N. Preclinical activity, pharmacodynamic, and pharmacokinetic properties of a selective HDAC6 inhibitor, ACY-1215, in combination with bortezomib in multiple myeloma. *Blood* **2012**, *119*, 2579–2589.

(12) (a) Lee, J. H.; Mahendran, A.; Yao, Y.; Ngo, L.; Venta-Perez, G.; Choy, M. L.; Kim, N.; Ham, W. S.; Breslow, R.; Marks, P. A. Development of a histone deacetylase 6 inhibitor and its biological effects. *Proc. Natl. Acad. Sci. U. S. A.* **2013**, *110*, 15704–15719. (b) Goracci, L.; Deschamps, N.; Randazzo, G. M.; Petit, C.; Dos Santos Passos, C.; Carrupt, P. A.; Simoes-Pires, C.; Nurisso, A. A rational approach for the identification of non-hydroxamate HDAC6-selective inhibitors. *Sci. Rep.* **2016**, *6*, 29086. (c) Wagner, F. F.; Olson, D. E.; Gale, J. P.; Kaya, T.; Weiwer, M.; Aidoud, N.; Thomas, M.; Davoine, E. L.; Lemerrier, B. C.; Zhang, Y. L.; Holson, E. B. Potent and selective inhibition of histone deacetylase 6 (HDAC6) does not require a surface-binding motif. *J. Med. Chem.* **2013**, *56*, 1772–1776. (d) Senger, J.; Melesina, J.; Marek, M.; Romier, C.; Oehme, I.; Witt, O.; Sippl, W.; Jung, M. Synthesis and biological investigation of oxazole hydroxamates as highly selective histone deacetylase 6 (HDAC6) inhibitors. *J. Med. Chem.* **2016**, *59*, 1545–1555. (e) Bergman, J. A.; Woan, K.; Perez-Villaruel, P.; Villagra, A.; Sotomayor, E. M.; Kozikowski, A. P. Selective histone deacetylase 6 inhibitors bearing substituted urea linkers inhibit melanoma cell growth. *J. Med. Chem.* **2012**, *55*, 9891–9899. (f) Butler, K. V.; Kalin, J.; Brochier, C.; Vistoli, G.; Langley, B.; Kozikowski, A. P. Rational design and simple chemistry yield a superior, neuroprotective

- HDAC6 inhibitor, tubastatin A. *J. Am. Chem. Soc.* **2010**, *132*, 10842–10856.
- (13) Dallavalle, S.; Pisano, C.; Zunino, F. Development and therapeutic impact of HDAC6-selective inhibitors. *Biochem. Pharmacol.* **2012**, *84*, 756–765.
- (14) Marek, L.; Hamacher, A.; Hansen, F. K.; Kuna, K.; Gohlke, H.; Kassack, M. U.; Kurz, T. Histone deacetylase (HDAC) inhibitors with a novel connecting unit linker region reveal a selectivity profile for HDAC4 and HDAC5 with improved activity against chemoresistant cancer cells. *J. Med. Chem.* **2013**, *56*, 427–436.
- (15) Lobera, M.; Madauss, K. P.; Pohlhaus, D. T.; Wright, Q. G.; Trocha, M.; Schmidt, D. R.; Baloglu, E.; Trump, R. P.; Head, M. S.; Hofmann, G. A.; Murray-Thompson, M.; Schwartz, B.; Chakravorty, S.; Wu, Z.; Mander, P. K.; Kruidenier, L.; Reid, R. A.; Burkhart, W.; Turunen, B. J.; Rong, J. X.; Wagner, C.; Moyer, M. B.; Wells, C.; Hong, X.; Moore, J. T.; Williams, J. D.; Soler, D.; Ghosh, S.; Nolan, M. A. Selective class IIa histone deacetylase inhibition via a nonchelating zinc-binding group. *Nat. Chem. Biol.* **2013**, *9*, 319–325.
- (16) Diedrich, D.; Hamacher, A.; Gertzen, C. G.; Alves Avelar, L. A.; Reiss, G. J.; Kurz, T.; Gohlke, H.; Kassack, M. U.; Hansen, F. K. Rational design and diversity-oriented synthesis of peptoid-based selective HDAC6 inhibitors. *Chem. Commun.* **2016**, *52*, 3219–3222.
- (17) Hai, Y.; Christianson, D. W. Histone deacetylase 6 structure and molecular basis of catalysis and inhibition. *Nat. Chem. Biol.* **2016**, *12*, 741–747.
- (18) Miyake, Y.; Keusch, J. J.; Wang, L.; Saito, M.; Hess, D.; Wang, X.; Melancon, B. J.; Helquist, P.; Gut, H.; Matthias, P. Structural insights into HDAC6 tubulin deacetylation and its selective inhibition. *Nat. Chem. Biol.* **2016**, *12*, 748–754.
- (19) Gohlke, H.; Klebe, G. DrugScore meets CoMFA: adaptation of fields for molecular comparison (AFMoC) or how to tailor knowledge-based pair-potentials to a particular protein. *J. Med. Chem.* **2002**, *45*, 4153–4170.
- (20) Sotriffer, C. A.; Gohlke, H.; Klebe, G. Docking into knowledge-based potential fields: a comparative evaluation of DrugScore. *J. Med. Chem.* **2002**, *45*, 1967–1970.
- (21) (a) Romine, J. L.; Martin, S. W.; Meanwell, N. A.; Epperson, J. R. Synthesis of 3-Hydroxypyrimidine-2,4-diones. Addition of anilines to benzyloxy isocyanate synthons to give N-hydroxyureas. *Synthesis* **1994**, *1994*, 846–850. (b) Khankischpur, M.; Hansen, F. K.; Geffken, D. Convenient synthesis of 5-substituted 2-Amino[1,2,4]triazolo[1,5-a][1,3,5]triazin-7(6H)-ones from N-triazolide imidates and 1,2,4-triazole-3,5-diamine. *Synthesis* **2010**, No. 10, 1645–1648.
- (22) (a) Gaisina, I. N.; Tueckmantel, W.; Ugolkov, A.; Shen, S.; Hoffen, J.; Dubrovskiy, O.; Mazar, A.; Schoon, R. A.; Billadeau, D.; Kozikowski, A. P. Identification of HDAC6-selective inhibitors of low cancer cell cytotoxicity. *ChemMedChem* **2016**, *11*, 81–92. (b) Lienlaf, M.; Perez-Villaruel, P.; Knox, T.; Pabon, M.; Sahakian, E.; Powers, J.; Woan, K. V.; Lee, C.; Cheng, F.; Deng, S.; Smalley, K. S.; Montecino, M.; Kozikowski, A.; Pinilla-Ibarz, J.; Sarnaik, A.; Seto, E.; Weber, J.; Sotomayor, E. M.; Villagra, A. Essential role of HDAC6 in the regulation of PD-L1 in melanoma. *Mol. Oncol.* **2016**, *10*, 735–750.
- (23) Asgar, M. A.; Senawong, G.; Sripa, B.; Senawong, T. Synergistic anticancer effects of cisplatin and histone deacetylase inhibitors (SAHA and TSA) on cholangiocarcinoma cell lines. *Int. J. Oncol.* **2016**, *48*, 409–420.
- (24) Duque-Afonso, J.; Yalcin, A.; Berg, T.; Abdelkarim, M.; Heidenreich, O.; Lubbert, M. The HDAC class I-specific inhibitor entinostat (MS-275) effectively relieves epigenetic silencing of the LAT2 gene mediated by AML1/ETO. *Oncogene* **2011**, *30*, 3062–3072.
- (25) Zingle, C.; Kuntz, L.; Tritsch, D.; Grosdemange-Billiard, C.; Rohmer, R. Isoprenoid biosynthesis via the methylerythritol phosphate pathway: structural variations around phosphonate anchor and spacer of fosmidomycin, a potent inhibitor of deoxyxylulose phosphate reductoisomerase. *J. Org. Chem.* **2010**, *75*, 3203–3207.
- (26) Ugwuegbulam, C. O.; Foy, J. E. Process for the preparation of anti-malarial drugs. US6479660 (B1), 2002.
- (27) Mills, N. ChemDraw Ultra 10.0. *J. Am. Chem. Soc.* **2006**, *128*, 13649–13650 (Computer software review).
- (28) Gerber, P. R.; Muller, K. MAB, a generally applicable molecular force field for structure modelling in medicinal chemistry. *J. Comput.-Aided Mol. Des.* **1995**, *9*, 251–268.
- (29) Millard, C. J.; Watson, P. J.; Celardo, I.; Gordiyenko, Y.; Cowley, S. M.; Robinson, C. V.; Fairall, L.; Schwabe, J. W. Class I HDACs share a common mechanism of regulation by inositol phosphates. *Mol. Cell* **2013**, *51*, 57–67.
- (30) Burli, R. W.; Luckhurst, C. A.; Aziz, O.; Matthews, K. L.; Yates, D.; Lyons, K. A.; Beconi, M.; McAllister, G.; Breccia, P.; Stott, A. J.; Penrose, S. D.; Wall, M.; Lamers, M.; Leonard, P.; Muller, I.; Richardson, C. M.; Jarvis, R.; Stones, L.; Hughes, S.; Wishart, G.; Haughan, A. F.; O'Connell, C.; Mead, T.; McNeil, H.; Vann, J.; Mangette, J.; Maillard, M.; Beaumont, V.; Munoz-Sanjuan, I.; Dominguez, C. Design, synthesis, and biological evaluation of potent and selective class IIa histone deacetylase (HDAC) inhibitors as a potential therapy for Huntington's disease. *J. Med. Chem.* **2013**, *56*, 9934–9954.
- (31) Decroos, C.; Clausen, D. J.; Haines, B. E.; Wiest, O.; Williams, R. M.; Christianson, D. W. Variable active site loop conformations accommodate the binding of macrocyclic largazole analogues to HDAC8. *Biochemistry* **2015**, *54*, 2126–2135.
- (32) (a) Osterberg, F.; Morris, G. M.; Sanner, M. F.; Olson, A. J.; Goodsell, D. S. Automated docking to multiple target structures: incorporation of protein mobility and structural water heterogeneity in AutoDock. *Proteins: Struct., Funct., Genet.* **2002**, *46*, 34–40. (b) Morris, G. M.; Goodsell, D. S.; Halliday, R. S.; Huey, R.; Hart, W. E.; Belew, R. K.; Olson, A. J. Automated docking using a Lamarckian genetic algorithm and an empirical binding free energy function. *J. Comput. Chem.* **1998**, *19*, 1639–1662.
- (33) (a) Radestock, S.; Bohm, M.; Gohlke, H. Improving binding mode predictions by docking into protein-specifically adapted potential fields. *J. Med. Chem.* **2005**, *48*, 5466–5479. (b) Gohlke, H.; Hendlich, M.; Klebe, G. Knowledge-based scoring function to predict protein-ligand interactions. *J. Mol. Biol.* **2000**, *295*, 337–356.
- (34) Gediya, L. K.; Chopra, P.; Purushottamachar, P.; Maheshwari, N.; Njar, V. C. A new simple and high-yield synthesis of suberoylanilide hydroxamic acid and its inhibitory effect alone or in combination with retinoids on proliferation of human prostate cancer cells. *J. Med. Chem.* **2005**, *48*, 5047–5051.
- (35) Gosepath, E. M.; Eckstein, N.; Hamacher, A.; Servan, K.; von Jonquieres, G.; Lage, H.; Gyroffly, B.; Royer, H. D.; Kassack, M. U. Acquired cisplatin resistance in the head-neck cancer cell line Cal27 is associated with decreased DKK1 expression and can partially be reversed by overexpression of DKK1. *Int. J. Cancer* **2008**, *123*, 2013–2019.
- (36) Eckstein, N.; Servan, K.; Girard, L.; Cai, D.; von Jonquieres, G.; Jaehde, U.; Kassack, M. U.; Gazdar, A. F.; Minna, J. D.; Royer, H. D. Epidermal growth factor receptor pathway analysis identifies amphiregulin as a key factor for cisplatin resistance of human breast cancer cells. *J. Biol. Chem.* **2008**, *283*, 739–750.
- (37) (a) Heltweg, B.; Trapp, J.; Jung, M. In vitro assays for the determination of histone deacetylase activity. *Methods* **2005**, *36*, 332–337. (b) Wegener, D.; Wirsching, F.; Riester, D.; Schwenhorst, A. A fluorogenic histone deacetylase assay well suited for high-throughput activity screening. *Chem. Biol.* **2003**, *10*, 61–68.
- (38) Heltweg, B.; Dequiedt, F.; Verdin, E.; Jung, M. Nonisotopic substrate for assaying both human zinc and NAD⁺-dependent histone deacetylases. *Anal. Biochem.* **2003**, *319*, 42–48.
- (39) Marek, M.; Kannan, S.; Hauser, A. T.; Moraes Mourao, M.; Caby, S.; Cura, V.; Stolfá, D. A.; Schmidtkunz, K.; Lancelot, J.; Andrade, L.; Renaud, J. P.; Oliveira, G.; Sippl, W.; Jung, M.; Cavarelli, J.; Pierce, R. J.; Romier, C. Structural basis for the inhibition of histone deacetylase 8 (HDAC8), a key epigenetic player in the blood fluke *Schistosoma mansoni*. *PLoS Pathog.* **2013**, *9*, e1003645.
- (40) Engelke, L. H.; Hamacher, A.; Proksch, P.; Kassack, M. U. Ellagic acid and resveratrol prevent the development of cisplatin resistance in the epithelial ovarian cancer cell line A2780. *J. Cancer* **2016**, *7*, 353–363.
- (41) Ciossek, T.; Julius, H.; Wieland, H.; Maier, T.; Beckers, T. A homogeneous cellular histone deacetylase assay suitable for compound profiling and robotic screening. *Anal. Biochem.* **2008**, *372*, 72–81.

(42) Bonfils, C.; Kalita, A.; Dubay, M.; Siu, L. L.; Carducci, M. A.; Reid, G.; Martell, R. E.; Besterman, J. M.; Li, Z. Evaluation of the pharmacodynamic effects of MGCD0103 from preclinical models to human using a novel HDAC enzyme assay. *Clin. Cancer Res.* **2008**, *14*, 3441–3449.

(43) Hoffmann, K.; Brosch, G.; Loidl, P.; Jung, M. A non-isotopic assay for histone deacetylase activity. *Nucleic Acids Res.* **1999**, *27*, 2057–2058.

(44) Schneider, C. A.; Rasband, W. S.; Eliceiri, K. W. NIH Image to ImageJ: 25 years of image analysis. *Nat. Methods* **2012**, *9*, 671–675.

Supporting Information

Alkoxyurea-based Histone Deacetylase Inhibitors Increase Cisplatin Chemosensitivity

Katharina Stenzel^{1,#}, Alexandra Hamacher^{1,#}, Finn K. Hansen¹, Christoph G. W. Gertzen¹, Johanna Senger², Viktoria Marquardt^{1,3,4,5}, Linda Marek¹, Martin Marek⁶, Christophe Romier⁶, Marc Remke^{3,4,5}, Manfred Jung², Holger Gohlke¹, Matthias U. Kassack^{1,Δ}, and Thomas Kurz^{1,Δ}

¹*Institut für Pharmazeutische und Medizinische Chemie, Heinrich-Heine-Universität Düsseldorf, Universitätsstr. 1, 40225 Düsseldorf, Germany.* ²*Institut für Pharmazeutische Wissenschaften, Albert-Ludwigs-Universität Freiburg, Albertstraße 25, 79104 Freiburg, Germany.* ³*Department of Pediatric Oncology, Hematology, and Clinical Immunology, Medical Faculty, Heinrich-Heine-University, Moorenstr. 5, 40225 Düsseldorf, Germany.* ⁴*Department of Neuropathology, Medical Faculty, Heinrich-Heine-University, Moorenstr. 5, 40225 Düsseldorf Germany.* ⁵*Division of Pediatric Neuro-Oncogenomics, German Cancer Consortium (DKTK) and German Cancer Research Center (DKFZ), Moorenstr. 5, 40225 Düsseldorf, Germany.* ⁶*Département de Biologie Structurale Intégrative, Institut de Génétique et Biologie Moléculaire et Cellulaire (IGBMC), Université de Strasbourg (UDS), CNRS, INSERM, 1 Rue Laurent Fries, 67404 Illkirch Cedex, France.*

Table of Contents

Chemistry	S2
References	S15

Chemistry**General**

All solvents and chemicals were used as purchased without further purification. The progress of all reactions was monitored on Merck precoated silica gel plates (with fluorescence indicator UV₂₅₄) using ethyl acetate/*n*-hexane as solvent system. Column chromatography was performed with Fluka silica gel 60 (230-400 mesh ASTM) with the solvent mixtures specified in the corresponding experiment. Spots were visualized by irradiation with ultraviolet light (254 nm) or staining in potassium permanganate solution following heating. Flash column chromatography was performed using prepacked silica cartridge with the solvent mixtures specified in the corresponding experiment. Melting points (mp) were taken in open capillaries on a Mettler FP 5 melting-point apparatus and are uncorrected. Proton (¹H) and carbon (¹³C) NMR spectra were recorded on a Bruker Avance 500 (500 MHz for ¹H and 125 MHz for ¹³C) or Bruker Avance 600 (600 MHz for ¹H and 150 MHz for ¹³C) using chloroform-*d* or DMSO-*d*₆ as solvent. Chemical shifts are given in parts per million (ppm), relative to residual solvent peak for ¹H and ¹³C. Elemental analysis was performed on a Perkin Elmer PE 2400 CHN elemental analyzer. Analytical HPLC analysis were carried out on a Varian Prostar system equipped with a Prostar 410 (autosampler), 210 (pumps) and 330 (UV-detector) using a Phenomenex Luna 5u C18(2) 1.8 μm particle (250 mm × 4.6 mm) column, supported by Phenomenex Security Guard Cartridge Kit C18 (4.0 mm × 3.0 mm). UV absorption was detected at 254 nm with a linear gradient. The purity of all final compounds was 95% or higher.

Synthesis of *N*-(Benzyloxy)-6-((1,3-dioxoisindolin-2-yl)oxy)hexanamide (3).

1) 6-Bromohexanoic acid (1.951 g, 10 mmol) was dissolved in anhydrous THF (25 mL) and cooled to -15 °C. This was treated with *N*-Methylmorpholine (1.012 g, 11 mmol) followed by isobutyl chloroformate (1.502 g, 11 mmol) to form the mixed anhydride. After 15 min *O*-benzylhydroxylamine (1.232 g, 10 mmol) was added dropwise. The reaction was warmed to RT over 3 h and subsequently filtrated. After removing the solvent in vacuo the residue was diluted in ethyl acetate/H₂O and extracted with ethyl acetate (3 x 60 mL). The combined extracts were washed with NaHCO₃ (50 mL) and the organic layer was dried over Na₂SO₄, filtered, and the solvent removed in vacuo to give the intermediate *N*-(benzyloxy)-6-bromohexanamide (2.49 g, 8.30 mmol, 83%). 2) *N*-Hydroxyphthalimide (1.35 g, 8.30 mmol) and *N*-(benzyloxy)-6-bromohexanamide (2.49 g, 8.30 mmol) were dissolved in acetonitrile (25 mL). Triethylamine (1.26 g, 12.45 mmol) was added and the reaction mixture was refluxed for 7 h. Upon completion (TLC analysis, eluent: ethyl acetate/*n*-hexane 1:1), the reaction mixture was poured into ice water (70 g) and extracted with ethyl acetate (3 x 75 mL). The combined organic layers were washed with a saturated solution of NaHCO₃ (3 x 75 mL), dried over Na₂SO₄ and evaporated under reduced pressure to provide **3** in 79% yield. All spectroscopic data were in agreement with the literature.[1]

Synthesis of 6-(Aminoxy)-*N*-(benzyloxy)hexanamide (4). Methylhydrazine (0.503 mL, 9.6 mmol) was added dropwise at -10 °C to a solution of compound **3** (2.29 g, 6 mmol) in dry CH₂Cl₂ (15 mL). The reaction mixture was stirred for 2.5 h and the precipitate was removed by filtration. The filtrate was evaporated under reduced pressure and treated with diethyl ether (5 mL). The precipitate was removed by filtration and a saturated solution of HCl in diethyl ether was added to the filtrate to obtain the hydrochloride of the product. The solid was collected by filtration and subsequently dissolved in water (40 mL). A saturated Na₂CO₃-solution was added until pH > 8 and the aqueous layer was extracted with ethyl acetate

(3 x 50 mL). The combined organic layers were dried over Na₂SO₄ and evaporated under reduced pressure to provide **4**. All spectroscopic data were in agreement with the literature.[1]

Synthesis of 4-Nitrophenyl ((6-((benzyloxy)amino)-6-oxohexyl)oxy)carbamate (5). The 6-(aminooxy)-*N*-(benzyloxy)hexanamide **4** (0.252 g, 1.0 mmol) was dissolved in dry CH₂Cl₂ (30 mL) and dry pyridine (0.110 mL, 1.4 mmol) was added. The reaction was cooled down to 0 °C and 4-nitrophenyl chloroformate (0.202 g, 1 mmol) was added under stirring in one portion. After stirring at RT for 3 h, the homogeneous solution was diluted with CH₂Cl₂ (100 mL) and washed with citric acid solution (10% w/w, 2 x 50 mL) and water (2 x 50 mL). The organic layer was dried over Na₂SO₄ and concentrated to afford **5** in 72% yield. Compound **5** was used directly in the next step without further purification.

Synthesis of the amine precursors

The amine intermediates and their precursors were synthesized according to established literature methods or were obtained from commercial suppliers. 2-Naphthylamine, 6-aminoquinoline, 8-aminoquinoline and 2-methyl-8-nitroquinoline were obtained from commercial suppliers (Sigma-Aldrich, TCI, Alfa Aesar) and used as purchased without further purification. 8-Amino-2-methylquinoline was synthesized from 2-methyl-8-nitroquinoline.^[2] The known intermediates 6-methoxy-4-methylquinolin-8-amine, 6-methoxyquinolin-8-amine and 2,6-dimethoxy-4-methylquinolin-8-amine and their precursors were synthesized according to established literature methods.[2] The novel 2-isopropoxy-6-methoxy-4-methyl-5-(3-(trifluoro-methyl)phenoxy)quinolin-8-amine was synthesized according to known procedures.[2]

Synthesis of 2-Isopropoxy-6-methoxy-4-methyl-8-nitro-5-(3-(trifluoromethyl)phenoxy)quinoline. A solution of the respective phenol (16.3 mmol) in DMSO (15 mL) and potassium hydroxide (0.92 g, 16.3 mmol) were heated to 100 °C for 0.5 h. The respective 2-alkoxy-5-

chloro-6-methoxy-4-methyl-8-nitroquinoline (14.2 mmol) was added in one portion. The resulting dark solution was stirred at 100 °C for 2.5 h. Water (30 mL) was added slowly while keeping the temperature above 60 °C. The resulting suspension was cooled to 10 °C. The crude product was separated by suction filtration, washed with water, and dried. The residue was then suspended in toluene (125 mL), heated to reflux in presence of activated charcoal, and filtered through kieselgur. Toluene (100 mL) was removed by distillation at ambient pressure. The solution was cooled to 70 °C and *n*-hexane was added (100 mL). The resulting suspension was cooled to 5 °C. The product was separated by suction filtration and washed with *n*-hexane.

2-Isopropoxy-6-methoxy-4-methyl-8-nitro-5-(3-(trifluoromethyl)phenoxy)quinoline.

Yellow solid; yield 64%; mp 155 °C. ¹H NMR (500 MHz, CDCl₃) δ = 7.75 (s, 1 H), 7.40 (dd, $J_1 = J_2 = 8.0$ Hz, 1 H), 7.32 (d, $J = 7.7$ Hz, 1 H), 7.09 (s, 1 H), 6.93 (d, $J = 8.2$ Hz, 1 H), 6.72 (s, 1 H), 5.41 (sept, $J = 6.2$ Hz, 1 H), 3.80 (s, 3 H), 2.61 (s, 3 H), 1.39 (d, $J = 6.2$ Hz, 6 H) ppm. ¹³C NMR (125 MHz, CDCl₃) δ = 161.70, 157.94, 146.23, 145.81, 144.36, 140.84, 135.20, 132.32 (q, $J = 32.7$ Hz), 130.35, 123.68 (q, $J = 273.2$ Hz), 121.74, 119.19 (q, $J = 3.6$ Hz), 118.18, 118.04, 112.23 (q, $J = 3.5$ Hz), 111.22, 69.42, 57.03, 23.10, 21.82. Anal. Calcd for C₂₁H₁₉F₃N₂O₅: C 57.80, H 4.39, N 6.42. Found: C 57.65, H 4.66, N 6.45.

Synthesis of 2-Isopropoxy-6-methoxy-4-methyl-5-(3-(trifluoromethyl)phenoxy)quinoline-8-amine. The respective 8-nitroquinoline (3.7 mmol) and Pd-C (10%) were suspended in dry ethanol (50 mL). The reaction mixture was heated to 60 °C, then hydrazine hydrate (0.93 g, 18.5 mmol) was added dropwise over 15 min. The reaction mixture was stirred at 60 °C for 4 h, then heated under reflux for 0.5 h. After cooling to 50 °C, Pd-C was removed by filtration through kieselgur, and washed with ethanol (20 mL). After cooling to RT, water (50 mL) was added slowly under vigorous stirring over 0.5 h. The resulting slurry was cooled to 5 °C, filtrated, and the residue was washed with a mixture of ethanol/H₂O (1:1).

2-Isopropoxy-6-methoxy-4-methyl-5-(3-(trifluoromethyl)phenoxy)quinoline-8-amine.

Colourless solid; yield 44%; mp 91 °C. ^1H NMR (500 MHz, CDCl_3) δ = 7.33 (dd, $J_1 = J_2 = 8.0$ Hz, 1 H), 7.21 (d, $J = 7.7$ Hz, 1 H), 7.05 (s, 1 H), 6.94 (dd, $J = 8.2, 2.0$ Hz, 1 H), 6.77 (s, 1 H), 6.61 (s, 1 H), 5.46 (sept, $J = 6.2$ Hz, 1 H), 4.69 (s, 2 H), 3.75 (s, 3 H), 2.54 (s, 3 H), 1.41 (d, $J = 6.2$ Hz, 6 H) ppm. ^{13}C NMR (126 MHz, CDCl_3) δ = 159.56, 158.87, 148.18, 146.00, 141.08, 131.89 (q, $J = 32.6$ Hz), 131.33, 129.98, 128.59, 123.93 (q, $J = 272.3$ Hz), 120.61, 118.20, 117.99 (q, $J = 3.8$ Hz), 116.36, 111.95 (q, $J = 3.7$ Hz), 99.25, 67.75, 56.68, 23.02, 22.00 ppm. Anal. Calcd for $\text{C}_{21}\text{H}_{21}\text{F}_3\text{N}_2\text{O}_3$: C 62.06, H 5.21, N 6.89. Found: C 62.01, H 5.60, N 6.80.

General procedure for the microwave-assisted synthesis of compounds 6 c-j.

4-Nitrophenyl-((6-((benzyloxy)amino)-6-oxohexyl)oxy)carbamate **5** (0.209 g, 0.5 mmol) in dry THF (1.5 mL) was placed into a 10 mL glass pressure microwave-tube equipped with a magnetic stirrer bar. Triethylamine (69 μL , 0.5 mmol) was added, before the tube was closed with a silicon septum and the reaction mixture was subjected to microwave irradiation for 0.5 h at 70 °C and 100 W. The reaction mixture was cooled to RT and transferred to a round bottomed flask. The solvent was evaporated, CH_2Cl_2 (100 mL) was added and the mixture was washed subsequently with a saturated, aqueous solution of sodium hydrogen carbonate (30 mL) and water (30 mL). The organic layer was dried over Na_2SO_4 , filtered and the solvent was evaporated. The remaining residues were purified by crystallization from appropriate solvents or the crude products were purified by flash column chromatography (prepacked silica cartridge, *n*-hexane/ethyl acetate, gradient: 90:10 \rightarrow 0:100 in 0.5 h) to yield the desired intermediates (yield: 83-91%).

***N*-(Benzyloxy)-6-((3-(naphthalen-2-yl)ureido)oxy)hexanamide (6c).** Colourless solid; yield 85%; mp 132°C. ^1H NMR (600 MHz, $\text{DMSO}-d_6$) δ = 10.96 (s, 1H), 9.54 (s, 1H), 8.87 (s, 1H), 8.15 (d, $J = 1.6$ Hz, 1H), 7.82 (s, 1H), 7.80 (s, 1H), 7.77 (d, $J = 8.2$ Hz, 1H), 7.69 (dd, $J = 2.0,$

8.9 Hz, 1H), 7.44 (t, $J = 7.5$ Hz, 1H), 7.41-7.30 (m, 6H), 4.78 (s, 2H), 3.79 (t, $J = 6.7$ Hz, 2H), 1.98 (t, $J = 7.2$ Hz, 2H), 1.69-1.59 (m, 2H), 1.57-1.48 (m, 2H), 1.37-1.26 (m, 2H) ppm. ^{13}C NMR (150 MHz, DMSO- d_6) $\delta = 169.22, 157.08, 136.64, 135.99, 133.34, 129.29, 128.66, 128.18, 128.09, 127.89, 127.29, 126.94, 126.14, 124.10, 120.63, 114.93, 76.66, 75.64, 32.08, 27.15, 24.73, 24.66$ ppm. Anal. Calcd. for $\text{C}_{24}\text{H}_{27}\text{N}_3$: C 68.39, H 6.46, N 9.97. Found: C 68.21, H 6.37, N 9.83.

***N*-(Benzyloxy)-6-((3-(quinolin-6-yl)ureido)oxy)hexanamide (6d)**. Colourless solid; yield 79%; mp 103 °C. ^1H NMR (600 MHz, DMSO- d_6) $\delta = 10.95$ (s, 1H), 9.62 (s, 1H), 9.03 (s, 1H), 8.75 (dd, $J = 4.0, 1.7$ Hz, 1H), 8.26-8.16 (m, 2H), 7.92 (s, 2H), 7.50-7.42 (m, 1H), 7.51-7.27 (m, 5H), 4.78 (s, 2H), 3.80 (t, $J = 6.7$ Hz, 2H), 1.98 (t, $J = 7.2$ Hz, 2H), 1.72-1.60 (m, 2H), 1.59-1.49 (m, 2H), 1.39-1.27 (m, 2H) ppm. ^{13}C NMR (151 MHz, DMSO- d_6) $\delta = 169.21, 157.00, 148.52, 144.32, 137.07, 136.00, 135.11, 129.01, 128.66, 128.18, 128.09, 123.94, 121.51, 114.53, 76.66, 75.69, 32.08, 27.14, 24.73, 24.65$ ppm. Anal. Calcd. for $\text{C}_{23}\text{H}_{26}\text{N}_4$: C 65.39, H 6.20, N 13.26. Found: C 65.11, H 6.11, N 13.01.

***N*-(Benzyloxy)-6-((3-(quinolin-8-yl)ureido)oxy)hexanamide (6e)**. Colourless solid; yield 77%; mp 94 °C. ^1H NMR (600 MHz, DMSO- d_6) $\delta = 10.97$ (s, 1H), 9.97 (s, 1H), 9.92 (s, 1H), 8.90 (d, $J = 2.9$ Hz, 1H), 8.49 (d, $J = 7.5$ Hz, 1H), 8.40 (d, $J = 7.1$ Hz, 1H), 7.66-7.52 (m, 3H), 7.43-7.30 (m, 5H), 4.77 (s, 2H), 3.89 (t, $J = 6.3$ Hz, 2H), 2.00 (t, $J = 7.2$ Hz, 2H), 1.74-1.64 (m, 2H), 1.62-1.51 (m, 2H), 1.51-1.42 (m, 2H) ppm. ^{13}C NMR (151 MHz, DMSO- d_6) $\delta = 169.21, 156.29, 148.74, 137.55, 136.54, 136.00, 134.43, 128.66, 128.17, 128.08, 127.73, 127.02, 122.10, 120.44, 114.05, 76.65, 75.96, 32.04, 27.42, 24.91, 24.73$ ppm. Anal. Calcd. for $\text{C}_{23}\text{H}_{26}\text{N}_4$: C 65.39, H 6.20, N 13.26. Found: C 65.34, H 6.05, N 13.23.

***N*-(Benzyloxy)-6-((3-(2-methylquinolin-8-yl)ureido)oxy)hexanamide (6f)**. Colourless solid; yield 89%; mp 110 °C. ^1H NMR (600 MHz, DMSO- d_6) $\delta = 10.93$ (s, 1H), 9.96 (s, 1H), 9.93 (s, 1H), 8.44 (dd, $J = 7.7, 1.4$ Hz, 1H), 8.27 (d, $J = 8.4$ Hz, 1H), 7.56-7.44 (m, 3H),

7.39-7.29 (m, 5H), 4.75 (s, 2H), 3.89 (t, $J = 6.5$ Hz, 2H), 2.70 (s, 3H), 1.96 (t, $J = 7.3$ Hz, 2H), 1.78-1.70 (m, 2H), 1.60-1.52 (m, 2H), 1.47-1.39 (m, 2H) ppm. ^{13}C NMR (151 MHz, DMSO- d_6) $\delta = 168.67, 156.67, 155.89, 136.43, 136.13, 135.51, 133.26, 128.16, 127.67, 127.59, 125.50, 125.41, 122.24, 119.71, 113.50, 76.14, 75.53, 31.47, 27.04, 24.37, 24.34, 24.22$ ppm. Anal. Calcd. for $\text{C}_{24}\text{H}_{28}\text{N}_4$ C 66.04, H 6.47, N 12.84. Found: C 66.07, H 6.33, N 12.77.

***N*-(Benzyloxy)-6-((3-(6-methoxyquinolin-8-yl)ureido)oxy)hexanamide (6g)**. Colourless solid; yield 91%; mp 102 °C. ^1H NMR (600 MHz, DMSO- d_6) $\delta = 10.96$ (s, 1H), 10.02 (s, 1H), 9.86 (s, 1H), 8.75-8.66 (m, 1H), 8.27 (dd, $J = 8.3, 1.7$ Hz, 1H), 8.15 (d, $J = 2.8$ Hz, 1H), 7.59-7.52 (m, 1H), 7.41-7.31 (m, 5H), 7.01 (d, $J = 2.8$ Hz, 1H), 4.78 (s, 2H), 3.96-3.81 (m, 5H), 2.00 (t, $J = 7.5$ Hz, 2H), 1.76-1.64 (m, 2H), 1.64-1.52 (m, 2H), 1.53-1.41 (m, 2H) ppm. ^{13}C NMR (151 MHz, DMSO- d_6) $\delta = 169.19, 157.63, 156.18, 146.02, 136.02, 135.37, 135.30, 134.24, 128.86, 128.67, 128.18, 128.09, 122.53, 106.51, 98.46, 76.65, 75.99, 55.39, 32.04, 27.41, 24.91, 24.74$ ppm. $\text{C}_{24}\text{H}_{28}\text{N}_4$: C 63.70, H 6.24, N 12.38. Found: C 63.41, H 6.09, N 12.23.

***N*-(Benzyloxy)-6-((3-(6-methoxy-4-methylquinolin-8-yl)ureido)oxy)hexanamide (6h)**.

Colourless solid; yield 78%; mp 110 °C. ^1H NMR (600 MHz, DMSO- d_6) $\delta = 10.95$ (s, 1H), 9.99 (s, 1H), 9.95 (s, 1H), 8.56 (d, $J = 4.2$ Hz, 1H), 8.15 (d, $J = 2.6$ Hz, 1H), 7.50-7.26 (m, 6H), 6.95 (d, $J = 2.6$ Hz, 1H), 4.76 (s, 2H), 3.91 (s, 3H), 3.86 (t, $J = 6.3$ Hz, 2H), 2.65 (s, 3H), 1.98 (t, $J = 6.2$ Hz, 2H), 1.75-1.62 (m, 2H), 1.61-1.51 (m, 2H), 1.51-1.40 (m, 2H) ppm. ^{13}C NMR (151 MHz, DMSO- d_6) $\delta = 169.18, 157.47, 156.19, 145.46, 143.43, 135.99, 135.81, 133.81, 128.65, 128.50, 128.16, 128.07, 123.01, 105.98, 95.19, 76.63, 75.95, 55.35, 32.01, 27.38, 24.87, 24.71, 18.44$ ppm. Anal. Calcd. for $\text{C}_{25}\text{H}_{30}\text{N}_4$: C 64.36, H 6.48, N 12.01. Found: C 64.13, H 6.43, N 12.15.

***N*-(Benzyloxy)-6-((3-(2,6-dimethoxy-4-methylquinolin-8-yl)ureido)oxy)hexanamide (6i).**

Colourless solid; yield 84%; mp 132 °C. ¹H NMR (600 MHz, DMSO-*d*₆) δ = 10.95 (s, 1H), 9.94 (s, 1H), 9.58 (s, 1H), 8.13 (d, *J* = 2.7 Hz, 1H), 7.42-7.30 (m, 5H), 6.93 (s, 1H), 6.90 (d, *J* = 2.8 Hz, 1H), 4.77 (s, 2H), 3.98 (s, 3H), 3.88 (m, 3.91-3.85, 5H), 2.57 (s, 3H), 1.96 (t, *J* = 7.3 Hz, 2H), 1.69-1.61 (m, 2H), 1.56-1.48 (m, 2H), 1.37-1.28 (m, 2H) ppm. ¹³C NMR (151 MHz, DMSO-*d*₆) δ = 169.14, 159.24, 156.29, 155.65, 147.15, 136.01, 134.09, 130.73, 128.67, 128.17, 128.08, 124.97, 113.02, 106.18, 96.48, 76.65, 75.80, 55.24, 52.57, 32.04, 27.48, 24.69, 18.42 ppm. Anal. Calcd. for C₂₆H₃₂N₄: C 62.89, H 6.50, N 11.28. Found: C 62.67, H 6.44, N 11.03.

***N*-(Benzyloxy)-6-((3-(2-isopropoxy-6-methoxy-4-methyl-5-(3-(trifluoromethyl)phenoxy)quinolin-8-yl)ureido)oxy)hexanamide (6j).**

Colourless solid; yield 83%; mp 109 °C. ¹H NMR (600 MHz, DMSO-*d*₆) δ = 10.95 (s, 1H), 10.01 (s, 1H), 9.67 (s, 1H), 8.56 (s, 1H), 7.52 (t, *J* = 8.1 Hz, 1H), 7.45-7.25 (m, 6H), 7.11 (s, 1H), 7.03 (dd, *J* = 8.5, 2.6 Hz, 1H), 6.84 (s, 1H), 5.44 (sept, *J* = 6.2 Hz, 1H), 4.78 (s, 2H), 3.90 (t, *J* = 6.9 Hz, 2H), 3.74 (s, 3H), 2.52 (s, 3H), 1.98 (t, *J* = 7.2 Hz, 2H), 1.73-1.64 (m, 2H), 1.62-1.47 (m, 2H), 1.39 (d, *J* = 9.5 Hz, 6H), 1.37- 1.30 (m, 2H) ppm. ¹³C NMR (151 MHz, DMSO-*d*₆) δ = 169.16, 158.67, 158.61, 156.38, 147.36, 146.17, 136.05, 131.96, 131.10, 131.07, 130.43 (q, *J* = 31.93 Hz), 130.39, 128.69, 128.20, 128.11, 123.79 (q, *J* = 272.79 Hz), 119.42, 118.59, 118.18, 116.32, 111.29, 103.70, 76.69, 75.80, 67.78, 56.34, 32.10, 27.47, 24.72, 24.69, 22.23, 21.64 ppm. Anal. Calcd. for C₃₅H₃₉N₄: C 61.40, H 5.74, N 8.18. Found: C 61.21, H 5.68, N 8.03.

Synthesis of *N*-(Benzyloxy)-6-((1,3-dioxoisindolin-2-yl)oxy)-*N*-methylhexanamide (7).

Sodium hydride 0,52 g (13.4 mmol, 60% dispersion in mineral oil) was added in portions to 4.59 g (12 mmol) *N*-(benzyloxy)-6-((1,3-dioxoisindolin-2-yl)oxy)hexanamide (3) in 115 ml THF followed by dropwise addition of methyl iodide (0.84 mL, 13.4 mmol). The reaction was stirred over night at RT before it was quenched with a saturated solution of NH₄Cl (100

mL) and extracted with ethyl acetate (3 x 100 mL). The organic layer was dried over Na₂SO₄, filtered and the solvent was removed in vacuo. The crude products were purified by flash column chromatography (prepacked silica cartridge, *n*-hexane/ethyl acetate, gradient: 90:10 → 50:50 in 0.5 h) to give the intermediate *N*-(benzyloxy)-6-((1,3-dioxoisindolin-2-yl)oxy)-*N*-methylhexanamide **7** in 92% yield.[3]

***N*-(Benzyloxy)-6-((1,3-dioxoisindolin-2-yl)oxy)-*N*-methylhexanamide (7)**. Oil; yield 59%.

¹H NMR (500 MHz, DMSO-*d*₆) δ = 7.86 (s, 4H), 7.52-7.30 (m, 5H), 4.89 (s, 2H), 4.11 (t, *J* = 6.5 Hz, 2H), 3.14 (s, 3H), 2.34 (t, *J* = 7.3 Hz, 2H), 1.71-1.58 (m, 2H), 1.57-1.44 (m, 2H), 1.44-1.34 (m, 2H) ppm. ¹³C NMR (125 MHz, DMSO-*d*₆) δ = 163.19, 134.64, 129.42, 128.58, 128.52, 128.38, 123.10, 77.47, 75.06, 31.11, 31.09, 27.41, 24.76, 23.60 ppm. HPLC analysis: retention time = 3.1 min; peak area: 95.34%. Method: Eluent A: 5 mM/L (385 mg/l) Ammonium acetate; Eluent B: HPLC-grade CH₃CN, linear gradient 5% B to 95% B over 20 min at a flow rate of 1.0 mL min⁻¹.

6-(Aminoxy)-*N*-(benzyloxy)-*N*-methylhexanamide (8). Synthetisized from **7** according to

(4).[1] Oil; yield 62%. ¹H NMR (500 MHz, DMSO-*d*₆) δ = 7.54-7.30 (m, 5H), 5.86 (s, 2H), 4.87 (s, 2H), 3.47 (t, *J* = 6.5 Hz, 2H), 3.13 (s, 3H), 2.30 (t, *J* = 7.5 Hz, 2H), 1.60-1.36 (m, 4H), 1.31-1.13 (m, 2H). ¹³C NMR (151 MHz, DMSO-*d*₆) δ = 173.70, 134.80, 129.41, 128.58, 128.38, 75.05, 74.65, 32.73, 31.18, 27.74, 25.29, 23.88 ppm. Anal. Calcd. for C₁₄H₂₂N₂ C 63.13, H 8.33, N 10.52 Found: C 63.11, H 8.60, N 10.39.

Synthesis of *N*-(Benzyloxy)-*N*-methyl-6-(3-naphthalen-1-ylureidooxy)hexanamide (9).

Synthesized from **8** according to literature.[1] A solution of 1-naphthylisocyanate (2.7 mmol) in dry CH₂Cl₂ (5 mL) was added dropwise to a solution of the aminoxyderivative **8** (3 mmol) in dry CH₂Cl₂ (15 mL). The reaction mixture was stirred over night at RT and subsequently treated with petroleum ether to precipitate the product. The resulting solid was collected, washed with petroleum ether (5 mL) and dried in vacuo.

***N*-(Benzyloxy)-*N*-methyl-6-(3-naphthalen-1-ylureidooxy)hexanamide (9)**. Oil; yield 59%. ^1H NMR (500 MHz, $\text{DMSO-}d_6$) δ = 9.55 (s, 1H), 8.82 (s, 1H), 7.95-7.91 (m, 2H), 7.75 (d, J = 8.18, 1H), 7.63 (d, J = 7.20 Hz, 1H), 7.57-7.34 (m, 8H), 4.87 (s, 2H), 3.86 (t, J = 6.69, 2H), 3.12 (s, 3H), 2.35 (t, J = 7.37 Hz, 2H), 1.71-1.61 (m, 2H), 1.78-1.70 (m, 2H), 1.56-1.44 (m, 2H), 1.34-1.25 (m, 2H) ppm. ^{13}C NMR (151 MHz, $\text{DMSO-}d_6$) δ = 170.24, 157.86, 134.79, 133.58, 133.55, 129.40, 128.57, 128.37, 128.26, 128.00, 125.80, 125.65, 125.49, 124.73, 122.33, 121.57, 75.72, 75.04, 31.16, 27.40, 25.03, 23.81 ppm. Anal. Calcd. for $\text{C}_{25}\text{H}_{29}\text{N}_3$ C 68.95, H 6.71, N 9.65. Found: C 68.75, H 6.89, N 9.20.

General procedure for the synthesis of compound 1c-j, 2. A solution of the respective *O*-benzyl-protected hydroxamic acid (**6c-j**, **9**) in methanol (50 mL) was hydrogenated (1 bar) at RT in the presence of a catalytic amount of Pd-C (10 wt%). Upon completion of the reaction, the crude mixture was filtered through Celite to remove the catalyst and the filtrate was concentrated under reduced pressure. The residue was purified by column chromatography using CH_2Cl_2 : CH_2Cl_2 /30% methanol (9:1) as Eluent (yield: 54-72%).

***N*-Hydroxy-6-((3-(naphthalen-2-yl)ureido)oxy)hexanamide (1c)**. Colourless solid; yield 65%; mp 195 °C. ^1H NMR (600 MHz, $\text{DMSO-}d_6$) δ = 10.35 (s, 1H), 9.54 (s, 1H), 8.88 (s, 1H), 8.67 (s, 1H), 8.15 (s, 1H), 7.96-7.64 (m, 4H), 7.50-7.33 (m, 2H), 3.80 (t, J = 6.8 Hz, 2H), 1.98 (t, J = 7.6 Hz, 2H), 1.81-1.59 (m, 2H), 1.61-1.48 (m, 2H), 1.42-1.28 (m, 2H) ppm. ^{13}C NMR (151 MHz, $\text{DMSO-}d_6$) δ = 168.98, 157.08, 136.67, 133.35, 129.28, 127.90, 127.30, 126.94, 126.15, 124.09, 120.61, 114.89, 75.67, 32.11, 27.18, 24.85 ppm. HPLC analysis: retention time = 8.13 min; peak area: 96.48%. Method: Eluent A: HPLC-grade water +0.1% TFA; Eluent B: HPLC-grade CH_3CN +0.1% TFA, linear gradient 30% B to 100% B over 20 min at a flow rate of 1.0 mL min^{-1} .

***N*-Hydroxy-6-((3-(quinolin-6-yl)ureido)oxy)hexanamide (1d)**. Colourless solid; yield 62%; mp 153 °C. ^1H NMR (600 MHz, $\text{DMSO-}d_6$) δ = 10.36 (s, 1H), 9.63 (s, 1H), 9.04 (s, 1H),

8.77-8.74 (m, 1H), 8.68 (s, 1H), 8.24 (m, 8.26-8.21, 2H), 7.93 (s, 2H), 7.54-7.36 (m, 1H), 3.80 (t, $J = 6.6$ Hz, 2H), 1.97 (t, $J = 7.4$ Hz, 2H), 1.72-1.60 (m, 2H), 1.60-1.47 (m, 2H), 1.40-1.28 (m, 2H) ppm. ^{13}C NMR (151 MHz, $\text{DMSO-}d_6$) $\delta = 168.96, 156.99, 148.52, 144.32, 137.07, 135.12, 129.01, 128.19, 123.95, 121.51, 114.54, 75.72, 32.12, 27.17, 24.85$ ppm. HPLC analysis: retention time = 7.09 min; peak area: 96.33% Method: Eluent A: HPLC-grade water +0.1% TFA; Eluent B: HPLC-grade CH_3CN +0.1% TFA, linear gradient 10% B to 100% B over 20 min at a flow rate of 1.0 mL min^{-1} .

***N*-Hydroxy-6-((3-(quinolin-8-yl)ureido)oxy)hexanamide (1e)**. Colourless solid; yield 57%; mp $123 \text{ }^\circ\text{C}$. ^1H NMR (600 MHz, $\text{DMSO-}d_6$) $\delta = 10.36$ (s, 1H), 9.96 (s, 1H), 9.91 (s, 1H), 8.92-8.87 (m, 1H), 8.67 (s, 1H), 8.48 (d, 1H), 8.41 (d, $J = 8.2, 1.7$ Hz, 1H), 7.68-7.51 (m, 3H), 3.89 (t, $J = 6.3$ Hz, 2H), 1.98 (t, $J = 7.3$ Hz, 2H), 1.76-1.64 (m, 2H), 1.61-1.52 (m, 2H), 1.51-1.42 (m, 2H) ppm. ^{13}C NMR (151 MHz, $\text{DMSO-}d_6$) $\delta = 169.02, 156.30, 148.78, 137.55, 136.55, 134.40, 127.74, 127.03, 122.14, 120.48, 114.06, 76.01, 32.10, 27.46, 25.05, 24.94$ ppm. HPLC analysis: retention time = 9.76 min; peak area: 95.44%. Method: Eluent A: HPLC-grade water +0.1% TFA; Eluent B: HPLC-grade CH_3CN +0.1% TFA, linear gradient 10% B to 100% B over 20 min at a flow rate of 1.0 mL min^{-1} .

***N*-Hydroxy-6-((3-(2-methylquinolin-8-yl)ureido)oxy)hexanamide (1f)**. Colourless solid; yield 72%; mp $153 \text{ }^\circ\text{C}$. ^1H NMR (600 MHz, $\text{DMSO-}d_6$) $\delta = 10.36$ (s, 1H), 9.97 (s, 1H), 9.94 (s, 1H), 8.68 (s, 1H), 8.49-8.42 (m, 1H), 8.27 (s, 1H), 7.61-7.40 (m, 3H), 3.91 (t, $J = 6.4$ Hz, 2H), 2.71 (s, 3H), 2.04-1.93 (m, 2H), 1.85-1.69 (m, 2H), 1.69-1.52 (m, 2H), 1.54-1.41 (m, 2H) ppm. ^{13}C NMR (151 MHz, $\text{DMSO-}d_6$) $\delta = 168.42, 156.68, 155.88, 136.42, 136.13, 133.25, 125.50, 125.41, 122.24, 119.71, 113.49, 75.56, 31.51, 27.08, 24.50, 24.43, 24.34$ ppm. HPLC analysis: retention time = 14.17 min; peak area: 96.99%. Method: Eluent A: HPLC-grade water +0.1% TFA; Eluent B: HPLC-grade CH_3CN +0.1% TFA, linear gradient 10% B to 100% B over 20 min at a flow rate of 1.0 mL min^{-1} .

***N*-Hydroxy-6-((3-(6-methoxyquinolin-8-yl)ureido)oxy)hexanamide (1g)**. Colourless solid; yield 59%; mp 176 °C. ¹H NMR (600 MHz, DMSO-*d*₆) δ = 10.35 (s, 1H), 10.01 (s, 1H), 9.85 (s, 1H), 8.70 (dd, *J* = 4.2, 1.6 Hz, 1H), 8.66 (s, 1H), 8.27 (d, *J* = 8.2 Hz, 1H), 8.14 (d, *J* = 2.5 Hz, 1H), 7.61-7.52 (m, 1H), 7.01 (d, *J* = 2.5 Hz, 1H), 3.97-3.82 (m, 5H), 1.98 (t, *J* = 7.2 Hz, 2H), 1.74-1.64 (m, 2H), 1.61-1.53 (m, 2H), 1.51-1.41 (m, 2H) ppm. ¹³C NMR (151 MHz, DMSO-*d*₆) δ = 168.94, 157.62, 156.17, 146.03, 135.36, 135.30, 134.22, 128.85, 122.54, 106.50, 98.46, 76.01, 55.38, 32.10, 27.45, 25.05, 24.94 ppm. HPLC analysis: retention time = 6.88 min; peak area: 95.42%. Method: Eluent A: HPLC-grade water +0.1% TFA; Eluent B: HPLC-grade CH₃CN +0.1% TFA, linear gradient 30% B to 100% B over 20 min at a flow rate of 1.0 mL min⁻¹.

***N*-Hydroxy-6-((3-(6-methoxy-4-methylquinolin-8-yl)ureido)oxy)hexanamide (1h)**. Colourless solid; yield 61%; mp 142 °C. ¹H NMR (600 MHz, DMSO-*d*₆) δ = 10.36 (s, 1H), 9.99 (s, 1H), 9.95 (s, 1H), 8.67 (s, 1H), 8.56 (dd, *J* = 4.3, 1.7 Hz, 1H), 8.19-8.11 (m, 1H), 7.42 (d, *J* = 4.1 Hz, 1H), 6.95 (s, 1H), 3.92 (s, 3H), 3.87 (t, *J* = 6.4, 1.8 Hz, 2H), 2.65 (s, 3H), 1.98 (t, *J* = 7.5, 1.7 Hz, 2H), 1.74-1.64 (m, 2H), 1.61-1.53 (m, 2H), 1.50-1.42 (m, 2H) ppm. ¹³C NMR (125 MHz, DMSO-*d*₆) δ = 168.95, 157.54, 156.19, 145.46, 143.41, 135.90, 133.90, 128.53, 123.00, 106.02, 95.31, 76.01, 55.39, 32.11, 27.45, 25.05, 24.92, 18.41 ppm. HPLC analysis: retention time = 9.62 min; peak area: 98.50%. Method: Eluent A: HPLC-grade water +0.1% TFA; Eluent B: HPLC-grade CH₃CN +0.1% TFA, linear gradient 10% B to 100% B over 20 min at a flow rate of 1.0 mL min⁻¹.

6-((3-(2,6-Dimethoxy-4-methylquinolin-8-yl)ureido)oxy)-*N*-hydroxyhexanamide (1i). Colourless solid; yield 55%; mp 162 °C. ¹H NMR (600 MHz, DMSO-*d*₆) δ = 10.34 (s, 1H), 9.94 (s, 1H), 9.59 (s, 1H), 8.66 (s, 1H), 8.13 (d, 1H), 6.96 (s, 1H), 6.92 (d, *J* = 2.7 Hz, 1H), 3.98 (s, 3H), 3.95-3.83 (m, 3H), 2.59 (s, 3H), 1.94 (t, *J* = 7.4 Hz, 2H), 1.70-1.60 (m, 2H), 1.56-1.47 (m, 2H), 1.38-1.29 (m, 2H) ppm. ¹³C NMR (151 MHz, DMSO-*d*₆) δ = 168.39,

158.73, 155.78, 155.14, 146.63, 133.58, 130.22, 124.45, 112.51, 105.68, 95.96, 75.34, 54.73, 52.06, 31.58, 27.02, 24.39, 24.32, 17.92 ppm. HPLC analysis: retention time = 14.17 min; peak area: 96.99%. Method: Eluent A: HPLC-grade water +0.1% TFA; Eluent B: HPLC-grade CH₃CN +0,1% TFA, linear gradient 10% B to 100% B over 20 min at a flow rate of 1.0 mL min⁻¹.

***N*-Hydroxy-6-((3-(2-isopropoxy-6-methoxy-4-methyl-5-(3(trifluoromethyl)phenoxy)**

quinolin-8-yl)ureido)oxy)hexanamide (1j). Colourless solid; yield 54%; mp 137 °C.

¹H NMR (600 MHz, DMSO-*d*₆) δ = 10.37 (s, 1H), 10.02 (s, 1H), 9.68 (s, 1H), 8.69 (s, 1H), 8.57 (s, 1H), 7.53 (t, *J* = 8.1, 1H), 7.37 (d, *J* = 7.8, 1H), 7.12 (s, 1H), 7.03 (d, *J* = 7.8, 1H), 6.84 (s, 1H), 5.45 (sept, *J* = 6.2, 1H), 3.91 (t, *J* = 7.1, 2H), 3.75 (s, 3H), 2.52 (s, 3 H), 1.98 (t, *J* = 7.4, 2H), 1.85-1.63 (m, 2H), 1.63-1.48 (m, 2H), 1.48-1.27(m, 8H) ppm. ¹³C NMR (151 MHz, DMSO-*d*₆) δ = 168.89, 158.66, 158.61, 156.36, 147.36, 146.18, 131.94, 131.08, 130.42 (q, *J* = 32.0 Hz), 130.38, 130.31, 123.78 (q, *J* = 272.9 Hz), 119.42, 118.59, 118.21, 118.19, 116.32, 111.28, 103.70, 75.83, 67.78, 56.34, 32.13, 27.49, 24.91, 24.79, 22.23, 21.64 ppm. HPLC analysis: retention time = 18.61 min; peak area: 96.49%. Method: Eluent A: HPLC-grade water +0.1% TFA; Eluent B: HPLC-grade CH₃CN +0,1% TFA, linear gradient 30% B to 100% B over 20 min at a flow rate of 1.0 mL min⁻¹.

***N*-(Benzyloxy)-*N*-methyl-6-((3-(naphthalen-1-yl)ureido)oxy)hexanamide (2)**. Oil; yield

54%. ¹H NMR (500 MHz, DMSO-*d*₆) δ = 9,76 (s, 1H), 9.55 (s, 1H), 8.83 (s, 1H), 8.07-7.87 (m, 2H), 7.75 (d, *J* = 8.20, 1H), 7.63 (d, *J* = 7.34, 1H), 7.60-7.46 (m, 3H), 3.88 (t, *J* = 6.7 Hz, 2H), 3.07 (s, 3H) 2.37 (t, *J* = 7.7 Hz, 2H), 1.77-1.66 (m, 2H), 1.61-1.49 (m, 2H), 1.47-1.34 (m, 2H) ppm. ¹³C NMR (125 MHz, DMSO-*d*₆) δ = 172.77, 157.88, 133.55, 128.26, 128.29, 128.00, 125.81, 125.67, 125.49, 124.75, 122.36, 121.62, 75.76, 35.58, 31.35, 27.40, 25.12, 24.01 ppm. Anal. Calcd. for C₁₈H₂₃N₃: C 60.51, H 8.07, N 12.45. Found: C 60.58, H 7.93, N 12.15.

Author Contributions

[#]These authors contributed equally to this work.

^ΔThese authors share the senior authorship.

References

- [1] Marek, L.; Hamacher, A.; Hansen, F. K.; Kuna, K.; Gohlke, H.; Kassack, M. U.; Kurz, T. Histone deacetylase (HDAC) inhibitors with a novel connecting unit linker region reveal a selectivity profile for HDAC4 and HDAC5 with improved activity against chemoresistant cancer cells. *J. Med. Chem.* **2013**, *56*, 427–436.
- [2] Ugwuegbulam, C. O.; Foy, J. E. US6479660 (B1) - Process for the preparation of anti-malarial drugs. 2002.
- [3] Zingle, C.; Kuntz, L.; Tritsch, D. Grosdemange-Billiard, C., Rohmer, R., Isoprenoid Biosynthesis via the Methylerythritol Phosphate Pathway: Structural Variations around Phosphonate Anchor and Spacer of Fosmidomycin, a Potent Inhibitor of Deoxyxylulose Phosphate Reductoisomerase. *J. Org. Chem.* **2010**, *75*, 3203–3207.

Manuscript II



DOI: 10.1002/cmdc.201700360

CHEM MED CHEM
Full Papers

Design and Synthesis of Terephthalic Acid-Based Histone Deacetylase Inhibitors with Dual-Stage Anti-*Plasmodium* Activity

Katharina Stenzel,^[a, b] Ming Jang Chua,^[b] Sandra Duffy,^[b] Yevgeniya Antonova-Koch,^[c] Stephan Meister,^[c] Alexandra Hamacher,^[a] Matthias U. Kassack,^[a] Elizabeth Winzeler,^[c] Vicky M. Avery,^[b] Thomas Kurz,^[a] Katherine T. Andrews,^{+, * [b]} and Finn K. Hansen^{+, * [a, d]}

In this work we aimed to develop parasite-selective histone deacetylase inhibitors (HDAC) inhibitors with activity against the disease-causing asexual blood stages of *Plasmodium* as well as causal prophylactic and/or transmission blocking properties. We report the design, synthesis, and biological testing of a series of 13 terephthalic acid-based HDAC inhibitors. All compounds showed low cytotoxicity against human embryonic kidney (HEK293) cells (IC_{50} : 8–>51 μM), with 11 also having sub-micromolar in vitro activity against drug-sensitive (3D7) and multidrug-resistant (Dd2) asexual blood-stage *P. falciparum* parasites (IC_{50} \approx 0.1–0.5 μM). A subset of compounds were examined for activity against early- and late-stage *P. falciparum*

gametocytes and *P. berghei* exo-erythrocytic-stage parasites. While only moderate activity was observed against gametocytes (IC_{50} > 2 μM), the most active compound (*N*'-(3,5-dimethylbenzyl)oxy)-*N*'-hydroxyterephthalamide, **1 f**) showed sub-micromolar activity against *P. berghei* exo-erythrocytic stages (IC_{50} 0.18 μM) and > 270-fold better activity for exo-erythrocytic forms than for HepG2 cells. This, together with asexual-stage in vitro potency (IC_{50} \approx 0.1 μM) and selectivity of this compound versus human cells (SI > 450), suggests that **1 f** may be a valuable starting point for the development of novel antimalarial drug leads with low host cell toxicity and multi-stage anti-plasmodial activity.

Introduction

Malaria remains one of the world's most significant infectious diseases. In 2015 the World Health Organization (WHO) estimated that there were > 200 million cases of malaria and 429 000 malaria related deaths, with most mortality due to *P. falciparum* parasitic infection.^[1] A widely effective malaria vaccine is still unavailable, with the most advanced candidate vaccine (RTS,S/AS01) being less efficacious than hoped in clinical trials in children in Africa.^[2] Despite the possible introduction of the RTS,S/AS01 vaccine into some regions in the future and on-going efforts to develop other vaccines with increased

efficacy,^[3] it is likely that malaria eradication will ultimately require an integrated strategy that includes vaccines, public health measures and effective drugs for prevention and treatment.^[4] Unfortunately, malaria parasite resistance or decreased clinical efficacy is now reported for all current antimalarial drugs, including the gold standard artemisinin-based combination therapies (ACTs). ACT failure has been reported in several countries in Asia^[1,5] and the threat of more widespread ACT resistance means that new antimalarial chemotypes, with novel mechanisms of action to limit impacts of cross-resistance, are required.

Over the past decades malaria drug development efforts have focused on a limited number of known chemical scaffolds and drug targets, mainly those targeting asexual blood-stage parasites. As the malaria research community strives toward elimination and ultimately eradication of malaria the focus has shifted to include discovery and development of drugs that can target liver-stage parasites (exo-erythrocytic forms) to prevent infection from being established and sexual blood-stage gametocytes to block parasite transmission to the mosquito vector.^[6] Here we address this issue by investigating histone deacetylase inhibitor (HDACi) type small molecules for anti-plasmodial activity.

HDACs are an essential part of eukaryotic epigenetic machinery, playing an important role in gene regulation and control of cell proliferation and differentiation.^[7] HDACs can be described as "eraser" enzymes as they cleave acetate from acety-

[a] K. Stenzel, Dr. A. Hamacher, Prof. Dr. M. U. Kassack, Prof. Dr. T. Kurz, Prof. Dr. F. K. Hansen^{*}
Institute of Pharmaceutical and Medicinal Chemistry, Heinrich Heine University Düsseldorf, 40225 Düsseldorf (Germany)

[b] K. Stenzel, M. J. Chua, S. Duffy, Prof. Dr. V. M. Avery, Prof. Dr. K. T. Andrews^{*}
Griffith Institute for Drug Discovery, Griffith University, Don Young Road, Nathan Campus, QLD 4111 (Australia)
E-mail: k.andrews@griffith.edu.au

[c] Dr. Y. Antonova-Koch, Dr. S. Meister, Prof. Dr. E. Winzeler
Department of Pediatrics, School of Medicine, University of California, San Diego, 9500 Gilman Drive 0741, La Jolla, CA 92093 (USA)

[d] Prof. Dr. F. K. Hansen^{*}
Pharmaceutical/Medicinal Chemistry, Institute of Pharmacy, Leipzig University, Brüderstraße 34, 04103 Leipzig (Germany)
E-mail: finn.hansen@uni-leipzig.de

[*] These authors contributed equally to this work.

Supporting information and the ORCID identification number(s) for the author(s) of this article can be found under <https://doi.org/10.1002/cmdc.201700360>.

lated ϵ -amino groups of lysine residues of both histone and non-histone proteins, thereby regulating chromatin remodeling and other cell processes.^[8] Mutations in HDAC genes and/or alterations in the expression of HDACs are associated with cancers and HDACi are validated and approved drugs for the treatment of some cancers (e.g., vorinostat (SAHA; Zolinza®; Figure 1), romidepsin (Istodax®), belinostat (Beleodaq®), panobinostat (LBH-589; Farydak®, Figure 1) and chidamide (Epidaza®).^[9] Furthermore, HDACi are under investigation for use against a wide range of diseases, including neurodegenerative diseases, HIV, cardiac diseases, inflammatory diseases, and parasitic diseases, illustrating their significant potential.^[9,10]

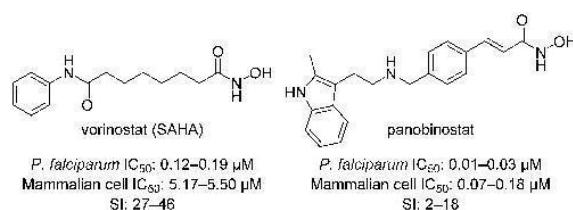


Figure 1. Structures and properties of two approved anticancer hydroxamate-based HDACi with anti-plasmodial activity. Selectivity index (SI): [mammalian cell IC₅₀]/[*P. falciparum* IC₅₀]; larger values indicate greater malaria parasite selectivity. *P. falciparum* and mammalian cell data from Ref. [10a].

HDACs have been shown to be important regulators of transcription in *P. falciparum* and the inhibition of *P. falciparum* HDACs (*Pf*HDACs) a possible mechanism to kill the parasite.^[10b,11]

Five HDAC encoding genes have been annotated in the genome of *P. falciparum*. Three have homology to human class I and II HDACs and two are class III (Sir2) homologues. *Pf*HDAC1 is transcribed across all life cycle stages in *P. falciparum* and has the highest similarity to HDACs of other species, with >50% amino acid identity to human HDAC1 and HDAC2. In contrast, *Pf*HDAC2 and *Pf*HDAC3 have limited homology to other class II HDAC proteins in other species.^[12] While *Pf*Sir2A and *Pf*Sir2B are not essential to asexual blood-stage *P. falciparum*,^[13] knockdown of *Pf*HDAC3 (also called *Pf*HDA2) has been shown to inhibit asexual blood-stage *P. falciparum* growth and to affect gametocytogenesis.^[12] A number of HDACi have been shown to have potent activity against asexual blood-stage parasites and to cause hyperacetylation of parasite histones, including clinically used anticancer HDACi drugs. However these compounds have varying selectivity for the parasite versus human cells (Figure 1).^[10b] Of the three *P. falciparum* class I/II HDAC homologues, recombinant protein is only available for *Pf*HDAC1.^[14] Although this enzyme is inhibited by different anti-plasmodial HDACi type compounds, its quality has been questioned.^[15] While the specificity of anti-plasmodial HDAC inhibitors for *Pf*HDAC1 versus the other *P. falciparum* HDACs is not yet known, we hypothesized that HDACi with potent activity against *P. falciparum* asexual blood stages and low activity against human class I enzymes and in particular against hHDAC1, are likely to be suitable starting points for the devel-

opment of anti-plasmodial HDACi with improved parasite-selectivity. This hypothesis was supported by a recent report from De Vreese et al., who showed that selective hHDAC6 inhibitors (with low activity against human class I HDACs) can possess potent and selective anti-plasmodial activity.^[16]

Previously we reported the synthesis and anti-plasmodial properties of the alkoxyamide-based HDACi of type I (see Figure 2). Several compounds from that series revealed potent

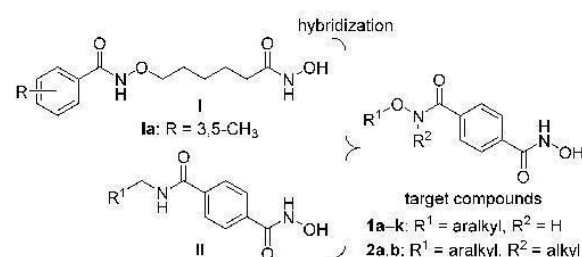


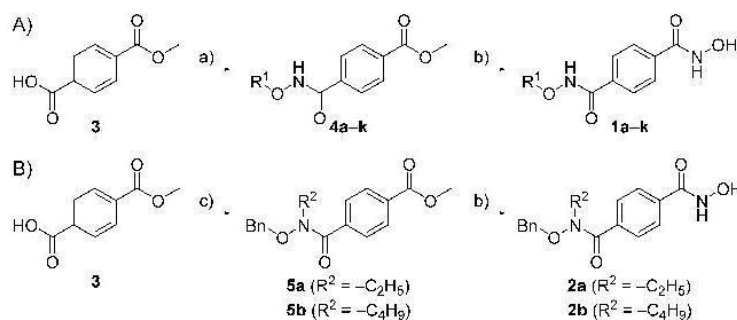
Figure 2. Design of terephthalic acid-based HDACi 1a–k, 2a and 2b featuring an alkoxyamide connecting unit linker region.^[17,19]

anti-plasmodial activity against asexual blood-stage *P. falciparum* parasites (IC₅₀ 0.09–1.12 μ M) as well as nanomolar to micromolar activity against late-stage (IV–V) *P. falciparum* gametocytes (*Pf*LSG IC₅₀ 0.25–> 120 μ M) and *P. berghei* exo-erythrocytic forms (*Pb*EEF IC₅₀ 0.16–7.91 μ M). While these results suggest that it may be possible to develop HDACi that target multiple malaria parasite life cycle stages, a limitation was that the alkoxyamide-based compounds with multi-stage targeting activity had only moderate selectivity for parasites versus mammalian cells (SI 13–27).^[17] With the aim of developing HDACi with improved selectivity for the parasites as well as increased potency against different *Plasmodium* parasite life cycle forms, herein we report the rational design, synthesis and bioactivity of a new type of anti-plasmodial HDACi with potent activity against asexual blood-stage parasites and exo-erythrocytic forms.

Results and Discussion

Design and synthesis of target compounds

Because the cytotoxicity of HDACi against mammalian cells is mainly attributed to the inhibition of human class I HDAC isoforms^[18] we hypothesized that HDACi with low activity against human class I enzymes and in particular against hHDAC1 are more likely to be suitable starting points for the development of anti-plasmodial HDACi with high parasite-selectivity. Interestingly, the *N*-hydroxy-benzamides II are known to show decreased inhibition of human class I isoforms (Figure 2).^[19] Thus, to identify potent anti-plasmodial HDACi with lower cytotoxicity, we designed the target compounds 1a–k and 2a,b by hybridizing our previously reported alkoxyamide connecting unit realized in I with a terephthalic acid-based linker (Figure 2).^[17]



Scheme 1. Synthesis of terephthalic acid-based HDACi A) **1a-k** and B) **2a** and **2b**. *Reagents and conditions:* a) isobutyl chloroformate, NMM, R¹ONH₂, THF, RT, 3 h, 67–93%; b) H₂NOH·HCl, Na, MeOH dry, 70 °C, 3 h, 41–83%; c) BnONHR², CDI, RT, 77–79%.

The preparation of the target compounds is summarized in Scheme 1. Compounds **1a-k** were synthesized using a simple two-step protocol starting from readily available *O*-substituted hydroxylamine derivatives and mono-methyl terephthalate **3**. First, mono-methyl terephthalate **3** was converted into a mixed anhydride and subsequently reacted with the respective *O*-substituted hydroxylamine to afford the key intermediates **4a-k** (67–93% yield, Scheme 1A). Secondly, **4a-k** were treated with a freshly prepared solution of hydroxylamine in a sealed tube at 70 °C for 3 h (Scheme 1A). The crude products were purified by flash column chromatography to afford the desired HDACi **1a-k** in 41–83% yield. Initial attempts to prepare the *N*-alkylated intermediates **5a** and **5b** using the mixed anhydride method provided both compounds only in relatively low yields (<30%). Thus, the *N*-alkylated intermediates **5a** and **5b** were prepared by a slightly modified procedure using 1,1'-carbonyldiimidazole (CDI) as coupling reagent.^[20] The CDI-mediated amide coupling reaction of mono-methyl terephthalate **3** with *N,O*-disubstituted hydroxylamines afforded the *N*-alkylated alkoxyamides **5a** and **5b** in 77% and 79% yield, respectively (Scheme 1B). The subsequent hydroxylaminolysis furnished the target compounds **2a** and **2b** (Scheme 1B).

In vitro activity against *P. falciparum* asexual blood-stage parasites

All synthesized compounds (**1a-k**, **2a** and **2b**) were tested for in vitro growth inhibition activity against the 3D7 line of *P. falciparum*. As summarized in Table 1 compounds **1a-k**, **2a** and **2b** showed anti-plasmodial activity ranging from 0.09 to 24.67 μM. The IC₅₀ value of the prototype compound **1a** (R¹ = Bn, R² = H; Pf3D7 IC₅₀ 0.14 μM) was similar to the activity of reference HDACi SAHA (Pf3D7 IC₅₀ 0.21 μM). Alkylation of the alkoxyamide connecting unit with an ethyl group resulted in decreased activity (**2a**, R¹ = Bn, R² = C₂H₅; Pf3D7 IC₅₀ 2.76 μM), and further elongation of the alkyl substitution to a butyl group resulted in a loss of anti-plasmodial activity (**2b**, R¹ = Bn, R² = C₄H₉; Pf3D7 IC₅₀ 24.67 μM). Thus, we focused our structural modification on compounds with a hydroxamic acid as ZBG and an unsubstituted alkoxyamide connecting unit. The phenylethyl homologue **1d** (Pf3D7 IC₅₀ 0.50 μM) displayed lower

Table 1. In vitro activity of **1a-k** and **2a,b** against asexual blood stages of *P. falciparum*.

Compd	R ¹	R ²	IC ₅₀ [μM] ^[a]		Ri ^[d]
			Pf3D7 ^[b]	PfDd2 ^[c]	
1a	Bn	H	0.14 ± 0.02	0.16 ± 0.01	1.1
1b	trityl	H	0.28 ± 0.12	0.26 ± 0.07	0.9
1c	4-CH ₃ -PhCH ₂	H	0.11 ± 0.02	0.13 ± 0.03	1.2
1d	PhCH ₂ CH ₂	H	0.50 ± 0.23	0.82 ± 0.25	1.6
1e	PhCH ₂ CH ₂ CH ₂	H	0.13 ± 0.06	0.18 ± 0.06	1.4
1f	3,5-CH ₃ -PhCH ₂	H	0.09 ± 0.03	0.11 ± 0.02	1.2
1g	1-naphthyl-CH ₂	H	0.17 ± 0.04	0.17 ± 0.02	1.0
1h	2,4-Cl-PhCH ₂	H	0.23 ± 0.02	0.22 ± 0.01	1.0
1i	3,4-Cl-PhCH ₂	H	0.21 ± 0.05	0.29 ± 0.02	1.4
1j	2,3-Cl-PhCH ₂	H	0.20 ± 0.04	0.23 ± 0.03	1.2
1k	3,4-FI-PhCH ₂	H	0.20 ± 0.03	0.32 ± 0.07	1.6
2a	Bn	C ₂ H ₅	2.76 ± 0.53	3.43 ± 1.2	1.2
2b	Bn	C ₄ H ₉	24.67 ± 6.19	n.d.	n.d.
1a			0.10 ± 0.02 ^[e]	n.d.	n.d.
SAHA			0.21 ± 0.06	0.18 ± 0.05	0.9
CQ ^[f]			0.006 ± 0.003	0.06 ± 0.03	

[a] In vitro 50% growth inhibition values; n.d.: not determined. [b] *P. falciparum* 3D7: data are the mean ± SD of three independent assays, each carried out in triplicate. [c] *P. falciparum* Dd2: data are the mean ± SD of at least two independent assays, each carried out in triplicate. [d] Resistance index (IC₅₀ PfDd2)/(IC₅₀ Pf3D7). [e] Data from Ref. [17]. [f] Chloroquine.

anti-plasmodial activity than **1a** (Pf3D7 IC₅₀ 0.14 μM). Further elongation of the linker to propyl (**1e**, Pf3D7 IC₅₀ 0.13 μM) resulted in a similar activity as in the benzyl-substituted prototype compound **1a**. Introducing a trityl group, as in **1b**, decreased activity (Pf3D7 IC₅₀ 0.28 μM). Further modifications on the aromatic cap group in **1a** were therefore investigated including chloro substituents and methyl groups as well as the replacement of the phenyl ring by a naphthyl group. The introduction of methyl groups to the cap group resulted in an improved activity, whereas chloro substituents as well as a naphthyl-based cap groups provided compounds with decreased activity relative to the prototype compound **1a**. The best activity against the 3D7 line of *P. falciparum* was observed for compound **1f** (R¹ = 3,5-CH₃-PhCH₂, R² = H; Pf3D7 IC₅₀ 0.09 μM; Table 1). Interestingly, **1f** showed a similar activity as com-

pound **1a** (*Pf*3D7 IC_{50} 0.10 μM , Table 1), a hit compound from our previous study also bearing a 3,5-dimethylphenyl-based cap (Figure 2).^[1]

Subsequently, all compounds with activity against the 3D7 line ($IC_{50} < 5 \mu\text{M}$) were screened for activity against the multi-drug resistant Dd2 line of *P. falciparum* (Table 1). A comparison of the resistance indices (RI) revealed that the compounds possess similar activity against both strains (RI: 0.9–1.6). In general, similar structure activity relationships were observed for *P. falciparum* Dd2 as observed against 3D7. For instance, the introduction of an ethyl group to the alkoxyamide moiety resulted in more than 20-fold decreased activity (see **1a** versus **2a**; Table 1). As for line 3D7, compound **1f** ($R^1 = 3,5\text{-CH}_3\text{-PhCH}_2$, $R^2 = \text{H}$) showed the highest activity of all synthesized compounds (*Pf*Dd2 IC_{50} 0.11 μM ; Table 1).

In vitro cytotoxicity against human cells and *P. falciparum* selectivity indices

To investigate the selectivity of our terephthalic acid-based HDACi for the parasites versus human cells, cytotoxicity of all compounds was evaluated against human embryonic kidney 293 (HEK293) cells (Table 2). The screening revealed IC_{50} values in the range of 8.3 to 51.3 μM . One compound displayed single-digit micromolar cytotoxicity (**1g**, HEK293 IC_{50} 8.3 μM), eight compounds (**1c**, **1e**, **1f**, **1h**, **1i**, **1j**, **1k** and **2a**) had moderate toxicity with IC_{50} values ranging from 10 to 20 μM , while four compounds (**1a**, **1b**, **1d** and **2b**) showed low cytotoxicity with IC_{50} s between 20.1 and 51.3 μM .

Notably, the five most active asexual blood-stage inhibitors (**1a**, **1c**, **1e**, **1f**, and **1g**) showed calculated selectivity indices (SI; human cell $IC_{50}/P. falciparum IC_{50}$) of greater than 100 (Table 2). In comparison, the reference anticancer HDACi SAHA showed high cytotoxicity against HEK293 cells (IC_{50} 1.49 μM) resulting in low parasite selectivity ($SI^{\text{HEK293}/3D7}$: 7 and $SI^{\text{HEK293}/Dd2}$:

8). As cytotoxicity is cell-line dependent, compounds **1a**, **1c**, **1e**, **1f**, and **1g** were further tested for cytotoxicity against the HepG2 human liver cancer cell line (Table 2), which is frequently used as a marker of in vitro liver toxicity.^[21] All compounds showed low cytotoxicity against HepG2 cells and four (**1a**, **1c**, **1e**, and **1f**) of the five compounds tested showed no cytotoxicity at the highest concentration examined (50 μM). The best parasite-selectivity was observed for compound **1f** ($SI^{\text{HepG2}/3D7} > 556$ and $SI^{\text{HepG2}/Dd2} > 455$). Of note, the hit compound from our previous study (**1a**) showed a remarkably higher cytotoxicity against the human HepG2 cell line (IC_{50} 1.26 μM) resulting in a relatively low selectivity index ($SI^{\text{HepG2}/3D7}$: 13).^[17] Keeping in mind that **1f** and **1a** both feature a 3,5-dimethylphenyl-based cap group, these data demonstrate that the parasite selectivity of HDACi can be improved by using a terephthalic acid linker instead of an alkyl linker.

As mentioned above, the high cytotoxicity of HDACi against mammalian cells is mainly attributed to the inhibition of human class I HDAC isoforms. To assess whether the lower cytotoxicity of our compounds compared to SAHA correlates with decreased activity against human class I HDACs, we tested the activity of **1a**, **1c**, **1e**, **1f**, and **1g** and the reference compound SAHA against recombinant hHDAC1. When we compared activity against recombinant hHDAC1, we found that **1a**, **1c**, **1e**, **1f**, and **1g** (IC_{50} 0.51 to 0.88 μM) showed 9- to 16-fold lower activity against hHDAC1 than SAHA (IC_{50} 0.056 μM , Table S1). Because our target compounds were designed based on the preferential hHDAC6 inhibitors of type II, compounds **1a**, **1c**, **1e**, **1f**, and **1g** were further tested for inhibition of recombinant hHDAC6. The screening revealed IC_{50} values ranging from 0.09 to 0.38 μM (Table S1). These results indicate a moderate preference for hHDAC6 over hHDAC1. While the preferential inhibition of hHDAC6 may contribute to the reduced cytotoxicity and improved selectivity indices observed for these compounds over SAHA in comparison with the activity against *P. falciparum* infected erythrocytes, we cannot confirm this. Furthermore, it cannot be ruled out that the parasite-specific activity arises from differences in cell permeability or efflux between the parasites and mammalian cells.

To elucidate whether the asexual blood-stage activity of our compounds is related to inhibition of class I or class II *Pf*HDACs, screening the compounds against all three zinc-dependent *Pf*HDACs would be required. However, of the three *P. falciparum* class I/II HDAC homologues, recombinant protein is only available for *Pf*HDAC1. Furthermore, in a recent study, the quality of recombinant *Pf*HDAC1 has been questioned,^[15] both in terms of the low purity of this commercially available enzyme and validity of its catalytic activity in the absence of endogenous cofactors. Thus, we decided to study the effect of selected compounds on parasitic deacetylase activity by means of *P. falciparum* hyperacetylation assays.

Asexual blood-stage *P. falciparum* hyperacetylation assays with terephthalic acid-based HDACi

The in situ hyperacetylation of histones in *P. falciparum* trophozoite-stage parasites by ten terephthalic acid-based HDACi

Compd	HEK293	SI	HepG2	SI
	IC_{50} [μM]	<i>Pf</i> 3D7/ <i>Pf</i> Dd2	IC_{50} [μM]	<i>Pf</i> 3D7/ <i>Pf</i> Dd2
1a	29.7 \pm 6.7	212/186	> 50	> 357/313
1b	51.3 \pm 18.8	183/197	n.d.	n.d.
1c	17.6 \pm 5.1	160/135	> 50	> 455/384
1d	20.6 \pm 5.6	41/25	n.d.	n.d.
1e	18.4 \pm 4.1	142/102	> 50	> 385/278
1f	11.9 \pm 1.9	132/108	> 50	> 556/455
1g	8.3 \pm 2.2	49/49	37.25	219/219
1h	15.6 \pm 5.1	67/71	n.d.	n.d.
1i	11.2 \pm 1.8	53/39	n.d.	n.d.
1j	11.8 \pm 3.1	59/51	n.d.	n.d.
1k	16.4 \pm 7.2	82/51	n.d.	n.d.
2a	16.6 \pm 7.2	6/5	n.d.	n.d.
2b	20.1 \pm 7.0	1/–	n.d.	n.d.
1a	n.d.	n.d.	1.26 ^[b]	13/n.d. ^[b]
SAHA	1.49 \pm 0.2	7/8	1.49 ^[b]	7/8

[a] *P. falciparum* 3D7 (*Pf*3D7), *P. falciparum* Dd2 (*Pf*Dd2); SI = selectivity index (mammalian cell $IC_{50}/P. falciparum IC_{50}$); larger values indicate greater malaria parasite selectivity; n.d.: not determined. [b] Data from Ref. [17].

(1a–c and 1e–k) was assessed in two independent experiments by western blot (Figure 3). The anti-(tetra)-acetyl histone H4 antibody detected an ~11 kDa band that corresponds to the expected size of H4, as well as a doublet of ~13–14 kDa and a band of ~16 kDa band which likely correspond to hyperacetylated forms of H2B/H2Bv and H2A.Z, respectively (see Experimental Section, *Histone hyperacetylation assays*), as previously reported.^[22] Using this antibody, all compounds, except 1b with a trityl in the R¹ position, caused a mean 1.5 to 3.4-fold increased signal relative to the vehicle control, irrespective of whether density of all bands (Figure 3; grey bars) or only the ~11 kDa band corresponding to H4 (Figure 3; white bars) were analyzed. As expected the control HDAC inhibitor SAHA, but not the negative control drug chloroquine, also caused hyperacetylation with mean ≈3-fold increased signal relative to vehicle control (Figure 3). While this suggests that all compounds, except 1b, can hyperacetylate *P. falciparum* histone H4 to some extent, it is important to note that these data only present single time-point snapshots of acetylation levels. Direct comparison of acetylation levels between compounds cannot be made as factors such as compound exposure dynamics (such as stability, cell permeability and efflux mechanisms), presence of differing isoforms and/or expression levels of potential target proteins within the parasite must be taken into account. Further analysis will be required to determine if the differences observed here, in particular for compound 1b,

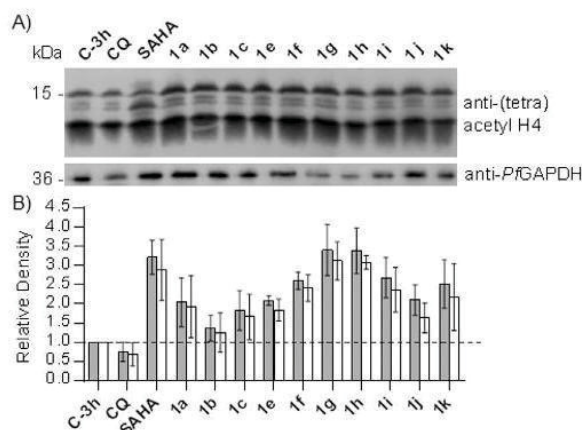


Figure 3. Hyperacetylation of *P. falciparum* histones by terephthalic acid-based HDACi. A) Western blot analysis of protein lysates prepared from trophozoite-stage *P. falciparum* 3D7-infected blood cells treated with SAHA, 1a–c, or 1e–k for 3 h. Parasite-infected blood cells treated for 3 h with 5 × IC₅₀ chloroquine (CQ) or vehicle only (0.1% DMSO; C-3h) are shown as a negative controls. Following western blot using anti-(tetra)-acetyl histone H4 (the ≈11 kDa band corresponds to the correct size of histone H4, with the doublet likely due to cross-reactivity with acetylated forms of H2B/H2Bv (≈13–14 kDa) and the ≈16 kDa band due to cross-reactivity with H2A.Z; see Experimental Section), the same membrane was re-probed with anti-PfGAPDH as loading control (representative blot shown). B) Densitometry analysis of two independent western blot results. Data are the mean (±SD) relative density of all bands (grey bars) or the ≈11 kDa band only (white bars) obtained using anti-(tetra)-acetyl histone H4 and compared with the band detected using anti-PfGAPDH on the same membrane and normalized to the C-3h control (set as 1.0; dotted line).

are related to target preferences, however as discussed above, this is currently limited by a lack of recombinant PfHDAC proteins.

Activity of terephthalic acid-based HDACi against *Plasmodium* exo-erythrocytic and gametocyte stages

Current antimalarial drug discovery efforts have moved toward elimination/eradication of malaria and aim to target exo-erythrocytic liver stages (prevention) and gametocyte-stage (transmission) parasites in addition to asexual blood stages.^[23] Thus, in addition to asexual blood-stage activity, it would be beneficial for new antimalarial agents to have activity against at least one of the non-dividing stages in order to provide additional prophylactic and/or transmission blocking potential. The five most potent asexual blood-stage inhibitors were therefore screened for activity against murine malaria (*P. berghei*) exo-erythrocytic forms and early-stage (stage I–III) and late-stage (stage IV–V) *P. falciparum* gametocytes. There are homologues for each of the three *P. falciparum* class I/II HDACs in *P. berghei*, with amino acid identities ranging from ≈35–95%, and highest identity seen for PfHDAC1 (see Supporting Information Table S2).

Plasmodium liver stages are clinically silent pre-erythrocytic life cycle stages and inhibition of this stage has the potential to lead to causal prophylaxis. When the activity of a subset of the terephthalic acid-based HDACi was evaluated against *P. berghei* exo-erythrocytic forms (PbEEF), three of the five compounds were found to have IC₅₀ values >1 μM (1c, 1e and 1g; Table 3), however, 1a and 1f showed nanomolar activity with IC₅₀ values of 0.53 μM and 0.18 μM, respectively (Table 3). Notably, the *Plasmodium* liver stages activity of 1f is similar to the activity of compound 1a from our former study (IC₅₀ 0.16 μM, Table 3).

A comparison of the PbEEF IC₅₀ of 1f with the HepG2 cell cytotoxicity indicates that 1f has >270-fold higher activity against *P. berghei* exo-erythrocytic stages versus human HepG2 cells. It is interesting to note that 1f was also the most parasite-selective *P. falciparum* asexual blood-stage inhibitor (Table 2). While some other hydroxamate HDACi (including SAHA (S^{HepG2/PbEEF}: 11) and 1a (S^{HepG2/PbEEF}: 8))^[17] have been shown to have sub-micromolar activity against exo-erythrocytic

Table 3. Activity of terephthalic acid-based HDACi against *P. berghei* exo-erythrocytic forms.

Compd	R ¹	R ²	PbEEF IC ₅₀ [μM] ^[a]	95% CI ^[b]
1a	Bn	H	0.53	0.34–0.84
1c	4-CH ₃ -PhCH ₂	H	9.51	7.28–12.39
1e	PhCH ₂ CH ₂ CH ₂	H	8.08	6.31–10.36
1f	3,5-CH ₃ -PhCH ₂	H	0.18	0.10–0.34
1g	1-naphthyl CH ₂	H	3.73	2.97–4.69
1a			0.16 ^[c]	0.12–0.21 ^[d]

[a] PbEEF, *P. berghei* exo-erythrocytic forms; atovaquone was used as reference compound (IC₅₀: 0.0565 nM). [b] 95% confidence interval for PbEEF IC₅₀ [μM]. [c] Data from Ref. [17].

ic-stage *P. berghei* parasites, to the best of our knowledge compound **1f** is the first anti-plasmodial HDACi with both nanomolar activity against *P. berghei* exo-erythrocytic forms in addition to high parasite-specific selectivity ($SI^{\text{HepG2/PbEEF}} > 270$).

Because four HDACi from our previous study including **1a** (IC_{50} 0.33 μM , Table 4) revealed sub-micromolar activity against late-stage *P. falciparum* gametocytes,^[17] we examined the activity of **1a**, **1c**, **1e**, **1f**, and **1g** against early-stage (stage I–III) and late-stage (stage IV–V) *P. falciparum* gametocytes using an imaging-based viability assay. In contrast to the activity observed against exo-erythrocytic forms, all five compounds were found to have only moderate activity ($IC_{50} \geq 2 \mu\text{M}$; Table 4).

Table 4. Activity of terephthalic acid-based HDACi against early-stage (I–III) and late-stage (IV–V) *P. falciparum* gametocytes.

Compd	R ¹	R ²	IC ₅₀ [μM]	
			PFESG ^[a]	PFLSG ^[b]
1a	Bn	H	4.27 ± 1.07 ^[a]	93% ^[c]
1c	4-CH ₃ -PhCH ₂	H	5.41 ± 1.88 ^[a]	5.77 ± 3.01 ^[b]
1e	PhCH ₂ CH ₂ CH ₂	H	4.85 ± 1.45 ^[a]	3.07 ± 0.78 ^[b]
1f	3,5-CH ₃ -PhCH ₂	H	2.62 ± 1.20 ^[a]	2.29 ± 0.21 ^[b]
1g	1-naphthyl-CH ₂	H	2.30 ± 0.20 ^[a]	2.06 ± 0.68 ^[b]
la		n.d.		0.33 ± 0.01 ^[a]
artesunate			0.003 ± 0.001 ^[a]	0.008 ± 0.0008 ^[b]
pyronaridine			0.029 ± 0.0010 ^[a]	1.710 ± 0.33 ^[b]
chloroquine			0.062 ± 0.016 ^[a]	68% ^[c]

[a] *P. falciparum* NF54 early-stage gametocytes (stage I–III): data are the mean ± SD of three independent assays, 16-point dose–response in duplicate wells. [b] *P. falciparum* NF54 late-stage gametocytes (IV–V): data are the mean ± SD of two independent assays, 16-point dose–response in duplicate wells. [c] Percent inhibition at 40 μM is provided when E_{max} plateau was not obtained to determine the IC_{50} value (see the Experimental Section for full description of analysis). [d] ESG data from two independent experiments. [e] Data from Ref. [17].

Conclusions

In summary, we have synthesized a mini-library of a novel type of anti-plasmodial compounds based on the HDACi pharmacophore. Several compounds have activity similar to that of the reference HDACi SAHA against drug-sensitive (3D7) and multi-drug resistant (Dd2) asexual blood-stage *P. falciparum* parasites, with five (**1a**, **1c**, **1e**, **1f**, and **1g**) having selectivity indices of >100 for *P. falciparum* versus human cells. The most active compound (**1f**; Pf3D7 IC_{50} 0.09 μM , PfDd2 IC_{50} 0.11 μM) was >455-fold more toxic against the asexual blood stages than toward mammalian HepG2 cells. Selected compounds were shown to cause hyperacetylation of *P. falciparum* histones in asexual blood-stage parasites, consistent with a mode of action targeting parasite deacetylase activity. Compounds **1a**, **1c**, **1e**, **1f**, and **1g** were further tested for activity against *P. berghei* exo-erythrocytic stages and early- and late-stage *P. falciparum* gametocytes. While this subset of terephthalic acid-based HDACi showed only moderate activity against gametocytes, compound **1f** showed potent and selective activity against *P. berghei* exo-erythrocytic stages. Notably, **1f** has >270-fold higher activity against *P. berghei* exo-erythrocytic

stages than against mammalian HepG2 cells. Thus, compound **1f** may be a useful starting point for further optimization toward anti-plasmodial HDACi with dual- or multi-stage activity and high parasite-specific activity.

Experimental Section

Chemistry

General: All chemicals and solvents were obtained from commercial suppliers (Sigma–Aldrich, Acros Organics, Carbolution Chemicals) and used as purchased without further purification. The synthesis of the required *O*-substituted and *N,O*-disubstituted hydroxylamine derivatives was performed according to literature procedures.^[20a, 24] The progress of all reactions was monitored by thin layer chromatography (TLC) using Merck pre-coated silica gel plates (with fluorescence indicator UV₂₅₄). Components were visualized by irradiation with ultraviolet light (254 nm) or staining in potassium permanganate solution followed by heating. Flash column chromatography was performed using prepacked silica cartridge with the solvent mixtures specified in the corresponding experiment. Melting points (mp) were taken in open capillaries on a Mettler FP 5 melting-point apparatus and are uncorrected. Proton (¹H) and carbon (¹³C) NMR spectra were recorded on a Bruker Avance 300, 500 or 600 using [D₆]DMSO or CDCl₃ as solvents. Chemical shifts are given in parts per million (ppm), relative to residual solvent peak for ¹H and ¹³C. Elemental analysis was performed on a PerkinElmer PE 2400 CHN elemental analyzer. High resolution mass spectra (HRMS) analysis was performed on a UHR-TOF maXis 4G, Bruker Daltonics, Bremen by electrospray ionization (ESI). Analytical HPLC analysis were carried out on a Varian Prostar system equipped with a Prostar 410 (autosampler), 210 (pumps) and 330 (UV-detector) using a Phenomenex Luna 5u C18(2) 1.8 μm particle (250 mm × 4.6 mm) column, supported by Phenomenex Security Guard Cartridge Kit C18 (4.0 mm × 3.0 mm). UV absorption was detected at 254 nm with a linear gradient of 10% B to 100% B in 20 min using HPLC-grade water + 0.1% TFA (solvent A) and HPLC-grade acetonitrile + 0.1% TFA (solvent B) for elution at a flow rate of 1 mLmin⁻¹. The purity of all final compounds was 95% or higher. General procedures for the synthesis and compound characterization data for HDACi **1a–k** and **2a,b** are given below. The synthesis of all other compounds is reported in the Supporting Information.

General procedure for the synthesis of 1a–k and 2a,b: Hydroxylamine hydrochloride (348 mg, 5.0 mmol, 10 equiv) was added to a sodium methanolate solution freshly prepared from dry methanol (8 mL) and sodium (175 mg, 7.5 mmol, 15 equiv). The mixture was stirred for 10 min before the respective ester **4a–k** and **5a,b** (0.5 mmol, 1.0 equiv) was added. The reaction mixture was stirred in a sealed tube for 3 h and 70 °C. The solvent was removed under reduced pressure, water (15 mL) was added, and the pH was adjusted to pH 7–8 using 4 M HCl. The mixture was extracted with ethyl acetate (3 × 50 mL), the combined organic layers were dried over anhydrous sodium sulfate, filtered, and concentrated in vacuum. The crude products were purified by flash column chromatography (prepacked silica cartridge, dichloromethane–dichloromethane/methanol (70:30), gradient: 90:10 → 70:30 in 20 min) to yield the desired hydroxamic acids **1a–k** and **2a,b**.

N¹-(Benzoyloxy)-N³-hydroxyterephthalamide 1a: Colorless solid; yield: 69%, mp: 189 °C; ¹H NMR (500 MHz, [D₆]DMSO): δ = 11.89 (s, 1H), 11.35 (s, 1H), 9.15 (s, 1H), 7.85–7.76 (m, 4H), 7.56–7.30 (m, 5H), 4.94 ppm (s, 2H); ¹³C NMR (151 MHz, [D₆]DMSO): δ = 163.72,

136.38, 135.91, 135.00, 129.40, 128.81, 127.62, 127.46, 77.45 ppm; t_R : 6.01 min, purity: 98.8%; HRMS (ESI) Anal. calcd for $C_{15}H_{15}N_2O_4$ 287.1026 $[M+H]^+$, found 287.1027.

***N*¹-Hydroxy-*N*⁴-(trityloxy)terephthalamide 1b:** Colorless solid; yield 59%; mp: 199 °C; ¹H NMR (500 MHz, $[D_6]DMSO$): δ = 11.26 (s, 1H), 11.05 (s, 1H), 9.09 (s, 1H), 7.69 (d, J = 8.0 Hz, 2H), 7.57–7.15 ppm (m, 17H); ¹³C NMR (151 MHz, $[D_6]DMSO$): δ = 163.28, 163.21, 142.31, 137.19, 134.88, 134.06, 134.81, 129.00, 127.38, 126.56, 92.44 ppm; t_R : 16.08 min, purity: 99.5%; HRMS (ESI) Anal. calcd for $C_{27}H_{22}N_2NaO_4$ 461.1472 $[M+Na]^+$, found 461.1471.

***N*¹-Hydroxy-*N*⁴-(4-methylbenzyl)oxy)terephthalamide 1c:** Colorless solid; yield: 68%; mp: 193 °C; ¹H NMR (600 MHz, $[D_6]DMSO$): δ = 11.84 (s, 1H), 11.34 (s, 1H), 9.15 (s, 1H), 7.85–7.76 (m, 4H), 7.35 (d, J = 7.5 Hz, 2H), 7.21 (d, J = 7.6 Hz, 2H), 4.89 (s, 2H), 2.32 ppm (s, 3H); ¹³C NMR (151 MHz, $[D_6]DMSO$): δ = 164.10, 163.85, 138.13, 135.91, 135.08, 133.28, 129.55, 129.36, 127.65, 127.46, 77.35, 21.30 ppm; t_R : 8.52 min, purity: 100.0%; HRMS (ESI) Anal. calcd for $C_{16}H_{17}N_2O_4$ 301.1183 $[M+H]^+$, found 301.1185.

***N*¹-Hydroxy-*N*⁴-phenethoxyterephthalamide 1d:** Colorless solid; yield 59%; mp: 173 °C; ¹H NMR (500 MHz, $[D_6]DMSO$): δ = 11.80 (s, 1H), 11.37 (s, 1H), 9.15 (s, 1H), 7.81 (s, 3H), 7.37–7.27 (m, 5H), 7.25–7.18 (m, 1H), 4.13 (t, J = 6.8 Hz, 2H), 2.96 ppm (t, J = 6.7 Hz, 2H); ¹³C NMR (151 MHz, $[D_6]DMSO$): δ = 163.79, 138.83, 135.86, 135.09, 129.35, 128.77, 127.64, 127.44, 126.67, 76.21, 34.52 ppm; t_R : 8.82 min, purity: 99.8%; Anal. calcd for $C_{16}H_{17}N_2O_4$ 301.1183 $[M+H]^+$, found 301.1181.

***N*¹-Hydroxy-*N*⁴-(3-phenylpropoxy)terephthalamide 1e:** Colorless solid; yield 86%; mp: 159 °C; ¹H NMR (500 MHz, $[D_6]DMSO$): δ = 11.73 (s, 1H), 11.40 (s, 1H), 9.16 (s, 1H), 7.85–7.77 (m, 4H), 7.33–7.23 (m, 4H), 7.18 (t, J = 7.2 Hz, 1H), 3.91 (m, 2H), 2.72 (t, J = 7.9 Hz, 2H), 1.94–1.86 ppm (m, 2H); ¹³C NMR (151 MHz, $[D_6]DMSO$): δ = 163.37, 163.17, 141.50, 135.31, 134.51, 128.28, 128.22, 127.03, 126.87, 125.70, 74.49, 31.34, 29.55 ppm; t_R : 10.16 min, purity: 99.6%; HRMS (ESI) Anal. calcd for $C_{17}H_{19}N_2O_4$ 315.1339 $[M+H]^+$, found 315.1341.

***N*¹-((3,5-Dimethylbenzyl)oxy)-*N*⁴-hydroxyterephthalamide 1f:** Colorless solid; yield 65%; mp: 149 °C; ¹H NMR (500 MHz, $[D_6]DMSO$): δ = 11.86 (s, 1H), 11.34 (s, 1H), 9.14 (s, 1H), 7.86–7.76 (m, 4H), 7.05 (s, 2H), 6.99 (s, 1H), 4.85 (s, 2H), 2.28 ppm (s, 6H); ¹³C NMR (151 MHz, $[D_6]DMSO$): δ = 163.56, 163.25, 137.20, 135.52, 135.34, 134.51, 129.58, 127.09, 126.89, 126.57, 77.01, 20.74 ppm; t_R : 11.50 min, purity: 99.6%; HRMS (ESI) Anal. calcd for $C_{17}H_{19}N_2O_4$ 315.1339 $[M+H]^+$, found 315.1344.

***N*¹-Hydroxy-*N*⁴-(naphthalen-1-ylmethoxy)terephthalamide 1g:** Colorless solid; yield 75%; mp: 140 °C; ¹H NMR (500 MHz, $[D_6]DMSO$): δ = 12.03 (s, 1H), 11.33 (s, 1H), 9.16 (s, 1H), 8.62 (s, 1H), 7.98 (d, J = 8.1 Hz, 2H), 7.85 (s, 4H), 7.70–7.44 (m, 4H), 5.39 ppm (s, 2H); ¹³C NMR (151 MHz, $[D_6]DMSO$): δ = 163.70, 163.21, 135.41, 134.40, 133.21, 131.93, 131.26, 129.33, 128.49, 128.16, 127.13, 126.92, 126.35, 125.94, 125.20, 124.83, 75.27 ppm; t_R : 10.85 min, purity: 97.1%; HRMS (ESI) Anal. calcd for $C_{19}H_{17}N_2O_4$ 337.1183 $[M+H]^+$, found 337.1182.

***N*¹-((2,4-Dichlorobenzyl)oxy)-*N*⁴-hydroxyterephthalamide 1h:** Colorless solid; yield: 71%; mp: 175 °C; ¹H NMR (500 MHz, $[D_6]DMSO$): δ = 11.89 (s, 1H), 11.36 (s, 1H), 9.16 (s, 1H), 8.27–7.30 (m, 7H), 5.04 ppm (s, 2H); ¹³C NMR (151 MHz, $[D_6]DMSO$): δ = 163.69, 163.18, 135.38, 134.21, 133.78, 132.66, 129.11, 128.71, 127.34, 127.08, 126.87, 72.97 ppm; t_R : 11.93 min, purity: 95.3%; HRMS (ESI) Anal. calcd for $C_{15}H_{13}N_2O_4$ 355.0247 $[M+H]^+$, found 355.0245.

***N*¹-((3,4-Dichlorobenzyl)oxy)-*N*⁴-hydroxyterephthalamide 1i:** Colorless solid; yield 73%; mp: 188 °C; ¹H NMR (600 MHz, $[D_6]DMSO$): δ = 11.88 (s, 1H), 11.35 (s, 1H), 9.14 (s, 1H), 8.02–7.72 (m, 5H), 7.67 (d, J = 8.1 Hz, 1H), 7.46 (d, J = 7.4 Hz, 1H), 4.95 ppm (s, 2H); ¹³C NMR (151 MHz, $[D_6]DMSO$): δ = 163.79, 163.24, 137.17, 135.44, 134.26, 130.85, 130.73, 130.56, 130.44, 128.92, 127.09, 126.92, 75.32 ppm; t_R : 12.12 min, purity: 99.2%; HRMS (ESI) Anal. calcd for $C_{15}H_{13}N_2O_4$ 355.0247 $[M+H]^+$, found 355.0248.

***N*¹-((2,3-Dichlorobenzyl)oxy)-*N*⁴-hydroxyterephthalamide 1j:** Colorless solid; yield: 64%; mp: 155 °C; ¹H NMR (600 MHz, $[D_6]DMSO$): δ = 11.91 (s, 1H), 11.35 (s, 1H), 9.13 (s, 1H), 7.98–7.73 (m, 4H), 7.66 (d, J = 7.7 Hz, 1H), 7.58 (d, J = 7.2 Hz, 1H), 7.42 (t, J = 7.8 Hz, 1H), 5.09 ppm (s, 2H); ¹³C NMR (151 MHz, $[D_6]DMSO$): δ = 163.78, 163.24, 136.03, 135.44, 134.25, 131.76, 131.18, 130.45, 129.76, 128.10, 127.12, 126.89, 74.12 ppm; t_R : 11.42 min, purity: 98.7%; HRMS (ESI) Anal. calcd for $C_{15}H_{13}N_2O_4$ 355.0247 $[M+H]^+$, found 355.0247.

***N*¹-((3,4-Difluorobenzyl)oxy)-*N*⁴-hydroxyterephthalamide 1k:** Colorless solid; yield 87%; mp: 192 °C; ¹H NMR (500 MHz, $[D_6]DMSO$): δ = 11.94 (s, 1H), 11.37 (s, 1H), 9.15 (s, 1H), 7.81 (q, J = 8.3 Hz, 4H), 7.61–7.51 (m, 1H), 7.50–7.42 (m, 1H), 7.33 (s, 1H), 4.93 ppm (s, 2H); ¹³C NMR (126 MHz, $[D_6]DMSO$): δ = 163.81, 163.32, 150.21 (ddd, J = 245.0, 12.6 Hz), 148.26 (ddd, J = 245.0, 12.4 Hz), 135.50, 134.39, 133.83, 127.13, 126.95, 125.64 (dd, J = 6.4, 3.2 Hz), 117.68 (d, J = 17.1 Hz), 117.24 (d, J = 17.1 Hz), 75.62 ppm; t_R : 7.79 min, purity: 99.6%; HRMS (ESI) Anal. calcd for $C_{15}H_{13}F_2N_2O_4$ 323.0838 $[M+H]^+$, found 323.0839.

***N*¹-(Benzyl)oxy)-*N*¹-ethyl-*N*⁴-hydroxyterephthalamide 2a:** Colorless solid; yield 54%; mp: 118 °C; ¹H NMR (600 MHz, $[D_6]DMSO$): δ = 11.34 (s, 1H), 9.12 (s, 1H), 7.80 (d, J = 8.0 Hz, 2H), 7.57 (d, J = 8.1 Hz, 2H), 7.37–7.25 (m, 3H), 7.10 (s, 2H), 4.75 (s, 2H), 3.75 (s, 2H), 1.20 ppm (t, J = 7.0 Hz, 3H); ¹³C NMR (151 MHz, $[D_6]DMSO$): δ = 168.43, 163.42, 137.40, 134.30, 133.97, 129.16, 128.50, 128.23, 127.35, 126.50, 75.44, 12.15 ppm; t_R : 11.57 min, purity: 96.6%; HRMS (ESI) Anal. calcd for $C_{17}H_{19}N_2O_4$ 315.1339 $[M+H]^+$, found 315.1343.

***N*¹-(Benzyl)oxy)-*N*¹-butyl-*N*⁴-hydroxyterephthalamide 2b:** Colorless solid; yield 51%; mp: 128 °C; ¹H NMR (600 MHz, $[D_6]DMSO$): δ = 11.35 (s, 1H), 9.13 (s, 1H), 7.81 (d, J = 8.3 Hz, 2H), 7.57 (d, J = 8.3 Hz, 2H), 7.35–7.23 (m, 3H), 7.07 (s, 2H), 4.72 (s, 2H), 3.75 (s, 2H), 1.67–1.59 (m, 2H), 1.38–1.28 (m, 2H), 0.89 ppm (t, J = 7.4 Hz, 3H); ¹³C NMR (151 MHz, $[D_6]DMSO$): δ = 168.40, 163.43, 137.39, 134.21, 133.94, 129.18, 128.52, 128.23, 127.43, 126.49, 75.31, 28.56, 19.21, 13.49 ppm; t_R : 13.58 min, purity: 97.6%; HRMS (ESI) Anal. calcd for $C_{19}H_{23}N_2O_4$ 343.1652 $[M+H]^+$, found 343.1655.

Biological evaluation

In vitro growth inhibition assays against asexual blood-stage *P. falciparum* parasites: Activity against asexual-stage *P. falciparum* parasites was determined using [³H]hypoxanthine incorporation, essentially as previously described.^[12a,25] Briefly, serial dilutions of compound or controls were prepared in parasite culture media (RPMI 1640 supplemented with 10% heat inactivated human serum) with no added hypoxanthine, followed by addition of synchronous ring-stage *P. falciparum* infected erythrocytes (0.25% parasitemia; 2.5% hematocrit). Following incubation for 48 h at 37 °C under standard parasite culture conditions, [³H]hypoxanthine (0.5 μ Ci per well) was added to each well, and the cultures incubated for a further 24 h. Assays were stopped by freezing at –20 °C and, after thawing, [³H]hypoxanthine incorporation measured by

136.38, 135.91, 135.00, 129.40, 128.81, 127.62, 127.46, 77.45 ppm; t_R : 6.01 min, purity: 98.8%; HRMS (ESI) Anal. calcd for $C_{15}H_{13}N_2O_4$ 287.1026 $[M+H]^+$, found 287.1027.

***N*¹-Hydroxy-*N*⁴-(trityloxy)terephthalamide 1b:** Colorless solid; yield 59%; mp: 199 °C; ¹H NMR (500 MHz, $[D_6]DMSO$): δ = 11.26 (s, 1H), 11.05 (s, 1H), 9.09 (s, 1H), 7.69 (d, J = 8.0 Hz, 2H), 7.57–7.15 ppm (m, 17H); ¹³C NMR (151 MHz, $[D_6]DMSO$): δ = 163.28, 163.21, 142.31, 137.19, 134.88, 134.06, 134.81, 129.00, 127.38, 126.56, 92.44 ppm; t_R : 16.08 min, purity: 99.5%; HRMS (ESI) Anal. calcd for $C_{27}H_{22}N_2NaO_4$ 461.1472 $[M+Na]^+$, found 461.1471.

***N*¹-Hydroxy-*N*⁴-(4-methylbenzoyloxy)terephthalamide 1c:** Colorless solid; yield: 68%; mp: 193 °C; ¹H NMR (600 MHz, $[D_6]DMSO$): δ = 11.84 (s, 1H), 11.34 (s, 1H), 9.15 (s, 1H), 7.85–7.76 (m, 4H), 7.35 (d, J = 7.5 Hz, 2H), 7.21 (d, J = 7.6 Hz, 2H), 4.89 (s, 2H), 2.32 ppm (s, 3H); ¹³C NMR (151 MHz, $[D_6]DMSO$): δ = 164.10, 163.85, 138.13, 135.91, 135.08, 133.28, 129.55, 129.36, 127.65, 127.46, 77.35, 21.30 ppm; t_R : 8.52 min, purity: 100.0%; HRMS (ESI) Anal. calcd for $C_{16}H_{17}N_2O_4$ 301.1183 $[M+H]^+$, found 301.1185.

***N*¹-Hydroxy-*N*⁴-phenethoxyterephthalamide 1d:** Colorless solid; yield 59%; mp: 173 °C; ¹H NMR (500 MHz, $[D_6]DMSO$): δ = 11.80 (s, 1H), 11.37 (s, 1H), 9.15 (s, 1H), 7.81 (s, 3H), 7.37–7.27 (m, 5H), 7.25–7.18 (m, 1H), 4.13 (t, J = 6.8 Hz, 2H), 2.96 ppm (t, J = 6.7 Hz, 2H); ¹³C NMR (151 MHz, $[D_6]DMSO$): δ = 163.79, 138.83, 135.86, 135.09, 129.35, 128.77, 127.64, 127.44, 126.67, 76.21, 34.52 ppm; t_R : 8.82 min, purity: 99.8%; Anal. calcd for $C_{16}H_{17}N_2O_4$ 301.1183 $[M+H]^+$, found 301.1181.

***N*¹-Hydroxy-*N*⁴-(3-phenylpropoxy)terephthalamide 1e:** Colorless solid; yield 86%; mp: 159 °C; ¹H NMR (500 MHz, $[D_6]DMSO$): δ = 11.73 (s, 1H), 11.40 (s, 1H), 9.16 (s, 1H), 7.85–7.77 (m, 4H), 7.33–7.23 (m, 4H), 7.18 (t, J = 7.2 Hz, 1H), 3.91 (m, 2H), 2.72 (t, J = 7.9 Hz, 2H), 1.94–1.86 ppm (m, 2H); ¹³C NMR (151 MHz, $[D_6]DMSO$): δ = 163.37, 163.17, 141.50, 135.31, 134.51, 128.28, 128.22, 127.03, 126.87, 125.70, 74.49, 31.34, 29.55 ppm; t_R : 10.16 min, purity: 99.6%; HRMS (ESI) Anal. calcd for $C_{17}H_{19}N_2O_4$ 315.1339 $[M+H]^+$, found 315.1341.

***N*¹-((3,5-Dimethylbenzoyloxy)-*N*⁴-hydroxyterephthalamide 1f:** Colorless solid; yield 65%; mp: 149 °C; ¹H NMR (500 MHz, $[D_6]DMSO$): δ = 11.86 (s, 1H), 11.34 (s, 1H), 9.14 (s, 1H), 7.86–7.76 (m, 4H), 7.05 (s, 2H), 6.99 (s, 1H), 4.85 (s, 2H), 2.28 ppm (s, 6H); ¹³C NMR (151 MHz, $[D_6]DMSO$): δ = 163.56, 163.25, 137.20, 135.52, 135.34, 134.51, 129.58, 127.09, 126.89, 126.57, 77.01, 20.74 ppm; t_R : 11.50 min, purity: 99.6%; HRMS (ESI) Anal. calcd for $C_{17}H_{19}N_2O_4$ 315.1339 $[M+H]^+$, found 315.1344.

***N*¹-Hydroxy-*N*⁴-(naphthalen-1-ylmethoxy)terephthalamide 1g:** Colorless solid; yield 75%; mp: 140 °C; ¹H NMR (500 MHz, $[D_6]DMSO$): δ = 12.03 (s, 1H), 11.33 (s, 1H), 9.16 (s, 1H), 8.62 (s, 1H), 7.98 (d, J = 8.1 Hz, 2H), 7.85 (s, 4H), 7.70–7.44 (m, 4H), 5.39 ppm (s, 2H); ¹³C NMR (151 MHz, $[D_6]DMSO$): δ = 163.70, 163.21, 135.41, 134.40, 133.21, 131.93, 131.26, 129.33, 128.49, 128.16, 127.13, 126.92, 126.35, 125.94, 125.20, 124.83, 75.27 ppm; t_R : 10.85 min, purity: 97.1%; HRMS (ESI) Anal. calcd for $C_{19}H_{17}N_2O_4$ 337.1183 $[M+H]^+$, found 337.1182.

***N*¹-((2,4-Dichlorobenzoyloxy)-*N*⁴-hydroxyterephthalamide 1h:** Colorless solid; yield: 71%; mp: 175 °C; ¹H NMR (500 MHz, $[D_6]DMSO$): δ = 11.89 (s, 1H), 11.36 (s, 1H), 9.16 (s, 1H), 8.27–7.30 (m, 7H), 5.04 ppm (s, 2H); ¹³C NMR (151 MHz, $[D_6]DMSO$): δ = 163.69, 163.18, 135.38, 134.21, 133.78, 132.66, 129.11, 128.71, 127.34, 127.08, 126.87, 72.97 ppm; t_R : 11.93 min, purity: 95.3%; HRMS (ESI) Anal. calcd for $C_{15}H_{13}N_2O_4$ 355.0247 $[M+H]^+$, found 355.0245.

***N*¹-((3,4-Dichlorobenzoyloxy)-*N*⁴-hydroxyterephthalamide 1i:** Colorless solid; yield 73%; mp: 188 °C; ¹H NMR (600 MHz, $[D_6]DMSO$): δ = 11.88 (s, 1H), 11.35 (s, 1H), 9.14 (s, 1H), 8.02–7.72 (m, 5H), 7.67 (d, J = 8.1 Hz, 1H), 7.46 (d, J = 7.4 Hz, 1H), 4.95 ppm (s, 2H); ¹³C NMR (151 MHz, $[D_6]DMSO$): δ = 163.79, 163.24, 137.17, 135.44, 134.26, 130.85, 130.73, 130.56, 130.44, 128.92, 127.09, 126.92, 75.32 ppm; t_R : 12.12 min, purity: 99.2%; HRMS (ESI) Anal. calcd for $C_{15}H_{13}N_2O_4$ 355.0247 $[M+H]^+$, found 355.0248.

***N*¹-((2,3-Dichlorobenzoyloxy)-*N*⁴-hydroxyterephthalamide 1j:** Colorless solid; yield: 64%; mp: 155 °C; ¹H NMR (600 MHz, $[D_6]DMSO$): δ = 11.91 (s, 1H), 11.35 (s, 1H), 9.13 (s, 1H), 7.98–7.73 (m, 4H), 7.66 (d, J = 7.7 Hz, 1H), 7.58 (d, J = 7.2 Hz, 1H), 7.42 (t, J = 7.8 Hz, 1H), 5.09 ppm (s, 2H); ¹³C NMR (151 MHz, $[D_6]DMSO$): δ = 163.78, 163.24, 136.03, 135.44, 134.25, 131.76, 131.18, 130.45, 129.76, 128.10, 127.12, 126.89, 74.12 ppm; t_R : 11.42 min, purity: 98.7%; HRMS (ESI) Anal. calcd for $C_{15}H_{13}N_2O_4$ 355.0247 $[M+H]^+$, found 355.0247.

***N*¹-((3,4-Difluorobenzoyloxy)-*N*⁴-hydroxyterephthalamide 1k:** Colorless solid; yield 87%; mp: 192 °C; ¹H NMR (500 MHz, $[D_6]DMSO$): δ = 11.94 (s, 1H), 11.37 (s, 1H), 9.15 (s, 1H), 7.81 (q, J = 8.3 Hz, 4H), 7.61–7.51 (m, 1H), 7.50–7.42 (m, 1H), 7.33 (s, 1H), 4.93 ppm (s, 2H); ¹³C NMR (126 MHz, $[D_6]DMSO$): δ = 163.81, 163.32, 150.21 (ddd, J = 245.0, 12.6 Hz), 148.26 (ddd, J = 245.0, 12.4 Hz), 135.50, 134.39, 133.83, 127.13, 126.95, 125.64 (dd, J = 6.4, 3.2 Hz), 117.68 (d, J = 17.1 Hz), 117.24 (d, J = 17.1 Hz), 75.62 ppm; t_R : 7.79 min, purity: 99.6%; HRMS (ESI) Anal. calcd for $C_{15}H_{13}F_2N_2O_4$ 323.0838 $[M+H]^+$, found 323.0839.

***N*¹-(Benzoyloxy)-*N*¹-ethyl-*N*⁴-hydroxyterephthalamide 2a:** Colorless solid; yield 54%; mp: 118 °C; ¹H NMR (600 MHz, $[D_6]DMSO$): δ = 11.34 (s, 1H), 9.12 (s, 1H), 7.80 (d, J = 8.0 Hz, 2H), 7.57 (d, J = 8.1 Hz, 2H), 7.37–7.25 (m, 3H), 7.10 (s, 2H), 4.75 (s, 2H), 3.75 (s, 2H), 1.20 ppm (t, J = 7.0 Hz, 3H); ¹³C NMR (151 MHz, $[D_6]DMSO$): δ = 168.43, 163.42, 137.40, 134.30, 133.97, 129.16, 128.50, 128.23, 127.35, 126.50, 75.44, 12.15 ppm; t_R : 11.57 min, purity: 96.6%; HRMS (ESI) Anal. calcd for $C_{17}H_{19}N_2O_4$ 315.1339 $[M+H]^+$, found 315.1343.

***N*¹-(Benzoyloxy)-*N*¹-butyl-*N*⁴-hydroxyterephthalamide 2b:** Colorless solid; yield 51%; mp: 128 °C; ¹H NMR (600 MHz, $[D_6]DMSO$): δ = 11.35 (s, 1H), 9.13 (s, 1H), 7.81 (d, J = 8.3 Hz, 2H), 7.57 (d, J = 8.3 Hz, 2H), 7.35–7.23 (m, 3H), 7.07 (s, 2H), 4.72 (s, 2H), 3.75 (s, 2H), 1.67–1.59 (m, 2H), 1.38–1.28 (m, 2H), 0.89 ppm (t, J = 7.4 Hz, 3H); ¹³C NMR (151 MHz, $[D_6]DMSO$): δ = 168.40, 163.43, 137.39, 134.21, 133.94, 129.18, 128.52, 128.23, 127.43, 126.49, 75.31, 28.56, 19.21, 13.49 ppm; t_R : 13.58 min, purity: 97.6%; HRMS (ESI) Anal. calcd for $C_{19}H_{23}N_2O_4$ 343.1652 $[M+H]^+$, found 343.1655.

Biological evaluation

In vitro growth inhibition assays against asexual blood-stage *P. falciparum* parasites: Activity against asexual-stage *P. falciparum* parasites was determined using [³H]hypoxanthine incorporation, essentially as previously described.^[12a,25] Briefly, serial dilutions of compound or controls were prepared in parasite culture media (RPMI 1640 supplemented with 10% heat inactivated human serum) with no added hypoxanthine, followed by addition of synchronous ring-stage *P. falciparum* infected erythrocytes (0.25% parasitemia; 2.5% hematocrit). Following incubation for 48 h at 37 °C under standard parasite culture conditions, [³H]hypoxanthine (0.5 μ Ci per well) was added to each well, and the cultures incubated for a further 24 h. Assays were stopped by freezing at –20 °C and, after thawing, [³H]hypoxanthine incorporation measured by

harvesting onto 1450 MicroBeta filter mats (Wallac) and counting using a 1450 MicroBeta liquid scintillation counter. Percentage inhibition of growth was determined relative to matched DMSO vehicle controls included in each assay (< 0.5% DMSO; nontoxic). At least three (*P. falciparum* line 3D7) or two (*P. falciparum* line Dd2) independent experiments were carried out, each in triplicate wells. Chloroquine and SAHA (vorinostat) were included in each assay as positive controls. IC₅₀ values were determined using log-linear interpolation of inhibition curves^[26] and are presented as mean (± SD) of the independent assays.

MTT cell viability assay: To assess cytotoxicity, the rate of cell-survival under the action of test substances was evaluated by an improved 3-(4,5-dimethylthiazol-2-yl)-2,5-diphenyltetrazolium bromide (MTT, Applichem, Germany) assay as previously described.^[27] In brief, HEK293 cells were seeded at a density of 5000 cells per well in 96well plates (Corning, Germany). After 24 h, cells were exposed to increased concentrations of the test compounds. Incubation was ended after 72 h and cell survival was determined by addition of MTT solution (5 mg mL⁻¹ in phosphate-buffered saline). The formazan precipitate was dissolved in DMSO (VWR, Germany). Absorbance was measured at 544 nm and 690 nm in a FLUOstar microplate reader (BMG LabTech, Offenburg, Germany). Concentration–effect curves were constructed with Prism 4.0 (GraphPad Inc., San Diego, CA, USA) by fitting the pooled data of at least three experiments performed in triplicates to the four parameter logistic equation.

Histone hyperacetylation assays: The effect of compounds on histone hyperacetylation was determined essentially as previously described.^[11a] Briefly, trophozoite-stage *P. falciparum* 3D7 parasites were incubated for 3 h under standard in vitro culture conditions with 5×IC₅₀ of test compounds, the antimalarial drug chloroquine (CQ) or the positive control SAHA. Vehicle (0.1% DMSO) served as a negative control, with samples taken at the start and end (termed C-3h) of the treatments. Protein lysates were prepared by lysis with 0.15% saponin (Sigma, USA) in phosphate-buffered saline (PBS; Invitrogen, USA) followed by extensively washing with PBS to remove hemoglobin. The resulting pellet was then resuspended in 1×SDS-PAGE loading dye and samples heat denatured (94 °C; 3 min) and sheared through a 27 gauge needle prior to analysis by 15% SDS-PAGE and western blotting using PVDF membrane (Roche, Switzerland). Membranes were blocked with Odyssey™ blocking buffer (LICOR Biosciences) for 1 h in RT prior to the addition of primary and secondary antibodies. The following antibodies were used: anti-(tetra)-acetyl histone H4 (Millipore; 1:2000 dilution) with IRDye 680RD goat anti-rabbit as secondary antibody (LICOR Biosciences; 1:10000 dilution); anti-glyceraldehyde 3-phosphate dehydrogenase (*PfGAPDH*; a gift from Dr. Matt Dixon, The University of Melbourne, Australia; 1:5000 dilution) with IRDye 800CW donkey anti-rabbit as secondary (LICOR Biosciences; 1:10000 dilution). Anti-(tetra)-acetyl histone H4 antibody recognizes acetylated histone H4 forms and may also cross-react with acetylated histone H2B and other acetylated histones, as reported by the manufacturer. Membranes were incubated with primary antibodies overnight at 4 °C, followed by washing and addition of secondary antibodies for 45 min at room temperature. Membranes were imaged using an Odyssey Classic (LI-COR biosciences) and densitometry analysis was carried out using Image Studio Lite version 5.2 (LI-COR biosciences).

***P. berghei*-Luciferase liver-stage assay and HepG2 Cytotoxicity assay:** HepG2-A16-CD81EGFP, human hepatocarcinoma HepG2 cells stably transformed to express the tetraspanin CD81 receptor^[28] and thus susceptible to *P. berghei* infection, were cultured at

37 °C in 5% CO₂ in DMEM (Life Technologies, CA, USA) supplemented with 10% FBS, 0.29 mg mL⁻¹ glutamine, 100 unit penicillin and 100 µg mL⁻¹ streptomycin. For the *P. berghei*-Luciferase and HepG2 cytotoxicity assays, 3×10³ of the HepG2-A16-CD81EGFP cells in 5 µL of assay medium (DMEM without Phenol Red (Life Technologies, CA), 5% FBS, and 5×Pen Strep Glutamine (Life Technologies, CA)) at concentration 6×10⁵ cells mL⁻¹ were seeded in 1536-well plates (Greiner BioOne white solid bottom custom GNF mold) 20–26 h prior to the actual infection. 18 h prior to infection, 50 nL of compound in DMSO (0.5 % final DMSO concentration per well) were transferred with Acoustic Transfer System (ATS) (Biosero) into the assay plates. Atovaquone and Puromycin (12-point serial dilution starting at 10 µM) were used as positive controls for *P. berghei* Liver-stage assay and HepG2 Cytotoxicity, respectively. 0.5% DMSO was used as negative control for the both assays. *A. stephensi* mosquitoes, infected with *P. berghei*-Luciferase (PbLuc), were provided by the New York University Insectary. PbLuc sporozoites were freshly dissected from the infected *A. stephensi* salivary glands, filtered twice through a 20 µm nylon net filter (Steriflip, Millipore), counted in a hemocytometer, and then adjusted to final concentration 200 sporozoites per µL in the assay media. For the *P. berghei* Liver-stage Assay, the HepG2-A16-CD81EGFP cells were then infected with 1×10³ sporozoites per well (5 µL) with a single tip Bottle Valve liquid handler (GNF), and the plates were spun down at 37 °C for 3 min at a centrifugal force of 330 g on normal acceleration and brake setting. The HepG2-A16-CD81EGFP cell designated for toxicity studies were left uninfected, with 5 µL of additional assay media added to each well to maintain equal concentrations of compounds with PbLuc infected plates. After incubation at 37 °C for 48 h the EEF growth and HepG2-A16-CD81EGFP cell viability were quantified by a bioluminescence measurement as follows: Media were removed by spinning the inverted plates at 150 g for 30 s; 2 µL per well of BrightGlo (Promega) or CellTiterGlo (Promega) reagent (diluted 1:2 with deionized water) for quantification of EEFs or HepG2-A16-CD81EGFP cell viability, respectively were dispensed with the MicroFlo (BioTek) liquid handler. Immediately after addition of the luminescence reagent, the plates were read by the Envision Multilabel Reader (PerkinElmer). For both assays IC₅₀ values were obtained using the normalized bioluminescence intensity and a non-linear variable slope four-parameter regression curve-fitting model in Prism 6 (GraphPad Software Inc.).

In vitro early- and late-stage gametocyte high content imaging assays: Early- and late-stage gametocyte production and the termination of compound gametocytocidal activity were performed as described in extensive detail elsewhere.^[29] In brief, NF54-pfs16-LUC-GFP transgenic parasites were cultured in RPMI 1640 medium, supplemented with glutamine, hypoxanthine, HEPES, 0.25 % AlbuMAX® II and 5 % Human serum, plus 2 µg mL⁻¹ Blasticidin (to maintain the expression plasmid). After one week in culture, a stress trigger was employed to induce gametocytogenesis.^[29a] For the early-stage gametocyte assay, stage I–II gametocytes were isolated by magnetic column and added to non-infected red blood cells to a final parasite percentage of 10% in 0.1% hematocrit in culture media supplemented with 50 mM *N*-acetylglucosamine (NAG). For the late-stage gametocyte assay stage IV gametocytes were isolated with the use of magnetic columns. Percent parasitemia was adjusted to 10% by the addition of non-infected RBCs and the hematocrit adjusted to 0.1 %. All compounds were solubilized to 10 mM in DMSO and serial dilutions in log dose–response were performed in 384-well polypropylene plates. 1 µL of compound concentrate was then diluted into 25 µL of sterile water in sterile 384-well polystyrene plates. Diluted compound (5 µL), including in plate controls (50 µM puromycin positive and 4% DMSO

negative control) was then transferred into empty 384-well imaging plates. 45 μL of early or late-stage gametocyte culture was then added to the compound containing imaging plates. The plates were sealed with a gas-permeable membrane and the plates incubated for 72 h in standard conditions. After incubation 5 μL of MitoTracker[®] Red CM-H2Xros dispensed into all wells. The plates were then incubated for a further 12–16 h before imaging on the Opera[®] High Content Screening System. The number of classified viable gametocytes for each compound treated well was identified and the data normalized to percent inhibition in relation to the in plate negative and positive control values. Percent inhibition data were subsequently plotted versus log concentration of each test or reference compound using GraphPad Prism 4, using nonlinear regression, sigmoidal dose response with no maximum and minimum constraints. IC_{50} values were obtained for compounds for which an E_{max} plateau of at least two doses was achieved. Compounds which did not achieve an E_{max} plateau of at least two compound doses were presented as percent inhibition of replication at the top screening dose.

Acknowledgements

K.S. thanks the Deutsche Akademischer Austausch Dienst (DAAD) for funding. This work was supported in part by the Deutsche Forschungsgemeinschaft (DFG) (HA 7783/1-1 to F.K.H.). K.T.A. acknowledges funding from the Australian National Health and Medical Research Council (grants APP1074016 and APP1093378) and A-PARADISE program funded under the European Union's Seventh Framework Programme. M.J.C. was supported by Griffith University GUIPRS and GUPRS scholarships. V.M.A. acknowledges funding from the Australian Research Council (grant number LP120200557). Y.A.K., S.M., and E.A.W. are supported by MMV12/0096 award. The authors thank the COST action CM1406 (Epigenetic Chemical Biology EPICHEMBO) for support. The DFG is acknowledged for funds used to purchase the UHR-TOF maXis 4G, Bruker Daltonics, and Bremen HRMS instruments used in this research. We thank the Australian Red Cross Blood Service for the provision of human blood and sera.

Conflict of interest

The authors declare no conflict of interest.

Keywords: anti-plasmodial · histone deacetylase · inhibitors · malaria · *Plasmodium falciparum*

- [1] WHO, *World Malaria Report 2016*, World Health Organization, Geneva, 2016, ISBN: 978-924-151171-1.
- [2] RTS,S Clinical Trials Partnership, *The Lancet* **2015**, *386*, 31–45.
- [3] B. Mordmüller, G. Surat, H. Lagler, S. Chakravarty, A. S. Ishizuka, A. Lalremruata, M. Gmeiner, J. J. Campo, M. Esen, A. J. Ruben, J. Held, C. L. Calle, J. B. Mengue, T. Gebru, J. Ibanez, M. Sulyok, E. R. James, P. F. Billingsley, K. C. Natasha, A. Manoj, T. Murshedkar, A. Gunasekera, A. G. Eappen, T. Li, R. E. Stafford, M. Li, P. L. Felgner, R. A. Seder, T. L. Richie, B. K. Sim, S. L. Hoffman, P. G. Kremsner, *Nature* **2017**, *542*, 445–449.
- [4] Malaria vaccine: WHO position paper—January 2016, *The Weekly Epidemiological Record (WER)*, World Health Organization, 2016, pp. 33–52; <http://www.who.int/wer/2016/wer9104.pdf?ua=1> (accessed September 5, 2017).
- [5] C. Wongsrichanalai, C. H. Sibley, *Clin. Microbiol. Infect.* **2013**, *19*, 908–916.
- [6] a) J. N. Burrows, E. Burlot, B. Campo, S. Cherbuin, S. Jeanneret, D. Leroy, T. Spangenberg, D. Waterson, T. N. Wells, P. Willis, *Parasitology* **2014**, *141*, 128–139; b) J. N. Burrows, R. H. van Huijsduijnen, J. J. Mohrle, C. Oeuvray, T. N. Wells, *Malar. J.* **2013**, *12*, 187–207.
- [7] P. A. Jones, S. B. Baylin, *Cell* **2007**, *128*, 683–692.
- [8] K. J. Falkenberg, R. W. Johnstone, *Nat. Rev. Drug Discovery* **2014**, *13*, 673–691.
- [9] a) S. Grant, C. Easley, P. Kirkpatrick, *Nat. Rev. Drug Discovery* **2007**, *6*, 21–22; b) V. Sandor, S. Bakke, R. W. Robey, M. H. Kang, M. V. Blagosklonny, J. Bender, R. Brooks, R. L. Piekarz, E. Tucker, W. D. Figg, K. K. Chan, B. Goldspiel, A. T. Fojo, S. P. Balcerzak, S. E. Bates, *Clin. Cancer Res.* **2002**, *8*, 718–728; c) H. M. Prince, M. J. Bishton, R. W. Johnstone, *Future Oncol.* **2009**, *5*, 601–612; d) J. C. Byrd, G. Marcucci, M. R. Parthun, J. J. Xiao, R. B. Klisovic, M. Moran, T. S. Lin, S. Liu, A. R. Sklenar, M. E. Davis, D. M. Lucas, B. Fischer, R. Shank, S. L. Tejaswi, P. Binkley, J. Wright, K. K. Chan, M. R. Grever, *Blood* **2005**, *105*, 959–967; e) Y. Shi, M. Dong, X. Hong, W. Zhang, J. Feng, J. Zhu, L. Yu, X. Ke, H. Huang, Z. Shen, Y. Fan, W. Li, X. Zhao, J. Qi, H. Huang, D. Zhou, Z. Ning, X. Lu, *Ann. Oncol.* **2015**, *26*, 1766–1771.
- [10] a) K. T. Andrews, T. N. Tran, A. J. Lucke, P. Kahnberg, G. T. Le, G. M. Boyle, D. L. Gardiner, T. S. Skinner-Adams, D. P. Fairlie, *Antimicrob. Agents Chemother.* **2008**, *52*, 1454–1461; b) J. A. Engel, A. J. Jones, V. M. Avery, S. D. Sumanadasa, S. S. Ng, D. P. Fairlie, T. S. Adams, K. T. Andrews, *Int. J. Parasitol. Drugs Drug Resist.* **2015**, *5*, 117–126; c) G. S. Hailu, D. Robaa, M. Forgione, W. Sippl, D. Rotili, A. Mai, *J. Med. Chem.* **2017**, *60*, 4780–4804.
- [11] a) S. D. Sumanadasa, C. D. Goodman, A. J. Lucke, T. Skinner-Adams, I. Sahama, A. Haque, T. A. Do, G. I. McFadden, D. P. Fairlie, K. T. Andrews, *Antimicrob. Agents Chemother.* **2012**, *56*, 3849–3856; b) G. S. Dow, Y. Chen, K. T. Andrews, D. Caridha, L. Gerena, M. Gettayacamin, J. Johnson, Q. Li, V. Melendez, N. Obaldia, 3rd, T. N. Tran, A. P. Kozikowski, *Antimicrob. Agents Chemother.* **2008**, *52*, 3467–3477; c) K. T. Andrews, A. P. Gupta, T. N. Tran, D. P. Fairlie, G. N. Gobert, Z. Bozdech, *PLoS One* **2012**, *7*, e31847; d) B. K. Chaal, A. P. Gupta, B. D. Wastuwidyaningtyas, Y. H. Luah, Z. Bozdech, *PLoS Pathog.* **2010**, *6*, e1000737; e) F. K. Hansen, T. S. Skinner-Adams, S. Duffy, L. Marek, S. D. Sumanadasa, K. Kuna, J. Held, V. M. Avery, K. T. Andrews, T. Kurz, *ChemMedChem* **2014**, *9*, 665–670; f) L. A. Alves Avelar, J. Held, J. A. Engel, P. Surechatchaiyan, F. K. Hansen, A. Hamacher, M. U. Kassack, B. Mordmüller, K. T. Andrews, T. Kurz, *Arch. Pharm.* **2017**, <https://doi.org/10.1002/ardp.201600347>.
- [12] B. I. Coleman, K. M. Skillman, R. H. Jiang, L. M. Childs, L. M. Altenhofen, M. Ganter, Y. Leung, I. Goldowitz, B. F. Kafsack, M. Marti, M. Llinas, C. O. Buckee, M. T. Duraisingh, *Cell Host Microbe* **2014**, *16*, 177–186.
- [13] a) C. J. Tonkin, C. K. Carret, M. T. Duraisingh, T. S. Voss, S. A. Ralph, M. Hommel, M. F. Duffy, L. M. Silva, A. Scherf, A. Ivens, T. P. Speed, J. G. Beeson, A. F. Cowman, *PLoS Biol.* **2009**, *7*, e1000084; b) C. J. Merrick, M. T. Duraisingh, *Eukaryotic Cell* **2007**, *6*, 2081–2091.
- [14] V. Patel, R. Mazitschek, B. Coleman, C. Nguyen, S. Urgaonkar, J. Cortese, R. H. Barker, E. Greenberg, W. Tang, J. E. Bradner, S. L. Schreiber, M. T. Duraisingh, D. F. Wirth, J. Clardy, *J. Med. Chem.* **2009**, *52*, 2185–2187.
- [15] J. M. Ontoria, G. Paonessa, S. Ponzi, F. Ferrigno, E. Nizi, I. Biancofiore, S. Malancona, R. Graziani, D. Roberts, P. Willis, A. Bresciani, N. Gennari, O. Cecchetti, E. Monteagudo, M. V. Orsale, M. Veneziano, A. Di Marco, A. Cellucci, R. Laufer, S. Altamura, V. Summa, S. Harper, *ACS Med. Chem. Lett.* **2016**, *7*, 454–459.
- [16] R. Vreese, C. Kock, P. J. Smith, K. Chibale, M. D'Hooghe, *Future Med. Chem.* **2017**, *9*, 357–364.
- [17] F. K. Hansen, S. D. Sumanadasa, K. Stenzel, S. Duffy, S. Meister, L. Marek, R. Schmetter, K. Kuna, A. Hamacher, B. Mordmüller, M. U. Kassack, E. A. Winzeler, V. M. Avery, K. T. Andrews, T. Kurz, *Eur. J. Med. Chem.* **2014**, *82*, 204–213.
- [18] a) J. H. Kalin, J. A. Bergman, *J. Med. Chem.* **2013**, *56*, 6297–6313; b) O. Witt, H. E. Deubzer, T. Milde, I. Oehme, *Cancer Lett.* **2009**, *277*, 8–21; c) D. Kim, C. L. Frank, M. M. Dobbin, R. K. Tsunemoto, W. Tu, P. L. Peng, J. S. Guan, B. H. Lee, L. Y. Moy, P. Giusti, N. Broodie, R. Mazitschek, I. DeLalle, S. J. Haggarty, R. L. Neve, Y. Lu, L. H. Tsai, *Neuron* **2008**, *60*, 803–817; d) I. N. Gaisina, W. Tueckmantel, A. Ugolkov, S. Shen, J. Hoffen, O. Dubrovskiy, A. Mazar, R. A. Schoon, D. Billadeau, A. P. Kozikowski, *ChemMedChem* **2016**, *11*, 81–92.

- [19] F. F. Wagner, D. E. Olson, J. P. Gale, T. Kaya, M. Weiwer, N. Aidoud, M. Thomas, E. L. Davoine, B. C. Lemerrier, Y. L. Zhang, E. B. Holson, *J. Med. Chem.* **2013**, *56*, 1772–1776.
- [20] a) K. Ramasamy, R. K. Olsen, T. Emery, *J. Org. Chem.* **1981**, *46*, 5438–5441; b) H. A. Staab, *Angew. Chem. Int. Ed.* **1962**, *1*, 351–367; *Angew. Chem.* **1962**, *74*, 407–423.
- [21] P. J. O'Brien, W. Irwin, D. Diaz, E. Howard-Cofield, C. M. Krejsa, M. R. Slaughter, B. Gao, N. Kaludercic, A. Angeline, P. Bernardi, P. Brain, C. Hougham, *Arch. Toxicol.* **2006**, *80*, 580–604.
- [22] M. J. Chua, M. S. Arnold, W. Xu, J. Lancelot, S. Lamotte, G. F. Spath, E. Prina, R. J. Pierce, D. P. Fairlie, T. S. Skinner-Adams, K. T. Andrews, *Int. J. Parasitol. Drugs Drug Resist.* **2017**, *7*, 42–50.
- [23] J. N. Burrows, S. Duparc, W. E. Gutteridge, R. Hooft van Huijsduijnen, W. Kaszubska, F. Macintyre, S. Mazzuri, J. J. Mohrle, T. N. Wells, *Malar. J.* **2017**, *16*, 26.
- [24] a) J. T. Welch, K. W. Seper, *J. Org. Chem.* **1988**, *53*, 2991–2999; b) J. Wild, N. Goetz, W. Will, R. D. Kohler, P. Plath (BASF AG), DE3615473 A1, **1987**, [*Chem. Abstr.* **1988**, *108*, 111952e].
- [25] R. E. Desjardins, C. J. Canfield, J. D. Haynes, J. D. Chulay, *Antimicrob. Agents Chemother.* **1979**, *16*, 710–718.
- [26] W. Huber, J. C. Koella, *Acta Trop.* **1993**, *55*, 257–261.
- [27] H. Mueller, M. U. Kassack, M. Wiese, *J. Biomol. Screening* **2004**, *9*, 506–515.
- [28] a) S. Yalaoui, S. Zougbede, S. Charrin, O. Silvie, C. Arduise, K. Farhati, C. Boucheix, D. Mazier, E. Rubinstein, P. Froissard, *PLoS Pathog.* **2008**, *4*, e1000010; b) O. Silvie, E. Rubinstein, J. F. Franetich, M. Prenant, E. Belnoue, L. Renia, L. Hannoun, W. Eling, S. Levy, C. Boucheix, D. Mazier, *Nat. Med.* **2002**, *9*, 93–96.
- [29] a) S. Duffy, S. Loganathan, J. P. Holleran, V. M. Avery, *Nat. Protoc.* **2016**, *11*, 976–992; b) S. Duffy, V. M. Avery, *Malar. J.* **2013**, *12*, 408.

Manuscript received: June 19, 2017

Revised manuscript received: August 13, 2017

Accepted manuscript online: August 15, 2017

Version of record online: September 13, 2017



Supporting Information

Design and Synthesis of Terephthalic Acid-Based Histone Deacetylase Inhibitors with Dual-Stage Anti-*Plasmodium* Activity

Katharina Stenzel,^[a, b] Ming Jang Chua,^[b] Sandra Duffy,^[b] Yevgeniya Antonova-Koch,^[c] Stephan Meister,^[c] Alexandra Hamacher,^[a] Matthias U. Kassack,^[a] Elizabeth Winzeler,^[c] Vicky M. Avery,^[b] Thomas Kurz,^[a] Katherine T. Andrews^{+, * [b]} and Finn K. Hansen^{+, * [a, d]}

cmdc_201700360_sm_miscellaneous_information.pdf

Supplementary data

Contents

1. Supplemental Tables	2
2. Chemistry	2
2.1. <i>General information</i>	2
2.2. <i>General procedure for the synthesis of 4a-k</i>	3
2.3. <i>General procedure for the synthesis of 5a,b</i>	3
2.4. <i>Experimental data</i>	4
3. Biological evaluation	7
4. References	8

1. Supplemental Tables

Table S1. Inhibition activities of selected compounds and the reference HDACi vorinostat (SAHA) against human HDAC1 (hHDAC1) and human HDAC6 (hHDAC6).

Comp.	R ¹	R ²	hHDAC1 IC ₅₀ [nM] ^a	hHDAC6 IC ₅₀ [nM] ^a
1a	Bn	H	0.736 ± 0.092	0.124 ± 0.002
1c	4-CH ₃ -PhCH ₂	H	0.880 ± 0.008	0.182 ± 0.015
1e	PhCH ₂ CH ₂ CH ₂	H	0.515 ± 0.067	0.167 ± 0.042
1f	3,5-CH ₃ -Ph CH ₂	H	0.690 ± 0.004	0.379 ± 0.086
1g	1-NaphthylCH ₂	H	0.508 ± 0.066	0.091 ± 0.020
SAHA		H	0.056 ± 0.008	0.045 ± 0.001

^a Values are the mean of two independent experiments, each in duplicate.

Table S2. *P. falciparum* and *P. berghei* HDAC amino acid identity and similarity

<i>P. falciparum</i> HDAC ^a	<i>P. berghei</i> ANKA HDAC homologue ^a	% amino acid identity ^b	% amino acid similarity ^b
<i>Pf</i>HDAC1[PF3D7_0925700]	PBANKA_0826500	94.6	98.9
<i>Pf</i>HDAC2[PF3D7_1472200]	PBANKA_1335400	35.2	46.4
<i>Pf</i>HDAC3[PF3D7_1008000]	PBANKA_1206200	39.2	50.8

^a PlasmoDB gene ID numbers are shown; [1] Pairwise sequence alignments carried out using EMBOSS Water (http://www.ebi.ac.uk/Tools/psa/emboss_water/)

2. Chemistry

2.1. General information

All chemicals and solvents were obtained from commercial suppliers (Sigma-Aldrich, Acros Organics, Carbolution Chemicals) and used as purchased without further purification. The synthesis of the required O-substituted and N,O-disubstituted hydroxylamine derivatives was performed according to literature procedures.[2-4] The progress of all reactions was monitored by thin layer chromatography (TLC) using Merck precoated silica gel plates (with fluorescence indicator UV₂₅₄). Components were visualized by irradiation with ultraviolet light (254 nm) or staining in potassium permanganate solution followed by heating. Flash column chromatography was performed using prepacked silica cartridge

with the solvent mixtures specified in the corresponding experiment. Melting points (mp) were taken in open capillaries on a Mettler FP 5 melting-point apparatus and are uncorrected. Proton (^1H) and carbon (^{13}C) NMR spectra were recorded on a Bruker Avance 300, 500 or 600 using $\text{DMSO-}d_6$ or CDCl_3 as solvents. Chemical shifts are given in parts per million (ppm), relative to residual solvent peak for ^1H and ^{13}C . Elemental analysis was performed on a Perkin Elmer PE 2400 CHN elemental analyzer. High resolution mass spectra (HRMS) analysis was performed on a UHR-TOF maXis 4G, Bruker Daltonics, Bremen by electrospray ionization (ESI). Analytical HPLC analysis were carried out on a Varian Prostar system equipped with a Prostar 410 (autosampler), 210 (pumps) and 330 (UV-detector) using a Phenomenex Luna 5u C18(2) 1.8 μm particle (250 mm \times 4.6 mm) column, supported by Phenomenex Security Guard Cartridge Kit C18 (4.0 mm \times 3.0 mm). UV absorption was detected at 254 nm with a linear gradient of 10% B to 100% B in 20 min using HPLC-grade water +0.1% TFA (solvent A) and HPLC-grade acetonitrile +0.1% TFA (solvent B) for elution at a flow rate of 1 mL/min. The purity of all final compounds was 95% or higher.

2.2. General procedure for the synthesis of **4a-k**

4-(Methoxycarbonyl)benzoic acid (1.802 g, 10 mmol, 1 eq) was dissolved in anhydrous THF (25 mL) and cooled to $-15\text{ }^\circ\text{C}$. The solution was treated with *N*-methylmorpholine (1.012 g, 11 mmol, 1.1 eq) followed by isobutyl chloroformate (1.502 g, 11 mmol, 1.1 eq) to form the mixed anhydride. After 15 min the respective *O*-benzylhydroxylamine derivative (10 mmol, 1 eq) dissolved in anhydrous THF was added dropwise. The reaction was warmed to room temperature over 3 h and subsequently filtrated. After removing the solvent in vacuo the residue was diluted with in ethyl acetate/ H_2O (40 mL/10 mL) and extracted with ethyl acetate (3 \times 60 mL). The combined extracts were washed with NaHCO_3 (50 mL) and the organic layer was dried over Na_2SO_4 , filtered, and the solvent removed in vacuo. The crude products were purified by flash column chromatography (prepacked silica cartridge, hexane/ethyl acetate, gradient: 90:10 \rightarrow 50:50 in 20 min) to yield the desired intermediates **4a-k** in 67 - 93% yield.

2.3. General procedure for the synthesis of **5a,b**

A solution of 4-(Methoxycarbonyl)benzoic acid (1.08 g, 6 mmol, 1 eq) in dry CH_2Cl_2 (3 mL) was added dropwise to a suspension of 1,1'-carbonyldiimidazole (CDI) (1.07 g, 6.6 mmol, 1.1 eq) in dry CH_2Cl_2 (5 mL). The reaction mixture was stirred for 0.5 h at room temperature. Afterwards, the respective

N,O-disubstituted hydroxylamine derivative was added and the reaction mixture was stirred over night and subsequently evaporated under reduced pressure. The residue was dissolved in ethyl acetate (20 mL) and the solution extracted with a saturated solution of NaHCO₃ (3 x 5 mL), water (5 mL), 1 M HCl (5 mL), dried over Na₂SO₄ and evaporated under reduced pressure. The crude product was purified by column chromatography using ethyl acetate as eluent (77 – 79% yield).

2.4. Experimental data

Methyl 4-((benzyloxy)carbamoyl)benzoate 4a: Colorless solid; yield 81%; mp: 157 °C; ¹H NMR (600 MHz, DMSO-*d*₆) δ 11.98 (s, 1H), 8.04 (d, *J* = 7.8 Hz, 2H), 7.87 (d, *J* = 8.7 Hz, 2H), 7.50 (m, 5H), 4.95 (s, 2H), 3.87 (s, 3H). ¹³C NMR (151 MHz, DMSO-*d*₆) δ 165.53, 163.39, 136.35, 135.69, 132.04, 129.16, 128.84, 128.25, 127.44, 76.98, 52.31. Anal. calcd. for C₁₆H₁₅NO₄: C 67.36, H 5.30, N 4.91, found: C 67.10, H 5.24, N 4.81.

Methyl 4-((trityloxy)carbamoyl)benzoate 4b: Colorless solid; yield 46%; mp: 153 °C; ¹H NMR (600 MHz, DMSO-*d*₆) δ 11.16 (s, 1H), 7.92 (d, *J* = 7.7 Hz, 2H), 7.52 (d, *J* = 6.1 Hz, 2H), 7.43 (d, *J* = 6.8 Hz, 6H), 7.39 – 7.19 (m, 9H), 3.84 (s, 3H). ¹³C NMR (151 MHz, DMSO-*d*₆) δ 165.56, 142.24, 136.80, 131.72, 129.03, 128.85, 127.72, 127.42, 92.58, 52.24. Anal. calcd. for C₂₈H₂₃NO₄: C 76.87, H 5.30, N 3.20, found: C 76.59, H 5.25, N 3.18.

Methyl 4-(((4-methylbenzyl)oxy)carbamoyl)benzoate 4c: Colorless solid; yield 54%; mp: 173 °C; ¹H NMR (500 MHz, DMSO-*d*₆) δ 11.93 (s, 1H), 8.09 – 8.01 (m, 2H), 7.86 (d, *J* = 8.1 Hz, 2H), 7.34 (d, *J* = 7.7 Hz, 2H), 7.21 (d, *J* = 7.7 Hz, 2H), 4.89 (s, 2H), 3.88 (s, 3H), 2.32 (s, 3H). ¹³C NMR (151 MHz, DMSO-*d*₆) δ 165.54, 163.33, 137.59, 136.40, 132.67, 132.02, 129.16, 128.98, 128.80, 127.45, 76.82, 52.31. Anal. calcd. for C₁₇H₁₇NO₄: C 68.22, H 5.72, N 4.68, found: C 67.97, H 5.73, N 4.57.

Methyl 4-(phenethoxycarbamoyl)benzoate 4d: Colorless solid; yield 69%; mp: 141 °C; ¹H NMR (500 MHz, DMSO-*d*₆) δ 11.92 (s, 1H), 8.04 (d, *J* = 8.1 Hz, 2H), 7.88 (d, *J* = 8.0 Hz, 2H), 7.36 – 7.18 (m, 5H), 4.14 (t, *J* = 6.8 Hz, 2H), 3.88 (s, 3H), 2.96 (t, *J* = 6.9 Hz, 2H). ¹³C NMR (126 MHz, DMSO-*d*₆) δ 165.53, 163.31, 138.23, 136.39, 132.00, 129.13, 128.78, 128.20, 127.48, 126.09, 75.69, 52.32, 33.91. Anal. calcd. for C₁₇H₁₇NO₄: C 68.22, H 5.72, N 4.68, found: C 68.18, H 5.82, N 4.92.

Methyl 4-((3-phenylpropoxy)carbamoyl)benzoate 4e: Colorless solid; yield 60%; mp: 126 °C; ^1H NMR (500 MHz, DMSO- d_6) δ 11.87 (s, 1H), 8.04 (d, J = 8.0 Hz, 2H), 7.88 (d, J = 8.1 Hz, 2H), 7.33 – 7.23 (m, 4H), 7.22 – 7.15 (m, 1H), 3.95 – 3.86 (m, 5H), 2.73 (t, J = 7.9 Hz, 2H), 1.96 – 1.86 (m, 2H). ^{13}C NMR (126 MHz, DMSO- d_6) δ 165.53, 163.24, 141.47, 136.44, 131.98, 129.16, 128.28, 128.21, 127.44, 125.70, 74.56, 52.31, 40.01, 29.52. Anal. calcd. for $\text{C}_{18}\text{H}_{19}\text{NO}_4$: C 69.00, H 6.11, N 4.47, found: C 68.86, H 6.03, N 4.45.

Methyl 4-(((3,5-dimethylbenzyl)oxy)carbamoyl)benzoate 4f: Colorless solid; yield 71%; mp: 121 °C; ^1H NMR (500 MHz, DMSO- d_6) δ 11.95 (s, 1H), 8.04 (d, J = 7.9 Hz, 2H), 7.87 (d, J = 7.9 Hz, 2H), 7.06 (s, 2H), 6.99 (s, 1H), 4.86 (s, 2H), 3.88 (s, 3H), 2.28 (s, 6H). ^{13}C NMR (126 MHz, DMSO- d_6) δ 165.53, 163.32, 137.21, 136.39, 135.47, 132.03, 129.61, 129.16, 127.46, 126.58, 77.03, 52.32, 20.74. Anal. calcd. for $\text{C}_{18}\text{H}_{19}\text{NO}_4$: C 69.00, H 6.11, N 4.47, found: C 68.90, H 6.07, N 4.47.

Methyl 4-((naphthalen-1-ylmethoxy)carbamoyl)benzoate 4g: Colorless solid; yield 78%; mp: 128 °C; ^1H NMR (500 MHz, DMSO- d_6) δ 12.13 (s, 1H), 8.61 (d, J = 8.5 Hz, 1H), 8.06 (d, J = 8.0 Hz, 2H), 7.98 (d, J = 8.2 Hz, 2H), 7.93 (d, J = 8.0 Hz, 2H), 7.72 – 7.47 (m, 4H), 5.40 (s, 2H), 3.89 (s, 3H). ^{13}C NMR (126 MHz, DMSO- d_6) δ 165.53, 163.51, 136.31, 133.21, 132.09, 131.93, 131.19, 129.38, 129.19, 128.53, 128.17, 127.52, 126.37, 125.95, 125.21, 124.81, 75.31, 52.33. Anal. calcd. for $\text{C}_{20}\text{H}_{17}\text{NO}_4$: C 71.63, H 5.11, N 4.18, found: C 71.78, H 5.13, N 4.28.

Methyl 4-(((2,4-dichlorobenzyl)oxy)carbamoyl)benzoate 4h: Colorless solid; yield 78%; mp: 150 °C; ^1H NMR (500 MHz, DMSO- d_6) δ 11.98 (s, 1H), 8.03 (d, J = 8.1 Hz, 2H), 7.85 (d, J = 8.2 Hz, 2H), 7.68 (s, 1H), 7.63 (d, J = 8.2 Hz, 1H), 7.49 (dd, J = 8.2, 1.9 Hz, 1H), 5.05 (s, 2H), 3.88 (s, 3H). ^{13}C NMR (126 MHz, DMSO- d_6) δ 165.51, 163.57, 136.16, 134.28, 133.84, 132.71, 132.56, 132.09, 129.15, 128.74, 127.50, 127.36, 73.06, 52.32. Anal. calcd. for $\text{C}_{16}\text{H}_{13}\text{Cl}_2\text{NO}_4$: C 54.26, H 3.70, N 3.95, found: C 53.97, H 3.77, N 3.82.

Methyl 4-(((3,4-dichlorobenzyl)oxy)carbamoyl)benzoate 4i: Colorless solid; yield 89%; mp: 174 °C; ^1H NMR (500 MHz, DMSO- d_6) δ 12.00 (s, 1H), 8.04 (d, J = 8.1 Hz, 2H), 7.85 (d, J = 8.2 Hz, 2H), 7.76 (s, 1H), 7.67 (d, J = 8.2 Hz, 1H), 7.47 (d, J = 8.1 Hz, 1H), 4.96 (s, 2H), 3.88 (s, 3H). ^{13}C NMR (151 MHz, DMSO- d_6) δ 165.01, 163.05, 136.65, 135.62, 131.61, 130.40, 130.27, 130.03, 129.94, 128.68,

128.38, 126.95, 74.88, 51.80. Anal. calcd. for $C_{16}H_{13}Cl_2NO_4$: C 54.26, H 3.70, N 3.95, found: C 54.22, H 3.66, N 3.90.

Methyl 4-(((2,3-dichlorobenzyl)oxy)carbamoyl)benzoate 4j: Colorless solid; yield 93%; mp: 158 °C; 1H NMR (600 MHz, DMSO- d_6) δ 12.03 (s, 1H), 8.04 (d, J = 8.0 Hz, 2H), 7.87 (d, J = 8.0 Hz, 2H), 7.66 (d, J = 7.8 Hz, 1H), 7.60 (d, J = 7.4 Hz, 1H), 7.42 (t, J = 7.8 Hz, 1H), 5.13 (s, 2H), 3.89 (s, 3H). ^{13}C NMR (151 MHz, DMSO- d_6) δ 165.05, 163.14, 135.66, 131.64, 131.35, 130.70, 129.97, 129.22, 128.69, 127.62, 127.02, 73.71, 51.83. Anal. Calcd. for $C_{16}H_{13}Cl_2NO_3$: C 54.26, H 3.70, N 3.95 found: C 54.25, H 3.68, N 3.92.

Methyl 4-(((3,4-difluorobenzyl)oxy)carbamoyl)benzoate 4k: Colorless solid; yield 80%; mp: 172 °C; 1H NMR (600 MHz, DMSO- d_6) δ 12.00 (s, 1H), 8.05 (d, J = 8.1 Hz, 2H), 7.88 (d, J = 8.2 Hz, 2H), 7.60 – 7.54 (m, 1H), 7.49 – 7.42 (m, 1H), 7.34 (s, 1H), 4.96 (s, 2H), 3.89 (s, 3H). ^{13}C NMR (151 MHz, DMSO- d_6) δ 165.09, 163.12, 149.61 (ddd, J = 244.9, 18.9, 12.4 Hz), 147.98 (ddd, J = 244.9, 17.8, 12.4 Hz), 135.76, 133.30, 131.69, 128.74, 127.03, 125.24, 117.27 (d, J = 17.2 Hz), 116.83 (d, J = 17.2 Hz), 75.18, 51.85. Anal. calcd. for $C_{16}H_{13}F_2NO_4$: C 59.82, H 4.08, N 4.36, found: C 59.88, H 4.08, N 4.38.

Methyl 4-((benzyloxy)(ethyl)carbamoyl)benzoate 5a: Colorless solid; yield 77%; mp: 61 °C; 1H NMR (600 MHz, DMSO- d_6) δ 8.00 (d, J = 8.2 Hz, 2H), 7.63 (d, J = 8.3 Hz, 2H), 7.36 – 7.24 (m, 3H), 7.09 (s, 2H), 4.75 (s, 2H), 3.89 (s, 3H), 3.77 (s, 2H), 1.21 (t, J = 7.0 Hz, 3H). ^{13}C NMR (151 MHz, DMSO- d_6) δ 168.24, 165.68, 139.41, 134.26, 130.69, 129.23, 128.80, 128.57, 128.28, 75.51, 52.32, 12.17. Anal. calcd. for $C_{18}H_{19}NO_4$: C 69.00, H 6.11, N 4.47, found: C 69.17, H 6.00, N 4.49.

Methyl 4-((benzyloxy)(butyl)carbamoyl)benzoate 5b: Colorless solid; yield 79%; mp: 79 °C; 1H NMR (600 MHz, DMSO- d_6) δ 8.00 (d, 2H), 7.61 (d, 2H), 7.36 – 7.22 (m, 3H), 7.04 (s, 2H), 4.72 (s, 2H), 3.89 (s, 3H), 3.77 (s, 2H), 1.75 – 1.51 (m, 2H), 1.44 – 1.23 (m, 2H), 0.89 (t, J = 7.4 Hz, 3H). ^{13}C NMR (151 MHz, DMSO- d_6) δ 167.68, 165.14, 138.85, 133.65, 130.10, 128.70, 128.24, 128.04, 127.73, 127.23, 74.82, 51.77, 28.04, 18.71, 12.99. Anal. calcd. for $C_{20}H_{23}NO_4$: C 70.36, H 6.79, N 4.10, found: C 70.34, H 7.03, N 4.05.

3. Biological evaluation

3.1. *In-vitro* human HDAC1 and human HDAC6 assay

OptiPlate-96 black microplates (Perkin Elmer) were used with an assay volume of 50 μ L. Human recombinant HDAC1 (10 ng/well; BPS Bioscience, Catalog #: 50051) or HDAC6 (35 ng/well; BPS Bioscience, Catalog #: 50006) were diluted in assay buffer (50 mM Tris-HCl, pH 8.0, 137 mM NaCl, 2.7 mM KCl, 1 mM MgCl₂, 0.1 mg/mL BSA), followed by addition of different concentrations of test compounds or controls diluted in assay buffer and 5 μ L of the fluorogenic substrate ZMAL (Z-(Ac)Lys-AMC)[5] (150 μ M) at 37 °C. After 90 min incubation at 37 °C, 50 μ L of 0.4 mg/mL trypsin in trypsin buffer (Tris-HCl 50 mM, pH 8.0, NaCl 100 mM) was added, followed by further incubation at 37 °C for 30 min. Fluorescence was measured with an excitation wavelength of 390 nm and an emission wavelength of 460 nm using a Spark 10 M microplate reader (Tecan).

4. References

- [1] C. Aurrecochea et al, 2009 PlasmoDB: a functional genomic database for malaria parasites. *Nucleic Acids Res*, 37, D539-43.
- [2] J. T. Welch, K. W. Seper. Synthesis, regioselective deprotonation, and stereoselective alkylation of fluoro ketimines, *J. Org. Chem.*, **1988**, 53, 2991-2999.
- [3] J. Wild, N. Goetz, W. Will, R. D. Kohler, P. Plath (BASF AG) Process for preparing O-substituted hydroxylamines. DE 3615473 A1, *ChemicalAbstracts*, **1988**, 108, 111952e.
- [4] K. Ramasamy, R. K. Olsen, T. Emery, N-Methylation of O-benzyl- α -N-(alkoxycarbonyl)- α -amino acid hydroxamate derivatives, *J. Org. Chem.*, **1981**, 46, 5438-5441.
- [5] B. Heltweg, F. Dequiedt, E. Verdin, M. Jung, Nonisotopic substrate for assaying both human zinc and NAD⁺-dependent histone deacetylases, *Anal. Biochem.*, **2003**, 319, 42-48.

Manuscript III

Full Paper

Isophthalic Acid-Based HDAC Inhibitors as Potent Inhibitors of HDAC8 from *Schistosoma mansoni*

Katharina Stenzel¹, Alokta Chakrabarti², Jelena Melesina³, Finn K. Hansen^{1,4}, Julien Lancelot⁵, Simon Herkenhöfner¹, Beate Lungerich¹, Martin Marek⁶, Christophe Romier⁶, Raymond. J. Pierce⁵, Wolfgang Sipp³, Manfred Jung², and Thomas Kurz ¹

¹ Institute of Pharmaceutical and Medicinal Chemistry, Heinrich-Heine-University, Düsseldorf, Germany

² Institute of Pharmaceutical Sciences, Albert-Ludwigs-University Freiburg, Freiburg, Germany

³ Institute of Pharmacy, Martin-Luther-University Halle-Wittenberg, Halle (Saale), Germany

⁴ Pharmaceutical/Medicinal Chemistry, Institute of Pharmacy, Leipzig University, Leipzig, Germany

⁵ Univ. Lille, CNRS, Inserm, CHU Lille, Institut Pasteur de Lille, U1019 UMR 8204CIL – Centre d'Infection et d'Immunité de Lille, Lille, France

⁶ IGBMC, Université de Strasbourg, Illkirch, France

Schistosoma mansoni histone deacetylase 8 (*SmHDAC8*) has been recently identified as a new potential target for the treatment of schistosomiasis. A series of newly designed and synthesized alkoxyamide-based and hydrazide-based HDAC inhibitors were tested for inhibitory activity against *SmHDAC8* and human HDACs 1, 6, and 8. The front runner compounds showed submicromolar activity against *SmHDAC8* and modest preference for *SmHDAC8* over its human orthologue hHDAC8. Docking studies provided insights into the putative binding mode in *SmHDAC8* and allowed rationalization of the observed selectivity profile.

Keywords: Docking studies / HDAC8 / Histone deacetylase inhibitors / *Schistosoma mansoni* / Schistosomiasis

Received: March 16, 2017; Revised: May 21, 2017; Accepted: May 22, 2017

DOI 10.1002/ardp.201700096



Additional supporting information may be found in the online version of this article at the publisher's web-site.

Introduction

The neglected parasitic disease schistosomiasis is endemic in 74 developing countries. The disease continues to spread to new geographic areas despite comprehensive anthelmintic drug therapy programs. There are two major forms of schistosomiasis – intestinal and urogenital – caused by *Schistosoma mansoni* and four further parasites of the genus *Schistosoma* that infect humans. Chronic disease contributes to major organ damage, and reducing the severity of

symptoms is critical to the management of schistosomiasis. Under risk are individuals having contact with freshwater sources and in particular children under age 14. According to World Health Organization (WHO) statistics at least 258 million people worldwide required preventive treatment and 62 million received treatment in 2014 [1, 2].

The life cycle of *S. mansoni* includes radical morphological modifications and exhibits diverse phenotypes [3, 4]. The complexity of the human endoparasite is reflected in a large genome, variable transcriptome profiles, and a dynamic epigenetic machinery in dependency of each life cycle stage [5, 6]. There is currently no vaccine available for the treatment of human schistosomiasis and no indication that a vaccine is likely to become available soon [7].

Since the anthelmintic drug praziquantel (PZQ) was approved for treatment of schistosomiasis it has been widely used for more than 30 years and remains to be the drug of choice till now [8]. The WHO strategy for schistosomiasis

Correspondence: Prof. Thomas Kurz, Institut für Pharmazeutische und Medizinische Chemie, Heinrich-Heine-Universität Düsseldorf, Universitätsstr. 1, 40225 Düsseldorf, Germany.
E-mail: thomas.kurz@uni-duesseldorf.de
Fax: +49 211 81-13847

control focuses on periodic large scale treatment with PZQ (preventive chemotherapy) of affected populations. However, the drug does not prevent reinfections and its mechanism of action is not exactly known. The application of PZQ is limited to adult worms, which has been shown in *in vitro* tests and confirmed by clinical data [9, 10]. PZQ is safe, effective and relatively cheap, but there is also a growing concern regarding reports from patients not cured by multiple doses [11, 12]. The development of resistance and stable resistance after removal of drug pressure has been demonstrated in the laboratory [13–15]. Moreover resistant isolates have already been characterized in endemic areas and the selection of field strains of schistosome that are resistant to PZQ is more and more likely [9].

Like other human parasites schistosomes share some properties with malignant tumors including intense metabolic activity and uncontrolled cell division [16–18]. Histone deacetylases (HDACs) are Zn²⁺- or NAD⁺-dependent lysine deacetylases that can modulate cell chromatin structure, transcription, and gene expression. Consequently, histone deacetylase inhibitors (HDACi) have emerged as a new class of anticancer drugs. Currently, three HDACi are approved by the US Food and Drug Administration (FDA) for the treatment of T-cell lymphoma (vorinostat, romidepsin, and belinostat) while panobinostat has been approved for combination therapy use in certain cases of multiple myeloma. Furthermore, the potential therapeutic use of HDACi in other diseases including inflammatory, immune, neurodegenerative, cardiac, viral, and parasitic diseases is currently under discussion [19–27].

Using the “piggyback” strategy it has been shown that the HDACi trichostatin A (TSA), vorinostat (SAHA), and valproic acid (VPA) inhibited *S. mansoni* histone deacetylase 8 (*SmHDAC8*) activity at all life cycle stages and TSA and VPA caused mortality of schistosomula and adult worms [25, 28, 29]. Till now only class I *S. mansoni* HDAC1, -3, and -8 and class III *S. mansoni* Sirt1, -2, -5, -6, -7 HDACs have been cloned and characterized [29, 30]. *S. mansoni* HDAC1, 3, and 8 mRNAs are expressed at all schistosome life cycle stages. In particular, *SmHDAC8* has been identified as a potential target for antiparasitic therapy [31]. Transcripts of *SmHDAC8* are expressed at higher levels than *SmHDAC1* and *SmHDAC3* during all life cycle stages, pointing at specific and vital functions in the parasite life cycle. At the same time human HDAC8 shows the lowest level of expression of the four class I HDACs in human and it has been reported that inhibition of hHDAC8 shows only limited effects in many cell types [32]. Different HDACi have already been shown to inhibit *SmHDAC8* and to induce histone hyperacetylation and apoptosis in *S. mansoni* [29, 31, 33].

Treatment of schistosomes with HDACi caused an accumulation of acetylated cellular proteins and dose-dependent mortality of schistosomula and adult worms [6, 28, 29]. Thus, the development of small-molecule *SmHDAC8* inhibitors represents a promising approach for the treatment of schistosomiasis and several HDACi with confirmed activity

against *SmHDAC8* have been identified in recent years (see Fig. 1 for selected examples) [32, 34]. Unfortunately, most known *SmHDAC8* inhibitors possess a higher activity against human HDAC8. Thus, there is a strong need for new types of HDACi with preferential activity for *SmHDAC8*. We herein present the design, synthesis, and biological evaluation of a novel series of *SmHDAC8* inhibitors.

Results and discussion

Design and synthesis of target compounds

We used the 3-acylamino benzohydroxamates of type I and II (Fig. 1), a series of potent and in some cases preferential *SmHDAC8* inhibitors, as starting point for this project [34]. In a previous study [21, 35] we identified an alkoxyamide group as a novel connecting unit which presumably can enable charge-assisted hydrogen bonds due to the additional polarization of the N–H bond. We therefore decided to retain the *meta*-substituted benzohydroxamate realized in I and to combine this motif with an alkoxyamide connecting unit and various cap groups. In addition, we designed compounds with hydrazide-based connecting units in order to probe whether these groups can serve as an alternative connecting unit.

The isophthalic acid-based target compounds **3a–i** and **5a,b** were synthesized using a straightforward two-step protocol as illustrated in Scheme 1. First, the 1,1'-carbonyldiimidazole (CDI)-mediated amide coupling reaction of mono-methyl isophthalate with *O*-substituted hydroxylamines and hydrazine derivatives provided the alkoxyamide intermediates **2a–i** and hydrazides **4a,b** (Scheme 1), respectively.

The subsequent treatment of **2a–i** and **4a,b** with an excess of hydroxylamine hydrochloride in the presence of methanolic sodium methoxide afforded the desired target compounds **3a–i** and **5a,b**. Using these synthetic methods allowed us to efficiently modify the cap region of our target compounds in order to potentially address the hydrophobic side pocket of *SmHDAC8*.

Primary screening

All synthesized compounds were first tested in a primary screen for inhibition of *SmHDAC8* and representative human HDAC isoforms (hHDAC1, hHDAC6, and hHDAC8) at a concentration of 1 μM (Table 1). The *in vitro* assays rely on the use of fluorogenic substrates containing an ϵ -acetyl lysine linked to a fluorescent moiety at the C-terminus. Only upon deacetylation the resulting peptide is a substrate for a protease which upon cleavage of the fluorogenic moiety releases the fluorophore for quantitation. For HDAC1 and 6 we used ZMAL (Z-Lys(Ac)-AMC) and trypsin as the protease. The commercially available Fluor de Lys-HDAC8 substrate has Arg-His-Lys(Ac)-Lys(Ac) as the substrate sequence. The exact identity of fluorophore and developer are not revealed [36, 37]. All compounds showed significant inhibition of *SmHDAC8* deacetylase activity, moderate inhibition of hHDAC6 and only very low inhibition of hHDAC1. However,

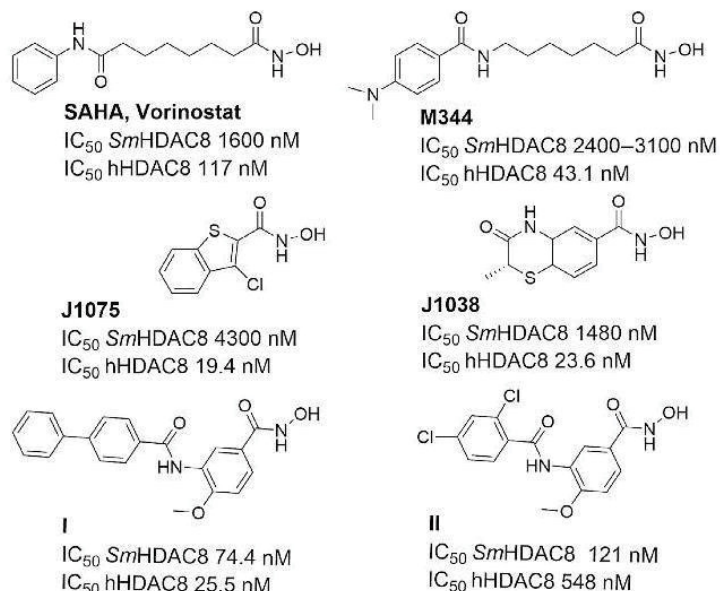


Figure 1. Chemical structures of selected HDAC inhibitors and IC₅₀ values of *SmHDAC8* and hHDAC8 [22, 24].

most compounds inhibited hHDAC8 in similar fashion as *SmHDAC8*. Interestingly, compounds **3d** and **5a** revealed a somewhat stronger inhibition of *SmHDAC8* in comparison to hHDAC8 (Table 1). Based on this primary screening, we decided to investigate the HDACi **3d**, **5a** and the unsubstituted prototype compound **3c** in more detail.

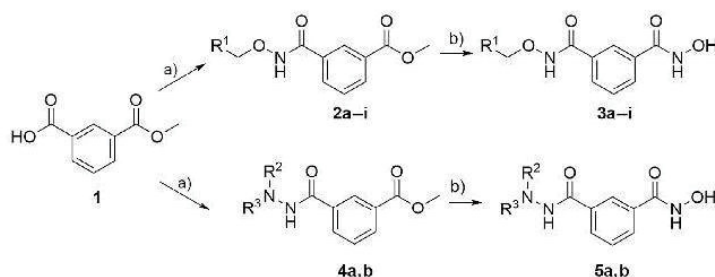
Inhibition of hHDAC1, hHDAC6, hHDAC8, and *SmHDAC8*

In order to study whether **3c**, **3d**, and **5a** can be considered as preferential *SmHDAC8* inhibitors, we determined IC₅₀ values against hHDAC1, hHDAC6, hHDAC8, and *SmHDAC8*. SAHA (vorinostat, suberoylanilide hydroxamic acid) was used as a reference pan-HDACi. The results are summarized in Table 2. Compounds **3c**, **3d**, and **5a** showed nanomolar activity against *SmHDAC8* with IC₅₀ values in the range of 0.33–0.75 μM and very good selectivity over hHDAC1. Furthermore, the

compounds possess approximately 10-fold preference over hHDAC6. The compound **3c** exhibited a stronger inhibition of hHDAC8 (IC₅₀: 0.09 μM) compared with *SmHDAC8* (IC₅₀: 0.33 μM) whereas **3d** (hHDAC8 IC₅₀: 0.63 μM vs. *SmHDAC8* IC₅₀: 0.40 μM) and **5a** (hHDAC8 IC₅₀: 1.31 μM vs. *SmHDAC8* IC₅₀: 0.75 μM) showed a very modest preference for *SmHDAC8*.

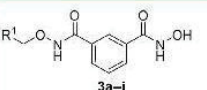
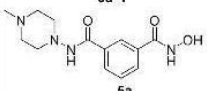
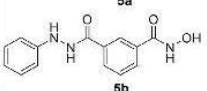
Docking study

To rationalize the obtained biochemical data, notably to understand the change of specificity between the schistosomal and human enzymes, the synthesized inhibitors were docked to the available crystal structures of *SmHDAC8*, hHDAC8, and hHDAC1. The applied docking method was first successfully validated on the X-ray structures of hHDAC8 and *SmHDAC8* (for details see the Experimental section). Using this docking setup consistent binding models were derived for both human and *SmHDAC8*. Comparison of the available X-ray structures of hHDAC8 and *SmHDAC8* showed a



Scheme 1. Synthesis of alkoxyamide-based and the hydrazide-based HDACi. Reagents and conditions: a) CDI, CH₂Cl₂, R¹-ONH₂, or R¹R²-NNH₂, r.t., 0.5 h, 12 h; b) 1) NaOMe, MeOH, NH₂OH·HCl, 70°C, 3–5 h, 2) NaOH, NH₂OH, MeOH, CH₂Cl₂, 0°C, r.t., 12 h.

Table 1. % Inhibition of hHDAC1, hHDAC6, hHDAC8, and *Sm*HDAC8 at 1 μ M.

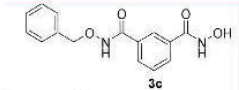
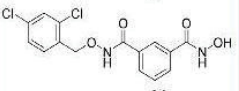
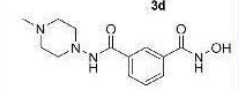
	% Inhibition at 1 μ M: Primary screen					
		R ¹	hHDAC1	hHDAC6	hHDAC8	<i>Sm</i> HDAC8
 3a-i	3a	Ph-CH ₂ -CH ₂	<10	65	81	87
	3b	Ph-CH ₂	<10	43	63	84
	3c	Ph	<10	31	79	89
 5a	3d	2,4-Cl-Ph	<10	20	56	86
	3e	2,3-Cl-Ph	<10	52	76	90
	3f	3,5-Me-Ph	<10	41	73	78
	3g	4-Me-Ph	<10	50	88	90
	3h	1-naphthyl	<10	51	78	84
 5b	3i	3,4-F-Ph	<10	41	72	82
	5a		<10	26	38	64
	5b		<10	49	70	87

high similarity especially within the binding pocket. The main differences are the substitution of Met274 in hHDAC8 to His292 in *Sm*HDAC8 and a flipped out conformation of Phe151 in *Sm*HDAC8 (for details see Fig. S1a and b in the Supporting Information). Docking of inhibitors **3c**, **3d**, and **5a** to *Sm*HDAC8 and hHDAC8 showed that the hydroxamate is perfectly coordinating the zinc ion as observed in *Sm*/hHDAC8-inhibitor crystal structures. In addition the hydroxamate group is making hydrogen bonds to conserved Tyr and His residues nearby the catalytic zinc ion (see Fig. 2A–C for details). Docking of **3c** and **3d**, having an alkoxyamide linker between the two aromatic rings, showed in case of *Sm*HDAC8 two additional hydrogen bonds to Lys20 and His292 (Fig. 2A, B). These interactions are also observed in the crystal structure of *Sm*HDAC8 in complex with an amide containing inhibitor (PDB ID 5FUE) [34]. Only compounds **3c** and **3d** are showing these two hydrogen bonds, whereas the weaker *Sm*HDAC8 inhibitor **5a** is not able to form these hydrogen bonds but interacts with Asp100. Additionally, the calculated binding energies of **3c** and **3d** are more favourable compared to **5a**

(see Supporting Information Table S1). The terminal aromatic group of **3c** and **3d** is interacting with the residues of the so-called side-pocket (His292, Pro293, Tyr306). The docking of **5a** showed that the piperazine ring is located nearby the acidic residue Asp100 (hydrogen bond in case of *Sm*HDAC8) whereas no interaction with the residues of the side-pocket was observed, which might explain the lower inhibitory activity.

In the hHDAC8 structure a methionine (Met274) is located at the same position as His292 in *Sm*HDAC8. The methionine is not able to form hydrogen bonds with the docked inhibitors. However, in the available crystal structures of hHDAC8 a conserved water molecule bound to the zinc coordinating histidine (His180 in hHDAC8) is observed which was found as a hydrogen bonding partner with **3c** and **3d** (Fig. 2D,E). The terminal aromatic ring of **3c** makes favorable van der Waals interaction with the side-pocket in hHDAC8 (Phe152, Pro273, Met274, Tyr341, Fig. 2) and shows a perfect fit to this hydrophobic subpocket (Fig. 3). This is reflected by favourable docking score and binding energy calculated for **3c** (Supporting Information Table S1). The docking of the

Table 2. IC₅₀ profiling against human hHDAC1, hHDAC6, hHDAC8, and *Sm*HDAC8.

		IC ₅₀ (μ M)			
		hHDAC1	hHDAC6	hHDAC8	<i>Sm</i> HDAC8
 3c	3c	136.1	2.95	0.09 \pm 0.12	0.33 \pm 0.04
	 3d	3d	47.5% @200 μ M	5.12	0.63 \pm 0.14
 5a		5a	15.3% @200 μ M	7.11	1.31 \pm 0.13
		SAHA	0.32	0.11	0.91 \pm 0.26

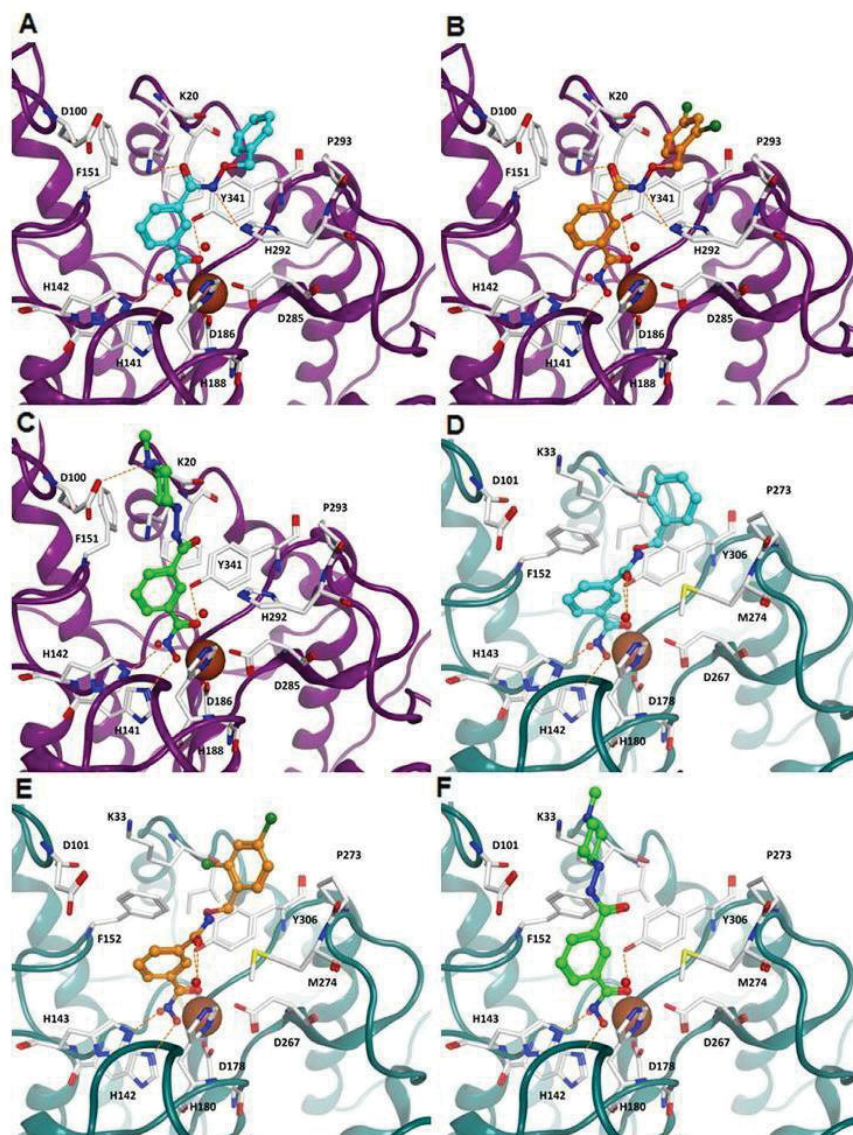


Figure 2. Docking poses calculated for inhibitor **3c** (colored cyan), **3d** (colored orange), and **5a** (colored green) at *SmHDAC8* (purple ribbon) and at hHDAC8 (turquoise ribbon). Only surrounding amino acid residues are shown for clarity. Hydrogen bonds are shown as orange dashed lines.

inhibitors to hHDAC1 showed that the hydroxamate is not able to coordinate in a favorable manner to the catalytic zinc ion due to a narrower binding pocket (Fig. 4).

Cytotoxicity and phenotypic activity

Parasite-specific HDACi should possess low toxicity to mammalian cells. We therefore tested **3d** and **5a** for cytotoxicity against HeK293T and HeLa cells. Vorinostat

was used as reference compound. The results are summarized in Fig. 5. As expected, vorinostat exhibited strong cytotoxicity against both HeK293T and HeLa cells. In contrast, compounds **3d** and **5a** showed only relatively low cytotoxicity (Fig. 5).

We next studied the phenotypic activity of **3d** and **5a** by testing their effects on the viability of the larvae (schistosomula) and the stability of adult worm pairs in culture exactly as

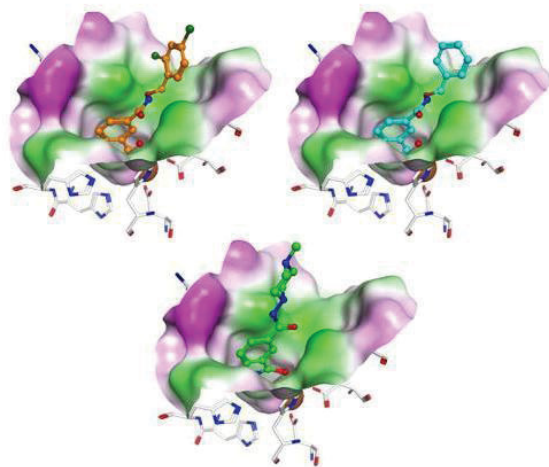


Figure 3. Molecular surface of the hHDAC8 binding pocket colored according to the hydrophobicity (green = hydrophobic, magenta = hydrophilic). The docking pose of inhibitor **3c** is shown in cyan, **3d** is shown in orange, and **5a** is shown in green.

previously described [34]. Using a fluorescence-based assay **3d** showed moderate toxicity toward schistosomula at 10 μ M, but this was not dose-dependent. **5a** showed only slight activity. Moreover, neither compound significantly affected adult worm pairing during 5 days of culture *in vitro* (Table 3). Of note, vorinostat is only moderately effective in the same assays (not shown), whereas other hydroxamate-based inhibitors are very active [29, 34]. The different abilities of the compounds to pass through the parasite tegument may provide a possible explanation for these differences.

Conclusion

In summary, we have designed and synthesized two new types of isophthalic acid-based *Sm*HDAC8 inhibitors. The alkoxyamide-based HDACi **3d** and the hydrazide-based HDACi **5a** were identified as potent inhibitors of *Sm*HDAC8 with a high preference over hHDAC1 and good preference over hHDAC6. Cytotoxicity studies revealed that the compounds showed relatively low effects on the proliferation of human cells. Molecular modeling and docking studies allowed rationalization of the observed biochemical data and suggest that two important hydrogen bonds of the alkoxyamide connecting unit to Lys20 and His292 contribute to the high activity of **3d** against *Sm*HDAC8. Even though the preference over hHDAC8 and the phenotypic activity need to be improved in the future, we believe that **3d** and **5a** are valuable starting points for the development of novel preferential *Sm*HDAC8 inhibitors.

Experimental

Chemistry

General procedure for the synthesis of **3a–i** and **5a,b**

Method A: Hydroxylamine hydrochloride (348 mg, 5.0 mmol, 10 eq) was added to a freshly prepared sodium methanolate solution (175 mg, 7.5 mmol, 15 eq) in dry methanol (8 mL). The mixture was stirred for 10 min before the respective ester **2a–i** or **4a** (0.5 mmol, 1.0 eq) was added. The reaction mixture was stirred in a high-pressure flask for 3–5 h at 70 °C. The solvent was removed under reduced pressure, water (15 mL) was added, and the pH was adjusted to pH 7–8 using 4 M HCl. The mixture was extracted with ethyl acetate (3 \times 20 mL), the combined organic layers were dried over anhydrous sodium sulfate, filtered, and concentrated in vacuum. The crude products were purified by flash column chromatography using a linear dichloromethane/methanol gradient (pre-packed silica cartridge, gradient: 97:3 to 91:9 in 20 min) to yield the desired hydroxamic acids **3a–i** and **5a–b** (yield: 60–91%). **Method B:** The respective ester **4b** (1 mmol, 1.0 eq) was dissolved in dry dichloromethane/methanol (1:3) and cooled down to 0 °C. Hydroxylamine (50 wt% in water, 30 mmol, 30 eq) and NaOH (0.4 g, 10 mmol, 10 eq) were added and stirred for 12 h at room temperature. The solvent was removed under reduced pressure, water (15 mL) was added, and the pH was adjusted to pH 7–8 using 4 M HCl. The mixture was extracted with ethyl acetate (3 \times 20 mL), the combined organic layers were dried over anhydrous sodium sulfate, filtered, and concentrated in vacuum (yield: 86%).

The InChI codes of the investigated compounds together with some biological activity data are provided as Supporting Information.

*N*¹-Hydroxy-*N*³-(3-phenylpropoxy)isophthalamide (**3a**)

Colorless solid; yield: 84%; mp: 130 °C; ¹H NMR (600 MHz, DMSO-*d*₆) δ 10.69 (s, 2H), 8.18 (s, 1H), 7.84–7.94 (m, 2H), 7.55 (t, *J* = 7.1 Hz, 1H), 7.42–7.22 (m, 4H), 7.22–7.07 (m, 1H), 3.92 (s, 2H), 2.73 (s, 2H), 1.92 (s, 2H). ¹³C NMR (151 MHz, DMSO) δ 162.95, 162.90, 141.01, 132.53, 132.07, 129.04, 128.96, 128.01, 127.79, 127.72, 125.32, 125.20, 73.96, 30.85, 29.05. *t*_R: 11.68 min, purity: 97.2%; HRMS (ESI) Anal. calcd. for C₁₇H₁₉N₂O₄ 315.1345 [M+H]⁺, Found 315.1342.

*N*¹-Hydroxy-*N*³-phenethoxyisophthalamide (**3b**)

Colorless solid; yield: 78%; mp: 128 °C; ¹H NMR (500 MHz, DMSO-*d*₆) δ 11.55 (s, 2H), 9.18 (s, 1H), 8.16 (s, 1H), 7.88 (t, *J* = 8.1 Hz, 2H), 7.55 (t, *J* = 7.7 Hz, 1H), 7.42–7.27 (m, 4H), 7.27–7.11 (m, 1H), 4.13 (t, *J* = 6.9 Hz, 2H), 2.97 (t, *J* = 6.9 Hz, 2H). ¹³C NMR (126 MHz, DMSO) δ 163.43, 138.27, 133.00, 132.49, 129.58, 129.48, 128.78, 128.51, 128.20, 126.09, 125.86, 75.64, 33.93. *t*_R: 10.65 min, purity: 97.5%; HRMS (ESI) Anal. calcd. for C₁₆H₁₇N₂O₄ 301.1188 [M+H]⁺, Found 301.1182.

*N*¹-(Benzyloxy)-*N*³-hydroxyisophthalamide (**3c**)

Colorless solid; yield: 60%; mp: 159 °C; ¹H NMR (500 MHz, DMSO-*d*₆) δ 11.92 (s, 1H), 11.34 (s, 1H), 9.14 (s, 1H), 8.16 (s, 1H),

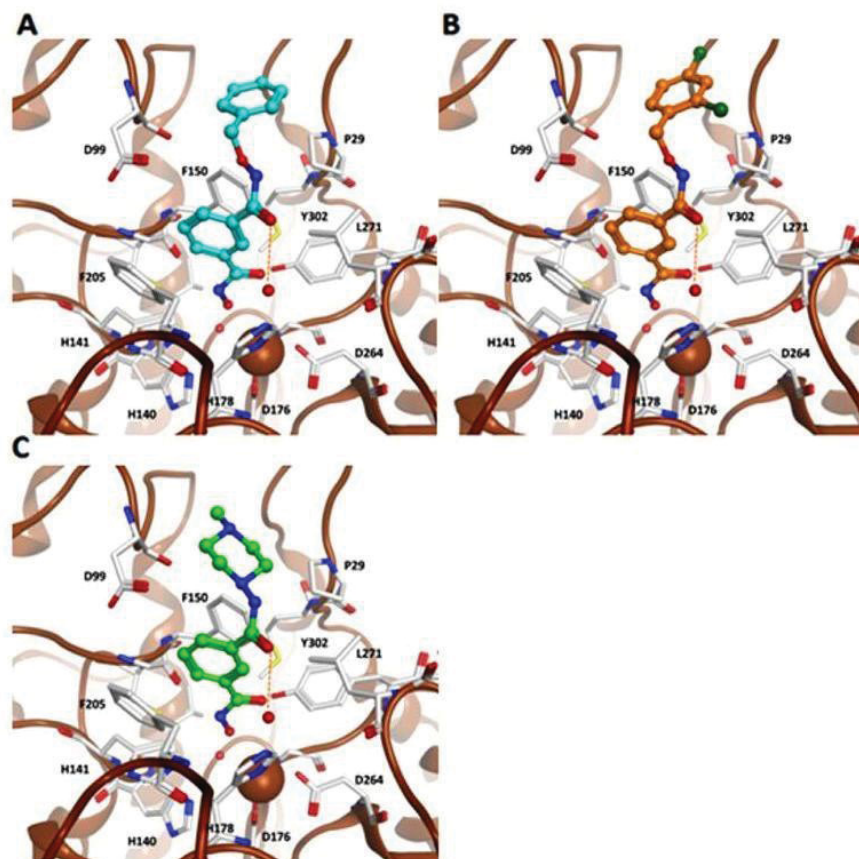


Figure 4. Docking poses calculated for inhibitor **3c** (colored cyan), **3d** (colored orange), and **5a** (colored green) at hHDAC1. Only surrounding amino acid residues are shown for clarity. Hydrogen bonds are shown as orange dashed lines.

8.05–7.75 (m, 2H), 7.62–7.26 (m, 6H), 4.94 (s, 2H). ^{13}C NMR (126 MHz, DMSO) δ 163.72, 163.46, 135.76, 132.98, 132.45, 129.62, 129.51, 128.82, 128.52, 128.23, 125.91, 76.93. t_R : 9.62 min, purity: 97.2%; HRMS (ESI) Anal. calcd. for $\text{C}_{15}\text{H}_{15}\text{N}_2\text{O}_4$ 287.1032 $[\text{M}+\text{H}]^+$, Found 287.1024.

*N*¹-((2,4-Dichlorobenzyl)oxy)-*N*³-hydroxyisophthalamide (**3d**)
Colorless solid; yield 82%; mp: 130°C; ^1H NMR (600 MHz, DMSO-*d*₆) δ 11.51 (s, 2H), 9.43 (s, 1H), 8.14 (s, 1H), 7.88 (d, *J* = 7.7 Hz, 1H), 7.84 (d, *J* = 7.6 Hz, 1H), 7.67 (s, 1H), 7.64 (d, *J* = 8.2 Hz, 1H), 7.53 (t, *J* = 7.7 Hz, 1H), 7.49 (dd, *J* = 8.3,

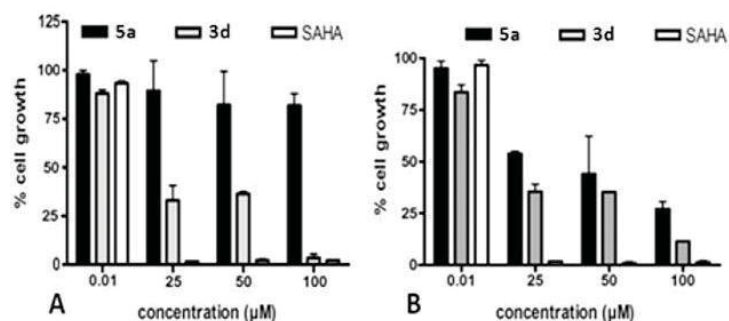


Figure 5. Comparison of cell viability of **3d** and **5a** in human cell lines. HeK293(A) and HeLa(B) cell lines were treated with the indicated concentrations of inhibitors for 72 h. Cell viability was measured using the 3-(4,5-dimethylthiazol-2-yl)-5-(3-carboxymethoxyphenyl)-2-(4-sulfo-phenyl)-2*H*-tetrazolium/phenazine methosulfate (MTS/PMS) reagent. Data represent S.E. of the mean (duplicates).

Table 3. Toxicity studies on *S. mansoni* adult worms and schistosomula.

Compound	% Pairing \pm SEM	% Viability \pm SD
3d		
10 μ M	95 \pm 5	76 \pm 6
20 μ M	85 \pm 5	75 \pm 4
5a		
10 μ M	95 \pm 5	90 \pm 9
20 μ M	95 \pm 5	79 \pm 3

Experimental conditions: Single dose at $D=0$, duration: 3 days data represent the means of three independent experiments. Adult worm pairing assay: Number of worms: 10/wells $n=2$ Alamar viability assay: Number of schistosomula: 100/well $n=2$.

2.2 Hz, 1H), 5.04 (s, 2H). ^{13}C NMR (151 MHz, DMSO) δ 163.12, 162.91, 133.63, 133.24, 132.47, 132.28, 132.03, 131.86, 129.11, 129.03, 128.20, 128.01, 126.83, 125.40, 72.46. t_{R} : 12.40 min, purity: 99.1%; HRMS (ESI) Anal. calcd. for $\text{C}_{15}\text{H}_{13}\text{Cl}_2\text{N}_2\text{O}_4$ 355.0252 $[\text{M}+\text{H}]^+$, Found 355.0244.

*N*¹-((2,3-Dichlorobenzyl)oxy)-*N*³-hydroxyisophthalamide (3e)

Colorless solid; yield 91%; mp: 116°C; ^1H NMR (600 MHz, DMSO-*d*₆) δ 11.75 (s, 1H), 11.47 (s, 1H), 9.13 (s, 1H), 8.13 (s, 1H), 7.89 (d, $J=7.6$ Hz, 1H), 7.84 (d, $J=7.7$ Hz, 1H), 7.67 (d, $J=7.9$ Hz, 1H), 7.60 (d, $J=7.5$ Hz, 1H), 7.55 (t, $J=7.7$ Hz, 1H), 7.42 (t, $J=7.8$ Hz, 1H), 5.11 (s, 2H). ^{13}C NMR (151 MHz, DMSO) δ 163.52, 162.93, 135.68, 135.63, 132.50, 131.76, 131.28, 130.60, 129.91, 129.15, 129.05, 128.03, 127.60, 125.42, 73.62. t_{R} : 12.10 min, purity: 96.3%; HRMS (ESI) Anal. calcd. for $\text{C}_{15}\text{H}_{13}\text{Cl}_2\text{N}_2\text{O}_4$ 355.0252 $[\text{M}+\text{H}]^+$, Found 355.0247.

*N*¹-((3,5-Dimethylbenzyl)oxy)-*N*³-hydroxyisophthalamide (3f)

Colorless solid; yield 84%; mp: 105°C; ^1H NMR (500 MHz, DMSO-*d*₆) δ 11.86 (s, 1H), 11.33 (s, 1H), 9.14 (s, 1H), 8.16 (s, 1H), 7.94–7.83 (m, 2H), 7.56 (t, $J=7.7$ Hz, 1H), 7.07 (s, 2H), 7.00 (s, 1H), 4.86 (s, 2H), 2.29 (s, 6H). ^{13}C NMR (126 MHz, DMSO-*d*₆) ^{13}C NMR (151 MHz, DMSO) δ 164.30, 164.06, 137.78, 136.13, 133.57, 133.12, 130.15, 129.10, 127.15, 126.51, 77.59, 21.32. t_{R} : 12.03 min, purity: 97.5%; HRMS (ESI) Anal. calcd. for $\text{C}_{17}\text{H}_{19}\text{N}_2\text{O}_4$ 315.1345 $[\text{M}+\text{H}]^+$, Found 315.1343.

*N*¹-Hydroxy-*N*³-((4-methylbenzyl)oxy)isophthalamide (3g)

Colorless solid; yield 78%; mp: 169°C; ^1H NMR (600 MHz, DMSO-*d*₆) δ 11.56 (s, 2H), 9.15 (s, 1H), 8.15 (s, 1H), 7.89 (d, $J=7.7$ Hz, 1H), 7.86 (d, $J=7.8$ Hz, 1H), 7.55 (t, $J=7.7$ Hz, 1H), 7.35 (d, $J=7.6$ Hz, 2H), 7.21 (d, $J=7.6$ Hz, 2H), 4.89 (s, 2H), 2.32 (s, 3H). ^{13}C NMR (151 MHz, DMSO) δ 163.16, 162.95, 137.02, 132.49, 132.28, 131.98, 129.04, 128.95, 128.43, 128.28, 128.01, 125.36, 76.24, 20.22. t_{R} : 10.85 min, purity: 97.1%; HRMS (ESI)

Anal. calcd. for $\text{C}_{16}\text{H}_{17}\text{N}_2\text{O}_4$ 301.1188 $[\text{M}+\text{H}]^+$, Found 301.1184.

*N*¹-Hydroxy-*N*³-(naphthalen-1-ylmethoxy)isophthalamide (3h)

Colorless solid; yield: 81%; mp: 137°C; ^1H NMR (600 MHz, DMSO-*d*₆) δ 11.97 (s, 1H), 11.09 (s, 1H), 9.17 (s, 1H), 8.62 (d, $J=8.0$ Hz, 1H), 8.22 (s, 1H), 7.98 (d, $J=8.1$ Hz, 2H), 7.91 (t, $J=6.5$ Hz, 2H), 7.68–7.55 (m, 4H), 7.49–7.54 (m, 1H), 5.39 (s, 2H). ^{13}C NMR (126 MHz, DMSO) δ 164.78, 164.37, 134.21, 134.09, 133.47, 132.91, 132.33, 130.59, 130.45, 130.24, 129.47, 129.36, 129.12, 127.29, 126.87, 126.15, 125.75, 76.23. t_{R} : 12.28 min, purity: 97.4%; HRMS (ESI) Anal. calcd. for $\text{C}_{19}\text{H}_{17}\text{N}_2\text{O}_4$ 337.1188 $[\text{M}+\text{H}]^+$, Found 337.1185.

*N*¹-((3,4-Difluorobenzyl)oxy)-*N*³-hydroxyisophthalamide (3i)

Colorless solid; yield 73%; mp: 120°C; ^1H NMR (600 MHz, DMSO-*d*₆) δ 11.57 (s, 2H), 9.28 (s, 1H), 8.18 (s, 1H), 7.88 (d, $J=7.5$ Hz, 1H), 7.91 (d, $J=7.6$ Hz, 1H), 7.64–7.50 (m, 2H), 7.49–7.42 (m, 1H), 7.33 (s, 1H), 4.95 (s, 2H). ^{13}C NMR (151 MHz, DMSO) δ 163.02, 162.89, 148.71 (dd, $J=245.4$, 10.5 Hz), 148.61 (dd, $J=245.2$, 11.9 Hz), 133.46, 132.45, 131.82, 129.14, 129.02, 128.03, 125.37, 125.07 (dd, $J=6.2$, 3.0 Hz), 117.11 (d, $J=17.3$ Hz), 116.74 (d, $J=17.1$ Hz), 74.96. t_{R} : 10.83 min, purity: 98.9%; HRMS (ESI) Anal. calcd. for $\text{C}_{15}\text{H}_{13}\text{F}_2\text{N}_2\text{O}_4$ 323.0843 $[\text{M}+\text{H}]^+$, Found 323.0835.

*N*¹-Hydroxy-*N*³-(4-methylpiperazin-1-yl)isophthalamide (5a)

Colorless solid; yield: 65%; mp: 155°C; ^1H NMR (600 MHz, DMSO-*d*₆) δ 11.40 (s, 1H), 9.72 (s, 1H), 9.15 (s, 1H), 8.24 (s, 1H), 7.94–7.86 (m, 2H), 7.53 (t, $J=7.5$ Hz, 1H), 2.97 (s, 4H), 2.66 (s, 4H), 2.33 (s, 3H). ^{13}C NMR (151 MHz, DMSO) δ 163.05, 162.98, 133.43, 132.21, 129.35, 128.88, 127.81, 125.47, 53.20, 52.32, 43.97. t_{R} : 4.79 min, purity: 98.1%; HRMS (ESI) Anal. calcd. for $\text{C}_{13}\text{H}_{19}\text{N}_4\text{O}_3$ 279.1457 $[\text{M}+\text{H}]^+$, Found 279.1453.

N-Hydroxy-3-(2-phenylhydrazine-1-carbonyl)benzamide (5b)

Colorless solid; yield 86%; mp: 182°C; ^1H NMR (600 MHz, DMSO-*d*₆) δ 11.34 (s, 1H), 10.44 (s, 1H), 9.14 (s, 1H), 8.29 (s, 1H), 8.04 (d, $J=7.7$ Hz, 1H), 7.99–7.89 (m, 2H), 7.59 (t, $J=7.7$ Hz, 1H), 7.16 (t, $J=7.9$ Hz, 2H), 6.81 (d, $J=7.8$ Hz, 2H), 6.73 (t, $J=7.3$ Hz, 1H). ^{13}C NMR (151 MHz, DMSO) δ 165.33, 163.07, 148.78, 132.73, 132.56, 129.21, 129.15, 128.14, 128.06, 125.61, 118.08, 111.74. t_{R} : 9.59 min, purity: 98.4% HRMS (ESI) Anal. calcd. for $\text{C}_{25}\text{H}_{25}\text{N}_2\text{O}_4$ 417.1804 $[\text{M}+\text{H}]^+$, Found 417.1809. HRMS (ESI) Anal. calcd. for $\text{C}_{14}\text{H}_{14}\text{N}_3\text{O}_3$ 272.1035 $[\text{M}+\text{H}]^+$, Found 272.1032.

Biological evaluation

Phenotypic screening of schistosomes

The viability of *S. mansoni* schistosomula in the presence of SmHDAC8 inhibitors was measured with a fluorescence-based assay using Alamar blue as previously described [24], as was

the effect of the compounds on the stability of adult worm pairing [24].

Computational methods

Crystal structures of *SmHDAC8* (PDB ID 5FUE), hHDAC8 (PDB ID 2V5X) and hHDAC1 (PDB ID 4BKX) were downloaded from the Protein Data Bank PDB [38]. Protein preparation was done using Schrödinger's Protein Preparation Wizard [39] by adding hydrogen atoms, assigning protonation states, and minimising the protein. Ligands were prepared in MOE [40] from smiles in neutral form. Multiple low energy starting conformations were generated with MOE within an energy window of 5 kcal/mol. Molecular docking was performed using program Glide software [39]. The same protocol was used as in a previous study [34]. Two conserved water molecules were included in the protein models, the best docking pose was selected based on the Glide SP score. All compounds were docked in neutral form.

In our previous study we found that rescoring the docking poses by using a MM-GB/SA protocol resulted in a significant correlation between calculated interaction energies and *in vitro* inhibition data. Therefore, the same protocol was applied to the compounds under study. To calculate binding free energy, we used the AMBER12EHT force field implemented in the MOE program together with the continuum solvation model GB/SA. The experimentally observed geometries of the zinc complexes were best reproduced using this setup. Partial charges were fixed using the MOE Protonate3D tool according to the used force-field followed by a short minimisation. An in-house script for minimising the protein–ligand complex and calculating the binding free energy was applied for all docking poses of ligands. During complex minimisation heavy atoms of protein were tethered with a deviation of 0.5 Å (force constant $(3/2) kT/(0.5)^2$).

The authors thank the COST action CM1406 (Epigenetic Chemical Biology EPICHEMbio) for support. This work and the authors of this article received funding from the European Union's Seventh Framework Programme for Research, Technological Development and Demonstration under Grant Agreements 241865 (SEtTReND) and 602080 (A-ParaDDisE). We thank Karin Schmidtkunz for technical assistance. The work of J. L. and R. P. was also supported by institutional funds from the CNRS, the Institut Pasteur de Lille and the Université de Lille.

The authors have declared no conflicts of interest.

References

- [1] World Health Organization, *Wkly. Epidemiol. Rec.* **2015**, *90*, 25–32 and schistosomiasis fact sheet; Available from: <http://www.who.int/mediacentre/factsheets/fs115/en> [accessed 08.12.16].
- [2] F. Mutapi, *Pediatrics* **2015**, *135*, 536–544.
- [3] M. Brown, *Schistosomiasis, Clin. Med. (Lond)* **2011**, *11*, 479–482.
- [4] B. Gryseels, K. Polman, J. Clerinx, L. Kestens, Human schistosomiasis, *Lancet* **2006**, *368*, 1106–1118.
- [5] M. Berriman, B. J. Haas, P. T. LoVerde, R. A. Wilson, G. P. Dillon, G. C. Cerqueira, S. T. Mashiyama, B. Al-Lazikani, L. F. Andrade, P. D. Ashton, M. A. Aslett, D. C. Bartholomeu, G. Blandin, C. R. Caffrey, A. Coghlan, R. Coulson, T. A. Day, A. Delcher, R. DeMarco, A. Djikeng, T. Eyre, J. A. Gamble, E. Ghedin, Y. Gu, C. Hertz-Fowler, H. Hirai, Y. Hirai, R. Houston, A. Ivens, D. A. Johnston, D. Lacerda, C. D. Macedo, P. McVeigh, Z. Ning, G. Oliveira, J. P. Overington, J. Parkhill, M. Perlea, R. J. Pierce, A. V. Protasio, M. A. Quail, M. A. Rajandream, J. Rogers, M. Sajid, S. L. Salzberg, M. Stanke, A. R. Tivey, O. White, D. L. Williams, J. Wortman, W. Wu, M. Zamanian, A. Zerlotini, C. M. Fraser-Liggett, B. G. Barrell, N. M. El-Sayed, *Nature* **2009**, *460*, 352–358.
- [6] R. J. Pierce, F. Dubois-Abdeselem, S. Caby, J. Trolet, J. Lancelot, F. Oger, N. Bertheaume, E. Roger, *Mem. Inst. Oswaldo Cruz* **2011**, *106*, 794–801.
- [7] A. A. Siddiqui, B. A. Siddiqui, L. Ganley-Leal, *Hum. Vaccin.* **2011**, *7*, 1192–1197.
- [8] D. Cioli, L. Pica-Mattocchia, A. Basso, A. Guidi, *Mol. Biochem. Parasitol.* **2014**, *195*, 23–29.
- [9] M. J. Doenhoff, J. R. Kusel, G. C. Coles, D. Cioli, *Trans. R. Soc. Trop. Med. Hyg.* **2002**, *96*, 465–469.
- [10] M. J. Doenhoff, L. Pica-Mattocchia, *Expert Rev. Anti-Infect. Ther.* **2006**, *4*, 199–210.
- [11] D. Alonso, J. Munoz, J. Gascon, M. E. Valls, M. Corachan, *Am. J. Trop. Med. Hyg.* **2006**, *74*, 342–344.
- [12] I. M. Silva, R. Thiengo, M. J. Conceicao, L. Rey, H. L. Lenzi, E. Pereira Filho, P. C. Ribeiro, *Mem. Inst. Oswaldo Cruz* **2005**, *100*, 445–449.
- [13] P. G. Fallon, M. J. Doenhoff, *Am. J. Trop. Med. Hyg.* **1994**, *51*, 83–88.
- [14] F. F. Couto, P. M. Coelho, N. Araujo, J. R. Kusel, N. Katz, L. K. Jannotti-Passos, A. C. Mattos, *Mem. Inst. Oswaldo Cruz* **2011**, *106*, 153–157.
- [15] S. M. Messerli, R. S. Kasinathan, W. Morgan, S. Spranger, R. M. Greenberg, *Mol. Biochem. Parasitol.* **2009**, *167*, 54–59.
- [16] U. E. Martinez-Outschoorn, R. G. Pestell, A. Howell, M. L. Tykocinski, F. Nagajyothi, F. S. Machado, H. B. Tanowitz, F. Sotgia, M. P. Lisanti, *Cell Cycle* **2011**, *10*, 4208–4216.
- [17] S. R. Choi, A. Pradhan, N. L. Hammond, A. G. Chittiboyina, B. L. Tekwani, M. A. Avery, *J. Med. Chem.* **2007**, *50*, 3841–3850.
- [18] F. Hirschhaeuser, U. G. Sattler, W. Mueller-Klieser, *Cancer Res.* **2011**, *71*, 6921–6925.
- [19] T. A. Rasmussen, O. Schmeltz Sogaard, C. Brinkmann, F. Wightman, S. R. Lewin, J. Melchjorsen, C. Dinarello,

- L. Ostergaard, M. Tolstrup, *Hum. Vaccin. Immunother* **2013**, *9*, 993–1001.
- [20] K. J. Falkenberg, R. W. Johnstone, *Nat. Rev. Drug Discov.* **2014**, *13*, 673–691.
- [21] F. K. Hansen, S. D. Sumanadasa, K. Stenzel, S. Duffy, S. Meister, L. Marek, R. Schmetter, K. Kuna, A. Hamacher, B. Mordmuller, M. U. Kassack, E. A. Winzeler, V. M. Avery, K. T. Andrews, T. Kurz, *Eur. J. Med. Chem.* **2014**, *82*, 204–213.
- [22] T. Harada, T. Hideshima, K. C. Anderson, *Int. J. Hematol.* **2016**, *104*, 300–309.
- [23] R. Benedetti, M. Conte, L. Altucci, *Antioxid. Redox Signal.* **2015**, *23*, 99–126.
- [24] J. A. Engel, A. J. Jones, V. M. Avery, S. D. Sumanadasa, S. S. Ng, D. P. Fairlie, T. S. Adams, K. T. Andrews, *Int. J. Parasitol. Drugs Drug Resist.* **2015**, *5*, 117–126.
- [25] C. Dissous, C. G. Grevelding, *Trends Parasitol.* **2011**, *27*, 59–66.
- [26] M. Marek, G. Oliveira, R. J. Pierce, M. Jung, W. Sippl, C. Romier, *Future Med. Chem.* **2015**, *7*, 783–800.
- [27] F. K. Hansen, T. S. Skinner-Adams, S. Duffy, L. Marek, S. D. Sumanadasa, K. Kuna, J. Held, V. M. Avery, K. T. Andrews, T. Kurz, *ChemMedChem* **2014**, *9*, 665–670.
- [28] F. Oger, F. Dubois, S. Caby, C. Noel, J. Cornette, B. Bertin, M. Capron, R. J. Pierce, *Biochem. Biophys. Res. Commun.* **2008**, *377*, 1079–1084.
- [29] F. Dubois, S. Caby, F. Oger, C. Cosseau, M. Capron, C. Grunau, C. Dissous, R. J. Pierce, *Mol. Biochem. Parasitol.* **2009**, *168*, 7–15.
- [30] J. Lancelot, S. Caby, F. Dubois-Abdeselem, M. Vanderstraete, J. Trolet, G. Oliveira, F. Bracher, M. Jung, R. J. Pierce, *PLoS Negl. Trop. Dis.* **2013**, *7*, e2428.
- [31] M. Marek, S. Kannan, A. T. Hauser, M. Moraes Mourao, S. Caby, V. Cura, D. A. Stolfa, K. Schmidtkunz, J. Lancelot, L. Andrade, J. P. Renaud, G. Oliveira, W. Sippl, M. Jung, J. Cavarelli, R. J. Pierce, C. Romier, *PLoS Pathog.* **2013**, *9*, e1003645.
- [32] A. Chakrabarti, I. Oehme, O. Witt, G. Oliveira, W. Sippl, C. Romier, R. J. Pierce, M. Jung, *Trends Pharmacol. Sci.* **2015**, *36*, 481–492.
- [33] D. A. Stolfa, M. Marek, J. Lancelot, A. T. Hauser, A. Walter, E. Leproult, J. Melesina, T. Rumpf, J. M. Wurtz, J. Cavarelli, W. Sippl, R. J. Pierce, C. Romier, M. Jung, *J. Mol. Biol.* **2014**, *426*, 3442–3453.
- [34] T. Heimbürg, A. Chakrabarti, J. Lancelot, M. Marek, J. Melesina, A. T. Hauser, T. B. Shaik, S. Duclaud, D. Robaa, F. Erdmann, M. Schmidt, C. Romier, R. J. Pierce, M. Jung, W. Sippl, *J. Med. Chem.* **2016**, *59*, 2423–2435.
- [35] L. Marek, A. Hamacher, F. K. Hansen, K. Kuna, H. Gohlke, M. U. Kassack, T. Kurz, *J. Med. Chem.* **2013**, *56*, 427–436.
- [36] B. Heltweg, F. Dequiedt, E. Verdin, M. Jung, *Anal. Biochem.* **2003**, *319*, 42–48.
- [37] B. Heltweg, F. Dequiedt, B. L. Marshall, C. Brauch, M. Yoshida, N. Nishino, E. Verdin, M. Jung, *J. Med. Chem.* **2004**, *47*, 5235–5243.
- [38] H. M. Berman, J. Westbrook, Z. Feng, G. Gilliland, T. N. Bhat, H. Weissig, I. N. Shindyalov, P. E. Bourne, The Protein Data Bank, *Nucleic Acids Res.* **2000**, *28*, 235–242.
- [39] S. Schrödinger Suite 2012 Protein Preparation Wizard; Epik Version 2.3, Schrödinger, LLC, New York, NY, 2012; Impact Version 5.8, Schrödinger, LLC, New York, NY, 2012; Prime Version 3.1, Schrödinger, LLC, New York, NY, 2012.
- [40] Molecular Operating Environment (Moe), 2012. 10; Chemical Computing Group Inc., 1010 Sherbooke St. West, Suite #910, Montreal, Qc, Canada, H3A 2r7, 2012.

8 References

1. P. A. Jones and S. B. Baylin. The epigenomics of cancer. *Cell* 2007, 128, 683-692.
2. S. Minucci and P. G. Pelicci. Histone deacetylase inhibitors and the promise of epigenetic (and more) treatments for cancer. *Nat.Rev. Cancer* 2006, 6, 38-51.
3. K. J. Falkenberg and R. W. Johnstone. Histone deacetylases and their inhibitors in cancer, neurological diseases and immune disorders. *Nat. Rev. Drug Discovery* 2014, 13, 673-691.
4. E. Seto and M. Yoshida. Erasers of histone acetylation: the histone deacetylase enzymes. *Cold Spring Harb Perspect Biol* 2014, 6, a018713.
5. J. G. Herman and S. B. Baylin. Promoter-region hypermethylation and gene silencing in human cancer. *Curr. Top. Microbiol. Immunol.* 2000, 249, 35-54.
6. A. Bird. DNA methylation patterns and epigenetic memory. *Genes Dev.* 2002, 16, 6-21.
7. A. Zemach, I. E. McDaniel, P. Silva and D. Zilberman. Genome-wide evolutionary analysis of eukaryotic DNA methylation. *Science* 2010, 328, 916-919.
8. S. B. Baylin and J. G. Herman. DNA hypermethylation in tumorigenesis: epigenetics joins genetics. *Trends Genet* 2000, 16, 168-174.
9. T. Jenuwein and C. D. Allis. Translating the histone code. *Science* 2001, 293, 1074-1080.
10. B. D. Strahl and C. D. Allis. The language of covalent histone modifications. *Nature* 2000, 403, 41-45.
11. B. A. Barber and M. Rastegar. Epigenetic control of Hox genes during neurogenesis, development, and disease. *Ann. Anat.* 2010, 192, 261-274.
12. K. Luger, A. W. Mader, R. K. Richmond, D. F. Sargent and T. J. Richmond. Crystal structure of the nucleosome core particle at 2.8 Å resolution. *Nature* 1997, 389, 251-260.
13. M. B. Eslaminejad, N. Fani and M. Shahhoseini. Epigenetic regulation of osteogenic and chondrogenic differentiation of mesenchymal stem cells in culture. *Cell J.* 2013, 15, 1-10.
14. Z. Wang, C. Zang, K. Cui, D. E. Schones, A. Barski, W. Peng and K. Zhao. Genome-wide mapping of HATs and HDACs reveals distinct functions in active and inactive genes. *Cell* 2009, 138, 1019-1031.
15. F. M. Rausa, 3rd, D. E. Hughes and R. H. Costa. Stability of the hepatocyte nuclear factor 6 transcription factor requires acetylation by the CREB-binding protein coactivator. *J. Biol. Chem.* 2004, 279, 43070-43076.
16. V. Giandomenico, M. Simonsson, E. Gronroos and J. Ericsson. Coactivator-Dependent Acetylation Stabilizes Members of the SREBP Family of Transcription Factors. *Mol. Cell. Biol.* 2003, 23, 2587-2599.
17. I. V. Gregoret, Y. M. Lee and H. V. Goodson. Molecular evolution of the histone deacetylase family: functional implications of phylogenetic analysis. *J. Mol. Biol.* 2004, 338, 17-31.
18. M. New, H. Olzscha and N. B. La Thangue. HDAC inhibitor-based therapies: can we interpret the code? *Mol. Oncol.* 2012, 6, 637-656.
19. M. Haberland, R. L. Montgomery and E. N. Olson. The many roles of histone deacetylases in development and physiology: implications for disease and therapy. *Nat. Rev. Genet.* 2009, 10, 32-42.
20. X. J. Yang and E. Seto. The Rpd3/Hda1 family of lysine deacetylases: from bacteria and yeast to mice and men. *Nat. Rev. Cell. Biol.* 2008, 9, 206-218.
21. M. Martin, R. Kettmann and F. Dequiedt. Class IIa histone deacetylases: regulating the regulators. *Oncogene* 2007, 26, 5450-5467.
22. C. Hubbert, A. Guardiola, R. Shao, Y. Kawaguchi, A. Ito, A. Nixon, M. Yoshida, X. F. Wang and T. P. Yao. HDAC6 is a microtubule-associated deacetylase. *Nature* 2002, 417, 455-458.
23. Y. Miyake, J. J. Keusch, L. Wang, M. Saito, D. Hess, X. Wang, B. J. Melancon, P. Helquist, H. Gut and P. Matthias. Structural insights into HDAC6 tubulin deacetylation and its selective inhibition. *Nat. Chem. Biol.* 2016, 12, 748-754.
24. H. Y. Kao, C. H. Lee, A. Komarov, C. C. Han and R. M. Evans. Isolation and characterization of mammalian HDAC10, a novel histone deacetylase. *J. Biol. Chem.* 2002, 277, 187-193.
25. A. R. Guardiola and T. P. Yao. Molecular cloning and characterization of a novel histone deacetylase HDAC10. *J. Biol. Chem.* 2002, 277, 3350-3356.
26. L. Gao, M. A. Cueto, F. Asselbergs and P. Atadja. Cloning and functional characterization of HDAC11, a novel member of the human histone deacetylase family. *J. Biol. Chem.* 2002, 277, 25748-25755.

-
27. A. Villagra, F. Cheng, H. W. Wang, I. Suarez, M. Glozak, M. Maurin, D. Nguyen, K. L. Wright, P. W. Atadja, K. Bhalla, J. Pinilla-Ibarz, E. Seto and E. M. Sotomayor. The histone deacetylase HDAC11 regulates the expression of interleukin 10 and immune tolerance. *Nat. Immunol.* 2009, 10, 92-100.
 28. X. J. Yang and E. Seto. HATs and HDACs: from structure, function and regulation to novel strategies for therapy and prevention. *Oncogene* 2007, 26, 5310-5318.
 29. M. D. Shahbazian and M. Grunstein. Functions of site-specific histone acetylation and deacetylation. *Annu. Rev. Biochem.* 2007, 76, 75-100.
 30. T. Heinzl, R. M. Lavinsky, T. M. Mullen, M. Soderstrom, C. D. Laherty, J. Torchia, W. M. Yang, G. Brard, S. D. Ngo, J. R. Davie, E. Seto, R. N. Eisenman, D. W. Rose, C. K. Glass and M. G. Rosenfeld. A complex containing N-CoR, mSin3 and histone deacetylase mediates transcriptional repression. *Nature* 1997, 387, 43-48.
 31. J. L. MacDonald and A. J. Roskams. Histone deacetylases 1 and 2 are expressed at distinct stages of neuro-glial development. *Dev. Dyn.* 2008, 237, 2256-2267.
 32. M. Bantscheff, C. Hopf, M. M. Savitski, A. Dittmann, P. Grandi, A. M. Michon, J. Schlegl, Y. Abraham, I. Becher, G. Bergamini, M. Boesche, M. Delling, B. Dumpelfeld, D. Eberhard, C. Huthmacher, T. Mathieson, D. PoECKel, V. Reader, K. Strunk, G. Sweetman, U. Kruse, G. Neubauer, N. G. Ramsden and G. Drewes. Chemoproteomics profiling of HDAC inhibitors reveals selective targeting of HDAC complexes. *Nat Biotechnol* 2011, 29, 255-265.
 33. S. A. Denslow and P. A. Wade. The human Mi-2/NuRD complex and gene regulation. *Oncogene* 2007, 26, 5433-5438.
 34. J. Zhang, M. Kalkum, B. T. Chait and R. G. Roeder. The N-CoR-HDAC3 Nuclear Receptor Corepressor Complex Inhibits the JNK Pathway through the Integral Subunit GPS2. *Molecular Cell* 2002, 9, 611-623.
 35. P. Karagianni and J. Wong. HDAC3: taking the SMRT-N-CoR road to repression. *Oncogene* 2007, 26, 5439-5449.
 36. W. Fischle, F. Dequiedt, M. J. Hendzel, M. G. Guenther, M. A. Lazar, W. Voelter and E. Verdin. Enzymatic activity associated with class II HDACs is dependent on a multiprotein complex containing HDAC3 and SMRT/N-CoR. *Mol. Cell.* 2002, 9, 45-57.
 37. I. Nusinzon and C. M. Horvath. Histone deacetylases as transcriptional activators? Role reversal in inducible gene regulation. *Sci STKE* 2005, 2005, re11.
 38. C. Choudhary, C. Kumar, F. Gnad, M. L. Nielsen, M. Rehman, T. C. Walther, J. V. Olsen and M. Mann. Lysine acetylation targets protein complexes and co-regulates major cellular functions. *Science* 2009, 325, 834-840.
 39. W. Gu and R. G. Roeder. Activation of p53 sequence-specific DNA binding by acetylation of the p53 C-terminal domain. *Cell* 1997, 90, 595-606.
 40. L. J. Juan, W. J. Shia, M. H. Chen, W. M. Yang, E. Seto, Y. S. Lin and C. W. Wu. Histone deacetylases specifically down-regulate p53-dependent gene activation. *J. Biol. Chem.* 2000, 275, 20436-20443.
 41. A. Tomita, M. Towatari, S. Tsuzuki, F. Hayakawa, H. Kosugi, K. Tamai, T. Miyazaki, T. Kinoshita and H. Saito. c-Myb acetylation at the carboxyl-terminal conserved domain by transcriptional co-activator p300. *Oncogene* 2000, 19, 444-451.
 42. O. Witt, H. E. Deubzer, T. Milde and I. Oehme. HDAC family: What are the cancer relevant targets? *Cancer Lett.* 2009, 277, 8-21.
 43. W. Krek, G. Xu and D. M. Livingston. Cyclin A-kinase regulation of E2F-1 DNA binding function underlies suppression of an S phase checkpoint. *Cell* 1995, 83, 1149-1158.
 44. J. J. Kovacs, P. J. Murphy, S. Gaillard, X. Zhao, J. T. Wu, C. V. Nicchitta, M. Yoshida, D. O. Toft, W. B. Pratt and T. P. Yao. HDAC6 regulates Hsp90 acetylation and chaperone-dependent activation of glucocorticoid receptor. *Mol. Cell.* 2005, 18, 601-607.
 45. X. Zhang, Z. Yuan, Y. Zhang, S. Yong, A. Salas-Burgos, J. Koomen, N. Olashaw, J. T. Parsons, X. J. Yang, S. R. Dent, T. P. Yao, W. S. Lane and E. Seto. HDAC6 modulates cell motility by altering the acetylation level of cortactin. *Mol. Cell.* 2007, 27, 197-213.
 46. A. D. Tran, T. P. Marmo, A. A. Salam, S. Che, E. Finkelstein, R. Kabarriti, H. S. Xenias, R. Mazitschek, C. Hubbert, Y. Kawaguchi, M. P. Sheetz, T. P. Yao and J. C. Bulinski. HDAC6 deacetylation of tubulin modulates dynamics of cellular adhesions. *J. Cell. Sci.* 2007, 120, 1469-1479.

-
47. B. T. Scroggins, K. Robzyk, D. Wang, M. G. Marcu, S. Tsutsumi, K. Beebe, R. J. Cotter, S. Felts, D. Toft, L. Karnitz, N. Rosen and L. Neckers. An acetylation site in the middle domain of Hsp90 regulates chaperone function. *Mol. Cell.* 2007, 25, 151-159.
 48. Y. Zhang, N. Li, C. Caron, G. Matthias, D. Hess, S. Khochbin and P. Matthias. HDAC-6 interacts with and deacetylates tubulin and microtubules in vivo. *EMBO J.* 2003, 22, 1168-1179.
 49. S. J. Haggarty, K. M. Koeller, J. C. Wong, C. M. Grozinger and S. L. Schreiber. Domain-selective small-molecule inhibitor of histone deacetylase 6 (HDAC6)-mediated tubulin deacetylation. *Proc. Natl. Acad. Sci. U. S. A.* 2003, 100, 4389-4394.
 50. M. Schapira. Structural biology of human metal-dependent histone deacetylases. 2011.
 51. A. Lahm, C. Paolini, M. Pallaoro, M. C. Nardi, P. Jones, P. Neddermann, S. Sambucini, M. J. Bottomley, P. Lo Surdo, A. Carfi, U. Koch, R. De Francesco, C. Steinkuhler and P. Gallinari. Unraveling the hidden catalytic activity of vertebrate class IIa histone deacetylases. *Proc. Natl. Acad. Sci. U. S. A.* 2007, 104, 17335-17340.
 52. P. Marks, R. A. Rifkind, V. M. Richon, R. Breslow, T. Miller and W. K. Kelly. Histone deacetylases and cancer: causes and therapies. *Nat Rev Cancer* 2001, 1, 194-202.
 53. A. Villar-Garea and M. Esteller. Histone deacetylase inhibitors: understanding a new wave of anticancer agents. *Int. J. Cancer.* 2004, 112, 171-178.
 54. C. Micelli and G. Rastelli. Histone deacetylases: structural determinants of inhibitor selectivity. *Drug. Discov. Today* 2015, 20, 718-735.
 55. F. F. Wagner, D. E. Olson, J. P. Gale, T. Kaya, M. Weiwer, N. Aidoud, M. Thomas, E. L. Davoine, B. C. Lemercier, Y. L. Zhang and E. B. Holson. Potent and selective inhibition of histone deacetylase 6 (HDAC6) does not require a surface-binding motif. *J. Med. Chem.* 2013, 56, 1772-1776.
 56. X. Ma, H. H. Ezzeldin and R. B. Diasio. Histone deacetylase inhibitors: current status and overview of recent clinical trials. *Drugs* 2009, 69, 1911-1934.
 57. J. M. Mariadason, G. A. Corner and L. H. Augenlicht. Genetic reprogramming in pathways of colonic cell maturation induced by short chain fatty acids: comparison with trichostatin A, sulindac, and curcumin and implications for chemoprevention of colon cancer. *Cancer Res* 2000, 60, 4561-4572.
 58. P. A. Marks, V. M. Richon and R. A. Rifkind. Histone deacetylase inhibitors: inducers of differentiation or apoptosis of transformed cells. *J Natl Cancer Inst* 2000, 92, 1210-1216.
 59. J. E. Bolden, M. J. Peart and R. W. Johnstone. Anticancer activities of histone deacetylase inhibitors. *Nat. Rev. Drug. Discov.* 2006, 5, 769-784.
 60. A. Nebbioso, N. Clarke, E. Voltz, E. Germain, C. Ambrosino, P. Bontempo, R. Alvarez, E. M. Schiavone, F. Ferrara, F. Bresciani, A. Weisz, A. R. de Lera, H. Gronemeyer and L. Altucci. Tumor-selective action of HDAC inhibitors involves TRAIL induction in acute myeloid leukemia cells. *Nat. Med.* 2005, 11, 77-84.
 61. R. R. Rosato, J. A. Almenara, Y. Dai and S. Grant. Simultaneous activation of the intrinsic and extrinsic pathways by histone deacetylase (HDAC) inhibitors and tumor necrosis factor-related apoptosis-inducing ligand (TRAIL) synergistically induces mitochondrial damage and apoptosis in human leukemia cells. *Mol Cancer Ther* 2003, 2, 1273-1284.
 62. R. W. Johnstone. Histone-deacetylase inhibitors: novel drugs for the treatment of cancer. *Nat. Rev. Drug. Discov.* 2002, 1, 287-299.
 63. R. R. Rosato and S. Grant. Histone deacetylase inhibitors in cancer therapy. *Cancer Biol. Ther.* 2003, 2, 30-37.
 64. A. Vannini, C. Volpari, G. Filocamo, E. C. Casavola, M. Brunetti, D. Renzoni, P. Chakravarty, C. Paolini, R. De Francesco, P. Gallinari, C. Steinkuhler and S. Di Marco. Crystal structure of a eukaryotic zinc-dependent histone deacetylase, human HDAC8, complexed with a hydroxamic acid inhibitor. *Proc. Natl. Acad. Sci. U. S. A.* 2004, 101, 15064-15069.
 65. J. S. Ungerstedt, Y. Sowa, W. S. Xu, Y. Shao, M. Dokmanovic, G. Perez, L. Ngo, A. Holmgren, X. Jiang and P. A. Marks. Role of thioredoxin in the response of normal and transformed cells to histone deacetylase inhibitors. *Proc. Natl. Acad. Sci. U. S. A.* 2005, 102, 673-678.
 66. V. M. Richon, T. W. Sandhoff, R. A. Rifkind and P. A. Marks. Histone deacetylase inhibitor selectively induces p21WAF1 expression and gene-associated histone acetylation. *Proc. Natl. Acad. Sci. U. S. A.* 2000, 97, 10014-10019.

-
67. V. Sandor, A. Senderowicz, S. Mertins, D. Sackett, E. Sausville, M. V. Blagosklonny and S. E. Bates. P21-dependent G1 arrest with downregulation of cyclin D1 and upregulation of cyclin E by the histone deacetylase inhibitor FR901228. *Br. J. Cancer* 2000, 83, 817-825.
 68. A. Leder and P. Leder. Butyric acid, a potent inducer of erythroid differentiation in cultured erythroleukemic cells. *Cell* 1975, 5, 319-322.
 69. V. M. Richon, S. Emiliani, E. Verdin, Y. Webb, R. Breslow, R. A. Rifkind and P. A. Marks. A class of hybrid polar inducers of transformed cell differentiation inhibits histone deacetylases. *Proc. Natl. Acad. Sci. U. S. A.* 1998, 95, 3003-3007.
 70. G. Zupkovitz, J. Tischler, M. Posch, I. Sadzak, K. Ramsauer, G. Egger, R. Grausenburger, N. Schweifer, S. Chiocca, T. Decker and C. Seiser. Negative and positive regulation of gene expression by mouse histone deacetylase 1. *Mol. Cell. Biol.* 2006, 26, 7913-7928.
 71. L. Rossig, H. Li, B. Fisslthaler, C. Urbich, I. Fleming, U. Forstermann, A. M. Zeiher and S. Dimmeler. Inhibitors of histone deacetylation downregulate the expression of endothelial nitric oxide synthase and compromise endothelial cell function in vasorelaxation and angiogenesis. *Circ. Res.* 2002, 91, 837-844.
 72. M. Michaelis, U. R. Michaelis, I. Fleming, T. Suhan, J. Cinatl, R. A. Blaheta, K. Hoffmann, R. Kotchetkov, R. Busse, H. Nau and J. Cinatl, Jr. Valproic acid inhibits angiogenesis in vitro and in vivo. *Mol. Pharmacol.* 2004, 65, 520-527.
 73. J. Joseph, G. Mudduluru, S. Antony, S. Vashistha, P. Ajitkumar and K. Somasundaram. Expression profiling of sodium butyrate (NaB)-treated cells: identification of regulation of genes related to cytokine signaling and cancer metastasis by NaB. *Oncogene* 2004, 23, 6304-6315.
 74. J. Mazieres, D. Tovar, B. He, J. Nieto-Acosta, C. Marty-Detraves, C. Clanet, A. Pradines, D. Jablons and G. Favre. Epigenetic regulation of RhoB loss of expression in lung cancer. *BMC Cancer* 2007, 7, 220.
 75. M. Dickinson, R. W. Johnstone and H. M. Prince. Histone deacetylase inhibitors: potential targets responsible for their anti-cancer effect. *Invest New Drugs* 2010, 28 Suppl 1, S3-20.
 76. H. Ozdag, A. E. Teschendorff, A. A. Ahmed, S. J. Hyland, C. Blenkins, L. Bobrow, A. Veerakumarasivam, G. Burt, T. Subkhankulova, M. J. Arends, V. P. Collins, D. Bowtell, T. Kouzarides, J. D. Brenton and C. Caldas. Differential expression of selected histone modifier genes in human solid cancers. *BMC Genomics* 2006, 7, 90.
 77. G. Eot-Houllier, G. Fulcrand, L. Magnaghi-Jaulin and C. Jaulin. Histone deacetylase inhibitors and genomic instability. *Cancer Lett* 2009, 274, 169-176.
 78. W. Weichert. HDAC expression and clinical prognosis in human malignancies. *Cancer Lett* 2009, 280, 168-176.
 79. Z. Zhang, H. Yamashita, T. Toyama, H. Sugiura, Y. Omoto, Y. Ando, K. Mita, M. Hamaguchi, S. Hayashi and H. Iwase. HDAC6 expression is correlated with better survival in breast cancer. *Clin. Cancer. Res.* 2004, 10, 6962-6968.
 80. L. Pasqualucci, D. Dominguez-Sola, A. Chiarenza, G. Fabbri, A. Grunn, V. Trifonov, L. H. Kasper, S. Lerach, H. Tang, J. Ma, D. Rossi, A. Chadburn, V. V. Murty, C. G. Mullighan, G. Gaidano, R. Rabadan, P. K. Brindle and R. Dalla-Favera. Inactivating mutations of acetyltransferase genes in B-cell lymphoma. *Nature*, 2011, 471, 189-195.
 81. N. Cancer Genome Atlas Research. Comprehensive molecular characterization of urothelial bladder carcinoma. *Nature* 2014, 507, 315-322.
 82. S. Spiegel, S. Milstien and S. Grant. Endogenous modulators and pharmacological inhibitors of histone deacetylases in cancer therapy. *Oncogene* 2012, 31, 537-551.
 83. L. M. Butler, D. B. Agus, H. I. Scher, B. Higgins, A. Rose, C. Cordon-Cardo, H. T. Thaler, R. A. Rifkind, P. A. Marks and V. M. Richon. Suberoylanilide hydroxamic acid, an inhibitor of histone deacetylase, suppresses the growth of prostate cancer cells in vitro and in vivo. *Cancer. Res.* 2000, 60, 5165-5170.
 84. I. B. Weinstein. Cancer. Addiction to oncogenes--the Achilles heel of cancer. *Science* 2002, 297, 63-64.
 85. A. Insinga, S. Monestiroli, S. Ronzoni, V. Gelmetti, F. Marchesi, A. Viale, L. Altucci, C. Nervi, S. Minucci and P. G. Pelicci. Inhibitors of histone deacetylases induce tumor-selective apoptosis through activation of the death receptor pathway. *Nat. Med.* 2005, 11, 71-76.

-
86. A. Burgess, A. Ruefli, H. Beamish, R. Warrener, N. Saunders, R. Johnstone and B. Gabrielli. Histone deacetylase inhibitors specifically kill nonproliferating tumour cells. *Oncogene* 2004, 23, 6693-6701.
 87. S. Grant, C. Easley and P. Kirkpatrick. Vorinostat. *Nat. Rev. Drug. Discov.* 2007, 6, 21-22.
 88. P. Reimer. New developments in the treatment of peripheral T-cell lymphoma - role of Belinostat. *Cancer Manag. Res.* 2015, 7, 145-151.
 89. V. Sandor, S. Bakke, R. W. Robey, M. H. Kang, M. V. Blagosklonny, J. Bender, R. Brooks, R. L. Piekarz, E. Tucker, W. D. Figg, K. K. Chan, B. Goldspiel, A. T. Fojo, S. P. Balcerzak and S. E. Bates. Phase I trial of the histone deacetylase inhibitor, depsipeptide (FR901228, NSC 630176), in patients with refractory neoplasms. *Clin. Cancer Res.* 2002, 8, 718-728.
 90. L. Liu, B. Chen, S. Qin, S. Li, X. He, S. Qiu, W. Zhao and H. Zhao. A novel histone deacetylase inhibitor Chidamide induces apoptosis of human colon cancer cells. *Biochem. Biophys. Res. Commun.* 2010, 392, 190-195.
 91. Y. Shi, M. Dong, X. Hong, W. Zhang, J. Feng, J. Zhu, L. Yu, X. Ke, H. Huang, Z. Shen, Y. Fan, W. Li, X. Zhao, J. Qi, H. Huang, D. Zhou, Z. Ning and X. Lu. Results from a multicenter, open-label, pivotal phase II study of chidamide in relapsed or refractory peripheral T-cell lymphoma. *Ann. Oncol.* 2015, 26, 1766-1771.
 92. H. M. Prince, M. J. Bishton and R. W. Johnstone. Panobinostat (LBH589): a potent pan-deacetylase inhibitor with promising activity against hematologic and solid tumors. *Future Oncol.* 2009, 5, 601-612.
 93. M. Bots and R. W. Johnstone. Rational combinations using HDAC inhibitors. *Clin. Cancer. Res.* 2009, 15, 3970-3977.
 94. L. Ding, L. Qiu, J. Zhang and B. Guo. Camptothecin-induced cell proliferation inhibition and apoptosis enhanced by DNA methyltransferase inhibitor, 5-aza-2'-deoxycytidine. *Biol. Pharm. Bull.* 2009, 32, 1105-1108.
 95. A. Merlo, J. G. Herman, L. Mao, D. J. Lee, E. Gabrielson, P. C. Burger, S. B. Baylin and D. Sidransky. 5' CpG island methylation is associated with transcriptional silencing of the tumour suppressor p16/CDKN2/MTS1 in human cancers. *Nat. Med.* 1995, 1, 686-692.
 96. G. Deng, A. Chen, J. Hong, H. S. Chae and Y. S. Kim. Methylation of CpG in a small region of the hMLH1 promoter invariably correlates with the absence of gene expression. *Cancer. Res.* 1999, 59, 2029-2033.
 97. E. A. Griffiths and S. D. Gore. DNA methyltransferase and histone deacetylase inhibitors in the treatment of myelodysplastic syndromes. *Semin. Hematol.* 2008, 45, 23-30.
 98. C. P. Miller, M. M. Singh, N. Rivera-Del Valle, C. A. Manton and J. Chandra. Therapeutic strategies to enhance the anticancer efficacy of histone deacetylase inhibitors. *J. Biomed. Biotechnol.* 2011, 2011, 514261.
 99. X. Y. Pei, Y. Dai and S. Grant. Synergistic induction of oxidative injury and apoptosis in human multiple myeloma cells by the proteasome inhibitor bortezomib and histone deacetylase inhibitors. *Clin. Cancer. Res.* 2004, 10, 3839-3852.
 100. J. P. Laubach, P. Moreau, J. F. San-Miguel and P. G. Richardson. Panobinostat for the Treatment of Multiple Myeloma. *Clin. Cancer. Res.* 2015, 21, 4767-4773.
 101. P. G. Richardson, R. D. Harvey, J. P. Laubach, P. Moreau, S. Lonial and J. F. San-Miguel. Panobinostat for the treatment of relapsed or relapsed/refractory multiple myeloma: pharmacology and clinical outcomes. *Expert Rev Clin Pharmacol* 2016, 9, 35-48.
 102. K. P. Garnock-Jones. Panobinostat: first global approval. *Drugs* 2015, 75, 695-704.
 103. A. Badros, A. M. Burger, S. Philip, R. Niesvizky, S. S. Kolla, O. Goloubeva, C. Harris, J. Zwiebel, J. Wright, I. Espinoza-Delgado, M. R. Baer, J. L. Holleran, M. J. Egorin and S. Grant. Phase I study of vorinostat in combination with bortezomib for relapsed and refractory multiple myeloma. *Clin. Cancer. Res.* 2009, 15, 5250-5257.
 104. A. Mazumder, D. H. Vesole and S. Jagannath. Vorinostat plus bortezomib for the treatment of relapsed/refractory multiple myeloma: a case series illustrating utility in clinical practice. *Clin. Lymphoma. Myeloma. Leuk.* 2010, 10, 149-151.
 105. T. Hideshima, J. E. Bradner, J. Wong, D. Chauhan, P. Richardson, S. L. Schreiber and K. C. Anderson. Small-molecule inhibition of proteasome and aggresome function induces synergistic antitumor activity in multiple myeloma. *Proc. Natl. Acad. Sci. U. S. A.* 2005, 102, 8567-8572.

-
106. T. Hideshima, R. Mazitschek, L. Santo, N. Mimura, G. Gorgun, P. G. Richardson, N. Raje and K. C. Anderson. Induction of differential apoptotic pathways in multiple myeloma cells by class-selective histone deacetylase inhibitors. *Leukemia* 2014, 28, 457-460.
107. M. P. Fenichel, FDA approves new agent for multiple myeloma, *J. Natl. Cancer. Inst.*, 2015, 107, djv165.
108. K. T. Thurn, S. Thomas, A. Moore and P. N. Munster. Rational therapeutic combinations with histone deacetylase inhibitors for the treatment of cancer. *Future Oncol.* 2011, 7, 263-283.
109. L. Marek, A. Hamacher, F. K. Hansen, K. Kuna, H. Gohlke, M. U. Kassack and T. Kurz. Histone deacetylase (HDAC) inhibitors with a novel connecting unit linker region reveal a selectivity profile for HDAC4 and HDAC5 with improved activity against chemoresistant cancer cells. *J. Med. Chem.* 2013, 56, 427-436.
110. M. Stiborova, T. Eckschlager, J. Poljakova, J. Hrabeta, V. Adam, R. Kizek and E. Frei. The synergistic effects of DNA-targeted chemotherapeutics and histone deacetylase inhibitors as therapeutic strategies for cancer treatment. *Curr. Med. Chem.* 2012, 19, 4218-4238.
111. P. S. Ong, X. Q. Wang, H. S. Lin, S. Y. Chan and P. C. Ho. Synergistic effects of suberoylanilide hydroxamic acid combined with cisplatin causing cell cycle arrest independent apoptosis in platinum-resistant ovarian cancer cells. *Int. J. Oncol.* 2012, 40, 1705-1713.
112. S. S. Ramalingam, M. L. Maitland, P. Frankel, A. E. Argiris, M. Koczywas, B. Gitlitz, S. Thomas, I. Espinoza-Delgado, E. E. Vokes, D. R. Gandara and C. P. Belani. Carboplatin and Paclitaxel in combination with either vorinostat or placebo for first-line therapy of advanced non-small-cell lung cancer. *J. Clin. Oncol.* 2010, 28, 56-62.
113. J. Shen, C. Huang, L. Jiang, F. Gao, Z. Wang, Y. Zhang, J. Bai, H. Zhou and Q. Chen. Enhancement of cisplatin induced apoptosis by suberoylanilide hydroxamic acid in human oral squamous cell carcinoma cell lines. *Biochem. Pharmacol.* 2007, 73, 1901-1909.
114. M. Suzuki, M. Endo, F. Shinohara, S. Echigo and H. Rikiishi. Enhancement of cisplatin cytotoxicity by SAHA involves endoplasmic reticulum stress-mediated apoptosis in oral squamous cell carcinoma cells. *Cancer Chemother. Pharmacol.* 2009, 64, 1115-1122.
115. M. S. Kim, M. Blake, J. H. Baek, G. Kohlhagen, Y. Pommier and F. Carrier. Inhibition of histone deacetylase increases cytotoxicity to anticancer drugs targeting DNA. *Cancer Res.* 2003, 63, 7291-7300.
116. Y. Zhang, M. Adachi, R. Kawamura, H. C. Zou, K. Imai, M. Hareyama and Y. Shinomura. Bmf contributes to histone deacetylase inhibitor-mediated enhancing effects on apoptosis after ionizing radiation. *Apoptosis* 2006, 11, 1349-1357.
117. Y. Zhang, M. Adachi, X. Zhao, R. Kawamura and K. Imai. Histone deacetylase inhibitors FK228, N-(2-aminophenyl)-4-[N-(pyridin-3-yl-methoxycarbonyl)amino- methyl]benzamide and m-carboxycinnamic acid bis-hydroxamide augment radiation-induced cell death in gastrointestinal adenocarcinoma cells. *Int. J. Cancer.* 2004, 110, 301-308.
118. K. P. Kim, S. J. Park, J. E. Kim, Y. S. Hong, J. L. Lee, K. S. Bae, H. Cha, S. K. Kwon, S. Ro, J. Cho and T. W. Kim. First-in-human study of the toxicity, pharmacokinetics, and pharmacodynamics of CG200745, a pan-HDAC inhibitor, in patients with refractory solid malignancies. *Invest. New. Drugs.* 2015, 33, 1048-1057.
119. S. A. Ganai. Novel Approaches Towards Designing of Isoform-Selective Inhibitors Against Class II Histone Deacetylases: The Acute Requirement for Targetted Anticancer Therapy. *Curr. Top. Med. Chem.* 2016, 16, 2441-2452.
120. Y. Minamiya, T. Ono, H. Saito, N. Takahashi, M. Ito, M. Mitsui, S. Motoyama and J. Ogawa. Expression of histone deacetylase 1 correlates with a poor prognosis in patients with adenocarcinoma of the lung. *Lung. Cancer.* 2011, 74, 300-304.
121. Z. Zhang, H. Yamashita, T. Toyama, H. Sugiura, Y. Ando, K. Mita, M. Hamaguchi, Y. Hara, S. Kobayashi and H. Iwase. Quantitation of HDAC1 mRNA expression in invasive carcinoma of the breast. *Breast Cancer Res. Treat.* 2005, 94, 11-16.
122. H. Adams, F. R. Fritzsche, S. Dirnhofer, G. Kristiansen and A. Tzankov. Class I histone deacetylases 1, 2 and 3 are highly expressed in classical Hodgkin's lymphoma. *Expert. Opin. Ther. Targets.* 2010, 14, 577-584.
123. F. R. Fritzsche, W. Weichert, A. Roske, V. Gekeler, T. Beckers, C. Stephan, K. Jung, K. Scholman, C. Denkert, M. Dietel and G. Kristiansen. Class I histone deacetylases 1, 2 and 3 are highly expressed in renal cell cancer. *BMC Cancer* 2008, 8, 381.

-
124. C. A. Krusche, P. Wulfig, C. Kersting, A. Vloet, W. Bocker, L. Kiesel, H. M. Beier and J. Alfer. Histone deacetylase-1 and -3 protein expression in human breast cancer: a tissue microarray analysis. *Breast Cancer Res. Treat.* 2005, 90, 15-23.
125. Y. Zhang, S. Kwon, T. Yamaguchi, F. Cubizolles, S. Rousseaux, M. Kneissel, C. Cao, N. Li, H. L. Cheng, K. Chua, D. Lombard, A. Mizeracki, G. Matthias, F. W. Alt, S. Khochbin and P. Matthias. Mice lacking histone deacetylase 6 have hyperacetylated tubulin but are viable and develop normally. *Mol. Cell Biol.* 2008, 28, 1688-1701.
126. D. Seigneurin-Berny, A. Verdel, S. Curtet, C. Lemerrier, J. Garin, S. Rousseaux and S. Khochbin. Identification of components of the murine histone deacetylase 6 complex: link between acetylation and ubiquitination signaling pathways. *Mol. Cell Biol.* 2001, 21, 8035-8044.
127. A. Rodriguez-Gonzalez, T. Lin, A. K. Ikeda, T. Simms-Waldrup, C. Fu and K. M. Sakamoto. Role of the aggresome pathway in cancer: targeting histone deacetylase 6-dependent protein degradation. *Cancer Res.* 2008, 68, 2557-2560.
128. C. Boyault, Y. Zhang, S. Fritah, C. Caron, B. Gilquin, S. H. Kwon, C. Garrido, T. P. Yao, C. Vourc'h, P. Matthias and S. Khochbin. HDAC6 controls major cell response pathways to cytotoxic accumulation of protein aggregates. *Genes. Dev.* 2007, 21, 2172-2181.
129. Y. Kawaguchi, J. J. Kovacs, A. McLaurin, J. M. Vance, A. Ito and T. P. Yao. The deacetylase HDAC6 regulates aggresome formation and cell viability in response to misfolded protein stress. *Cell* 2003, 115, 727-738.
130. H. C. Drexler. Activation of the cell death program by inhibition of proteasome function. *Proc. Natl. Acad. Sci. U. S. A.* 1997, 94, 855-860.
131. P. Masdehors, S. Omura, H. Merle-Beral, F. Mentz, J. M. Cosset, J. Dumont, H. Magdelenat and J. Delic. Increased sensitivity of CLL-derived lymphocytes to apoptotic death activation by the proteasome-specific inhibitor lactacystin. *Br. J. Haematol.* 1999, 105, 752-757.
132. J. E. Amengual, P. Johannet, M. Lombardo, K. Zullo, D. Hoehn, G. Bhagat, L. Scotto, X. Jirau-Serrano, D. Radeski, J. Heinen, H. Jiang, S. Cremers, Y. Zhang, S. Jones and O. A. O'Connor. Dual Targeting of Protein Degradation Pathways with the Selective HDAC6 Inhibitor ACY-1215 and Bortezomib Is Synergistic in Lymphoma. *Clin. Cancer Res.* 2015, 21, 4663-4675.
133. D. T. Vogl, N. S. Raje, S. Jagannath, P. G. Richardson, P. Hari, R. Z. Orlowski, J. G. Supko, D. Tamang, M. Yang, S. S. Jones, C. Wheeler, R. J. Markelewicz and S. Lonial. Ricolinostat, the first selective histone deacetylase 6 inhibitor, in combination with bortezomib and dexamethasone for relapsed or refractory multiple myeloma. *Clin. Cancer Res.* 2017, DOI: 10.1158/1078-0432.CCR-16-2526.
134. L. Santo, T. Hideshima, A. L. Kung, J. C. Tseng, D. Tamang, M. Yang, M. Jarpe, J. H. van Duzer, R. Mazitschek, W. C. Ogier, D. Cirstea, S. Rodig, H. Eda, T. Scullen, M. Canavese, J. Bradner, K. C. Anderson, S. S. Jones and N. Raje. Preclinical activity, pharmacodynamic, and pharmacokinetic properties of a selective HDAC6 inhibitor, ACY-1215, in combination with bortezomib in multiple myeloma. *Blood* 2012, 119, 2579-2589.
135. P. Bali, M. Pranpat, J. Bradner, M. Balasis, W. Fiskus, F. Guo, K. Rocha, S. Kumaraswamy, S. Boyapalle, P. Atadja, E. Seto and K. Bhalla. Inhibition of histone deacetylase 6 acetylates and disrupts the chaperone function of heat shock protein 90: a novel basis for antileukemia activity of histone deacetylase inhibitors. *J. Biol. Chem.* 2005, 280, 26729-26734.
136. A. Edwards, J. Li, P. Atadja, K. Bhalla and E. B. Haura. Effect of the histone deacetylase inhibitor LBH589 against epidermal growth factor receptor-dependent human lung cancer cells. *Mol. Cancer Ther.* 2007, 6, 2515-2524.
137. G. I. Aldana-Masangkay and K. M. Sakamoto. The role of HDAC6 in cancer. *J. Biomed. Biotechnol.* 2011, 2011, 875824.
138. Y. S. Lee, K. H. Lim, X. Guo, Y. Kawaguchi, Y. Gao, T. Barrientos, P. Ordentlich, X. F. Wang, C. M. Counter and T. P. Yao. The cytoplasmic deacetylase HDAC6 is required for efficient oncogenic tumorigenesis. *Cancer Res.* 2008, 68, 7561-7569.
139. J. Liu, J. Gu, Z. Feng, Y. Yang, N. Zhu, W. Lu and F. Qi. Both HDAC5 and HDAC6 are required for the proliferation and metastasis of melanoma cells. *J. Transl. Med.* 2016, 14, 7.
140. T. Sakuma, K. Uzawa, T. Onda, M. Shiiba, H. Yokoe, T. Shibahara and H. Tanzawa. Aberrant expression of histone deacetylase 6 in oral squamous cell carcinoma. *Int. J. Oncol.* 2006, 29, 117-124.
141. S. Saji, M. Kawakami, S. Hayashi, N. Yoshida, M. Hirose, S. Horiguchi, A. Itoh, N. Funata, S. L. Schreiber, M. Yoshida and M. Toi. Significance of HDAC6 regulation via estrogen signaling for

-
- cell motility and prognosis in estrogen receptor-positive breast cancer. *Oncogene* 2005, 24, 4531-4539.
142. C. A. Bradbury, F. L. Khanim, R. Hayden, C. M. Bunce, D. A. White, M. T. Drayson, C. Craddock and B. M. Turner. Histone deacetylases in acute myeloid leukaemia show a distinctive pattern of expression that changes selectively in response to deacetylase inhibitors. *Leukemia* 2005, 19, 1751-1759.
143. A. G. Kazantsev and L. M. Thompson. Therapeutic application of histone deacetylase inhibitors for central nervous system disorders. *Nat. Rev. Drug. Discov.* 2008, 7, 854-868.
144. D. M. Chuang, Y. Leng, Z. Marinova, H. J. Kim and C. T. Chiu. Multiple roles of HDAC inhibition in neurodegenerative conditions. *Trends Neurosci.* 2009, 32, 591-601.
145. D. R. Grayson, M. Kundakovic and R. P. Sharma. Is there a future for histone deacetylase inhibitors in the pharmacotherapy of psychiatric disorders? *Mol. Pharmacol.* 2010, 77, 126-135.
146. H. Jia, J. Pallos, V. Jacques, A. Lau, B. Tang, A. Cooper, A. Syed, J. Purcell, Y. Chen, S. Sharma, G. R. Sangrey, S. B. Darnell, H. Plasterer, G. Sadri-Vakili, J. M. Gottesfeld, L. M. Thompson, J. R. Rusche, J. L. Marsh and E. A. Thomas. Histone deacetylase (HDAC) inhibitors targeting HDAC3 and HDAC1 ameliorate polyglutamine-elicited phenotypes in model systems of Huntington's disease. *Neurobiol. Dis.* 2012, 46, 351-361.
147. M. R. Shakespear, M. A. Halili, K. M. Irvine, D. P. Fairlie and M. J. Sweet. Histone deacetylases as regulators of inflammation and immunity. *Trends Immunol.* 2011, 32, 335-343.
148. H. S. Lin, C. Y. Hu, H. Y. Chan, Y. Y. Liew, H. P. Huang, L. Lepescheux, E. Bastianelli, R. Baron, G. Rawadi and P. Clement-Lacroix. Anti-rheumatic activities of histone deacetylase (HDAC) inhibitors in vivo in collagen-induced arthritis in rodents. *Br. J. Pharmacol.* 2007, 150, 862-872.
149. A. M. Grabiec, O. Korchynskiy, P. P. Tak and K. A. Reedquist. Histone deacetylase inhibitors suppress rheumatoid arthritis fibroblast-like synoviocyte and macrophage IL-6 production by accelerating mRNA decay. *Ann. Rheum. Dis.* 2012, 71, 424-431.
150. B. S. Ferguson and T. A. McKinsey. Non-sirtuin histone deacetylases in the control of cardiac aging. *J. Mol. Cell. Cardiol.* 2015, 83, 14-20.
151. S. Chang, T. A. McKinsey, C. L. Zhang, J. A. Richardson, J. A. Hill and E. N. Olson. Histone deacetylases 5 and 9 govern responsiveness of the heart to a subset of stress signals and play redundant roles in heart development. *Mol. Cell. Biol.* 2004, 24, 8467-8476.
152. C. L. Zhang, T. A. McKinsey, S. Chang, C. L. Antos, J. A. Hill and E. N. Olson. Class II histone deacetylases act as signal-responsive repressors of cardiac hypertrophy. *Cell* 2002, 110, 479-488.
153. R. B. Vega, K. Matsuda, J. Oh, A. C. Barbosa, X. Yang, E. Meadows, J. McAnally, C. Pomajzl, J. M. Shelton, J. A. Richardson, G. Karsenty and E. N. Olson. Histone deacetylase 4 controls chondrocyte hypertrophy during skeletogenesis. *Cell* 2004, 119, 555-566.
154. R. L. Montgomery, C. A. Davis, M. J. Potthoff, M. Haberland, J. Fielitz, X. Qi, J. A. Hill, J. A. Richardson and E. N. Olson. Histone deacetylases 1 and 2 redundantly regulate cardiac morphogenesis, growth, and contractility. *Genes. Dev.* 2007, 21, 1790-1802.
155. D. Ritchie, R. L. Piekarz, P. Blombery, L. J. Karai, S. Pittaluga, E. S. Jaffe, M. Raffeld, J. E. Janik, H. M. Prince and S. E. Bates. Reactivation of DNA viruses in association with histone deacetylase inhibitor therapy: a case series report. *Haematologica* 2009, 94, 1618-1622.
156. D. M. Margolis. Histone deacetylase inhibitors and HIV latency. *Curr. Opin. HIV AIDS* 2011, 6, 25-29.
157. N. M. Archin, A. L. Liberty, A. D. Kashuba, S. K. Choudhary, J. D. Kuruc, A. M. Crooks, D. C. Parker, E. M. Anderson, M. F. Kearney, M. C. Strain, D. D. Richman, M. G. Hudgens, R. J. Bosch, J. M. Coffin, J. J. Eron, D. J. Hazuda and D. M. Margolis. Administration of vorinostat disrupts HIV-1 latency in patients on antiretroviral therapy. *Nature* 2012, 487, 482-485.
158. J. A. Engel, A. J. Jones, V. M. Avery, S. D. Sumanadasa, S. S. Ng, D. P. Fairlie, T. S. Adams and K. T. Andrews. Profiling the anti-protozoal activity of anti-cancer HDAC inhibitors against Plasmodium and Trypanosoma parasites. *Int. J. Parasitol. Drugs. Drug. Resist.* 2015, 5, 117-126.
159. S. J. Darkin-Rattray, A. M. Gurnett, R. W. Myers, P. M. Dulski, T. M. Crumley, J. J. Allocco, C. Cannova, P. T. Meinke, S. L. Colletti, M. A. Bednarek, S. B. Singh, M. A. Goetz, A. W.

-
- Dombrowski, J. D. Polishook and D. M. Schmatz. Apicidin: a novel antiprotozoal agent that inhibits parasite histone deacetylase. *Proc. Natl. Acad. Sci. U. S. A.* 1996, 93, 13143-13147.
160. S. R. Choi, A. Pradhan, N. L. Hammond, A. G. Chittiboyina, B. L. Tekwani and M. A. Avery. Design, synthesis, and biological evaluation of Plasmodium falciparum lactate dehydrogenase inhibitors. *J. Med. Chem.* 2007, 50, 3841-3850.
161. F. Hirschhaeuser, U. G. Sattler and W. Mueller-Klieser. Lactate: a metabolic key player in cancer. *Cancer Res* 2011, 71, 6921-6925.
162. W. G. Kaelin, Jr. and S. L. McKnight. Influence of metabolism on epigenetics and disease. *Cell* 2013, 153, 56-69.
163. U. E. Martinez-Outschoorn, R. G. Pestell, A. Howell, M. L. Tykocinski, F. Nagajyothi, F. S. Machado, H. B. Tanowitz, F. Sotgia and M. P. Lisanti. Energy transfer in "parasitic" cancer metabolism: mitochondria are the powerhouse and Achilles' heel of tumor cells. *Cell Cycle* 2011, 10, 4208-4216.
164. A. Loukas, M. K. Jones, L. T. King, P. J. Brindley and D. P. McManus. Receptor for Fc on the surfaces of schistosomes. *Infect. Immun.* 2001, 69, 3646-3651.
165. T. J. Templeton. The varieties of gene amplification, diversification and hypervariability in the human malaria parasite, Plasmodium falciparum. *Mol. Biochem. Parasitol.* 2009, 166, 109-116.
166. C. Kidgell, S. K. Volkman, J. Daily, J. O. Borevitz, D. Plouffe, Y. Zhou, J. R. Johnson, K. Le Roch, O. Sarr, O. Ndir, S. Mboup, S. Batalov, D. F. Wirth and E. A. Winzeler. A systematic map of genetic variation in Plasmodium falciparum. *PLoS Pathog.* 2006, 2, e57.
167. K. T. Andrews, G. Fisher and T. S. Skinner-Adams. Drug repurposing and human parasitic protozoan diseases. *Int. J. Parasitol. Drugs Drug Resist.* 2014, 4, 95-111.
168. S. Nwaka and A. Hudson. Innovative lead discovery strategies for tropical diseases. *Nat. Rev. Drug. Discov.* 2006, 5, 941-955.
169. E. L. Flannery, A. K. Chatterjee and E. A. Winzeler. Antimalarial drug discovery - approaches and progress towards new medicines. *Nat. Rev. Microbiol.* 2013, 11, 849-862.
170. S. D. Sumanadasa, C. D. Goodman, A. J. Lucke, T. Skinner-Adams, I. Sahama, A. Haque, T. A. Do, G. I. McFadden, D. P. Fairlie and K. T. Andrews. Antimalarial activity of the anticancer histone deacetylase inhibitor SB939. *Antimicrob. Agents Chemother.* 2012, 56, 3849-3856.
171. G. S. Dow, Y. Chen, K. T. Andrews, D. Caridha, L. Gerena, M. Gettayacamin, J. Johnson, Q. Li, V. Melendez, N. Obaldia, 3rd, T. N. Tran and A. P. Kozikowski. Antimalarial activity of phenylthiazolyl-bearing hydroxamate-based histone deacetylase inhibitors. *Antimicrob. Agents Chemother.* 2008, 52, 3467-3477.
172. K. T. Andrews, A. Haque and M. K. Jones. HDAC inhibitors in parasitic diseases. *Immunol. Cell Biol.* 2012, 90, 66-77.
173. M. Marek, S. Kannan, A. T. Hauser, M. Moraes Mourao, S. Caby, V. Cura, D. A. Stolfa, K. Schmidtkunz, J. Lancelot, L. Andrade, J. P. Renaud, G. Oliveira, W. Sippl, M. Jung, J. Cavarelli, R. J. Pierce and C. Romier. Structural basis for the inhibition of histone deacetylase 8 (HDAC8), a key epigenetic player in the blood fluke Schistosoma mansoni. *PLoS Pathog.* 2013, 9, e1003645.
174. C. J. Sutherland, N. Tanomsing, D. Nolder, M. Oguike, C. Jennison, S. Pukrittayakamee, C. Dolecek, T. T. Hien, V. E. do Rosario, A. P. Arez, J. Pinto, P. Michon, A. A. Escalante, F. Nosten, M. Burke, R. Lee, M. Blaze, T. D. Otto, J. W. Barnwell, A. Pain, J. Williams, N. J. White, N. P. Day, G. Snounou, P. J. Lockhart, P. L. Chiodini, M. Imwong and S. D. Polley. Two nonrecombining sympatric forms of the human malaria parasite Plasmodium ovale occur globally. *J. Infect. Dis.* 2010, 201, 1544-1550.
175. A. Calderaro, G. Piccolo, C. Gorrini, S. Rossi, S. Montecchini, M. L. Dell'Anna, F. De Conto, M. C. Medici, C. Chezzi and M. C. Arcangeletti. Accurate identification of the six human Plasmodium spp. causing imported malaria, including Plasmodium ovale wallikeri and Plasmodium knowlesi. *Malar. J.* 2013, 12, 321.
176. D. M. Langhi, Jr. and J. O. Bordin. Duffy blood group and malaria. *Hematology* 2006, 11, 389-398.
177. A. V. Hill. Vaccines against malaria. *Philos. Trans. R. Soc. Lond. B. Biol. Sci.* 2011, 366, 2806-2814.
178. L. M. Coronado, C. T. Nadovich and C. Spadafora. Malarial hemozoin: from target to tool. *Biochim. Biophys. Acta.* 2014, 1840, 2032-2041.

-
179. G. A. Josling and M. Llinas. Sexual development in Plasmodium parasites: knowing when it's time to commit. *Nat. Rev. Microbiol.* 2015, 13, 573-587.
180. B. F. Kafsack, N. Rovira-Graells, T. G. Clark, C. Bancells, V. M. Crowley, S. G. Campino, A. E. Williams, L. G. Drought, D. P. Kwiatkowski, D. A. Baker, A. Cortes and M. Llinas. A transcriptional switch underlies commitment to sexual development in malaria parasites. *Nature* 2014, 507, 248-252.
181. WHO, World Malaria Report, 2016. Geneva: World Health Organization.
182. WHO, World Malaria Report, 2015. Geneva: World Health Organization.
183. C. L. Mackintosh, J. G. Beeson and K. Marsh. Clinical features and pathogenesis of severe malaria. *Trends Parasitol.* 2004, 20, 597-603.
184. D. J. Weatherall and J. B. Clegg. Genetic variability in response to infection: malaria and after. *Genes Immun.* 2002, 3, 331-337.
185. N. J. White. Preventing antimalarial drug resistance through combinations. *Drug Resist. Updat.* 1998, 1, 3-9.
186. K. Maitland and K. Marsh. Pathophysiology of severe malaria in children. *Acta. Trop.* 2004, 90, 131-140.
187. R. L. Pullan, H. Bukirwa, S. G. Staedke, R. W. Snow and S. Brooker. Plasmodium infection and its risk factors in eastern Uganda. *Malar. J.* 2010, 9, 2.
188. A. O. Osunkentan and D. Evans. Chronic adverse effects of long-term exposure of children to dichlorodiphenyltrichloroethane (DDT) through indoor residual spraying: A systematic review. *Rural. Remote. Health* 2015, 15, 2889.
189. B. M. Greenwood, K. Bojang, C. J. Whitty and G. A. Targett. Malaria. *Lancet* 2005, 365, 1487-1498.
190. G. Zuccotti and C. D. DeAngelis. Malaria 2007-progressing research, persisting challenges. *JAMA* 2007, 297, 2285-2286.
191. R. G. Feachem and O. J. Sabot. Global malaria control in the 21st century: a historic but fleeting opportunity. *JAMA* 2007, 297, 2281-2284.
192. B. Greenwood. Anti-malarial drugs and the prevention of malaria in the population of malaria endemic areas. *Malar. J.* 2010, 9 Suppl 3, S2.
193. G. Krause, I. Schoneberg, D. Altmann and K. Stark. Chemoprophylaxis and malaria death rates. *Emerg. Infect. Dis.* 2006, 12, 447-451.
194. S. L. Hoffman, J. Vekemans, T. L. Richie and P. E. Duffy. The march toward malaria vaccines. *Vaccine* 2015, 33 Suppl 4, D13-23.
195. A. Opar. Quarter-century quest for malaria vaccine shows signs of success. *Nat. Rev. Drug. Discov.* 2011, 10, 887-888.
196. A. Olotu, G. Fegan, J. Wambua, G. Nyangweso, A. Leach, M. Lievens, D. C. Kaslow, P. Njuguna, K. Marsh and P. Bejon. Seven-Year Efficacy of RTS,S/AS01 Malaria Vaccine among Young African Children. *N. Engl. J. Med.* 2016, 374, 2519-2529.
197. RTS,S Clinical Trials Partnership, Efficacy and safety of RTS,S/AS01 malaria vaccine with or without a booster dose in infants and children in Africa: final results of a phase 3, individually randomised, controlled trial. *The Lancet* 2016, 386, 31-45.
198. B. Mordmuller, G. Surat, H. Lagler, S. Chakravarty, A. S. Ishizuka, A. Lalremruata, M. Gmeiner, J. J. Campo, M. Esen, A. J. Ruben, J. Held, C. L. Calle, J. B. Mengue, T. Gebru, J. Ibanez, M. Sulyok, E. R. James, P. F. Billingsley, K. C. Natasha, A. Manoj, T. Murshedkar, A. Gunasekera, A. G. Eappen, T. Li, R. E. Stafford, M. Li, P. L. Felgner, R. A. Seder, T. L. Richie, B. K. Sim, S. L. Hoffman and P. G. Kremsner. Sterile protection against human malaria by chemoattenuated PfSPZ vaccine. *Nature* 2017, DOI: 10.1038/nature21060.
199. P. H. Schlesinger, D. J. Krogstad and B. L. Herwaldt. Antimalarial agents: mechanisms of action. *Antimicrob. Agents. Chemother.* 1988, 32, 793-798.
200. P. L. Olliaro and Y. Yuthavong, An overview of chemotherapeutic targets for antimalarial drug discovery. *Pharmacol. Ther.* 1999, 81, 91-110.
201. D. A. Fidock, P. J. Rosenthal, S. L. Croft, R. Brun and S. Nwaka. Antimalarial drug discovery: efficacy models for compound screening. *Nat. Rev. Drug. Discov.* 2004, 3, 509-520.
202. T. E. Wellems and C. V. Plowe. Chloroquine-resistant malaria. *J. Infect. Dis.* 2001, 184, 770-776.
203. C. V. Plowe, O. K. Doumbo, A. Djimde, K. Kayentao, Y. Diourte, S. N. Doumbo, D. Coulibaly, M. Thera, T. E. Wellems and D. A. Diallo. Chloroquine treatment of uncomplicated Plasmodium

-
- falciparum malaria in Mali: parasitologic resistance versus therapeutic efficacy. *Am. J. Trop. Med. Hyg.* 2001, 64, 242-246.
204. R. E. Howes, F. B. Piel, A. P. Patil, O. A. Nyangiri, P. W. Gething, M. Dewi, M. M. Hogg, K. E. Battle, C. D. Padilla, J. K. Baird and S. I. Hay. G6PD deficiency prevalence and estimates of affected populations in malaria endemic countries: a geostatistical model-based map. *PLoS Med.* 2012, 9, e1001339.
205. D. C. Warhurst, Antimalarial drugs: mode of action and resistance. *J. Antimicrob. Chemother.* 1986, 18 Suppl B, 51-59.
206. A. Gregson and C. V. Plowe. Mechanisms of resistance of malaria parasites to antifolates, *Pharmacol. Rev.* 2005, 57, 117-145.
207. P. M. O'Neill, V. E. Barton and S. A. Ward. The molecular mechanism of action of artemisinin--the debate continues. *Molecules* 2010, 15, 1705-1721.
208. L. Cui, S. Mharakurwa, D. Ndiaye, P. K. Rathod and P. J. Rosenthal. Antimalarial Drug Resistance: Literature Review and Activities and Findings of the ICEMR Network. *Am. J. Trop. Med. Hyg.* 2015, 93, 57-68.
209. S. Krishna, A. C. Uhlemann and R. K. Haynes. Artemisinins: mechanisms of action and potential for resistance. *Drug Resist. Updat.* 2004, 7, 233-244.
210. D. R. Hill, J. K. Baird, M. E. Parise, L. S. Lewis, E. T. Ryan and A. J. Magill. Primaquine: report from CDC expert meeting on malaria chemoprophylaxis I. *Am. J. Trop. Med. Hyg.* 2006, 75, 402-415.
211. T. E. Wellems and L. H. Miller. Two worlds of malaria. *N. Engl. J. Med.* 2003, 349, 1496-1498.
212. W. Sirawaraporn. Dihydrofolate reductase and antifolate resistance in malaria. *Drug Resist. Updat.* 1998, 1, 397-406.
213. J. E. Hyde. Antifolate resistance in Africa and the 164-dollar question. *Trans. R. Soc. Trop. Med. Hyg.* 2008, 102, 301-303.
214. A. M. McCollum, A. C. Poe, M. Hamel, C. Huber, Z. Zhou, Y. P. Shi, P. Ouma, J. Vulule, P. Bloland, L. Slutsker, J. W. Barnwell, V. Udhayakumar and A. A. Escalante. Antifolate resistance in *Plasmodium falciparum*: multiple origins and identification of novel dhfr alleles. *J. Infect. Dis.* 2006, 194, 189-197.
215. A. Nzila, S. A. Ward, K. Marsh, P. F. Sims and J. E. Hyde. Comparative folate metabolism in humans and malaria parasites (part I): pointers for malaria treatment from cancer chemotherapy. *Trends. Parasitol.* 2005, 21, 292-298.
216. N. Gonen and Y. G. Assaraf. Antifolates in cancer therapy: structure, activity and mechanisms of drug resistance. *Drug Resist. Updat.* 2012, 15, 183-210.
217. P. L. Olliaro, R. K. Haynes, B. Meunier and Y. Yuthavong. Possible modes of action of the artemisinin-type compounds. *Trends. Parasitol.* 2001, 17, 122-126.
218. H. C. Lai, N. P. Singh and T. Sasaki. Development of artemisinin compounds for cancer treatment. *Invest. New. Drugs.* 2013, 31, 230-246.
219. R. T. Eastman and D. A. Fidock. Artemisinin-based combination therapies: a vital tool in efforts to eliminate malaria. *Nat Rev Microbiol* 2009, 7, 864-874.
220. C. Wongsrichanalai and C. H. Sibley. Fighting drug-resistant *Plasmodium falciparum*: the challenge of artemisinin resistance. *Clin Microbiol Infect* 2013, 19, 908-916.
221. S. Mok, M. Imwong, M. J. Mackinnon, J. Sim, R. Ramadoss, P. Yi, M. Mayxay, K. Chotivanich, K. Y. Liong, B. Russell, D. Socheat, P. N. Newton, N. P. Day, N. J. White, P. R. Preiser, F. Nosten, A. M. Dondorp and Z. Bozdech. Artemisinin resistance in *Plasmodium falciparum* is associated with an altered temporal pattern of transcription. *BMC Genomics* 2011, 12, 391.
222. J. E. Hyde. Drug-resistant malaria - an insight. *FEBS J.* 2007, 274, 4688-4698.
223. C. Tacoli, P. P. Gai, C. Bayingana, K. Sift, D. Geus, J. Ndoli, A. Sendegeya, J. B. Gahutu and F. P. Mockenhaupt. Artemisinin Resistance-Associated K13 Polymorphisms of *Plasmodium falciparum* in Southern Rwanda, 2010-2015. *Am. J. Trop. Med. Hyg.* 2016, 95, 1090-1093.
224. T. Mita, A. Kaneko, J. K. Lum, B. Bwijo, M. Takechi, I. L. Zungu, T. Tsukahara, K. Tanabe, T. Kobayakawa and A. Bjorkman. Recovery of chloroquine sensitivity and low prevalence of the *Plasmodium falciparum* chloroquine resistance transporter gene mutation K76T following the discontinuance of chloroquine use in Malawi. *Am. J. Trop. Med. Hyg.* 2003, 68, 413-415.
225. J. N. Burrows, S. Duparc, W. E. Gutteridge, R. Hooft van Huijsduijnen, W. Kaszubska, F. Macintyre, S. Mazzuri, J. J. Mohrle and T. N. Wells. New developments in anti-malarial target candidate and product profiles. *Malar J.* 2017, 16, 26.

-
226. J. N. Burrows, R. H. van Huijsduijnen, J. J. Mohrle, C. Oeuvray and T. N. Wells. Designing the next generation of medicines for malaria control and eradication. *Malar J.* 2013, 12, 187.
227. J. N. Burrows, E. Burlot, B. Campo, S. Cherbuin, S. Jeanneret, D. Leroy, T. Spangenberg, D. Waterson, T. N. Wells and P. Willis. Antimalarial drug discovery - the path towards eradication. *Parasitology* 2014, 141, 128-139.
228. K. T. Andrews, T. N. Tran and D. P. Fairlie. Towards histone deacetylase inhibitors as new antimalarial drugs. *Curr. Pharm. Des.* 2012, 18, 3467-3479.
229. T. N. Wells, R. Hooft van Huijsduijnen and W. C. Van Voorhis. Malaria medicines: a glass half full? *Nat. Rev. Drug. Discov.* 2015, 14, 424-442.
230. T. Rodrigues, R. Moreira and F. Lopes. New hope in the fight against malaria? *Future Med. Chem.* 2011, 3, 1-3.
231. E. Beutler. The hemolytic effect of primaquine and related compounds: a review. *Blood*, 1959, 14, 103-139.
232. T. Rodrigues, M. Prudencio, R. Moreira, M. M. Mota and F. Lopes. Targeting the liver stage of malaria parasites: a yet unmet goal. *J. Med. Chem.* 2012, 55, 995-1012.
233. D. Mazier, L. Renia and G. Snounou. A pre-emptive strike against malaria's stealthy hepatic forms. *Nat. Rev. Drug. Discov.* 2009, 8, 854-864.
234. M. Cunha-Rodrigues, M. Prudencio, M. M. Mota and W. Haas. Antimalarial drugs - host targets (re)visited. *Biotechnol J.* 2006, 1, 321-332.
235. C. T. Williams and A. F. Azad. Transcriptional analysis of the pre-erythrocytic stages of the rodent malaria parasite, *Plasmodium yoelii*. *PLoS One* 2010, 5, e10267.
236. K. G. Le Roch, Y. Zhou, P. L. Blair, M. Grainger, J. K. Moch, J. D. Haynes, P. De La Vega, A. A. Holder, S. Batalov, D. J. Carucci and E. A. Winzeler. Discovery of gene function by expression profiling of the malaria parasite life cycle. *Science* 2003, 301, 1503-1508.
237. S. J. Westenberger, C. M. McClean, R. Chattopadhyay, N. V. Dharia, J. M. Carlton, J. W. Barnwell, W. E. Collins, S. L. Hoffman, Y. Zhou, J. M. Vinetz and E. A. Winzeler. A systems-based analysis of *Plasmodium vivax* lifecycle transcription from human to mosquito. *PLoS Negl. Trop. Dis.* 2010, 4, e653.
238. S. Meister, D. M. Plouffe, K. L. Kuhlen, G. M. Bonamy, T. Wu, S. W. Barnes, S. E. Bopp, R. Borboa, A. T. Bright, J. Che, S. Cohen, N. V. Dharia, K. Gagaring, M. Gettayacamin, P. Gordon, T. Groessl, N. Kato, M. C. Lee, C. W. McNamara, D. A. Fidock, A. Nagle, T. G. Nam, W. Richmond, J. Roland, M. Rottmann, B. Zhou, P. Froissard, R. J. Glynn, D. Mazier, J. Sattabongkot, P. G. Schultz, T. Tuntland, J. R. Walker, Y. Zhou, A. Chatterjee, T. T. Diagana and E. A. Winzeler. Imaging of *Plasmodium* liver stages to drive next-generation antimalarial drug discovery. *Science* 2011, 334, 1372-1377.
239. D. A. Baker. Malaria gametocytogenesis. *Mol Biochem Parasitol* 2010, 172, 57-65.
240. C. Drakeley, C. Sutherland, J. T. Bousema, R. W. Sauerwein and G. A. Targett. The epidemiology of *Plasmodium falciparum* gametocytes: weapons of mass dispersion. *Trends Parasitol.* 2006, 22, 424-430.
241. O. Dechy-Cabaret and F. Benoit-Vical. Effects of antimalarial molecules on the gametocyte stage of *Plasmodium falciparum*: the debate. *J. Med. Chem.* 2012, 55, 10328-10344.
242. F. Ay, E. M. Bunnik, N. Varoquaux, J. P. Vert, W. S. Noble and K. G. Le Roch. Multiple dimensions of epigenetic gene regulation in the malaria parasite *Plasmodium falciparum*: gene regulation via histone modifications, nucleosome positioning and nuclear architecture in *P. falciparum*. *Bioessays* 2015, 37, 182-194.
243. B. I. Coleman, K. M. Skillman, R. H. Jiang, L. M. Childs, L. M. Altenhofen, M. Ganter, Y. Leung, I. Goldowitz, B. F. Kafsack, M. Marti, M. Llinas, C. O. Buckee and M. T. Duraisingh. A *Plasmodium falciparum* histone deacetylase regulates antigenic variation and gametocyte conversion. *Cell. Host. Microbe.* 2014, 16, 177-186.
244. L. H. Freitas-Junior, R. Hernandez-Rivas, S. A. Ralph, D. Montiel-Condado, O. K. Ruvalcaba-Salazar, A. P. Rojas-Meza, L. Mancio-Silva, R. J. Leal-Silvestre, A. M. Gontijo, S. Shorte and A. Scherf. Telomeric heterochromatin propagation and histone acetylation control mutually exclusive expression of antigenic variation genes in malaria parasites. *Cell* 2005, 121, 25-36.
245. P. C. Bull, B. S. Lowe, M. Kortok, C. S. Molyneux, C. I. Newbold and K. Marsh. Parasite antigens on the infected red cell surface are targets for naturally acquired immunity to malaria. *Nat. Med.* 1998, 4, 358-360.

-
246. D. J. Roberts, A. G. Craig, A. R. Berendt, R. Pinches, G. Nash, K. Marsh and C. I. Newbold. Rapid switching to multiple antigenic and adhesive phenotypes in malaria. *Nature* 1992, 357, 689-692.
247. B. K. Chaal, A. P. Gupta, B. D. Wastuwidyaningtyas, Y. H. Luah and Z. Bozdech. Histone deacetylases play a major role in the transcriptional regulation of the *Plasmodium falciparum* life cycle. *PLoS Pathog.* 2010, 6, e1000737.
248. F. K. Hansen, T. S. Skinner-Adams, S. Duffy, L. Marek, S. D. Sumanadasa, K. Kuna, J. Held, V. M. Avery, K. T. Andrews and T. Kurz. Synthesis, antimalarial properties, and SAR studies of alkoxyurea-based HDAC inhibitors. *ChemMedChem*, 2014, 9, 665-670.
249. F. K. Hansen, S. D. Sumanadasa, K. Stenzel, S. Duffy, S. Meister, L. Marek, R. Schmetter, K. Kuna, A. Hamacher, B. Mordmuller, M. U. Kassack, E. A. Winzeler, V. M. Avery, K. T. Andrews and T. Kurz. Discovery of HDAC inhibitors with potent activity against multiple malaria parasite life cycle stages. *Eur. J. Med. Chem.* 2014, 82, 204-213.
250. K. T. Andrews, T. N. Tran, A. J. Lucke, P. Kahnberg, G. T. Le, G. M. Boyle, D. L. Gardiner, T. S. Skinner-Adams and D. P. Fairlie. Potent antimalarial activity of histone deacetylase inhibitor analogues. *Antimicrob. Agents Chemother.* 2008, 52, 1454-1461.
251. G. Giannini, G. Battistuzzi and D. Vignola. Hydroxamic acid based histone deacetylase inhibitors with confirmed activity against the malaria parasite. *Bioorg. Med. Chem. Lett.* 2015, 25, 459-461.
252. M. B. Joshi, D. T. Lin, P. H. Chiang, N. D. Goldman, H. Fujioka, M. Aikawa and C. Syin. Molecular cloning and nuclear localization of a histone deacetylase homologue in *Plasmodium falciparum*. *Mol. Biochem. Parasitol.* 1999, 99, 11-19.
253. J. H. Kalin and J. A. Bergman. Development and therapeutic implications of selective histone deacetylase 6 inhibitors. *J. Med. Chem.* 2013, 56, 6297-6313.
254. D. Kim, C. L. Frank, M. M. Dobbin, R. K. Tsunemoto, W. Tu, P. L. Peng, J. S. Guan, B. H. Lee, L. Y. Moy, P. Giusti, N. Broodie, R. Mazitschek, I. Delalle, S. J. Haggarty, R. L. Neve, Y. Lu and L. H. Tsai. Deregulation of HDAC1 by p25/Cdk5 in neurotoxicity. *Neuron.* 2008, 60, 803-817.
255. J. Melesina, D. Robaa, R. J. Pierce, C. Romier and W. Sippl. Homology modeling of parasite histone deacetylases to guide the structure-based design of selective inhibitors. *J. Mol. Graph. Model.* 2015, 62, 342-361.
256. T. Heimbürg, A. Chakrabarti, J. Lancelot, M. Marek, J. Melesina, A. T. Hauser, T. B. Shaik, S. Duclaud, D. Robaa, F. Erdmann, M. Schmidt, C. Romier, R. J. Pierce, M. Jung and W. Sippl. Structure-Based Design and Synthesis of Novel Inhibitors Targeting HDAC8 from *Schistosoma mansoni* for the Treatment of Schistosomiasis. *J. Med. Chem.* 2016, 59, 2423-2435.
257. S. Agbor-Enoh, C. Seudieu, E. Davidson, A. Dritschilo and M. Jung. Novel inhibitor of *Plasmodium* histone deacetylase that cures *P. berghei*-infected mice. *Antimicrob. Agents Chemother.* 2009, 53, 1727-1734.
258. A. F. Adenowo, B. E. Oyinloye, B. I. Ogunyinka and A. P. Kappo. Impact of human schistosomiasis in sub-Saharan Africa. *Braz. J. Infect. Dis.* 2015, 19, 196-205.
259. M. Brown. Schistosomiasis. *Clin. Med.* 2011, 11, 479-482.
260. W. G. Jordan P., Sturrock R.F., ed. *Human schistosomiasis* CAB International Wallingford 1993.
261. World Health Organization. *Wkly. Epidemiol. Rec.*, 2015, 90, 25-32.
262. F. Mutapi. Changing policy and practice in the control of pediatric schistosomiasis. *Pediatrics* 2015, 135, 536-544.
263. D. G. Colley, A. L. Bustinduy, W. E. Secor and C. H. King. Human schistosomiasis. *Lancet* 2014, 383, 2253-2264.
264. T. Elbaz and G. Esmat. Hepatic and intestinal schistosomiasis: review. *J. Adv. Res.* 2013, 4, 445-452.
265. J. I. Odegaard and M. H. Hsieh. Immune responses to *Schistosoma haematobium* infection. *Parasite Immunol.* 2014, 36, 428-438.
266. M. Berriman, B. J. Haas, P. T. LoVerde, R. A. Wilson, G. P. Dillon, G. C. Cerqueira, S. T. Mashiyama, B. Al-Lazikani, L. F. Andrade, P. D. Ashton, M. A. Aslett, D. C. Bartholomeu, G. Blandin, C. R. Caffrey, A. Coghlan, R. Coulson, T. A. Day, A. Delcher, R. DeMarco, A. Djikeng, T. Eyre, J. A. Gamble, E. Ghedin, Y. Gu, C. Hertz-Fowler, H. Hirai, Y. Hirai, R. Houston, A. Ivens, D. A. Johnston, D. Lacerda, C. D. Macedo, P. McVeigh, Z. Ning, G. Oliveira, J. P. Overington, J. Parkhill, M. Pertea, R. J. Pierce, A. V. Protasio, M. A. Quail, M. A. Rajandream, J. Rogers, M. Sajid, S. L. Salzberg, M. Stanke, A. R. Tivey, O. White, D. L. Williams, J. Wortman, W. Wu, M.

-
- Zamanian, A. Zerlotini, C. M. Fraser-Liggett, B. G. Barrell and N. M. El-Sayed. The genome of the blood fluke *Schistosoma mansoni*. *Nature* 2009, 460, 352-358.
267. R. S. Barsoum. Urinary schistosomiasis: review. *J. Adv. Res.* 2013, 4, 453-459.
268. D. Cioli, L. Pica-Mattocchia, A. Basso and A. Guidi. Schistosomiasis control: praziquantel forever? *Mol. Biochem. Parasitol.* 2014, 195, 23-29.
269. A. A. Siddiqui, B. A. Siddiqui and L. Ganley-Leal. Schistosomiasis vaccines. *Hum. Vaccin.* 2011, 7, 1192-1197.
270. J. R. Doenhoff, G. Kusel, C. Coles and D. Cioli. Resistance of *Schistosoma mansoni* to praziquantel: is there a problem? *Trans. R. Soc. Trop. Med. Hyg.* 2002, 96, 465-469.
271. M. J. Doenhoff and L. Pica-Mattocchia. Praziquantel for the treatment of schistosomiasis: its use for control in areas with endemic disease and prospects for drug resistance. *Expert. Rev. Anti. Infect. Ther.* 2006, 4, 199-210.
272. F. F. Couto, P. M. Coelho, N. Araujo, J. R. Kusel, N. Katz, L. K. Jannotti-Passos and A. C. A. Mattos. *Schistosoma mansoni*: a method for inducing resistance to praziquantel using infected *Biomphalaria glabrata* snails, *Mem. Inst. Oswaldo Cruz*, 2011, 106, 153-157.
273. D. Alonso, J. Munoz, J. Gascon, M. E. Valls and M. Corachan. Failure of standard treatment with praziquantel in two returned travelers with *Schistosoma haematobium* infection. *Am. J. Trop. Med. Hyg.* 2006, 74, 342-344.
274. I. M. Silva, R. Thiengo, M. J. Conceicao, L. Rey, H. L. Lenzi, E. Pereira Filho and P. C. Ribeiro. Therapeutic failure of praziquantel in the treatment of *Schistosoma haematobium* infection in Brazilians returning from Africa. *Mem. Inst. Oswaldo Cruz.* 2005, 100, 445-449.
275. P. G. Fallon and M. J. Doenhoff. Drug-Resistant Schistosomiasis - Resistance to Praziquantel and Oxamniquine Induced in *Schistosoma-Mansoni* in Mice Is Drug-Specific. *Am. J. Trop. Med. Hyg.* 1994, 51, 83-88.
276. S. M. Messerli, R. S. Kasinathan, W. Morgan, S. Spranger and R. M. Greenberg. *Schistosoma mansoni* P-glycoprotein levels increase in response to praziquantel exposure and correlate with reduced praziquantel susceptibility. *Mol. Biochem. Parasitol.* 2009, 167, 54-59.
277. W. Wang, L. Wang and Y. S. Liang. Susceptibility or resistance of praziquantel in human schistosomiasis: a review. *Parasitol. Res.* 2012, 111, 1871-1877.
278. A. Cabezas-Cruz, J. Lancelot, S. Caby, G. Oliveira and R. J. Pierce. Epigenetic control of gene function in schistosomes: a source of therapeutic targets? *Front. Genet.* 2014, 5, 317.
279. A. Azzi, C. Cosseau and C. Grunau. *Schistosoma mansoni*: developmental arrest of miracidia treated with histone deacetylase inhibitors. *Exp. Parasitol.* 2009, 121, 288-291.
280. F. Dubois, S. Caby, F. Oger, C. Cosseau, M. Capron, C. Grunau, C. Dissous and R. J. Pierce. Histone deacetylase inhibitors induce apoptosis, histone hyperacetylation and up-regulation of gene transcription in *Schistosoma mansoni*. *Mol. Biochem. Parasitol.* 2009, 168, 7-15.
281. F. Oger, F. Dubois, S. Caby, C. Noel, J. Cornette, B. Bertin, M. Capron and R. J. Pierce. The class I histone deacetylases of the platyhelminth parasite *Schistosoma mansoni*. *Biochem. Biophys. Res. Commun.* 2008, 377, 1079-1084.
282. R. J. Pierce, F. Dubois-Abdeselem, S. Caby, J. Trolet, J. Lancelot, F. Oger, N. Bertheaume, E. Roger. Chromatin regulation in schistosomes and histone modifying enzymes as drug targets. *Mem. Inst. Oswaldo Cruz.* 2011, 106, 794-801.
283. S. Kannan, J. Melesina, A. T. Hauser, A. Chakrabarti, T. Heimburg, K. Schmidtkunz, A. Walter, M. Marek, R. J. Pierce, C. Romier, M. Jung and W. Sippl. Discovery of inhibitors of *Schistosoma mansoni* HDAC8 by combining homology modeling, virtual screening, and in vitro validation. *J. Chem. Inf. Model.* 2014, 54, 3005-3019.
284. M. Marek, Kannan, S., Hauser, A. T., Moraes Mourao, M., Caby, S., Cura, V., Stofa, D. A., Schmidtkunz, K., Lancelot, J., Andrade, L., Renaud, J. P., Oliveira, G., Sippl, W., Jung, M., Cavarelli, J., Pierce, R. J., Romier, C. Structural basis for the inhibition of histone deacetylase 8 (HDAC8), a key epigenetic player in the blood fluke *Schistosoma mansoni*. *PLoS Pathog.* 2013, 9, e1003645.
285. R. J. Pierce, F. Dubois-Abdeselem, J. Lancelot, L. Andrade and G. Oliveira. Targeting schistosome histone modifying enzymes for drug development. *Curr. Pharm. Des.* 2012, 18, 3567-3578.
286. R. Brunmeir, S. Lagger and C. Seiser. Histone deacetylase HDAC1/HDAC2-controlled embryonic development and cell differentiation. *Int. J. Dev. Biol.* 2009, 53, 275-289.

-
287. J. Lancelot, S. Caby, F. Dubois-Abdesselem, M. Vanderstraete, J. Trolet, G. Oliveira, F. Bracher, M. Jung and R. J. Pierce. Schistosoma mansoni Sirtuins: characterization and potential as chemotherapeutic targets. *PLoS Negl. Trop. Dis.* 2013, 7, e2428.
288. M. Nakagawa, Y. Oda, T. Eguchi, S. Aishima, T. Yao, F. Hosoi, Y. Basaki, M. Ono, M. Kuwano, M. Tanaka and M. Tsuneyoshi. Expression profile of class I histone deacetylases in human cancer tissues. *Oncol. Rep.* 2007, 18, 769-774.
289. M. Marek, G. Oliveira, R. J. Pierce, M. Jung, W. Sippl and C. Romier. Drugging the schistosome zinc-dependent HDACs: current progress and future perspectives. *Future Med. Chem.* 2015, 7, 783-800.
290. D. A. Stolfa, M. Marek, J. Lancelot, A. T. Hauser, A. Walter, E. Leproult, J. Melesina, T. Rumpf, J. M. Wurtz, J. Cavarelli, W. Sippl, R. J. Pierce, C. Romier and M. Jung. Molecular basis for the antiparasitic activity of a mercaptoacetamide derivative that inhibits histone deacetylase 8 (HDAC8) from the human pathogen schistosoma mansoni. *J. Mol. Biol.* 2014, 426, 3442-3453.
291. M. Mottamal, S. Zheng, T. L. Huang and G. Wang. Histone deacetylase inhibitors in clinical studies as templates for new anticancer agents. *Molecules* 2015, 20, 3898-3941.
292. M. Guha. HDAC inhibitors still need a home run, despite recent approval. *Nat. Rev. Drug Discov.* 2015, 14, 225-226.
293. I. N. Gaisina, W. Tueckmantel, A. Ugolkov, S. Shen, J. Hoffen, O. Dubrovskiy, A. Mazar, R. A. Schoon, D. Billadeau and A. P. Kozikowski. Identification of HDAC6-Selective Inhibitors of Low Cancer Cell Cytotoxicity. *ChemMedChem* 2016, 11, 81-92.
294. K. Kanno, S. Kanno, H. Nitta, N. Uesugi, T. Sugai, T. Masuda, G. Wakabayashi and C. Maesawa. Overexpression of histone deacetylase 6 contributes to accelerated migration and invasion activity of hepatocellular carcinoma cells. *Oncol. Rep.* 2012, 28, 867-873.
295. L. Goracci, N. Deschamps, G. M. Randazzo, C. Petit, C. Dos Santos Passos, P. A. Carrupt, C. Simoes-Pires and A. Nurisso. A Rational Approach for the Identification of Non-Hydroxamate HDAC6-Selective Inhibitors. *Sci. Rep.* 2016, 6, 29086.
296. Y. Mishima, L. Santo, H. Eda, D. Cirstea, N. Nemani, A. J. Yee, E. O'Donnell, M. K. Selig, S. N. Quayle, S. Arastu-Kapur, C. Kirk, L. H. Boise, S. S. Jones and N. Raje. Ricolinostat (ACY-1215) induced inhibition of aggresome formation accelerates carfilzomib-induced multiple myeloma cell death. *Br. J. Haematol.*, 2015, 169, 423-434.
297. H. V. Diyabalanage, M. L. Granda and J. M. Hooker. Combination therapy: histone deacetylase inhibitors and platinum-based chemotherapeutics for cancer. *Cancer Lett.* 2013, 329, 1-8.
298. M. A. Asgar, G. Senawong, B. Sripan and T. Senawong. Synergistic anticancer effects of cisplatin and histone deacetylase inhibitors (SAHA and TSA) on cholangiocarcinoma cell lines. *Int. J. Oncol.* 2016, 48, 409-420.
299. J. Senger, J. Melesina, M. Marek, C. Romier, I. Oehme, O. Witt, W. Sippl and M. Jung. Synthesis and Biological Investigation of Oxazole Hydroxamates as Highly Selective Histone Deacetylase 6 (HDAC6) Inhibitors. *J. Med. Chem.* 2016, 59, 1545-1555.
300. H. Mueller, M. U. Kassack and M. Wiese. Comparison of the usefulness of the MTT, ATP, and calcein assays to predict the potency of cytotoxic agents in various human cancer cell lines. *J. Biomol. Screening* 2004, 9, 506-515.
301. T. Ciossek, H. Julius, H. Wieland, T. Maier and T. Beckers. A homogeneous cellular histone deacetylase assay suitable for compound profiling and robotic screening. *Anal. Biochem.* 2008, 372, 72-81.
302. C. Bonfils, A. Kalita, M. Dubay, L. L. Siu, M. A. Carducci, G. Reid, R. E. Martell, J. M. Besterman and Z. Li. Evaluation of the pharmacodynamic effects of MGCD0103 from preclinical models to human using a novel HDAC enzyme assay. *Clin. Cancer. Res.* 2008, 14, 3441-3449.
303. E. M. Gosepath, N. Eckstein, A. Hamacher, K. Servan, G. von Jonquieres, H. Lage, B. Gyorffy, H. D. Royer and M. U. Kassack. Acquired cisplatin resistance in the head-neck cancer cell line Cal27 is associated with decreased DKK1 expression and can partially be reversed by overexpression of DKK1. *Int. J. Cancer.* 2008, 123, 2013-2019.
304. N. Eckstein, K. Servan, L. Girard, D. Cai, G. von Jonquieres, U. Jaehde, M. U. Kassack, A. F. Gazdar, J. D. Minna and H. D. Royer. Epidermal growth factor receptor pathway analysis identifies amphiregulin as a key factor for cisplatin resistance of human breast cancer cells. *J. Biol. Chem.* 2008, 283, 739-750.
305. T. N. Wells, P. L. Alonso and W. E. Gutteridge. New medicines to improve control and contribute to the eradication of malaria. *Nat. Rev. Drug. Discov.* 2009, 8, 879-891.

-
306. K. V. Butler, J. Kalin, C. Brochier, G. Vistoli, B. Langley and A. P. Kozikowski, Rational design and simple chemistry yield a superior, neuroprotective HDAC6 inhibitor, tubastatin A. *J. Am. Chem. Soc.* 2010, 132, 10842-10846.
307. J. A. Bergman, K. Woan, P. Perez-Villarroel, A. Villagra, E. M. Sotomayor and A. P. Kozikowski. Selective histone deacetylase 6 inhibitors bearing substituted urea linkers inhibit melanoma cell growth. *J. Med. Chem.* 2012, 55, 9891-9899.
308. WHO, Preventative Chemotherapy in Helminthiasis: coordinated use of antihelminthic drugs in control interventions: a manual for health professionals and programme managers., World Health Organization, Geneva, 2006.
309. I. Rettig, E. Koenke, F. Trippel, W. C. Mueller, J. Burhenne, A. Kopp-Schneider, J. Fabian, A. Schober, U. Fernekorn, A. von Deimling, H. E. Deubzer, T. Milde, O. Witt and I. Oehme. Selective inhibition of HDAC8 decreases neuroblastoma growth in vitro and in vivo and enhances retinoic acid-mediated differentiation. *Cell. Death Dis.* 2015, 6, e1657.
310. I. Oehme, H. E. Deubzer, M. Lodrini, T. Milde and O. Witt. Targeting of HDAC8 and investigational inhibitors in neuroblastoma. *Expert. Opin. Investig. Drugs* 2009, 18, 1605-1617.
311. B. Heltweg, F. Dequiedt, E. Verdin and M. Jung. Nonisotopic substrate for assaying both human zinc and NAD⁺-dependent histone deacetylases. *Anal. Biochem.* 2003, 319, 42-48.